The Systematic Development of Direct Write (DW) Technology for the Fabrication of Printed Antennas for the Aerospace and Defence Industry

Sandeep Raja
December 2013

This thesis is submitted in fulfilment for the Engineering Doctorate in Systems Engineering at Loughborough University. The work was carried out during the three years 2006 – 2010 at BAE Systems Advanced Technology Centre, Bristol.

ABSTRACT

Low profile, conformal antennas have considerable advantages for Aerospace and Military platforms where conventional antenna system add weight and drag. Direct Write (DW) technology has been earmarked as a potential method for fabricating low profile antennas directly onto structural components. This thesis determines the key design rules and requirements for DW fabrication of planar antennas. From this, three key areas were investigated: the characterisation of DW ink materials for functionality and durability in harsh environments, localised processing of DW inks and the optimisation of DW conductive ink material properties for antenna fabrication. This study mainly focused on established DW technologies such as micro-nozzle and inkjet printing due to their ability to print on conformal surfaces.

From initial characterisation studies it was found that silver based micro-nozzle PTF inks had greater adhesion then silver nano-particle inkjet inks but had lower conductivity (2% bulk conductivity of silver as opposed to 8% bulk conductivity). At higher curing temperatures (>300°C) inkjet inks were able to achieve conductivities of 33% bulk conductivity of silver. However, these temperatures were not suitable for processing on temperature sensitive surfaces such as carbon fibre. Durability tests showed that silver PTF inks were able to withstand standard aerospace environments apart from Skydrol immersion.

It was found that DW inks should achieve a minimum conductivity of 30% bulk silver to reduce antenna and transmission line losses. Using a localised electroplating process (known as brush plating) it was shown that a copper layer could be deposited onto silver inkjet inks and thermoplastic PTF inks with a copper layer exhibiting a bulk conductivity of 66% bulk copper and 57% bulk copper respectively. This was an improvement on previous electroless plating techniques which reported bulk copper conductivities of 50% whilst also enabling DW inks to be plated without the need for a chemical bath.

One of the limitations of many DW ink materials is they require curing or sintering before they become functional. Conventional heat treatment is performed using an oven which is not suitable when processing DW materials onto large structural component. Previous literature has investigated laser curing as means of overcoming this problem. However, lasers are monochromatic and can therefore be inefficient when curing materials that have absorption bands that differ from the laser wavelength. To investigate this, a laser diode system was compared to a broadband spot curing

system. In the curing trials it was found that silver inks could be cured with much lower energy density (by a factor of 10) using the broadband white light source. Spectroscopy also revealed that broadband curing could be more advantageous when curing DW dielectric ink materials as these inks absorb at multiple wavelengths but have low heat conductivity.

Themodynamical modelling of the curing process with the broadband heat source was also performed. Using this model it was shown that the parameters required to cure the ink with the broadband heat source only caused heat penetration by a few hundred micro-metres into the top surface of the substrate at very short exposure times (~1s). This suggested that this curing method could be used to process the DW inks on temperature sensitive materials without causing any significant damage.

Using a combination of the developments made in this thesis the RF properties of the DW inks were measured after broadband curing and copper plating. It was found that the copper plated DW ink tracks gave an equivalent transmission line loss to a copper etched line. To test this further a number of GPS patch antennas were fabricated out of the DW ink materials. Again the copper plated antenna gave similar properties to the copper etched antenna.

To demonstrate the printing capabilities of the micro-nozzle system a mock wireless telecommunications antenna was fabricated on to a GRP UAV wing. In this demonstrator a dielectric and conductive antenna pattern was fabricated on to the leading edge of the wing component using a combination of convection curing and laser curing (using an 808nm diode laser).

ACKNOWLEDGEMENTS

I would like to express my sincere thanks to my supervisors Dr. Jagjit Sidhu and Jennifer McDonald at BAE Systems Advanced Technology Centre and Dr. Chris Tuck and Prof. Richard Hague at Loughborough University who gave me the opportunity to take part in the Engineering Doctorate programme and also gave me invaluable technical help and support.

I would also like to thank the team at the Systems Engineering Doctorate Centre (SEDC) at Loughborough University, Sharon Henson and Dr. Roger Dixon who organised the doctorate programme and associated teaching modules. This allowed me to develop and gain understanding behind the principles of Systems Engineering and applications within industry.

The work conducted in this thesis could not have been completed without access to specific equipment. I would therefore like to thank Dr. Liang Hao at Exeter University who allowed me to use their polymer characterisation equipment, Dr. Paul Warr at Bristol University for giving me access to their anechoic chamber for antenna gain measurements and Richard Orton at BAE systems for assisting me with antenna modelling and transition line measurements. Furthermore, I would like to mention the partners in the DW: EASY project, Steve Jones at Printed Electronics (PEL) and John Lowe (APT) for their invaluable advice regarding Inkjet and electroplating technologies.

Finally without the support and encouragement of my work colleagues, friends and family specifically, Dr Emma Ashcroft, Dr Robert Scudamore, Kevin Chan, Andy Wescott, Alan Proudfoot, Mom (Chandrika Raja) and Dad (Pravin Raja), I would never have been able to complete this piece of work.

CONTENTS

APT	Additive Process Technologies
AUT	Antenna Under Test
BW	Band Width
CAD	Computer Aided Design
COTS	Commercial Off The Shelf
CVD	Chemical Vapour Deposition
DMA	Dynamic Mechanical Analysis
DSC	Dynamic Scanning Calorimetry
DTI	Department of Trade and Industry
DW	Direct Write
FWHM	Full Width Half Maxima
GEM	Gwent Electronic Materials
GPS	Global Positioning System
GRP	Glass Reinforced Plastic
HTCC	High Temperature Co-fired Ceramic
IR	Infra-Red
LTCC	Low Temperature Co-fired Ceramic
M3D	Maskless Mesoscale Deposition
MAPLE	Matrix Assisted Pulsed Laser Evaporation
PTF	Polymer Thick Film
PVD	Physical Vapour Deposition
QFD	Quality Functional Deployment
RCS	Radar Cross-Section
RF	Radio Frequency
RFID	Radio Frequency Identification
RL	Return Loss
SE	Systems Engineering
SHM	Structural Health Monitoring
SLS	Selective Laser Sintering
TGA	Thermo Gravimetric Analysis
UAV	Unmanned Autonomous Vehicle

UV	Ultra Violet
VOC	Volatile Organic Components
VNA	Vector Network Analyser

λ	wavelength
D_{min}	Largest dimension of the antenna
r_{min}	Minimum distance from the antenna
Z_{in}	Input Impedance
R_{in}	Antenna resistance at the terminals
X_{in}	Antenna reactance at the terminals
e_t	Total antenna efficiency
e_r	Reflection (impedance mismatch) efficiency
e_c	Conduction efficiency
e_d	Dielectric efficiency
D	Antenna directivity
U	Radiation intensity of the antenna
U_i	Radiation intensity of the reference source
P_r	Total power radiated
G	Antenna gain
RL	Return loss
Γ	Reflection coefficient
BW	Band Width
f_h	Highest frequency
f_L	Lowest frequency
f_c	Center frequency
Q	Quality Factor
ω	Angular frequency
W	Stored energy
P_l	Total power loss in the antenna
P_c	Conductor power loss
P_d	Dielectric power loss
$\tan\delta_d$	Dielectric loss tangent
α_d	Microstrip dielectric loss
α_c	Microstrip conductor loss
ε_r	Relative permittivity

ε_o	Free space permittivity
W	Width of the conductor
R_s	Surface resistivity
σ_c	Conductivity of the micro-strip
Z_m	Characteristic impedance
L	Inductance per unit length
G_c	Conductance per unit length
C	Capacitance per unit length
R_l	Resistance per unit length
Z_0	Impedance of free space
w_{eff}	Effective width of the strip
h	Height of the dielectric
t	Thickness of the metal conductor
δ_z	Skin depth
Ra_D	RMS surface roughness of the conductor
R	Resistivity
L	Track length
A	Cross-section area of the conductor
V	Voltage
I	Current
R_a	Surface roughness
tanδ	Mechanical loss tangent
R	Resistance
R_{sq}	Sheet Resistance
E	Young's modulus
E'	Storage modulus
E''	Loss modulus
r_c	Number of cross-links per gram
T_g	Glass transition temperature
n	Valence number
m	Mass
M	Molar mass
Q_c	Electric charge
F	Faraday constant

T	Transmission percentage
I_0	Intensity of incident light
I	intensity
α	Absorption coefficient
δ_p	Penetration depth
D_{sp}	Laser spot diameter
V_s	Laser scanning rate
E_l	Energy density of laser beam
k	Thermal conductivity
Q_h	Heat energy
c	Heat capacity
T	Temperature
t	Time
A_{amp}	Amplitude of incident beam
N	Gaussian normalisation factor
g	Gaussian factor
r_d	Material density
C_p	Specific heat capacity
$\vec{n}$	Normal vector
q_o	Inward heat flux

LIST OF FIGURES

1. General Introduction

Chapter 1 describes the subject matter of this thesis. This will include the research aims and a description of the novelty of the work conducted. A brief introduction of Direct Write (DW) technology and its advantages for conformal, low profile antenna manufacture will also be given. This will then lead into uses and limitations of the current state of the art of this technology, concluding with an outline of this thesis.

1.1 The need for integrated conformal antennas

The Aerospace and Defence industry is striving to increase the efficiency of its vehicles by reducing weight and drag. One of the areas where this is of particular concern is the size and number of current antenna systems. A typical modern aircraft, for example, can have between 20 to 70 different antenna protruding from its surface as depicted in Figure 1:1 [1]. These antennas can cause considerable drag, increased fuel consumption and additional weight. Military defence systems also have requirements for antennas that have covert or stealthy properties such that the antenna does not backscatter microwave radiation when illuminated by a hostile radar transmitter [2].

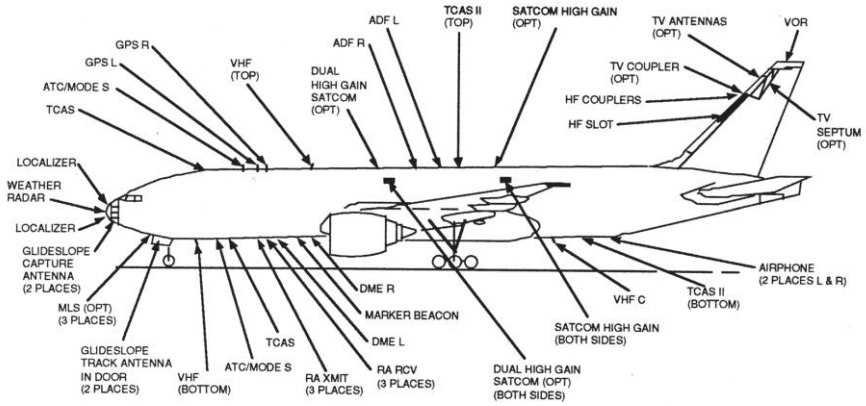

Antenna Systems on an Aircarft from [2]

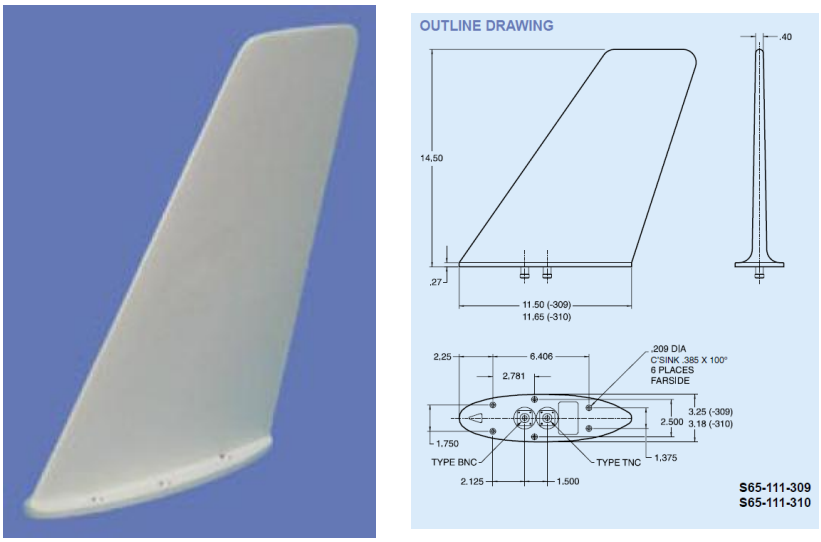

A typically large 225-400MHz blade antenna which is bolted on to the fuselage of an aircraft [3]

Figure 1:1: At least 20-30 different antennas can protrude from the aircraft skin increasing both drag and weight (from Sensor Systems Inc [3] and Josefsson, L et al. [2])

It has become increasingly desirable to have antennas with flat profiles that can be integrated on to the walls of vehicles and aircraft bodies [4]. The need to provide this capability is even more pronounced as large scale apertures are required for over the horizon communications such as satellite communications and military airborne surveillance radars. In addition, these antennas must be capable of withstanding the harsh environments imposed by the aircraft and maintain a low radar cross-section (RCS) [5].

One method of overcoming this problem is to embed the antenna within the vehicle structure as shown in Figure 1:2. The advantages of this solution are that the antenna remains flush to the surface and is visually undetectable. However, in order to mount the antenna a large section of the structure must be removed from the vehicle, this will affect its flightworthiness and would need to go through stringent qualification processes.

Figure 1:2: Embedded annular slot antenna integrated on to a wing structure (from Engle, R [6])

An alternative solution is to use a conformal antenna design whereby the complete antenna can be integrated on to the 'skin' of the structure. A conformal antenna is an antenna whose structure conforms to a prescribed shape. There are various factors other than electromagnetic considerations which prescribe the shape and orientation of a conformal antenna [7]. The IEEE standard definition of terms (IEEE Std 145-1993) for antennas gives the following definition for conformal antennas:

"*An antenna that conforms to a surface whose shape is determined by considerations other than electromagnetic; for example, aerodynamic or hydrodynamic*"

The micro-strip antenna allows conformal, low profile antennas to be realised. This type of antenna assembly is physically very simple and flat. The upper surface of a dielectric substrate supports a conducting strip while the entire lower surface of the substrate is backed by a conducting ground plane [8]. Figure 1:3 gives some examples of microstrip antennas.

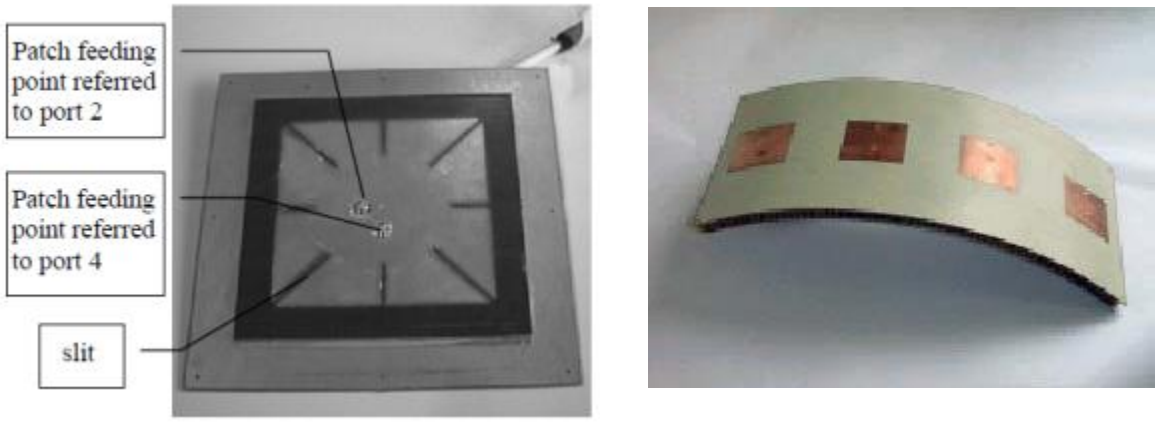

GPS Patch Antenna [9] Conformal Patch Antenna Array [10]

Figure 1:3: Examples of microstrip patch antennas (from Alboni, E et al. [9] and Kabacik, P et al. [10])

Micro-strip antennas are conventionally fabricated using conventional Printed Circuit Board (PCB) type techniques on to a suitable dielectric material. This process does not lend itself well for integrating these antennas on to structures with complex curvatures. This is primarily because it can be difficult to fit and attach the antenna accurately on to the surface of the structural component. Alternatively the antenna can be embedded within the structure similar to the example given in Figure 1:2 but this method is not desirable for aircraft or military vehicles.

The aim of this thesis is to investigate Direct Write (DW) printing technology for the fabrication of conformal, micro-strip antennas on to the surface of large military and aircraft structures. The term DW describes a family of additive methods that can deposit a pattern of material on to a substrate with controlled architecture and properties.

1.2 Direct Write Printing Technology

Material deposition occurs by moving a DW printing head or substrate component along a predefined path using suitable robotics. Whilst the structural architecture is achieved during the deposition process, the material properties are defined during the post-processing step that usually involves some form of heat-treatment. DW processes include inkjet printing, micro-nozzle deposition, Maskless Mesoscale Material Deposition (M3D) and thermal spray technologies, these processes are described in more detail in Chapter 2.

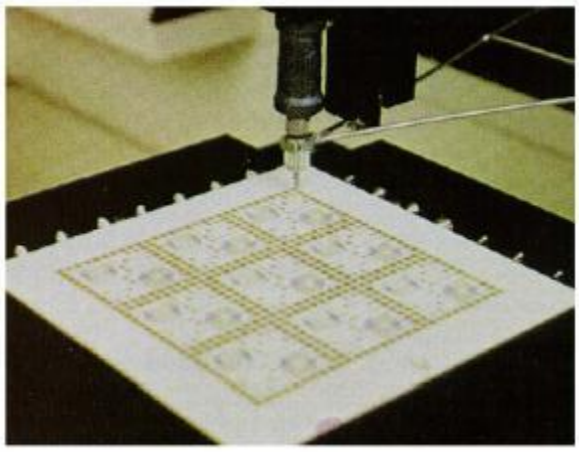

Figure 1:4: Example of the DW micro-nozzle system being used to produce an electrical device (from King, B H et al. [11])

One of the most promising application areas of DW technology is the ability to print novel, meso-scale, electrical components and devices directly onto complex 3D surfaces targeting both consumer, aerospace and defence markets. In the past DW has been used to fabricate electrical interconnects [12], passive electrical components [13], sensors for Structural Health Monitoring

(SHM) [14] and inductors for RFID tags [15]. DW has also found applications in both optical and biological applications [16].

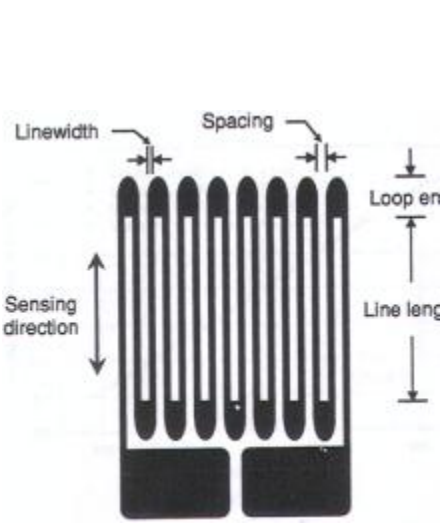

Printed pattern of thermally sprayed strain gauge [14]

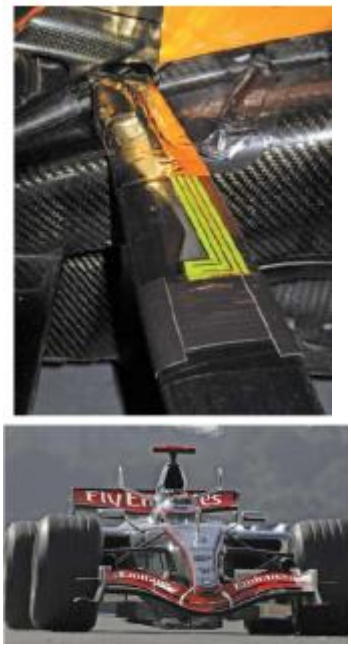

DW micronozzle used to print electrical interconnects on a F1 racing car [12]

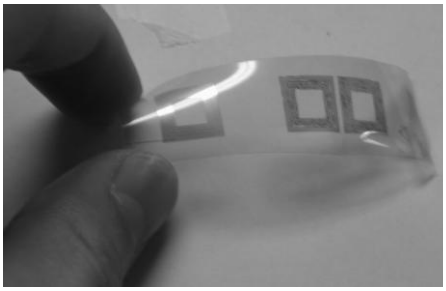

Inductors printed on to plastic using inkjet printing [15]

Figure 1:5: Example of DW devices (from Chen, Q et al. [14], Birch, S [12] and Subramanian, V [15])

While these devices are not yet capable of challenging the performance of traditional electronics especially in the micro-electronics industry, they have considerable potential when the main market drivers are size, weight and cost as opposed to performance. In addition unique applications can be found where volumes are small but the ability to easily customise designs is important.

In 2004 the UK Department of Trade and Industry produced a report highlighting some of the key drivers and benefits of DW technology [17]:

- The ability to fabricate multi-functional 'complete devices' using a single deposition method
- The ability to rapidly prototype circuits without the need for masks or hard tooling
- The reduction in the size and weight of devices by fabricating components directly on to surfaces thereby eliminating the need for an interfacial substrate

- The fabrication of low cost devices without material waste
- The fabrication of flexible devices on to temperature sensitive materials
- To realise a smaller production scale footprint for devices that is CAD/CAM compatible

1.3 DW technology for conformal antenna fabrication

Due to the perceived benefits of DW technology it is increasingly finding applications in printing large conformal antennas [18] & [19]. Figure 1:6 shows an example of a conformal GPS antenna printed on to a fibreglass dome printed using Laser DW.

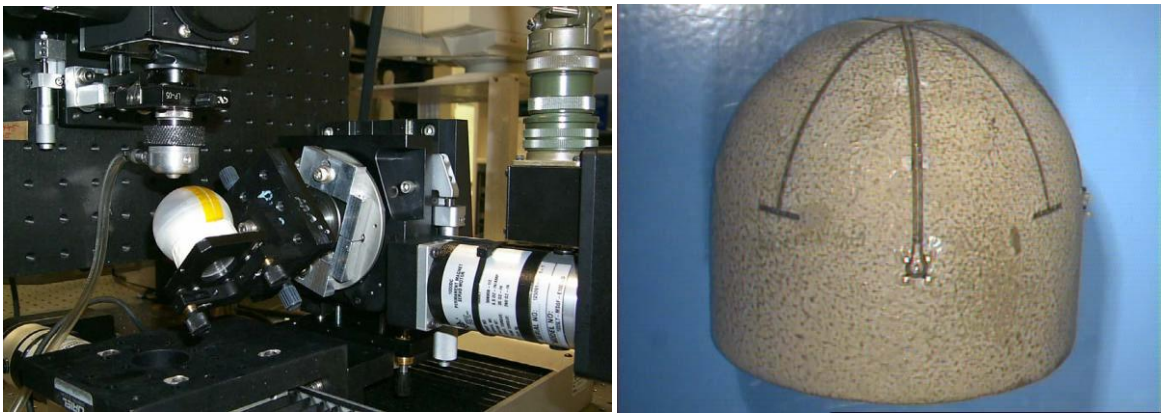

Figure 1:6: Laser deposited conformal GPS antenna on to a fibreglass dome (from Pique, A et al. [20])

The potential advantages of DW printing for conformal antenna fabrication are:

- Accurate positioning of the antenna device through precision robotics
- Conformal deposition of the antenna through CAD/CAM robotic systems
- Manufacture of the complete antenna device through the deposition of all functional material including conductors and dielectrics
- Ability to fabricate the antenna without effecting the flightworthiness of the vehicle using additive approaches

Another key driver for using DW technology to fabricate conformal antennas is the potential to be able to deposit and process functional materials on to structures, such as carbon fibre composites, which have relatively low tolerance to high temperatures (>100°C). This is important as the aerospace and defence industry is increasingly using carbon fibre composites to manufacture structural components such as whole wing and fuselage sections [21] [22] [23].

DW technology currently has a number of limitations that prevent it from being used today for conformal antenna fabrication. Research is required in terms of improving the printing process and

material properties. Furthermore there has been little work in qualifying DW antennas for functionality and durability which is a key requirement for any device used in aerospace or military applications. These areas of development will be discussed further in Chapter 2, 3 and 4.

1.4 Outline of Thesis

The aims and objectives of this thesis are summarised in Figure 1:7 along with an outline of the thesis structure. To meet these objectives the research plan was designed in such a way as to first identify the current limitations in DW technology and then to look at a number of key technologies which could be used to address these limitations. To validate the developments made in this thesis a demonstrator DW antenna is fabricated to measure the RF properties against a conventionally manufactured microstrip antenna.

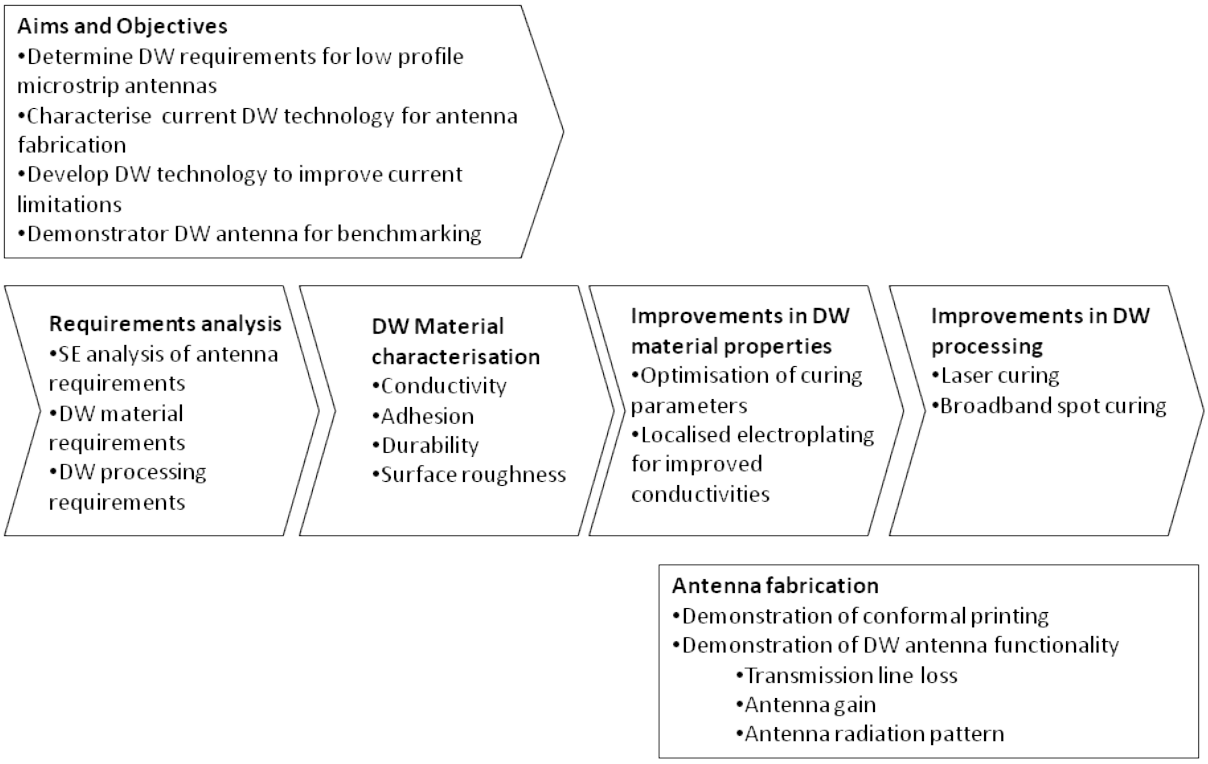

Figure 1:7: Flow diagram to illustrate thesis outline

A description of each chapter in this thesis is given below:

Chapter 2 gives an introduction and history of development of DW technology. An overview of the current printing technologies will be given including their suitability for conformal printing. An assessment of current DW materials, processes and past work in antenna fabrication will also be given.

Chapter 3 details the basic theory behind antenna operation and lists some of the antenna types that are currently being used today. A focus will be given to micro-strip antenna designs which are particularly suitable for conformal low profile antennas. The equations and physics related to the design of these antennas will be given. From the relationships dictated in these equation a set of requirements and design rules (or guidelines) for antenna fabrication using DW technology will be determined.

Chapter 4; from the information gathered in Chapter 2 and Chapter 3 the requirements for the production of a conformal DW antenna will be captured using a 'systems' approach. In this chapter an introduction of Systems Engineering (SE) will be given as well as how it can be applied to research and development projects. Using a number of SE tools the requirements for DW technology and printed DW antennas will be captured using both systems architecture and functional analysis. This chapter will conclude by defining a set of technical performance parameters and measures which can be used to monitor the developments made in this thesis with regards to the defined requirements.

Chapter 5 outlines the main experimental techniques carried out in this thesis. This will include details of the DW printing technologies and why they were selected for antenna fabrication. This thesis will primarily investigate micro-nozzle deposition for conformal antenna printing with some analysis of inkjet printing as well.

Chapter 6 analyses some of the fundamental properties of DW ink materials that could be used for antenna fabrication. This thesis will concentrate on characterising a number of conductive ink compositions specifically designed for DW applications, some additional work will also be presented on dielectric inks. Initial measurements of the functional properties of the ink, such as adhesion and conductivity, will be made using (manufacturer's) recommended and elevated curing parameters. To optimise the curing parameters, and hence material properties, of PTF inks the curing kinetics will be

investigated using polymer characterisation techniques. The environmental durability of a select number of DW materials will also be investigated using Airbus approved standards.

Chapter 7 shows the development of a localised electroplating technique to improve the conductivity of the DW ink material. Using the first iteration of the electroplating tool head the conductivity copper plated DW ink tracks will be measured and the plating efficiency calculated. From these results recommendations will be made on the DW ink best suited for electroplating.

Chapter 8 outlines the development of suitable curing methods. Conventionally, DW ink material is cured in an oven. This is not suitable for a number of applications earmarked for DW technology. Previous work has analysed laser-curing techniques as a means of solving this problem. The work conducted in Chapter 8 will consider a fibre delivered broadband white light source as an alternative means of curing DW ink materials. By investigating the spectral properties of DW inks and comparing results obtained from laser curing trials an assessment will be made on the advantages of using broadband radiation to process DW inks.

Chapter 9 outlines a thermodynamical modelling analysis of the localised curing process using the COMSOL software suite. The purpose of the model will be to determine if the heat exposure from the heat source is high enough to cause damage to the composite substrate material underneath a DW coating.

Chapter 10 combines the processing parameters and techniques suggested in this thesis to fabricate DW micro-strip transmission lines and GPS patch antennas onto a Commercial Off The Shelf (COTS) dielectric. The RF properties of these devices will then be investigated and compared to benchmark copper etched variants on the same substrate. A brief analysis of the RF carrying capability of DW dielectric materials will also be performed.

Chapter 11 concludes the work conducted in this thesis based on the results obtained in the previous chapters. An overview of the key developments will be made along with their importance to improving low profile antenna fabrication onto aerospace grade structures. The key contribution to knowledge is the implementation of localised broadband curing of DW ink materials and localised electroplating which improves antenna fabrication and antenna functionality respectively. Recommendations will also be given on where further study is required to take this technology further.

2 Background Literature Review of Direct Write Technology

Chapter 2 reviews the relevant research and theory in the area of DW technology. This will include the historic development of DW and the main DW printing technologies and materials with respect to their advantages and disadvantages for conformal antenna fabrication. Finally Chapter 2 ends with a summary of the requisite literature and identification of the current gaps in the field.

2.1 Direct Write (DW) Technology a Market Pull

Advances in integrated circuits and electronics for semi-conductor devices have increased rapidly over the last decade. This has led to smaller more compact chips with a larger numbers of transistors and the development of Micro-Electro-Mechanical System (MEMS) devices. However, technologies for developing electronic feature sizes in the mesoscopic range were not as forthcoming. The mesoscopic regime encompasses electronic devices that straddle the size range between conventional microelectronics (sub-micron range) and traditional surface mount components (10mm range) [16]. Meso-scale devices are particularly important for packaging applications and for adding functionality to existing devices or components such as wireless communications and sensors [16]. The meso-electronic components encompass passive components (resistors, capacitors, inductors), as well as active components such as antennae and batteries [24]. These types of devices form a complimentary role to micro-electronic devices and integrated circuits.

DW was recognised by the UK Department for Trade and Industry (DTI) as an additive manufacturing method that allows the fabrication and integration of mesoscopic devices. The definition of the DW process is given as [17]:

“The ability to fabricate (including post deposition processing), two or three dimensional functional structures, usually in situ and directly on to complex shapes, that may be large, possibly in short production runs that are not carried out in a vacuum”

As DW is an additive process it has relatively low geometrical constraints on the manufacturing process. This allows for greater design flexibility as too often the development of devices is limited by the processes which define them.

The DTI highlighted a number of markets where the benefits of DW can be exploited [17]. Possibly the greatest sector where DW can have an impact is in the Printed Circuit Board (PCB) industry. The European PCB market value was forecasted at approximately £3.4 billion in 2010 [25]. This market breaks down into single and multilayer devices on to rigid and flexible surfaces. In 2002 rigid multilayer devices dominated the market; however, with advent of disposable electronics (such as RFID tags), the flexible sector has grown in value [17]. Some of these application are increasing the demand for electronic devices to be constructed on to temperature sensitive surfaces (such as polymers, composites and glass), an area which can be achieved using DW technology.

Another area where DW can provide advantages is through weight reduction. Weight reduction even by a few grams can often be paramount in aerospace and defence applications. An example of this is the printing of conformal low weight interconnects and devices on the surface of a military helmet (Figure 2:1). This has been highlighted as a potential high value application by defence industries [17].

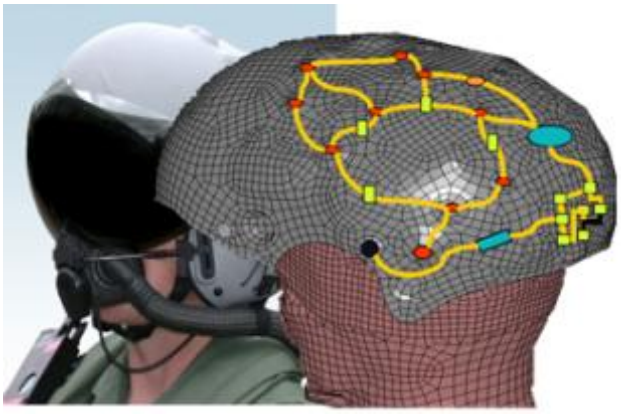

Figure 2:1: Potential application to fabricate DW interconnects on a helmet leading to reduced weight and cost (from Sidhu, J [26])

2.2 Printed Electronics: the development of Direct Write

Electronic features can be deposited using thick and thin film printing technologies as well as particle dispensing units [27]. These processes deliver electrically functional material (such as conductors) to the substrate. Depending on the material type there is an additional post-processing step before the material becomes functional. This step is usually but not exclusively in the form of heat treatment.

One of the earliest types of thin film deposition techniques are Chemical Vapour Deposition (CVD) and Physical Vapour Deposition (PVD), these processes use either a solid or gaseous precursor. In PVD a thin film coating is applied to a workpiece in a high temperature vacuum evaporation

chamber using condensation or plasma sputtering to apply the material. CVD uses one or more volatile precursors which reacts or decompose on the substrate surface [17]. Other technologies involve sputtering thin film material using electro-physical processes. Patterning techniques conventionally involve masking or lithography (selectively etching) type processes. Thin film deposition techniques allow for film thickness of 3nm to 2,500 nm and near bulk conductivities to be obtained [17] [28]. These processes require certain environmental conditions (such as vacuum chambers), resulting in costly procedures and limits to the type of substrate/component material that can be written on and the type of material that can be deposited. Thin film materials and techniques are mainly used for the fabrication of micro-electronic circuits rather than surface mounted mesoscale components and are thus not considered as DW techniques.

Prior to DW, screen printing was the most established method for meso-scale deposition of thick-film electronic material. The screen printing process has the ability to deposit highly accurate patterns on to a substrate using different masks or screens [27]. The use of mask and screen reduce flexibility of the technique and reduces the potential for Rapid Prototyping and mass customisation. The process is also confined to writing on flat surfaces only [16].

In 1999 the Defence Advanced Research Projects Agency (DARPA) launched the Mesoscale Integrated Conformal Electronics (MICE) program [24]. The specific aims of this program were to develop technologies which could provide industry with rapid prototyping and just-in-time electronics manufacturing on conformal surfaces [16]. This requires the fabrication of electronic devices directly from CAD files without the fabrication of a mask, which in turn allows the economical fabrication of low-batch runs because of minimal capital costs for new designs [28]. MICE also considered the morphological requirements of the structural surface, whereby neither the patterning nor the post processing steps should heat the substrate/surface above its damage threshold. This has led to continued material development of thick film inks with lower processing temperatures.

Through the auspices of the MICE program four different deposition techniques were developed which enabled the deposition of different functional materials on to different substrate materials and shapes. These DW technologies are:

- DW syringe process, or micronozzle (MicroPen ® ohmcraft, n-Scrypt)
- Thermal spraying

- Matrix Assisted Pulsed Laser Evaporation (MAPLE)
- Maskless Mesoscale Material Deposition (M3D)

In addition to these technologies Ink-Jet printing has been developing as capable method of depositing functional quasi-thin film material [16]. In general the resolution of DW tracks can be on the micrometer scale, speeds can be in excess of 200 mm/s, and the electronic material properties are comparable to those of conventional screen-printed materials [29]. Ultimately however, each DW technique is a compromise between material selection, accuracy and speed.

As a result of the MICE program the potential of direct write technologies for fabricating passive elements on a range of planar and conformal substrates was demonstrated. Physical values (capacitance, inductance, conductance), however, were generally lower than those required for most applications. For example the conductivities of DW features have been measured as ranging from a few percent to 50% of the bulk material value. Since the advent of the DARPA funded MICE project there has been significant improvement in the understanding and development of materials for DW.

2.3 Deposition Techniques

DW is an 'additive' processes that can directly pattern material on to a surface without the need for an 'adhesive layer'. Additive processes have the advantage of low material waste and the potential to rapidly manufacture components or devices. There are also some techniques that use a combination of both additive and subtractive processes whereby the deposited material is trimmed after deposition to enhance the pattern morphology.

The rest of section 2 will consider mature additive material deposition techniques. A review of the current capabilities for fabricating conformal antenna type devices will also be carried out.

2.3.1 Conventional Deposition Techniques

The most common additive patterning technique is screen-printing. The screen-printing process is illustrated in Figure 2:2.

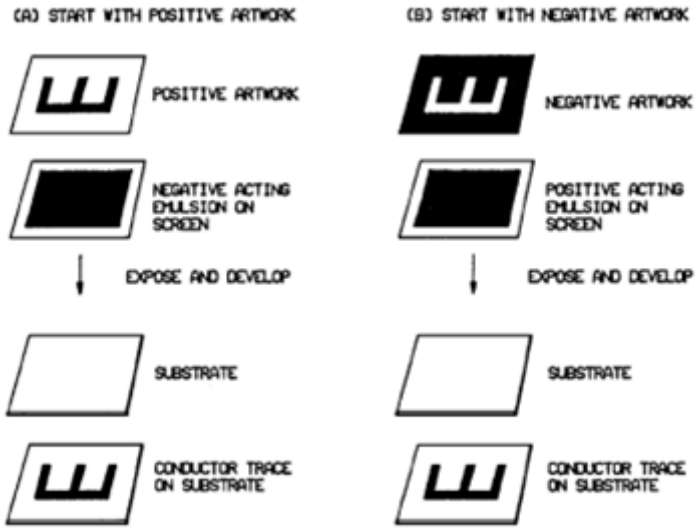

Figure 2:2: The screen-printing process (modified from Piqué, A [16])

The feature sizes that can be printed using this technique are limited by the thickness and resolution of the image mesh. Fine screens composing of high mesh numbers, 325-400, have been shown to consistently produce lines and spacing of 75-100µm [27]. Traditional screen-printing inks consisted of thick film ceramic (or cermet) inks. Once the inks have been printed they need to be post treated (fired) before they become functional. These temperatures are usually relatively high (850°C-1000°C) and limit the acceptable substrates to ceramics [27].

Another technique that has been used to print electronics is Low-Temperature Co-fired Ceramic (LTCC) process [27]. This process can print multiple layers of functional material, with the added benefit of embedding passive electronics (e.g. resistors, capacitors etc.) in the LTCC material. The technology is a descendant of the High-Temperature Co-fired Ceramic (HTCC) which requires the device to be fired at a much higher temperature (1600°C rather than 850°C). The LTCC process involves screen-printing on to green (alumina mixed with organics and binders) substrates [27]. Additionally, holes can be punched through the green ribbon to form vias (i.e. an electrical contact point between layers). Once the layers are deposited and aligned they are fired together allowing the production of high density electronics to be fabricated.

Both these techniques are very mature technologies and have been used to print highly reliable PCB's (screen printing) or hybrid circuits (LTCC). These techniques are restricted by the materials which require high firing temperature requirements. Screen printing has since evolved from this with

the implementation of Polymeric Thick Film (PTF) inks which have low 'cure' temperatures in the region of 100-165°C [16] [27]. PTF inks will be covered later on in this chapter.

The limitations of screen printing processes for the fabrication of antenna on to structural surfaces summarised as:

- Method requires contact with the substrate surface
- High firing temperatures of inks and pastes used in HTCC and LTCC which can limit the materials and composites that can be deposited on to
- Limited or no conformal writing capabilities
- Limited for rapid-prototyping applications or one-off designs as the processes require the use of screens or masks which need to be developed for each new pattern
- Multilayer devices require subsequent masks to be accurately aligned to one another [27]

2.3.2 Ink-jet Printing

Ink-jet printing is one of the most common modes of direct writing, although the technology has mainly seen mass commercialisation in other areas such as graphics printing. The technology provides a means of directing an extremely repeatable formation of fluid droplets on to a location with a large degree of accuracy. Currently there are two typical ink-jet mechanisms:

1. **Bubble jet**: The bubble (thermal) ink-jet uses an electrical micro-heater to heat the ink locally to form a rapidly expanding vapour bubble that ejects the ink as a droplet (see Figure 2:3. Thermal jetting usually uses water as a solvent and may therefore impose restrictions on some of the inks (such as polymeric compounds) that can be used [30] [31].
2. **Piezoelectric Inkjet**: the piezoelectric ink-jet relies on the deformation of piezoelectric material to cause a sudden pressure wave and hence generate an acoustic pulse through the material (see Figure 2:3) [31].

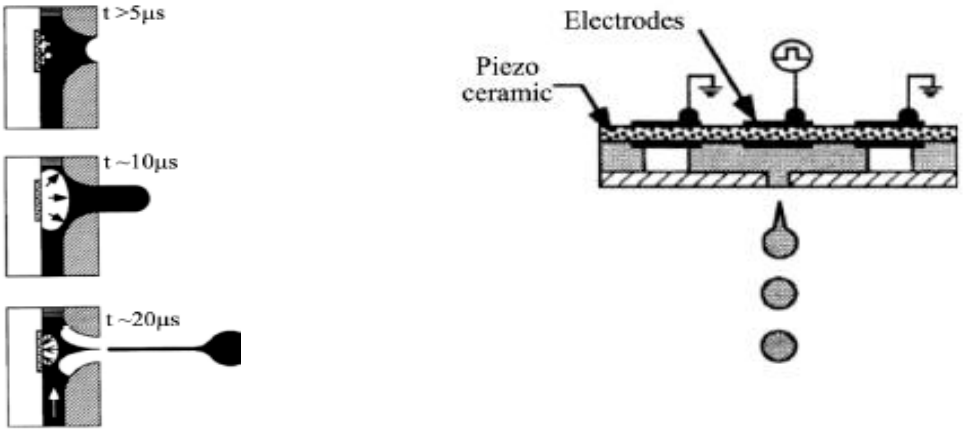

Bubble-jet Piezoelectric

Figure 2:3: Inkjet printing techniques (modified from Lin, L et al. [30])

Ink-jetting can operate in either a drop-on-demand fashion or in a continuous mode. In continuous mode ink-jet printing a cylindrical jet of liquid is formed by forcing a fluid under pressure through an orifice. Surface tension forces create instabilities in the jet causing it to break into drops. By applying a controlled frequency disturbance to the jet the fluid can be forced to break up at precise time intervals into uniform diameter droplets. The droplets are then charged and deflected by an electrostatic charge to either a substrate or catcher/gutter for recycling [30] [31].

Continuous mode ink-jet printing systems produce droplets that are approximately twice the orifice diameter. Droplets produced using this technology can have drop diameters as large as 1mm and as small as 20μm, however 150μm is more typical [31]. Continuous mode printing has very high throughput capabilities but lack the high quality print capabilities of drop-on-demand mode inkjet printing.

Demand mode ink jet printing employs a small transducer to displace the ink creating a pressure wave which enables the deposition of a droplet at the orifice. Either a single droplet can be produced or a group of droplets in a time interval. Droplets deposited using these techniques are usually the same size as the orifice diameter, typically diameters of 15-100μm have been observed [31]. Drop-on-demand printing has the advantage over continuous mode printing in that smaller drop sizes and higher placement accuracy can be achieved and is one of the primary technologies used for DW [32].

The most crucial constraint on ink-jet printability is the material rheology requirements especially the viscosity and surface tension. The surface tension should be higher than 30mN/m and the pressure low enough to prevent dripping of the ink from the nozzle [33]. Ideally the fluid should be relatively Newtonian and the viscosity must be suitably low as the power generated by the piezoelectric and heater membrane is limited. Low viscosity is also important to allow the channel within the inkjet nozzle to be refilled within a 100μs. For these reasons viscosities tend to be below 20mPa.s [34]. One of the downsides to inkjet printing is that feature sizes tend to be limited in both size, due to spreading effects on the substrate, and print thickness, due to viscosity limits. Particle size can be an issue and should be less than 5% of the orifice diameter [16], otherwise nozzle clogging problems can persist. Inkjet printing, however, can have very high throughputs with fast deposition rates and/or multiple nozzles. Multiple nozzles can also be used to deliver different materials allowing for a multi-functional device to be fabricated relatively quickly [30].

2.3.3 Maskless Mesoscale Material Deposition (M3D)

The M3D technology consists of three different processes, aerosolisation, deposition, and heat treatment of the deposition. Aerosolisation is accomplished using an ultrasonic transducer or pneumatic nebulizer. The aerosol is entrained in an air stream and carried to the deposition head. The aerosol stream is then focused using a flow guidance deposition head, which forms an annular, co-axial flow between the aerosol stream and a sheath gas stream [35]. The focused air stream travels through a final nozzle and is directed on to the substrate. For optimal conditions the nozzle should stand off from the substrate between 1-5mm [36]. In the final step the material must be functionalized using either a thermal or photochemical process. The M3D process is illustrated in Figure 2:4.

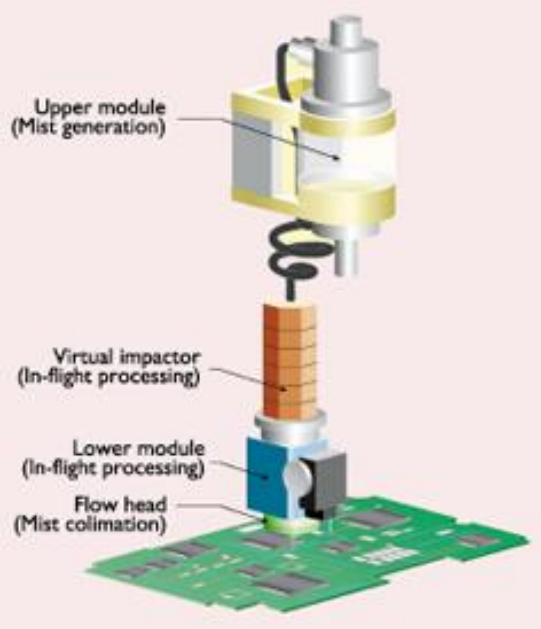

Figure 2:4: Illustration of the M3D (from King, B [35])

The M3D technology can write fine feature sizes in the order of 10μm with deposition rates of 200mms^{-1} [37]. The main material requirement for M3D is that the deposition material should have a viscosity between 1 and 1000cP, if the material is outside this regime then atomization cannot take place. Furthermore solvents with long evaporation times are preferred because fast evaporation can cause the materials to dry out before they reach the substrate [35]. The M3D system has since been rebranded as Aersol Jet Lab system and can be purchased from Optomec [38].

2.3.4 Thermal Spray

Thermal spray development for Direct Write (DW) of electronic components on conformal surfaces has been established at the Centre of Thermal Spray Research at Stony Brook, USA [39]. Thermal spray is a continuous, directed, melt-spray process in which particles (e.g., 1–50μm in diameter) of virtually any material are melted and accelerated to high velocities, through either a combustion flame or a DC or RF non-transferred thermal-plasma arc. These molten or semi-molten droplets impinge on a substrate with high kinetic energy where they flatten and solidify to form a series of 'splats'. The deposit is built up by successive impingement and inter-bonding among the splats, generally, with a thickness greater than 10μm [16] [40].

Thermal spray has both a high throughput and conformal writing capabilities. The technology is able to deposit materials such as metals, ceramics, and polymers in the form of wire, rod or powder with

near bulk materials properties [16]. Once the material is deposited there is no need for further treatment to cure or process the material.

The major disadvantage of conventional thermal spray techniques is that feature sizes are relatively coarse of approximately 500μm being reported with the use of suitable masks [16]. Higher resolution feature sizes can be accomplished using laser ablation techniques [41]. To achieve finer features without the need for additional masks or processes a novel multistage aperture collimator system developed at the State University of New York (SUNY) [42], using this system features in the order of 200μm were deposited [43].

Thermal sprayed microstructures have also been reported to have an abundance of imperfections comprising a variety of particle sizes, volume densities, morphologies, and sometimes orientations. These imperfections, which depend on the spray process and materials used, can significantly influence a wide number of properties, for example, elastic moduli, fracture strength, thermal conductivity, and electric and dielectric effects. Pores and micro-cracks are the major defects observed in brittle materials (e.g. ceramic oxides), while metals generally display porosity and oxides [40].

2.3.5 MAPLE

Matrix-Assisted Pulsed Laser Evaporation (MAPLE) and MAPLE Direct Write (MAPLE-DW) are laser-based processes that transfer material from a transparent carrier on to an acceptor substrate [16]. MAPLE is a soft deposition technique i.e. deposition is achieved at low laser fluence (0.2J/cm^2) and lower particle velocities compared to similar material transfer techniques such as Laser Induced Forward Transfer (LIFT) [44]. This process uses inks formed by dissolving the material to be deposited in an organic matrix. The matrix is typically frozen at low temperatures to form a 1-20 μm layer. The layer is supported from the substrate by ~5 cm and the entire process takes place in a vacuum. A suitably tuned laser can cause the material in the layer to be desorbed from the organic matrix and transferred on to a substrate. A pattern can be generated by placing a shadow mask over the substrate.

In MAPLE-DW, the ribbon (or frozen layer) is placed in close proximity to the substrate (25-100μm) in a forward transfer configuration. A UV laser is focused on to the ink-support interface. The organic material absorbs the UV radiation and is rapidly heated and vaporized. This provides a pressure pulse which pushes the material out and deposits it on to the substrate. The substrate or laser can

be translated to create very precise patterns. The entire process takes place in ambient conditions and does not heat the substrate. In addition, the highly focused laser beam can also be used for in-situ micromachining or any other surface treatment by removing the ribbon from the laser path. A schematic of the Maple DW process is shown in Figure 2:5.

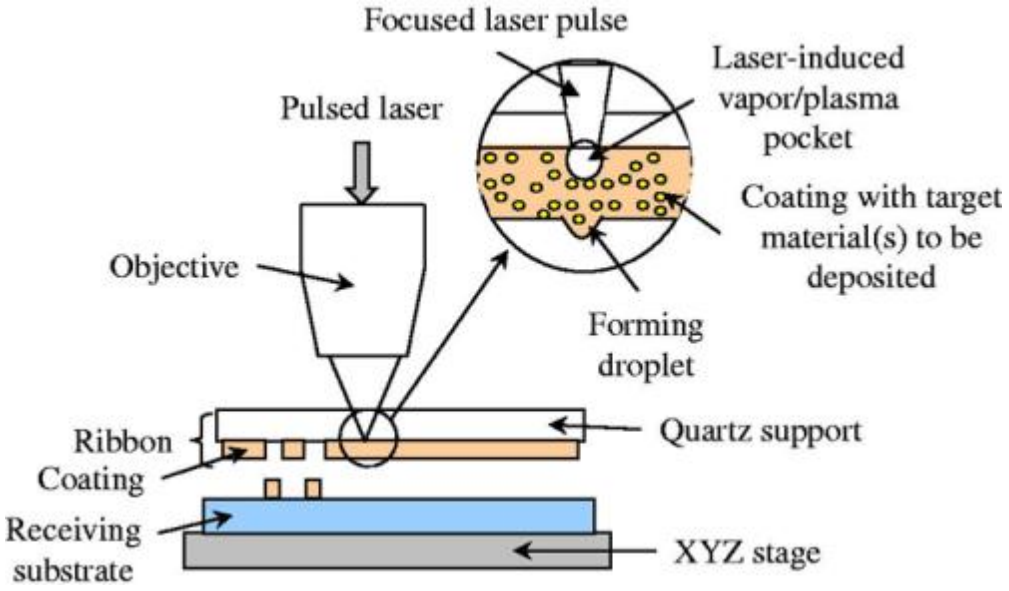

Figure 2:5: Maple DW diagram (from Lin, Y et al. [45])

MAPLE-DW is essentially a wet process, the wet ribbon has a very short shelf life which makes it difficult for real production. Also since the material is transferred across a gap the lateral resolution decreases as the gap increases which make true conformal 3D writing difficult. To overcome this problem a dry MAPLE-DW process was developed using low temperature co-fired ceramic materials [46]. In this technique, the material mixture is coated on to a flexible optically transparent backing film and dried at low temperatures (below 100°C). The ribbon is then put in direct contact with the substrate. After irradiation with the laser the ribbon is peeled off, leaving the desired pattern. The advantage of using this process is that feature sizes are greatly enhanced (feature sizes of 10μm have been reported [46]) because the overspray is minimised.

The main drawback from using this method is the amount of material waste, not all of the ribbon is utilised in the laser transfer process. For small runs or elements this may not be an issue but for large devices or long interconnects this process may be unsuitable. MAPLE also does not lend itself to conformal printing as it can be difficult to manipulate the ribbon around complex geometries.

2.3.6 Micronozzle system

The micronozzle system is a computer automated device for precision printing of liquid ink or particulate slurries developed by Ohmcraft Inc (Honeoye Falls, NY) and N-Scrypt (Orlando) [16]. Dispensing systems and nozzles can also be purchased from Intertronics [47]. The system uses a computer driven x-y stage for printing, incorporating CAD software which is used to define the print pattern [16]. The micronozzle system is essentially a small nozzle which is kept in close proximity (10-150µm) of a substrate as it traces a predefined pattern (see Figure 2:6).

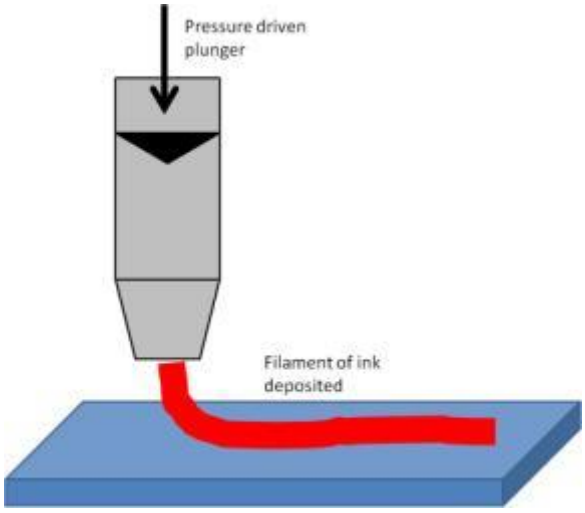

Figure 2:6: Schematic of the micronozzle system

The cross-sectional area of the printed features is determined by the nozzle dimensions, the deposition rate (i.e. the speed of the nozzle relative to the surface), and the nozzle tip to substrate offset. The smallest nozzles have an inner diameter of 25 µm although diameters ranging from 100 to 250µm are more typical [48]. The ink is delivered through this aperture by using a pumping block. To maintain the print characteristics a feedback mechanism is used which holds the tip to substrate distance constant. Traditionally a force feedback mechanism has been used whereby feedback is achieved by balancing the upward force on the pen due to the extruding slurry and the downward force applied by an electromagnet [16] [48]. An alternative to this is to use a non-contact approach with a laser displacement sensor. This DW approach has been demonstrated to be capable of producing feature sizes down to 150 µm [27].

The same thick-film pastes and PTF inks that are used for screen printing can be used as the base ink for the Micronozzle system. Almost any electronic material can be deposited, including dielectrics and resistive inks with multiple sheet resistances, as well as biological and polymer sensing

materials. The micro-nozzle system can also be easily integrated with robotic CAD/CAM system to enable conformal printing.

2.3.7 Direct Write Deposition Overview

Table 2:1 shows a comparison of some of the DW deposition techniques that could be used for printing of conformal devices. The technique with the least material requirements is the micronozzle syringe process. This system can use almost any off-the-shelf thick film inks and can be integrated easily on to a CAD/CAM robot system for 3D deposition. The micronozzle is limited to feature sizes above 150μm and cannot deposit solid particulate materials. Finer feature sizes can be obtained using M3D and MAPLE-DW techniques or using a combination of both additive and subtractive techniques (e.g. laser ablation). M3D and inkjet lend themselves well to conformal deposition of electrically functional material, however, it must be noted that as more inkjet nozzles are used the less suitable it becomes for conformal printing due to the increased size of the deposition head. Inkjet is preferred as it has the advantages of being more cost effective than the M3D process. Thermal spray can provide perhaps the best material properties but requires masks or laser machining to provide accurate and fine feature sizes.

Technology	**Feature Size (μm)**	**3D Printing capability**	**Deposition Speed (mms^{-1})**	**Capitol Cost ($'000)**	**Contact**	**Material viscosity requirement (mPa.s)**
Ink-Jet	150	Yes	200	100	No	<20
Micronozzle	150	Yes	50	300	No	None
Maple DW	10	limited	1000	20-250	No	None
M3D	10	Yes	200	500	No	<5000
Thermal spray	500	Yes	500	250	No	molten form

Table 2:1: Summary of mature Direct-Write deposition techniques (Adapted from the TMS annual meeting 2006 [46]

2.4 Direct Write Ink Materials

As discussed earlier there are a number of deposition methods which are capable of depositing solid (particulate) and liquid (ink, pastes) material. Inks (low viscosity liquids) and pastes (high viscosity liquids) are the most common types of DW material. The chemical composition of Ink materials can be altered more easily than their solid counterparts to include additional functionalities such as adhesion and electrical properties. Commercial Off-the shelf inks used for screen printing and ink-jet applications are already available on the market.

This section will concentrate on the different type of ink and paste compositions used for printed electronics. A review of each ink composition will be done focusing on their functional and rheological properties, as well as their suitability for different DW deposition techniques.

2.4.2 Material Design Requirements

Inks and pastes need to be specially designed with application and deposition methods in mind. For example, if the application requires the fabrication of interconnects printed via inkjet printing, the ink formulation will need to have a functional element as well as the right viscosity for deposition. Most inks are comprised of a number of different components including:

- ***Functional material***: DW inks can be loaded with appropriate particulate material to obtain conductive, resistive and dielectric properties.
- ***Solvent:*** The solvent acts as the vehicle for the ink. It is an important part of the chemical makeup of the ink as it provides the composition with the necessary viscosity to disperse the solid ingredients in the liquid and allow for deposition. The solvent is normally removed after deposition by drying or post treatment (firing) of the ink.
- ***Binder:*** There are two types of binders, a temporary binder and a permanent binder. The temporary binder is also used as a vehicle to hold the other ingredients together and provide rheological (flow control) properties [17]. The permanent Binder fuses the functional part of the composition together as well as adhering it to the substrate upon post heat processing.

When the ink is particle based, the volume fraction of the functional particles is generally maintained above the percolation threshold, the minimum volume fraction required for inter-particle connectivity [49]. Depending on the deposition method however, the amount of particle loading may become an issue. The inks used for ink-jet printing for example typically have a low solids loading per volume (<5%) to keep the viscosity low [50]. Thick film inks on the other hand can have 25-35% volume solids loading, higher percentages up to around 60% solid loading are available for thicker more conductive inks [26] but have a much higher viscosities [50].

Ink formulation designed for printing will usually have both a liquid (printing) and a solid (functional) phase. Identifying the functionality of the solid or dry ink phase requires understanding of the print processing requirements and therefore the properties of the ink in the liquid phase. The main issues in the liquid phase are the compatibility, wetting, adhesion and issues associated with dispensing the

fluid, primarily the fluid rheology. The factors governing the choice and development of a functional ink are summarized in the flow chart depicted in Figure 2:7.

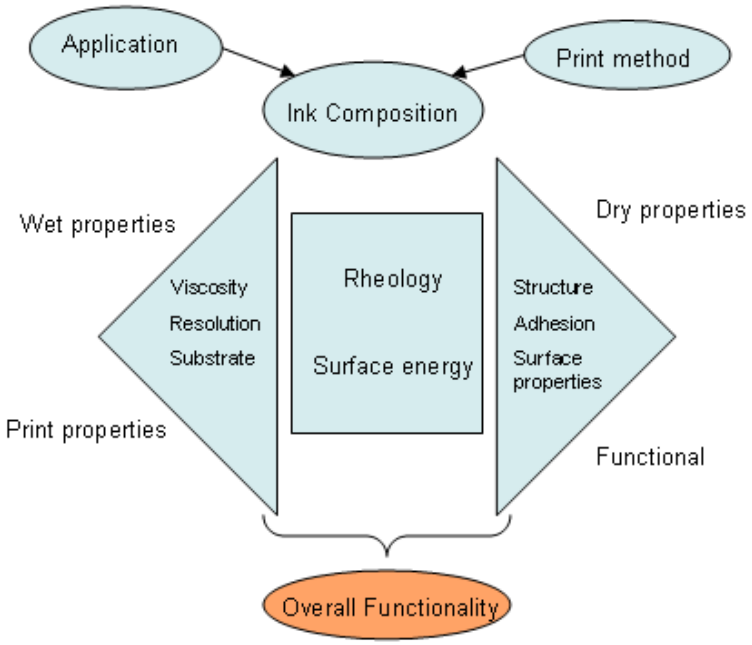

Figure 2:7: Factors governing the development of printed inks (adapted from Piqué, A [16])

2.4.3 Material Printing Requirements

To obtain a controlled well defined print quality the ink rheology and wetting properties must be understood. The required rheology for printing depends on the intended printing process, the specific printing equipment, ambient conditions, production parameters and chemical makeup. There are three types of rheological behaviour for fluids, Newtonian, non-Newtonian and thixotropic behaviour [16]. Low viscosity fluids usually exhibit Newtonian characteristics whereby the viscosity is independent of stress. Ideally for high viscosity thick film pastes non-Newtonian behaviour is preferred, whereby sheer thinning is induced i.e. the viscosity decreases with increasing stress. In this scenario the fluid would readily flow through an aperture under a force but will then thicken and hold its shape when stress is removed. What tends to happen is that most ink formulations have a third rheological property where the viscosity is time dependant. In this thixotropic regime the fluid will take time to recover from its un-stressed state [27]. The second key property that will affect the print quality of an ink is the material wet-ability. The wet-ability is affected by the surface tension of the material and the substrate roughness.

2.4.4 Inorganic Thick Film Inks

Thick film inks are one of the most commercially available inks on the market and offer electrical properties with strong adhesion to a number of different surfaces. They are primarily designed for screen printing applications, but more of these types of inks are being modified for DW applications (such as reducing processing temperatures). All pastes consist of four generic ingredients, a functional material, a solvent, a temporary binder (an organic compound) and a permanent binder (which is composed of glasses or frit). The firing temperatures for these types of compositions are usually above 1000^{o}C (High temperature co-fired ceramic inks HTCC) where the frit melts and re-solidifies thus wetting the particles and fusing them together forming a mechanical bond with the substrate [17].

The lowest electrical resistivity of a silver loaded LTCC paste is approximately 2x10^{-6} Ωcm about 75% bulk conductivity of pure silver [27]. However, these types of inks are unsuitable as they require high firing temperatures to sinter the silver particles within the ink. High firing temperatures are also a consequence of the permanent binder used in the chemical composition on the ink. Low temperature frit-less molecular bonded inks have been produced which reduce the firing temperature between the narrow range of 950-1000^{o}C. The adhesion here is predominately a chemical mechanism. The narrow temperature must be met to obtain the best adhesion between the ink and the substrate. To overcome this limitation, a third type of mixed bonded paste was formed combining both mechanisms to produce a low temperature co-fired ceramic (LTCC) ink in the range of 850^{o}C-1000^{o}C [27].

2.4.5 Organic Polymeric Inks

Polymeric organic inks have been developed over the past decade to combat the high firing temperatures of their ceramic thick-film counterparts. Low value passive electronics will need to be fabricated on many different material types some of which are not temperature resistant (e.g. organic materials such as carbon or glass composites). The advantage of using polymeric materials is that they are flexible, lightweight and easily processed. Printed organic electronics are advantageous as they offer a processing window near or at atmospheric pressure and room temperature and are environmentally friendly [46].

Conducting polymer inks are generally made by doping polymers with an oxidizing agent, a reducing agent, or a protonic acid, to generate delocalized polycations or polyanions. The polymer can be made conductive or semi-conductive by tuning the chemical composition, configuration and

conformation of the polymer backbone, by the nature of the dopant, by the degree of doping, and the volume fraction of the conducting polymer in the printing composition [46].

The two most common conductive polymers are polyaniline (PANI) and poly (3,4-ethylenedioxythiophene) doped with poly(styrenesulfonate) (PEDOT:PSS). PEDOT is a water-based dispersion of conductive polymer in submicron size gel particles, which forms a continuous film upon drying. This poses an additional advantage over inorganic inks as the annealing and fuctionalisation temperature is very low (50^{o}C). The downside however, is that carrier densities are low and therefore the resistivities are higher, for PEDOT the resistivity is 2.5Ωcm [51].

Dielectric polymeric inks have also been made such as polyimide and poly-4 vinylphenol (PVP). PVP has been reported as a material that could also be used to produce a low cost transistor [52].

Polymeric devices still have a long way to go. Conductivities are too low to be used for interconnects and high Q inductors. In a perspective review done by Nanomarkets [53] they concluded that polymer inks have not yet established themselves for broad commercialisation in the printed electronics market. One of the biggest drawbacks for polymer inks is their sensitivity to the environment especially to water and air [53].

2.4.5 Polymer Thick Film (PTF) Inks

Polymer Thick Film (PTF) pastes are composed of a polymeric resin or binder which can be loaded with dielectric, graphite and conductive particles. These inks have very high viscosities ranging from 4Pa.s-100Pa.s [54], making them unsuitable for ink-jet printing and M3D processes and more suitable for screen printing and micronozzle printing. The major advantage of using PTF's is that they can be processed at relatively low temperatures (100^{o}C-220^{o}C) [16] [17]. The heat treatment here has a different mechanism to the one employed with Cermet thick film pastes where the resin is sintered off. PTF's instead undergo a 'curing' phase whereby a chemical reaction is initiated in the polymer resin. This chemical reaction causes the polymer chains in the system to cross-link, increasing the viscosity of the paste solidifying it and making the paste functional. The cured polymer provides integrity to the film and adhesion to the substrate. Additionally, the cross-linked polymer systems confer improved abrasion resistance, chemical resistance and environmental resistance to the printed film [54]. As the polymer resin stays with the final structure the electrical functionality (e.g. reduced conductivities) of the deposited can suffer due to dilution of the loaded

particles. This structure however, offers greater mechanical flexibility which could be an advantage on structural components subjected to mechanical stresses and in flexible electronics [54].

PTF inks containing copper, gold and silver micron sized particles have been printed to form conductive tracks on to a variety of substrates. Silver based inks however are more frequently used due to having the best tradeoffs between conductivity and cost. Silver is more reactive than gold in that it forms a wider range of compounds for dispersion in organic solvents and unlike copper a careful control of the oxygen content in the processing atmosphere is not needed [55]. The amount of metal loading in PTF varies between 40-77% and conductivities can be 1-20% of bulk values [27].

2.4.6 Nano-Particle Inks

Nano-particle inks have recently entered the forefront of modern day printed electronics, especially for the fabrication of conductive elements. Nano-particles typically measure 1 to 100nm in diameter and consist of clusters of metallic, semi-conducting or insulating atoms. Gold, copper and silver have both been made into nano-particle ink suspensions. Silver is so far the most promising of the three as it offers relatively high conductivity at a lower cost than gold (approximately 50 times cheaper in 2012 [56]).

Significantly for DW, nano-particles exhibit lower melting temperatures (approximately 200-400°C) than bulk silver because of their comparatively high surface area to volume ratio, this allows bonds to readily form between neighbouring particles [57]. Figure 2:8 shows SEM images of a silver nano-particle ink sintered at different temperatures. These images show how the volume fraction of silver increases with increasing temperatures and also how the particles readily form bonds with one another.

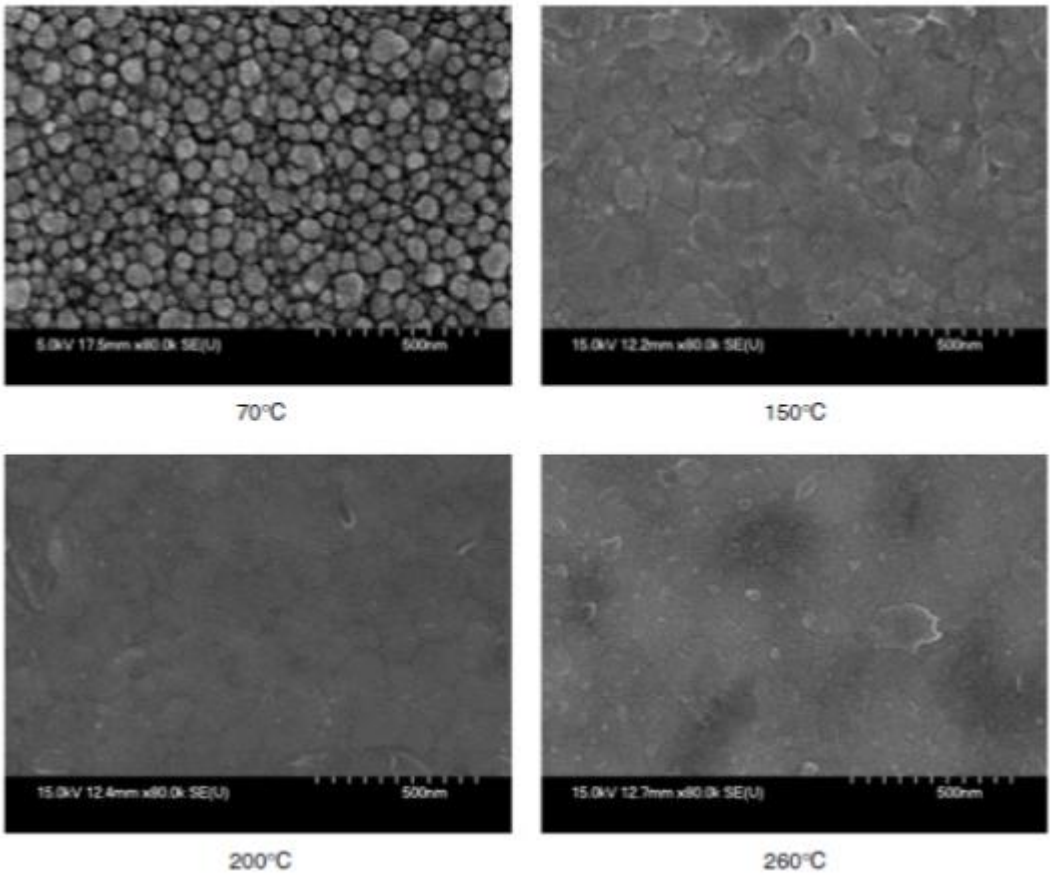

Figure 2:8: SEM image of surface morphologies of a silver nano-particle ink after different temperature treatments (from Hsien-Hsueh, L et al. [58])

Most of the current research being conducted on nano-particle inks concern silver nano-particles suspended in a variety of solvents. Most of these inks are being deposited using ink-jet printing. This causes some design challenges on the ink being deposited as agglomeration of particles in the ink-jet printing head can cause clogging problems. To avoid this problem the viscosity and nano-particle concentrations are kept low [57]. Silver nano-particle inks have been reported to have relatively high conductivity given the low concentrations of metal loading within the suspensions. The silver nano-particle inks have been measured with conductivities equivalent to 10-56% bulk silver [59].

In the work conducted by Fuller et al [57], printing at room temperature caused lines and plates of ink to pinch and bulge due to surface tensions, and the ink to wet the surface unevenly, and any surface defects on the substrate to be filled with ink by capillary action. To overcome this problem the substrate was heated at 100-300^{o}C thereby causing the liquid in the ink-jet drops to flash evaporates on contact.

Another effect when printing silver nano-particle solutions is preferential drying at the edges of the ink track. This causes the silver nano-paricles within the solution to migrate to the edges causing an uneven distribution of particles across the profile of the track, this is known as the 'coffee staining' effect. Similar to the work done by Fuller et al this affect can be reduced by preheating the substrate in order to cause uniform evaporation of the solvent with the ink [60].

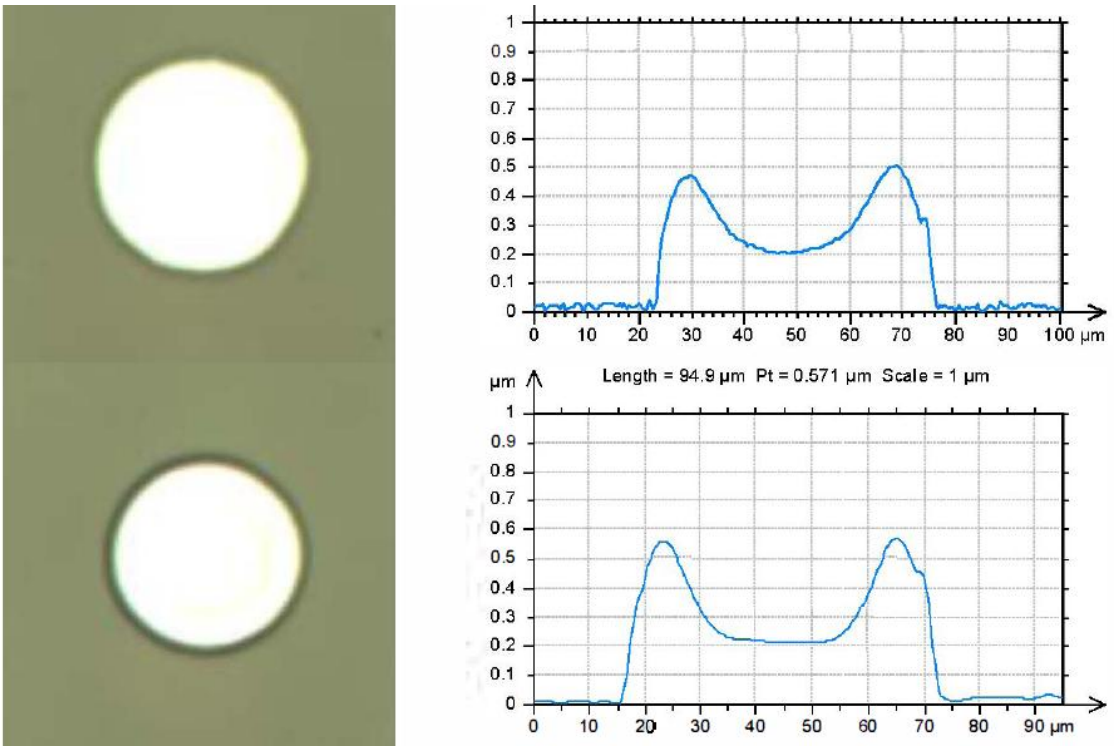

Figure 2:9: Printed silver ink drop showing 'coffee staining' effect (from Mei, J et al. [61])

Many of the current nano-particle solutions also use what can be classified as Volatile Organic Compounds (VOC's) as the solvent; Toluene and α-terpineol both fall into this category. However nano-particle ink formulation consisting of silver, water and diethylene glycol (DET) has been used which is more environmentally friendly than Toluene and α-terpineol [62]. The results from this work produced conductive tracks with a resistivity of $1.6 \times 10^{-5} \Omega$.cm, with similar printing problems as those found in Fuller et al. [57] work. Although this experiment demonstrates the use of non-VOC's as solvents the conductivities are 10 times worse than bulk silver.

2.4.7 Particle-Free Silver Inks

Nano-particle silver inks have shown much progress for fabricating conductive elements. However, nano-particles have also been known to sediment due agglomeration and settling, causing clogging

problems and reduced shelf-life. A solution is therefore desirable especially if the ink is being deposited through a small orifice. Metallo-organic decomposition (MOD) precursors can offer a route to solving this problem.

Silver neodecanoate has been prominently used as an MOD precursor to form silver tracks. Silver neodecanoate starts decomposing to silver at 170^{o}C, and full decomposition is achieved at 250^{o}C [61]. The final structure will leave a silver trace composed of silver nano-particles in contact with one another. Dearden, et al [63], has shown silver MOD inks to produce resistivities of 3-5$\mu\Omega$.cm (2-3 times the resistivity of bulk silver) when cured between the range of 150-200^{o}C. Curing at 300^{o}C increases the conductivity to 2.4$\mu\Omega$.cm [61].

One of the drawbacks of using silver aqueous solutions to form conductive tracks is the porosity in the final cured structure. Porosity can lead to adverse effects on electrical conductivity, mechanical strength and adhesion. As the metallic silver is the only effective component of the ink that contributes to the electrical conductivity and mechanical strength (adhesion) porosity can cause a huge problem. This was emphasised in the work done by Mei, J., et al [61] where a silver trace which had been cured at 300°C exhibited a brittle fracture pattern after 20 cycles of wear (see Figure 2:10).

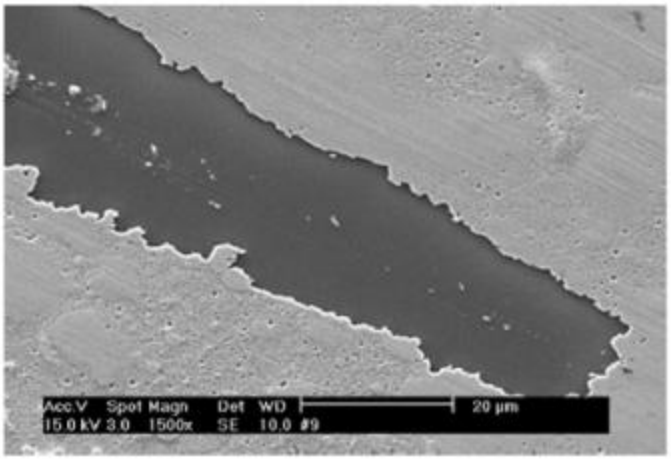

Figure 2:10: Brittle nature of a silver aqueous solution cured at 300^{o}C after 120g loading for 20 cycles (from Mei, J et al. [61])

To decrease the porosity of the structure and increase the structural strength the silver trace can be further annealed in an oven at 580°C for 30min. At this elevated temperature the silver will effectively sinter and densify the structure, producing an intimate interface with the substrate

surface (see Figure 2:11). This technique has been shown to increase the electrical conductivity of the silver trace with value of 2μΩ.cm (80% bulk conductivity of silver) [61].

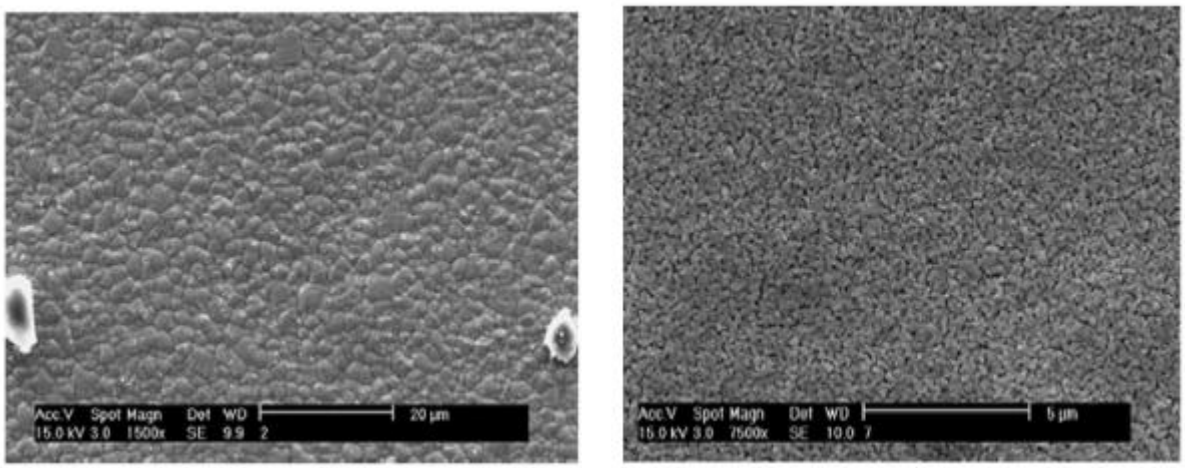

Figure 2:11: SEM images showing the micro-structure of a silver solution cured at 300°C (left picture) and conditioned at 580°C (right picture) (from Mei, J et al. [61])

Another example of how spreading of MOD inks can be reduced is the use of VOC as a solvent for the ink. Recently, an organo-metallic silver ink has been used which was dissolved in toluene, after heat treatment at 150°C for 60min a resistivity of 2-3μΩ.cm was measured. This experiment demonstrated that using a high VOC as a solvent for the organo-metallic ink can be advantageous for controlling the deposition of a silver track. Because the solvent evaporates relatively quickly once deposited the ink tends to be pinned to the surface. Additionally, as the spreading of the ink is decreased it becomes easier to predict the final dimensions of a printed track when ink-jetting [64].

2.4.8 UV Curable Inks

Ultra Violet (UV) curable inks have the potential to address some of the problem that can occur when processing Direct Write materials which require high curing temperatures. These types of inks are made of fluid oligomers, monomors and initiators which cure or polymerise upon incident UV light [65], typical values for curing powers are 160-200mjW/cm^2 [66]. One of the main advantages of these inks is that they are resistant to drying and therefore clogging problems do not occur.

Despite these advantages UV curable inks are not widely used for DW applications. This is because there are many constraints for using UV inks especially for printed electronics. UV inks in their nature are required to be transparent or translucent for full absorption of the UV light. The curing

mechanism is also very sensitive; any over-cure for example may cause the cured structure to become brittle and can have detrimental effects to the adhesion [65]. UV inks tend to have relatively high viscosities, and use of a solvent to thin them is not permitted unless the solvent is evaporated before applying the UV curing mechanism [65]. These constraints limit the types of functionalities the ink can posses. However, conductive silver inks have been produced as well as dielectrics and protective coatings which is where these inks excel. In terms of conductive UV inks, their performance is the poorest with resistivity values ranging between 500-1000$\mu\Omega$.cm (almost 300 times more resistive than bulk silver) being reported [66].

2.5 Material Post Processing

DW inks have two phases, a liquid phase which enables deposition, and a dry / solid phase which is functional. To activate this functional phase most DW compositions require some form of post-processing, usually in the form of heat treatment. Heat treatment is conventionally applied through an oven furnace. Depending on the material type the temperature and chemical mechanism that the heat treatment invokes can vary.

- **Thick film inks**: for thick film inks the organic part of the material must be driven off and the conductive/dielectric/resistive particle must fuse by sintering. The functionalisation temperature for most thick film inks is 850^{o}C, alternatively a ceramic metal thick film ink can be used which fires at 500^{o}C.
- **Organic polymeric inks**: functionalised by drying at 50^{o}C
- **PTF inks**: functionalise by a cross-linking mechanism at around 150^{o}C. The conductive/resistive/dielectric particles are brought into contact by this cross linking mechanism.
- **Nano-particle inks**: nano-particle ink suspensions cure at temperatures greater than 220^{o}C. Heat treatment at these temperatures causes the solvent in the ink to evaporate and the nano-particles to sinter forming bonds with one another.

Low processing temperatures are desirable for DW applications where the substrate can be temperature sensitive or needs to have highly controlled properties (e.g. in the aerospace industry). In addition to this the application may involve printing devices on to large structures whereby conventional oven curing is not practical. One method to overcome this problem is to locally process the material using for example a laser source. Some of these techniques will be considered in this section.

2.5.1 Selective Laser Sintering/Curing

Selective laser sintering has previously been recognised for building 3D metallic and polymeric structures [67]. The technique has also been used for sintering nano-particle ink suspensions. The work conducted by Marinov, [68], demonstrated laser curing for silver nano-particle inks. This was a three step-process which involved depositing the ink via M3D, heat treating the sample via an oven at 80^{o}C to remove any volatile solvents and finally laser sintering of the sample with a 50mW Nd:YAG continuous wave (CW) laser at 1mms^{-1}. It is essential to include the second step for fast laser scans because if the volatile organics remain in the compound during laser sintering they will expand so rapidly that the printed pattern could become damaged [68]. For lower scan speeds and powers this effect can be mitigated against as the organic solvent is driven off through conductive heating [68]. The measured bulk resistivity of the laser sintered sample was 16μΩ.cm this was compared to a 150^{o}C oven sintered sample which was 1.6mΩ.cm [68].

One of the reported drawbacks of using lasers for sintering is the inhomogeneous temperature field in the sintered material. This is highlighted by Chun et al. studies on sintering gold nano-particle inks [69]. The gold nano-particle ink was sintered using a 100mW argon laser with a Gaussian profile at 0.2mms^{-1}. Due to thermocapillary flow and evaporation of solvent near the incident laser flux the final structure of the ink exhibited a U-shaped convex meniscus structure, with thorn microstructures being observed at the edges of ink structure (Figure 2:12).

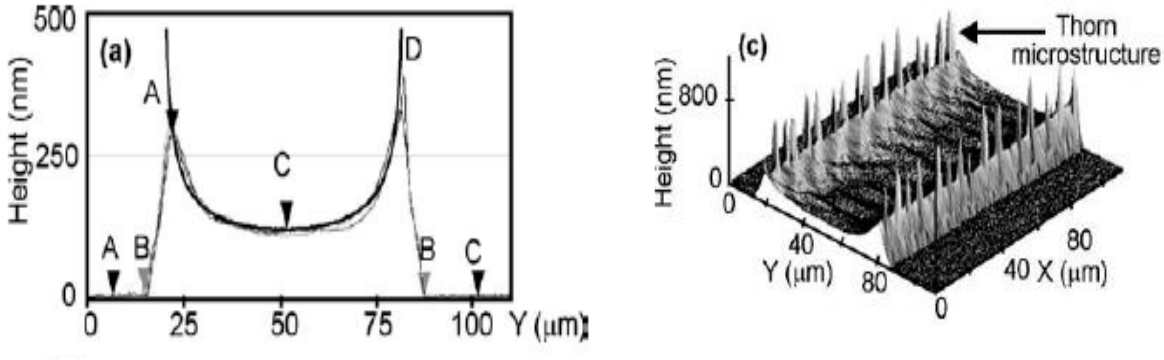

Figure 2:12: Atomic force microscope image of the cross-section of a Gold nano-particle ink sintered with a single Laser pass at 100mW (from Chung, J et al. [69])

To optimise the sintering temperature a planar waveform is desired, thereby increasing the uniformity of the temperature field within the ink. Chung, J., et al [69] used a beam-splitter to form a

heart shaped laser distribution pattern. This contributed to a near uniform energy distribution within the printed sample removing the meniscus like structure that was previously observed (Figure 2:13).

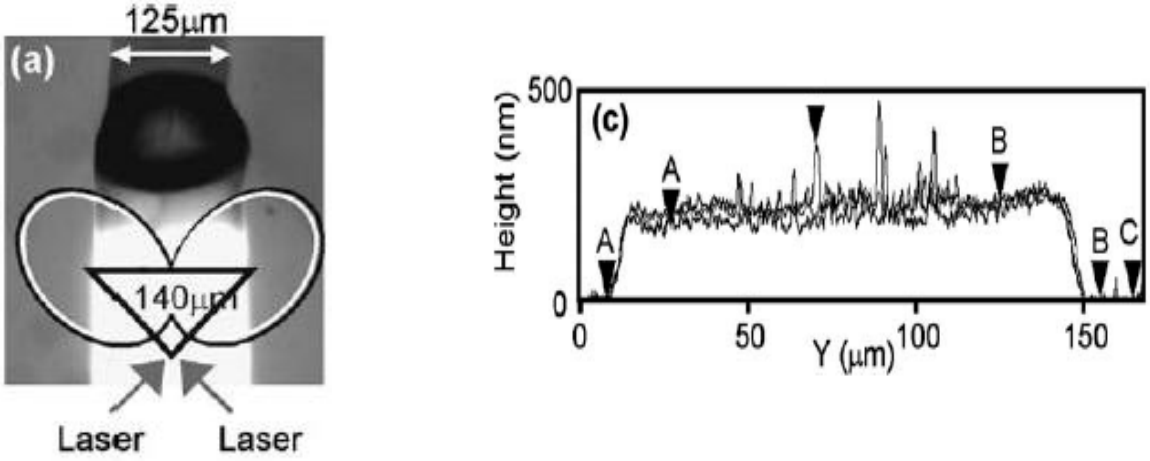

Figure 2:13: Optimisation of the beam profile can produce a flatter structure as indicated by the AFM image of the final structure (from Chung, J et al. [69])

The final power of the incident laser beam was 1206mW which reportedly produced near bulk conductive gold tracks. However, a trade-off must always be met between the degree of sintering of the ink (i.e. the level of laser power used) and the heat transferred to the substrate material.

The effect of laser processing on the substrate has been investigated by Kinzel [28]. In this experiment commercial thick-film fritted silver ink (Heraeus C8772) was laser sintered on to a FR4 glass epoxy substrate. Heraeus C8772 has sintering temperature of 475-525^{o}C lower than conventional thick film inks but still much higher than the glass transition temperature, T_g =140°C, of FR4. At a laser power of 1.121W and scanning speed of 0.4 m/s, 57% of the inks specified conductivity was reached. The degree of laser sintering was shown to be a function of scan speed and laser powers. However, there is a threshold where the substrate can be visibly damaged affecting the sintering and electrical performance of the ink. Following on from this work a Finite Element Model (FEM) was constructed to map the thermal profile within the ink and substrate material. This model showed a thermal discontinuity at the interface between the ink layer and substrate. Thus if the ratio between the thermal conductivity of the ink and substrate is increased, the rate at which thermal energy is transferred to the substrate would decrease thereby decreasing the damage to the substrate [28].

The FEM was used to determine the thermal penetration depth of the laser for given powers and speeds. Figure 2:14 shows that even for very high powers (above the melting point of silver) incident on the surface of the silver ink the thermal energy transferred to the substrate is minimised to within just a few microns [28]. Although it must be noted that the temperatures quoted here are still very high and could cause damage to the substrate.

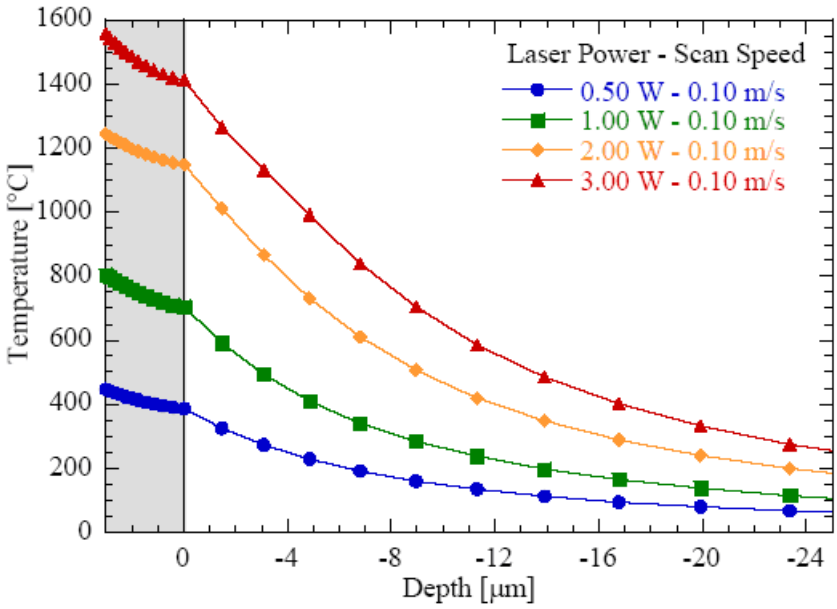

Figure 2:14: Maximum thermal profile attained using a scan speed of 0.1m/s for different laser powers. The grey region is the ink layer (from Kinzel, E C [28])

This type of analysis is essential to optimise laser printing parameters, although, more detailed work needs to be done to accurately model laser absorptions and temperature distributions of different DW materials on temperature sensitive substrates.

Sato et al [70] has also investigated laser curing of conductive PTF inks using both CO_2 and Er:YAG laser. It was found that the resistance of conductive DW material could be reduced by using multiple passes or scans with a laser beam. Comparison between the CO_2 laser and fibre laser showed that the CO_2 laser gave lower ink resistances and surface roughness properties although the practicality of using a fibre delivered laser may suit the process better for in-situ curing. It was also reported that the thermal conductivity of the substrate directly affected the curing properties of the ink. It was concluded in this investigation that substrates with lower conductivity increase the heat encapsulated within the ink composition allowing better curing properties to be achieved.

2.5.2 Microwave Sintering

Microwave heating is another alternative method for processing directly written materials. In this process the material absorbs incident microwave radiation due to coupling with charge carriers or rotating dipoles. Microwave sintering has two main advantages over conventional laser or oven sintering techniques. Firstly sintering times are dramatically shortened and. secondly the technique does little or no damage to organic polymer substrates. This is because the rotational freedom of any dipoles present in thermoplastic polymers below the glass transition temperature (T_g) is limited, therefore rendering the absorption to microwave radiation negligible [71].

The downside to microwave sintering of conductive materials is the extremely low penetration depth of microwave radiation for example at 2.54GHz microwave frequency the penetration depth for silver, gold and copper falls between 1.3 to 1.6μm [71]. However, despite this, the sintering process has been demonstrated for silver nano-particle tracks with a larger profile than the penetration depth of the microwave radiation. This is because in reality as the material sinters, the thermal conductivity increases, thereby transferring heat to lower levels of the material.

For a track with an average height of 4.1μm consisting of a silver nano particle paste sintered using a micro-wave reactor operating at 2.54GHz at 300W for 240s a resistivity of $3.0 \times 10^{-5}\Omega.cm$ (5% bulk conductivity of silver) was obtained [71]. Longer sintering times resulted in no increase to the bulk conductivity (see Figure 2:15). This result was in close comparison with an oven cured sample at 220^{o}C for 60min, however no additional experiment was performed to see how the process compared to laser sintering.

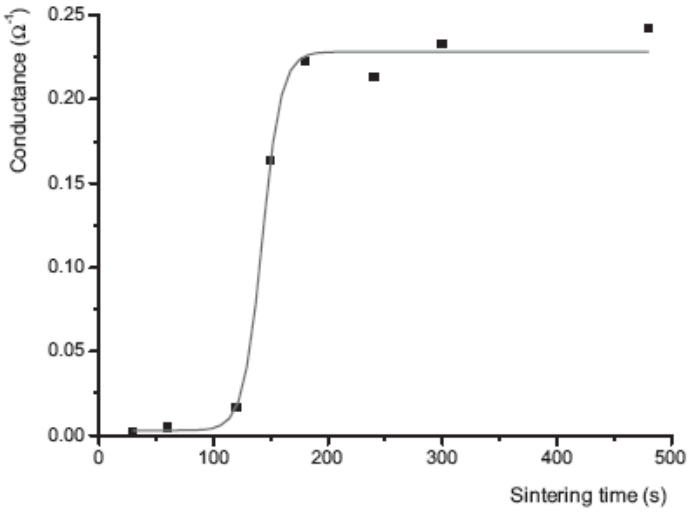

Figure 2:15: Conductance as a function of time for the microwave sintering of track consisting of silver nano-paste (from Perelaer, J et al. [71])

2.6 DW for Antenna applications

This section will review the current state of the art regarding the fabrication of RF devices such as antenna systems using DW.

2.6.1 RF signal carrying properties of DW deposits

So far there has been only limited work in investing gating the RF signal carrying properties of DW interconnects. In the work conducted by Marinov et al [72] an enhanced M3D process was used to fabricate high quality conductive tracks for the transmission of RF frequencies. This process used a laser to etch a 10μm high channel in the substrate where material could be deposited. The channel was filled with a nano-particle ink and then sintered. Using this process improved line precision and edge acuity was observed. At 6Ghz the average signal loss of the track was below 0.02dB/mm, this falls within the acceptable range for high frequency interconnects and was much lower than a film printed with the conventional M3D approach, 0.3dB/mm (see Figure 2:16).

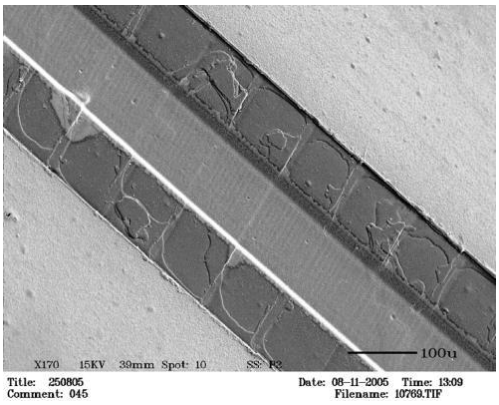

Enhanced M3D process by micromachining channels

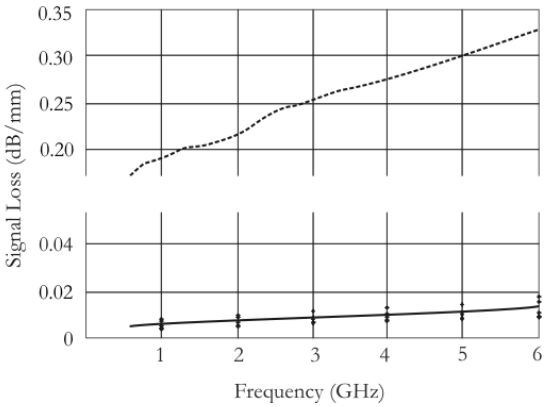

Reduced signal loss (solid line) as a result of improved M3D process compared to the conventional M3D process.

Figure 2:16: enhanced M3D process shows improved RF carrying characteristics (from Marinov, V et al. [72])

Electroless plating has also been used to improve the RF signal carrying capabilities of inkjet deposited conductive tracks [73]. From this it was shown that copper plating of silver inkjet tracks could exhibit equivalent RF carrying capabilities as bulk copper material. Whilst this technique is promising one of the downsides to the electroless plating technique is that it is not suitable for plating on to large structural components as large plating baths would be required.

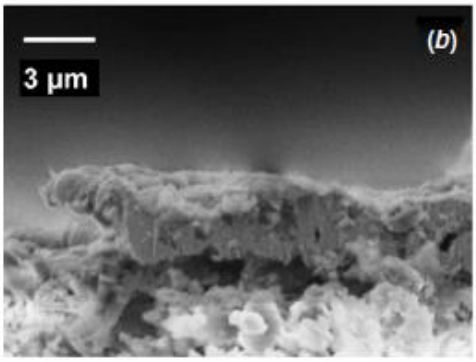

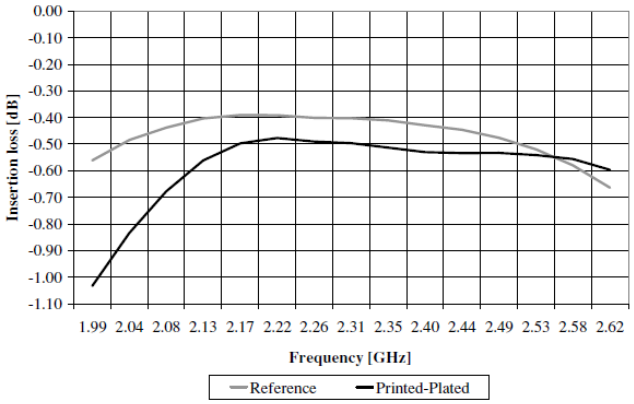

Inkjet deposited track

Line loss of printed line against reference

Figure 2:17: Electroless plating of copper plated inkjet tracks for improved RF performance (from Sridhar, A et al [73])

2.6.2 DW Antenna Printing

Full microstrip antennas have been fabricated using DW. In one example a combination of Inkjet and micro-nozzle printing was used [74]. This highlights the benefits of both technologies where the high accuracy control of the inkjet system is used to deposit the conductive tracks and the thick-film printing capabilities of the micro-nozzle system for printing the polyimide dielectric material. To improve the properties of the DW antenna it was capacitively coupled with another antenna which was made from much thicker commercially obtained dielectric material (see Figure 2:18). This underlines one of the downsides to DW technology in that it can be difficult to print the large dielectric thicknesses that are required to be able to reduce losses and increase bandwidth in the antenna (this is discussed further in Chapter 3 and 10).

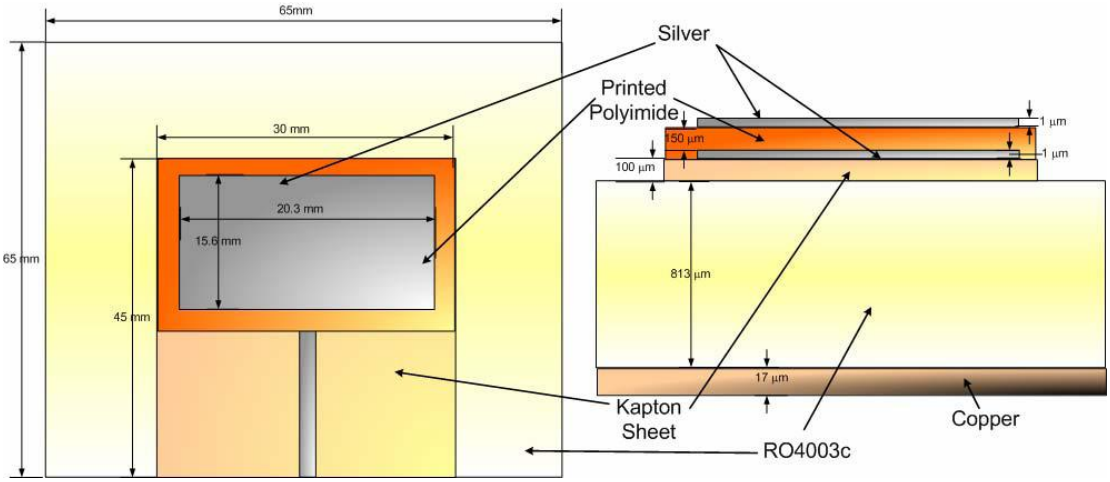

Figure 2:18: Geometry and design of capacitively coupled DW antenna (from Kirschenmann, K et al. [74])

Fabrication of a conformal GPS antenna has also been demonstrated by depositing a conductive PTF ink on to a fibreglass dome [75]. In this particular example the substrate itself acts the dielectric and the conductor is printed using DW as shown in Figure 2:19. This study reported that the resulting gain patterns were shown to have relatively good approximation to predicted values [75].

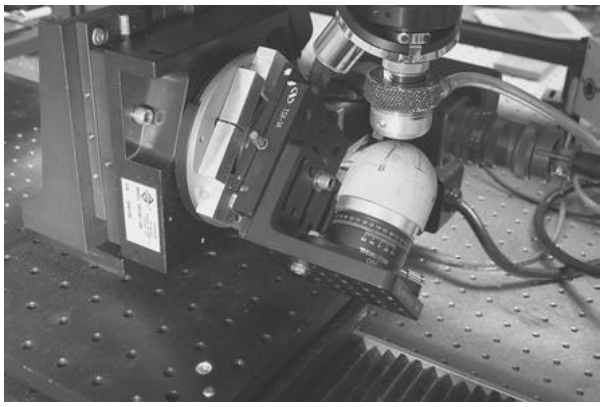

Figure 2:19: Conformal printing of a GPS antenna (from Auyeung, R C Y et al.) [75]

Similarly in work published by Adams J. J. et al. DW techniques were used to fabricate an Electrically Small Antenna (ESA) onto a glass dome using a nano-particle ink with a micro-nozzle type system. By filling a spherical volume the antennas effective size is increased which can lead to bandwidth improvements relative to their linear and planar counterparts [76]. It was found that these ESA had a measured centre frequency of 1.73GHz with a 5.83:1 bandwidth of 15.2%. This represented a 50% improvement in bandwidth over a helical antenna design and nearly an order of magnitude higher than a conventional monopole design.

In this experiment the inks were heat treated to 550^{o}C to achieve a resistivity of approximately 5x10$^{6}\Omega$cm. The author noted that using a copper antenna would only give an increase in antenna efficiently of 5-10% [76].

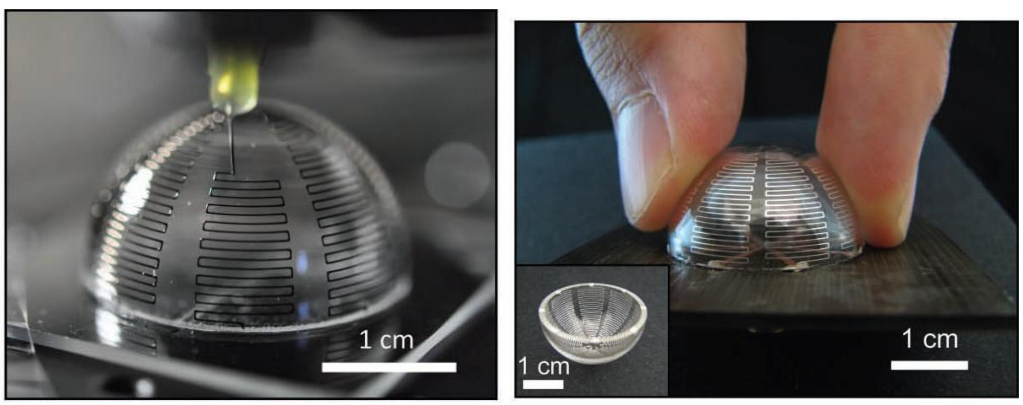

Figure 2:20: Printed ESA antenna on a glass dome with a centre frequency of 1.73GHz (from Adams, J J et al. [76])

Inkjet printing of wearable antennas has also been discussed on a variety of substrates including a polyurethane coated stretchable textile and a polyester cotton with a screen printed polyurethane acrylate based interface paste used to reduce the surface roughness of the material [77]. Figure 2:21 shows a half wavelength dipole antenna printed onto these substrate materials. This investigation highlights once of the limitations of DW which is the relatively high cure temperatures when processing on temperature sensitive substrates. For example the polyurethane stretchable textile has a maximum operating temperature of 80^{o}C, however it was found there were no discernible effects when processing the ink at 150^{o}C for 10mins.

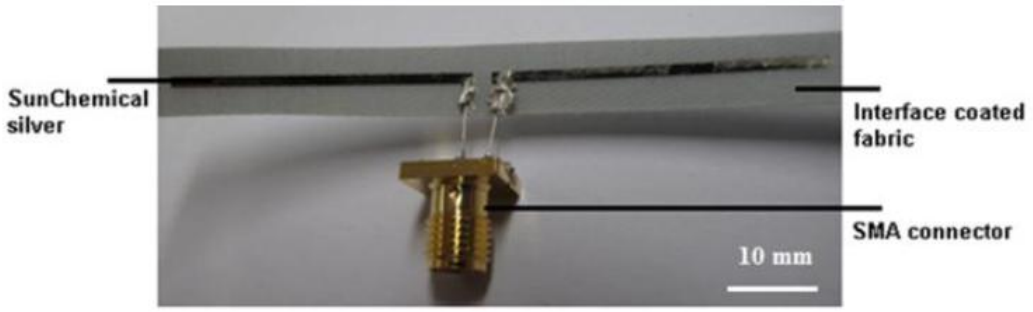

Inkjet printed 2.4 GHz dipole antenna on screen printed interface layer coated textile.

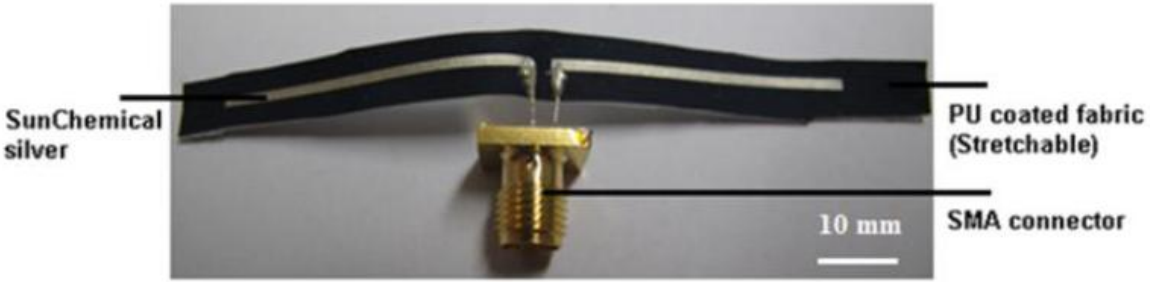

Inkjet printed 2.4 GHz dipole antenna on Plastibert (PU coated stretchable textile).

Figure 2:21: Printed dipole antenna on different textile substrates (from Chauraya, A et al. [77])

A number of papers have also highlighted that a high conductor thickness is key to reducing antenna losses [78] [79]. In general the conductor thickness should be higher than the skin depth (described in Chapter 3), this is especially important at lower frequencies where the skin depth is higher. Figure 2:22 shows the reflection coefficient (or return loss described in chapter 3) and antenna efficiency for an L-shaped monopole antenna printed at various thicknesses. The thickness was increased by printing multiple layers with the inkjet system. As can be seen the best return loss and antenna efficiency is obtained with the highest conductor thickness.

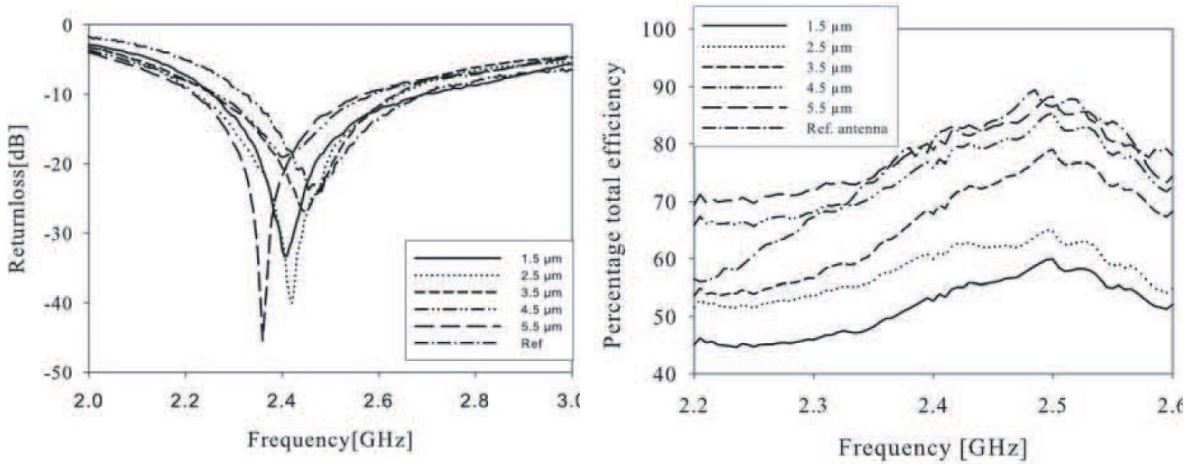

Figure 2:22: Return loss and antenna efficiency of an L-shaped monople antenna printed at various thicknesses (from Sowpati, A K et al. [78])

One potential way to reduce the amount of ink (and processing time) used to print an inkjet antenna is to only increase the layer thickness around areas of high current density [79]. The efficiency for a printed 2.4GHz narrow wire-type inverted F antenna (IFA) is given in Figure 2:23. It was seen that increased sintering (and hence conductivity) and layer thickness increase antenna efficiency. Comparison with a two layer local print (whereby the second layer is only printed in the areas of high current density) showed that the efficiency could give equivalent values to a full two layer print if sintered for long enough (in this case 60mins). The local two layer antennas reduced the amount of ink material by approximately 62%.

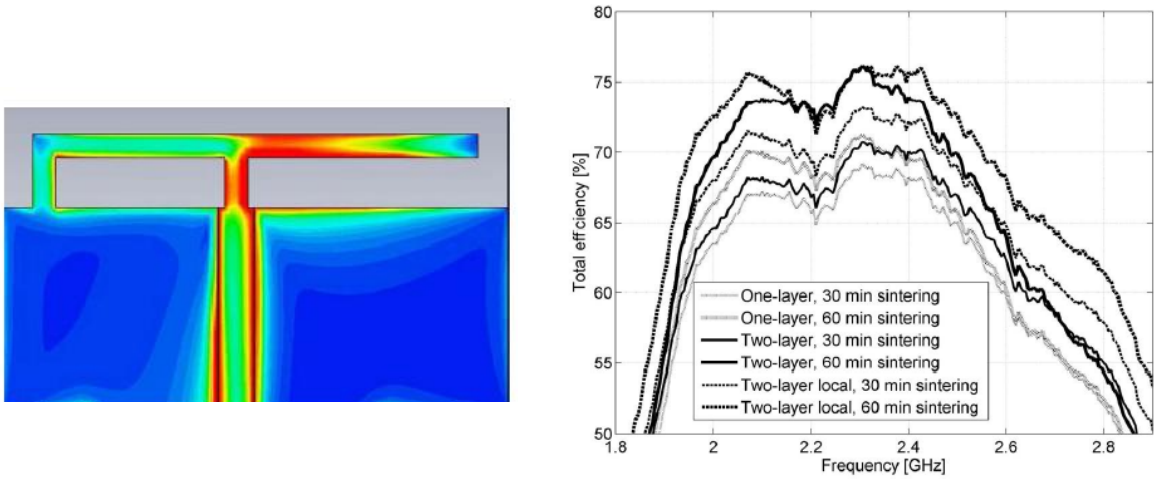

Figure 2:23: Antenna efficiency for a printed IFA antenna printed with different thickness and reduced second layer print areas (from Pynttäri, V et al. [79])

The defence market has previously investigated DW conformal antennas on an advanced combat helmet that could be used for applications such as voice communication, direction finding, jamming, situational awareness, GPS, remote sensor data and video [80]. These types of applications require a

bandwidth between 750-2700MHz. In order to cover this range a genetically optimised monopole antenna was considered. The main advantages of the conformal DW antenna were improved space, weight and covertness. This report highlighted several manufacturing challenges associated with integrating a DW antenna. For example if the antenna is integrated within the helmet shell it would need undergo high temperature and pressure cycles needed to consolidate the shell material. On the other hand if the antenna is printed onto the outside surface of the shell it is subject to environmental effects and low velocity impacts due to normal use of a helmet system. Figure 2:24 shows the micro-nozzle printed DW antenna and the optimised antenna pattern a when printed onto the Kevlar shell. Again similar to previous experiments the results show that if microwave dielectrics (such as Duroid) are not used then the antenna tends to behave differently from the model.

Broadband antenna and ground plane written on military helmet

Optimised antenna design

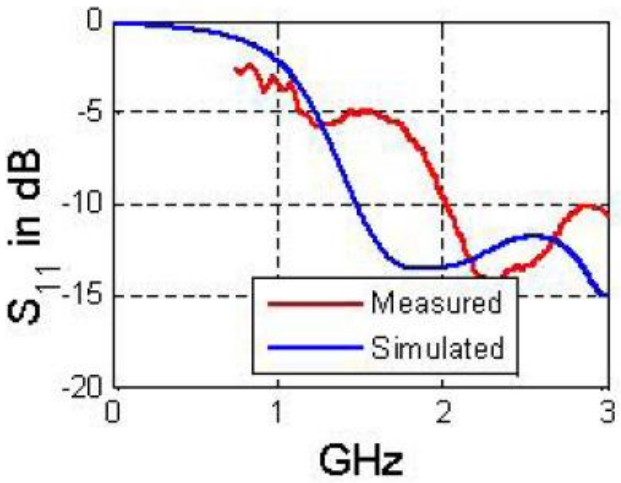

Return loss of optimised antenna design

Figure 2:24: Micro-nozzle printed monopole antenna on an advanced combat helmet (from Herold, D et al. [80])

The main limitations of fabricating antennas using DW methods as highlighted from the published work is optimising both material conductivity and print thickness whilst maintaining low cure/sintering temperatures. It is also evident that there is a lack of available printable materials to allow for fabrication of the dielectric layer via DW technology. Other factors that need to be considered for real world applications are the environmental durability of DW antenna and how they are integrated within component structures.

2.6.3 Inductors and RFID Tags

Related to the development of microstrip and conformal antennas has been the development of low-cost mass-manufactured printed Radio Frequency Identification (RFID) tags' or 'smart cards' (see Figure 2:25). These are essentially compact wireless technologies without the need for Line of Sight (LoS) to communicate with its reader i.e. the tag is ominidirectional [81]. These tags will contain unique ID's allowing them to be selectively activated from a remote device. Such tags will find market in commercial, industrial and defence markets where identification, tracking and sensing are key. [82]

Figure 2:25: Typical smart Card design (from DuPont [83])

RFID tags compose of an onboard integrated circuit (IC) chip and antenna. There are two main types of tags, passive and active. Passive RFID tags have no internal power supply which means that the antenna has to be designed to both collect powers from the incoming signal and also to transmit the outbound backscatter signal. Active RFID tags have their own internal power source, which is used to power the IC and broadcast the signal to the reader. There is currently a market push to produce RFID tags operating at high communication bands typically in the gigahertz range although currently 13.56Mhz is the choice frequency of operation especially for passive tags [15].

So far two materials have been used to produce inductance coils which meet the specifications of RFID tags. These materials are conductive nano-particle inks [15] and PTF pastes [83]. Dupont have suggested that PTF pastes have two main advantages for RFID printing [83]. The first is that they are thick film meaning thick track dimensions can be obtained without the need for multiple passes or layers, and secondly they have relatively low curing temperatures.

One of the biggest pitfalls of using DW technology for RFID fabrication is the cost of manufacture. Silver for example is used in most conductive DW materials due to its high conductivity but is more costly than copper. Furthermore DW does not lend itself well to markets which involve mass manufacturing due to comparatively low processing speeds of many DW technologies.

2.7 Summary

This chapter has introduced the main DW printing, material and processing technologies that could be used for to fabricate a conformal antenna on to a large structural component. A number of the printing technologies can be integrated with appropriate robotics to enable 3D writing capabilities although there is not a great deal of literature or examples of DW demonstrators that show this. Some of the key developments in DW have been on improving the properties of the ink materials especially in terms of conductivity and print control. There have been a number of examples where a number of additional processes such as micromachining and electroplating have also been used to improve the RF signal carrying properties of DW conductive materials. Of significant development is the successful use of lasers to locally cure or sinter DW materials removing the need to put the whole structure (which can be large) in an oven. Past investigations have shown that laser curing processes could restrict the heat into the substrate which may enable high temperature curing inks to be processes on temperature sensitive substrates.

From the literature some of the current limitations in DW technology for low profile antenna fabrication can be summarised as:

- Lack of literature regarding the implementation of DW ink materials and processing requirements for antenna fabrication
- Limited information on the durability of DW ink materials in harsh environments (such as high/low temperature, solvent and humidity resistance)
- Lack of specimens which show Heat Affected Zone (HAZ) inspection after laser curing

- Implementation of conventional electroplating techniques to improve ink conductivities which is not suitable when processing on large structures
- Little characterisation of the RF properties of PTF and inkjet conductive and dielectric ink compositions

This thesis will aim to address some of these limitations by first identifying the key design requirements for antenna fabrication and then investigate areas where the technology can be improved in terms of processing and material properties.

3. Determining the Design Rules for DW Antenna Fabrication

This chapter aims to understand antenna theory in more detail particularly focusing on the key considerations when designing a micro-strip patch antenna. From this the main requirements on the DW printing process can be determined.

3.1 Introduction to Antennas

Antennas are metallic structures that are designed for radiating or receiving electromagnetic energy in the radio and microwave frequencies. The antenna structure essentially acts as the transition between a guided wave (e.g. a transmission line) and a free-space wave [84].

In aerospace and defence communication systems the antenna is one of the most critical components. A good antenna design can improve overall system performance and reduce system integration requirements. Through the use of more intensive computer aided designs (such as phased array antennas) antennas have advanced significantly in the last decade in order to meet the system requirements of today's communication systems and the increasing demand on their performance [85].

In this chapter the key antenna parameters will be described along with some examples of some conventional antenna configurations.

3.1.1 Radiation Pattern

The radiation pattern depicts the far-field field strength transmitted from or received by the antenna as function of the spatial co-ordinates which are specified by the elevation angle, θ, and the azimuth angle, ϕ. The spherical co-ordinate system for antenna radiation patterns is given in Figure 3:1. The z-axis is taken to be the vertical axis and the xy plane is the horizontal axis. The xz plane is the elevation plane or the E-plane, or electric field vector and direction of maximum radiation. The XY plane is the azimuthal plane ($\theta=\pi/2$) or H-plane which is the plane containing the magnetic field vector of maximum radiation.

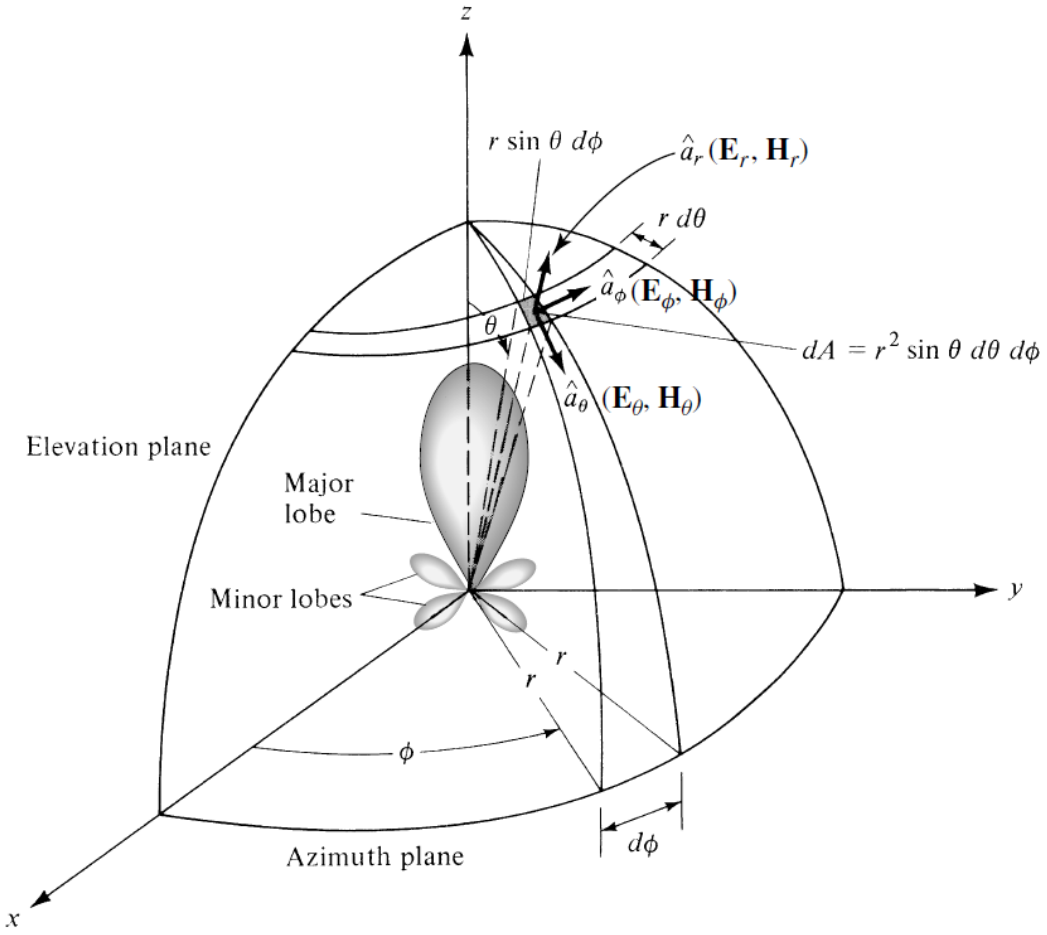

Figure 3:1: Spherical Co-ordinate system (from Balanis, C A [86])

The radiation pattern or intensity distribution from the antenna is observed in the Far-Field (Fraunhofer) region where the field distribution is essentially independent of the distance from the antenna. The far-field region is defined as [86]:

$$r_{\min} = \frac{2D_{\min}^{\ 2}}{\lambda}$$ **Equation 3:1**

Where, r_{min} is the minimum distance from the antenna, D_{min}, is the largest dimension of the antenna and, λ, is the wavelength.

Radiation patterns are measured at a single frequency, one polarization, and one plane cut. The polarization of an antenna refers to the polarization of the electric field vector of the radiated wave. Radiation patterns are usually taken at both co-polar (desired or actual polarization of the antenna) and cross-polar (orthogonal to the desired polarization of the antenna) configurations.

The radiation pattern has a number of features which are referred to as lobes. Most practical antennas are considered directional in that they radiate more power in some directions, the main lobe, and less power in other directions, known as minor lobes. The minor lobes usually represent radiation in undesired directions and so should be minimised. The Half-power beam-width (HPBW) is defined as the angle subtended by the half power points of the main lobe [87].

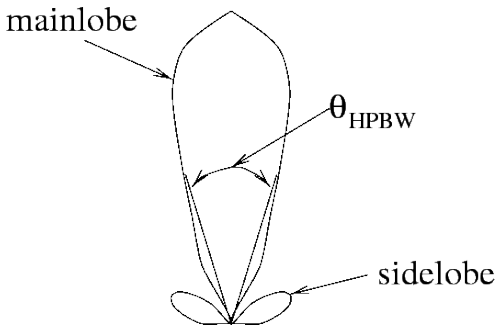

Figure 3:2: Radiation pattern of a generic directional antenna (from Chengalur, J N et al. [88])

3.1.2 Input Impedance

The input impedance, Z_{in}, is defined as 'the impedance presented by an antenna at its terminals or the ratio of the voltage to the current at the pair of terminals [86]. The impedance can be given by

$$Z_{in} = R_{in} + jX_{in}$$ **Equation 3:2**

Where R_{in} is the antenna resistance at the terminals and X_{in} is the antenna reactance at the terminals. The antenna reactance is the opposition to changes in electric current or voltage, due to its inductance or capacitance. The reactance can be eliminated by operating at the antennas resonant frequency where capacitive and inductive reactances are equal and opposite.

The imaginary part of the input impedance represents the power stored in the near field of the antenna. The resistive part of the input impedance consists of two components, the radiation resistance R_r and the loss resistance R_L. The power associated with the radiation resistance is the power radiated by the antenna, while the power dissipated in the loss resistance is lost as heat in the antenna itself due to dielectric or conducting losses.

3.1.3 Antenna efficiency

The antenna efficiency takes into account the losses at the terminals (i.e. where there is connection to a transmission line) of the antenna. The losses are attributed to reflection (due to impedance mismatch between the transmission line and antenna), dielectric and conductor losses where [86]

$$e_t = e_r e_c e_d$$ **Equation 3:3**

Where $e_{t,}$ is the total antenna efficiency, $e_{r,}$ is the reflection (impedance mismatch) efficiency, e_c is the conduction efficiency and e_d is the dielectric efficiency.

3.1.4 Directivity and Gain

The directivity of an antenna is the ratio of radiation intensity in a given direction (usually maximum radiation intensity or main lobe on the antenna radiation pattern) from the antenna against the intensity of an isotropic antenna (which has equal radiation intensity in all directions). The radiation pattern gives an indication of the directivity of the antenna, for example an antenna which has a narrow main lobe would have higher directivity then an antenna with a broad main lobe. The directivity is given by [86]

$$D = \frac{U}{U_i} = \frac{4\pi U}{P_r}$$ **Equation 3:4**

Where U is the radiation intensity of the antenna, U_i is the radiation intensity of the reference source and P_r is the total power radiated.

The antenna gain G, is simply the antenna efficiency e, multiplied by the directivity D [89]

$$G = eD = e\frac{U}{U_i}$$ **Equation 3:5**

With reference to an isotropic radiator the Gain can be defined as [89]

$$G_{dBi} = 10\log_{10}(e\frac{4\pi U}{P_r})$$ **Equation 3:6**

Where U, is the radiation intensity of the antenna, U_i, is the radiation intensity of the reference source, P_r is the total power radiated and e, is the efficiency of the antenna.

Gain is a dimensionless quantity, since it is the ratio of two radiation intensities, hence, it is generally expressed in dB.

The antenna gain is always related to the main lobe in the direction of maximum radiation unless indicated. Depending on the application either high or low gain is required, for example GPS antennas may want to have higher gain towards the zenith (highest point in the sky). In radar applications low side lobes are desired to avoid detecting large targets when they are illuminated by side lobes [85].

3.1.4 Return loss

The return loss, RL, is the amount of power reflected back to the transmitter for a given input power the rest of the power is either radiated or absorbed by the antenna as losses. The return loss is given by [90]

$$RL = -20\log_{10}|\Gamma| \qquad \textbf{Equation 3:7}$$

Where Γ is the reflection coefficient. For perfect matching between the transmitter and the antenna $\Gamma = 0$ and RL = ∞, i.e. no power is reflected back. The return loss with a positive sign is identical to the magnitude of the reflection coefficient in decibels but of opposite sign.

3.1.5 Voltage Standing Wave Ratio (VSWR)

The VSWR measures how well a load (such as a receiver or transmitter) is matched to a source. A perfectly impedance matched load has a VSWR of 1:1, this means that all the power is transmitted from source to the load, i.e. there is no reflected power and the *return loss* Is said to be infinity. The higher the VSWR the more power that is lost to impedance mismatching and the lower the return loss as more power is reflected away [91]. For many practical applications a VSWR of 2 is acceptable which corresponds to a RL of -9.54dB [84].

3.1.6 Bandwidth

The bandwidth, BW, of an antenna is the range of usable frequencies (either side of the centre frequency) over which the VSWR is below 2. The BW can be given by [86]

$$BW = 100\text{x}\frac{f_H - f_L}{f_c} \qquad \textbf{Equation 3:8}$$

Where f_h is the highest frequency in the band, f_L is the lowest frequency and f_c is the center frequency.

3.2 Types of Antennas

Many types of antennas have been developed for use in a number of different applications ranging from radio and television broadcasting, cellular and wireless phone communications, marine and satellite communications. The characteristics of an antenna are very much determined by its shape, size and material that it is made of. Some of the commonly used antennas are briefly described in this section.

3.2.1 Wire Antennas

Wire antennas are some of the simplest type of antenna designs and are used in everyday life in various applications. Wire antennas include single wire (dipole), loop and helical type configurations (see Figure 3:3). The most common type of wire antenna is the half-wave dipole (where the length of the wire is equivalent to half the wavelength) which has a typical gain of 2dB (the ratio of power when compared to an isotropic antenna is approximately 3/2) [92].

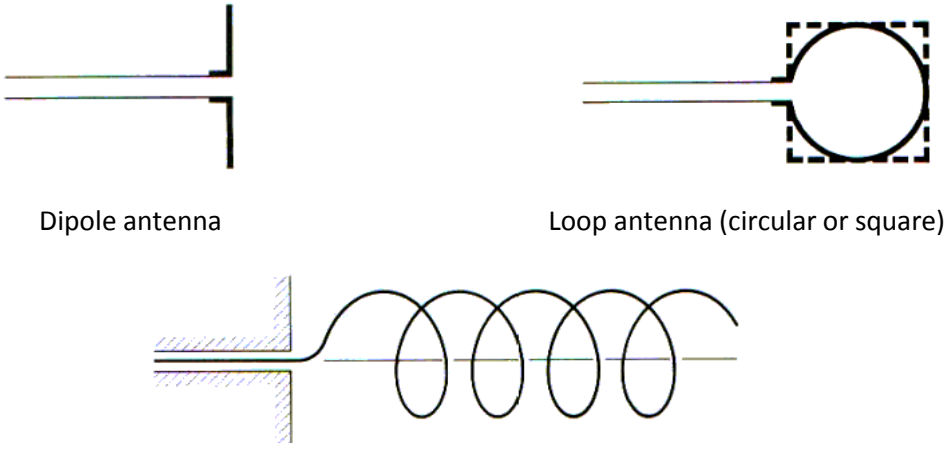

Dipole antenna

Loop antenna (circular or square)

Helical antenna

Figure 3:3: Wire antenna designs (from Balanis, C A [86])

3.2.2 Horn Antennas

Antennas which use an aperture are typically used at gigahertz (microwave) frequencies. The most common type of aperture antenna is the horn antenna which is essentially a waveguide whose end walls are flared out (see Figure 3:4). The aperture of the horn can be circular, rectangular or elliptical. Horn antennas are advantageous as they provide high gain, low VSWR with relatively low bandwidth [86]. These antennas are used in aircraft and spacecraft applications.

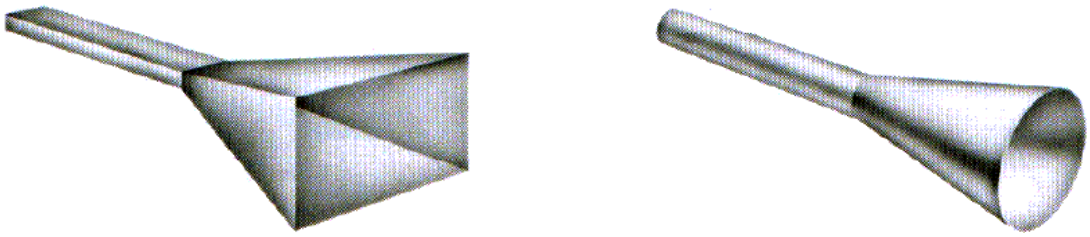

Pyramidal Horn Conical Horn

Figure 3:4: Horn Antennas (from Balanis, C A [86])

3.2.3 Microstrip Antennas

As discussed in Chapter 1 the microstrip antenna is advantageous due to its low profile and low weight. Microstrip patch antennas can take many different forms but rectangular and circular patches are the most common because of their ease of fabrication and radiation characteristics. Microstrip patch antennas have increasingly found extensive use in wireless communication systems and can have applications in aircraft and military applications as well. One of the major drawbacks of conventional microstrip antenna designs is that they offer relatively narrow bandwidth (see Section 3.3), typically 5% with respect to the centre frequency, although this can be improved with novel designs [93].

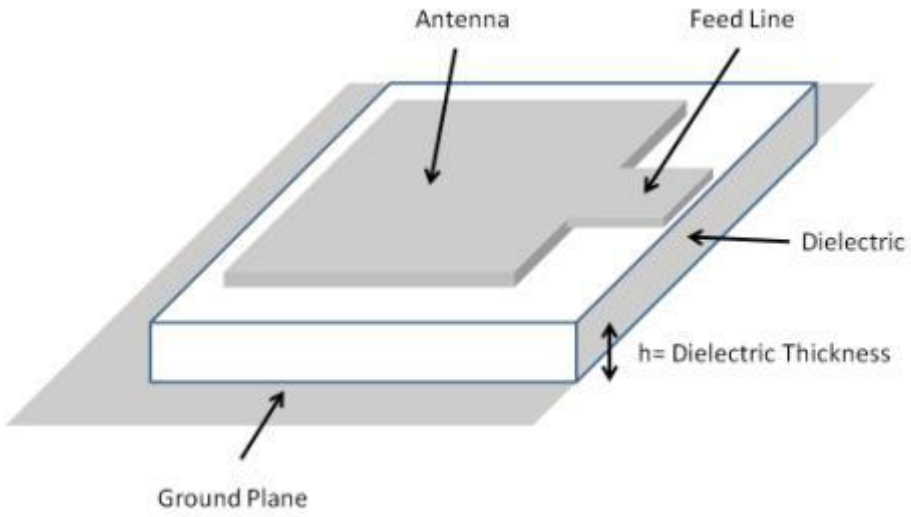

Figure 3:5: Microstrip patch antenna (modified from James, J R et al. [94])

3.3 Micro-Strip Patch Antenna Design Considerations

The micro-strip patch antenna essentially consists of two main components, the antenna itself and the feed or transmission line used to connect the antenna to the power source and signal generator/receiver. These components are made from a dielectric medium sandwiched between two conductive elements as shown in Figure 3:5. Conventional antennas are usually made with low loss dielectrics such as Duroid 4350 and the conductors are usually copper which is photo-etched on the surface [91].

Ideally it is desirable that the energy generated by the source is totally radiated by the antenna. However, in practice this energy is lost in the transmission line and the antenna patch (by conductor and dielectric losses). Reflection losses also occur at the interface between the transmission line and the antenna which can also reduce efficiency. By optimising both the design of the antenna and the materials used these losses can be reduced. This section will mainly focus on what key design elements are used to minimise conductor and dielectric loss therefore improve antenna efficiency.

3.3.1 Antenna Efficiency

When designing an antenna it is useful to start with the bandwidth requirements and resonant frequency. The bandwidth of a patch antenna is the range of frequencies over which the antenna can receive or radiate energy above an acceptable loss. The bandwidth is inversely proportional to the quality factor of the antenna and can therefore be approximated to [94]:

$$BW \approx \frac{1}{Q}$$ **Equation 3:9**

Where Q is the quality factor. The quality factor is essentially the ratio between the stored and energy lost in the antenna. The quality factor is given by:

$$Q = \omega \frac{W}{P_l}$$ **Equation 3:10**

Where ω is the angular frequency (at the resonant frequency of the antenna), W is the stored energy and P_l is the total power loss in the antenna.

The total power loss in the antenna originates from three main loss mechanisms, the conductor loss P_c, dielectric loss P_d and radiation loss P_r [94]. The total quality factor Q_t is thus given by [8]:

$$Q_t = \frac{2\pi f \mathrm{E}(1/h)}{P_r + P_c + P_d}$$ **Equation 3:11**

Where $\mathrm{E}(1/h)$ is the stored energy and $2\pi f$ is the angular frequency

From Equation 3:11 it can be seen that as the frequency of the antenna increases the Q factor increases thereby reducing the antenna bandwidth (Equation 3:9). Interestingly power losses (from the conductor and dielectric) essentially increase the bandwidth of the antenna. However, the antenna efficiency depends on the ratio of radiated power to total input power (Equation 3:12) so any increase in bandwidth due to these losses is matched by a proportional reduction in antenna efficiency [8].

$$e_t = \frac{P_r}{P_r + P_d + P_c} \mathrm{x}100\%$$ **Equation 3:12**

3.3.2 Transmission Line model of dielectric and conductive losses

To get a better idea of how the dielectric and conductor losses affect the antenna performance we can use the transmission line model. Other models for determining the performance of a patch

antenna include the cavity line model and full wave model. Whilst the transmission line model is not as accurate as the other models it gives a good approximation of the behaviour of a patch antenna and field distribution for transverse electromagnetic (TEM) TEM_{00n} modes which propagate in the longitudinal direction (along the strip). The field distribution along the x and y axes is assumed uniform. The cavity model on the other hand is a more general model of the patch which imposes open-end conditions at the side edges of the patch however this model and the full wave model are more complex to calculate and was therefore not considered here [87].

Micro-strip dielectric loss

In the case of a strip transition line the signal is mostly of the transverse electromagnetic (TEM) mode of propagation. The dielectric loss, α_d, in this type of system is independent of dimensions and can be approximated to:

$$\alpha_d = \frac{\omega}{2}(\mu\varepsilon_0\varepsilon_r)^{\frac{1}{2}}\tan\delta_d \qquad \textbf{Equation 3:13}$$

Where ε_r is the relative permittivity of the material and ε_o is the free space permittivity and 'tan δ_d' is the dielectric loss tangent. The loss tangent is a measure of the rate of energy lost to a mode of oscillation in a dissipative system. It can apply to both electrical systems (i.e. dielectrics losses in the presence of alternating current) and mechanical systems such as the one described in Chapter 6.

From Equation 3:13 the transmission line loss increases with frequency. Line losses also increase with high dielectric constants (relative permittivity) and loss tangents.

Micro-strip conductor loss

The micro-strip conductor loss α_c, is proportional to the length of the line and the surface resistivity of the conductor.

$$\alpha_c = 8.68\text{x}\frac{R_s}{wZ_m} \qquad \textbf{Equation 3:14}$$

$$R_s = \left(\frac{\omega\mu_o}{2\sigma_c}\right)^{\frac{1}{2}} \qquad \textbf{Equation 3:15}$$

Where w is the width of the conductor, R_s is the surface resistivity, σ_c is the conductivity of the micro-strip and Z_m, is the characteristic impedance of the micro-strip and is a function of the dielectric constant, the width of the conductor and the height of the dielectric.

Characteristic Impedance

The Characteristic Impedance or input impedance of a finite transmission line is the ratio of the amplitudes of a single voltage wave to its current waves propagating along the line in the absence of reflections. The characteristic impedance is given by [95]:

$$Z_m = \sqrt{\frac{R_l + j\omega L}{G_c + j\omega C}} \qquad \textbf{Equation 3:16}$$

Where, L, is the inductance per unit length, G_c is the conductance per unit length, C is the capacitance per unit length and ω is the angular frequency and R_l is the resistance per unit length.

If the transmission line is considered lossless, the characteristic impedance is purely real and appears like a resistor in a normal electrical circuit. A transmission line of finite length (lossless or lossy) that is terminated at one end with a resistor equal to the characteristic impedance ($Z_m = Z_0$) appears to the source like an infinitely long transmission line.

When connecting the transmission line to a device that is not matched ($Z_m \neq Z$), some of the electrical energy cannot be transferred between the lines and is reflected back along the line towards the transmitter, thereby increasing RF energy losses. The superposition of the reflected wave with the forward wave causes standing waves patterns within the line and is characterised by the VSWR.

Most RF coax cables come with a 50Ω rating, the transmission line must therefore be designed to match this impedance. Transmission line impedance varies as a function of the frequency of operation, the height above ground (the dielectric height), the width of the conductor and the thickness of the conductor. An approximation of the characteristic impedance of the line is given by [96]:

$$Z_0 = \frac{Z_0}{2\pi\sqrt{2(1+\varepsilon_r)}} ln\left[1 + \frac{4h}{w_{eff}}\left(\frac{14+\frac{8}{\varepsilon_r}}{11} * \frac{4h}{w_{eff}} + \sqrt{\frac{14+\frac{8}{\varepsilon_r}}{11}\frac{4h}{w_{eff}} + \pi^2\frac{1+\varepsilon_r}{2}}\right)\right] \quad \textbf{Equation 3:17}$$

$$W_{eff} = w + t(\frac{1+\frac{1}{\varepsilon_r}}{2\pi}) ln\left[\left(\frac{4e}{\left(\frac{t}{h}\right)^2 + \left(\frac{1}{\pi} * \frac{1}{\frac{w}{t}+\frac{11}{10}}\right)^2}\right)\right] \quad \textbf{Equation 3:18}$$

Where Z_0 is the impedance of free space, w is the width of the strip, w_{eff} is the effective width of the strip, h is the height of the dielectric and t is the thickness of the metal conductor.

Skin Depth Considerations

The skin depth determines the penetration depth of the RF signal into the conductive medium in the transmission line and antenna, and is given by Equation 3:19.

$$\partial_z = \sqrt{\frac{1}{\pi f \mu \sigma}} \quad \textbf{Equation 3:19}$$

As the conductivity of the material increases the skin depth reduces and the signal becomes increasingly confined to the surface of the conductor. The effects of skin depth on antenna loss have are related by the following equation [8]:

$$\alpha_{cr} = \alpha_c \left\{1 + \frac{2}{\pi}\arctan 1.4\left(\frac{Ra_\Delta}{z}\right)^2\right\} \quad \textbf{Equation 3:20}$$

Where Ra_Δ is the RMS surface roughness of the conductor. To reduce the effect of surface roughness & skin depth effects on antenna loss it has been suggested that the maximum surface roughness of a conductive track should be equal to or lower than the skin depth and the thickness of the conductor should be three times the skin depth [8] [97].

It can be important to identify whether the current travels through either the top or bottom surface of a microstrip transmission line as this will determine surface roughness requirements). To do this,

current density within a microstrip line was modelled using FEKO electromagnetic suite by Richard Orton at BAE systems, Great Baddow. In this simulation the conductor track height was modelled to be significantly greater than the skin depth. In this circumstance the microstrip line is being fed through the bottom of the conductor using embedded SMA connectors. This was chosen as it was thought to be close to how a DW microstrip would be connected. The results are shown in Figure 3:6.

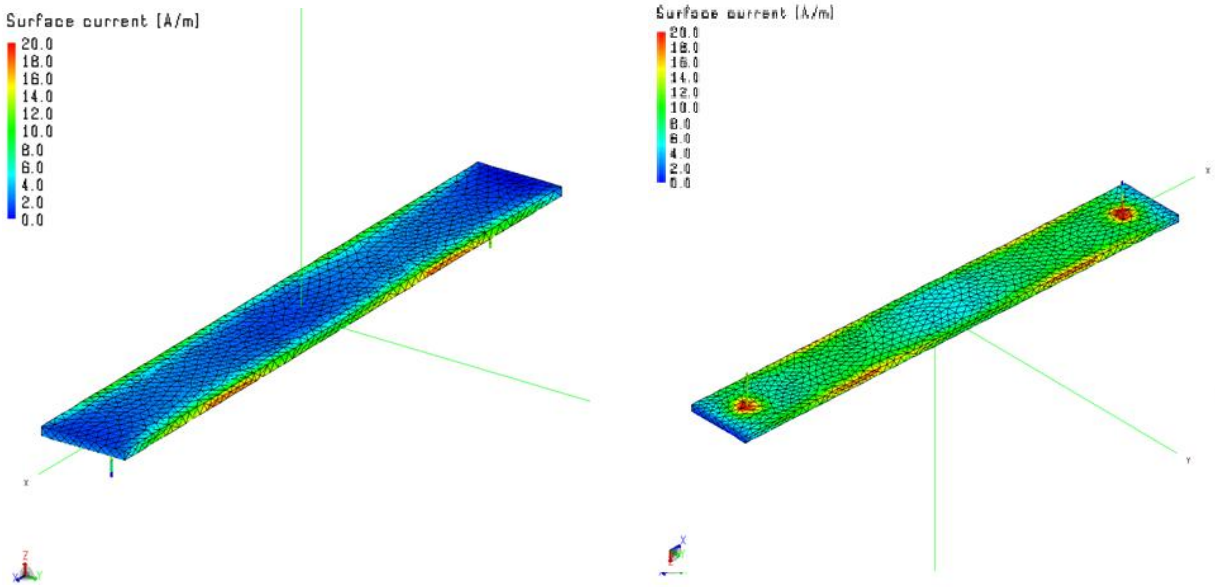

Top Surface of conductor in microstrip line with low current density

Bottom Surface of conductor at dielectric interface high current density

Figure 3:6: Current Density measured at 1GHz for a silver micro-strip line on a dielectric surface where the dielectric height>>Skin depth.[1]

This analysis shows that the majority of the current density within the conductor is located at interface between the dielectric and the conductor when operating at frequencies of 1Ghz. In terms of DW it is therefore important that the dielectric has a smooth surface in order to allow the conductive ink to flow over it uniformly. Any curing approach used to process the dielectric or the conductor must also consider surface roughness effects.

[1] These models were creaed by Richard Orton at BAE systems

Modelling the Microstrip Transmission Line Loss

To understand how dielectric thickness affects the loss in a micro-strip a micro-strip program, TX-line [98] was used. The following transmission line parameters were selected for this simulation:

- Conductivity of silver, $6.14 \times 10^7\ Sm^{-1}$
- Dielectric constant, $\varepsilon_r = 5$
- Loss tangent = 0.001
- Impedance = 50Ω
- Conductor height = 0.1mm
- Conductor length =100mm
- GPS Frequency =1.575 GHz

The dielectric constants were chosen at values similar to those required for microwave applications i.e. low loss tangent and dielectric constant (Duroid has a loss tangent of 0.001 and a dielectric constant of 2.16 [99]). To maintain the characteristic impedance of 50Ω the dielectric width will also vary with the thickness of the dielectric. The results are shown in Figure 3:7.

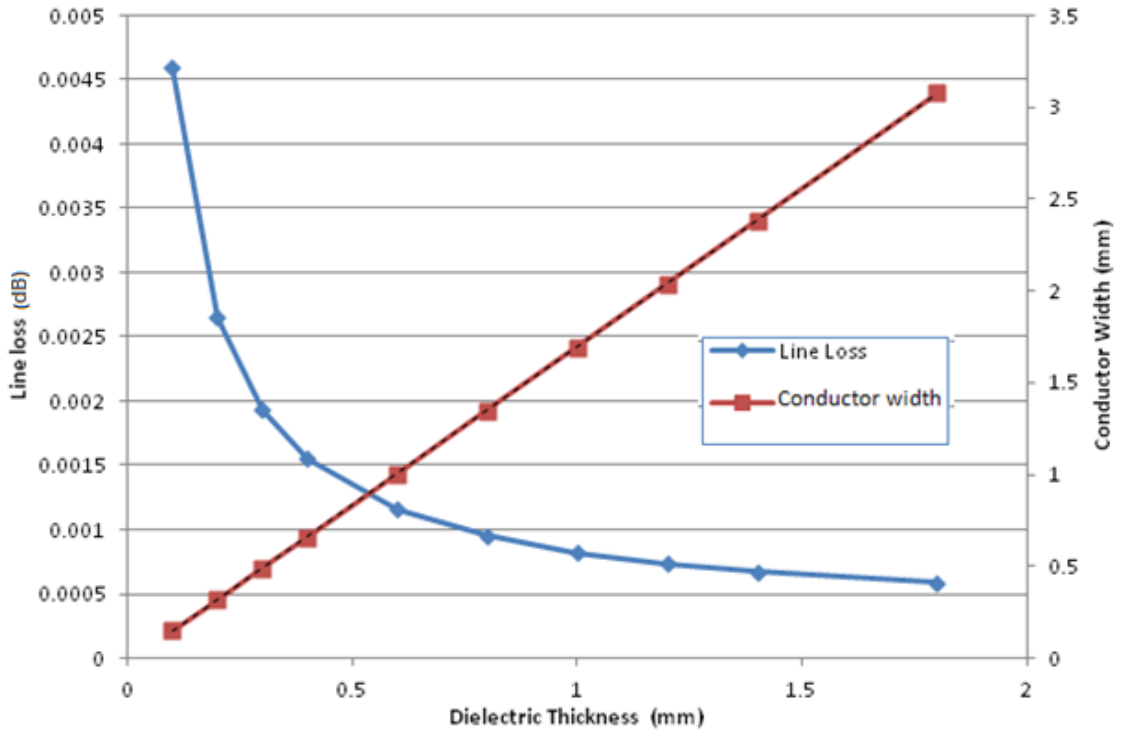

Figure 3:7: Effect of substrate thickness on micro-strip loss calculated using TX-line, where the line loss is plotted against dielectric thickness and the corresponding conductor width is plotted against dielectric thickness.

The micro-strip loss decreases asymptotically with increasing dielectric height. When the thickness is greater than 1mm the loss becomes more constant at around 0.001dB.

A similar investigation was conducted to determine the effects of conductivity on transmission line loss (known as insertion loss). In this model a value of 1mm was used for the dielectric thickness and the loss was measured over a range of frequencies. The normalised loss measurements as a percentage of the bulk conductivity of silver are given in Figure 3:8. Silver was chosen as the reference material because most conductive DW ink materials use silver as the conductive element.

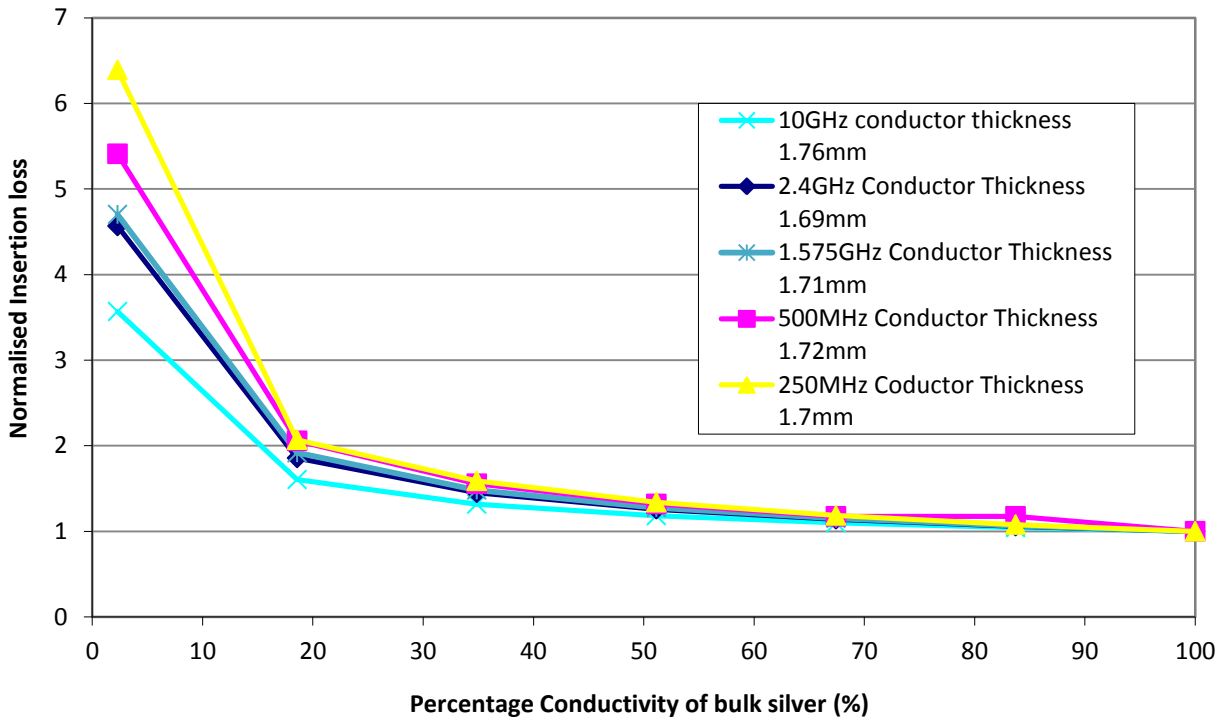

Figure 3:8: Normalised transmission line loss against the percentage conductivity of bulk silver.

As expected as the conductivity increases to bulk metal values the transmission line loss reduces. It is reasonable to say that for bulk silver conductivities greater than 30% the reduction in line loss is less significant for all operating frequencies and so this can be used as the minimum target conductivity for DW ink materials.

A final simulation was conducted to measure the line loss as a function of the dielectric constant for different frequencies. For this measurement the height of the dielectric was kept at 1mm and the loss tangent at 0.001. The results are shown in Figure 3:9.

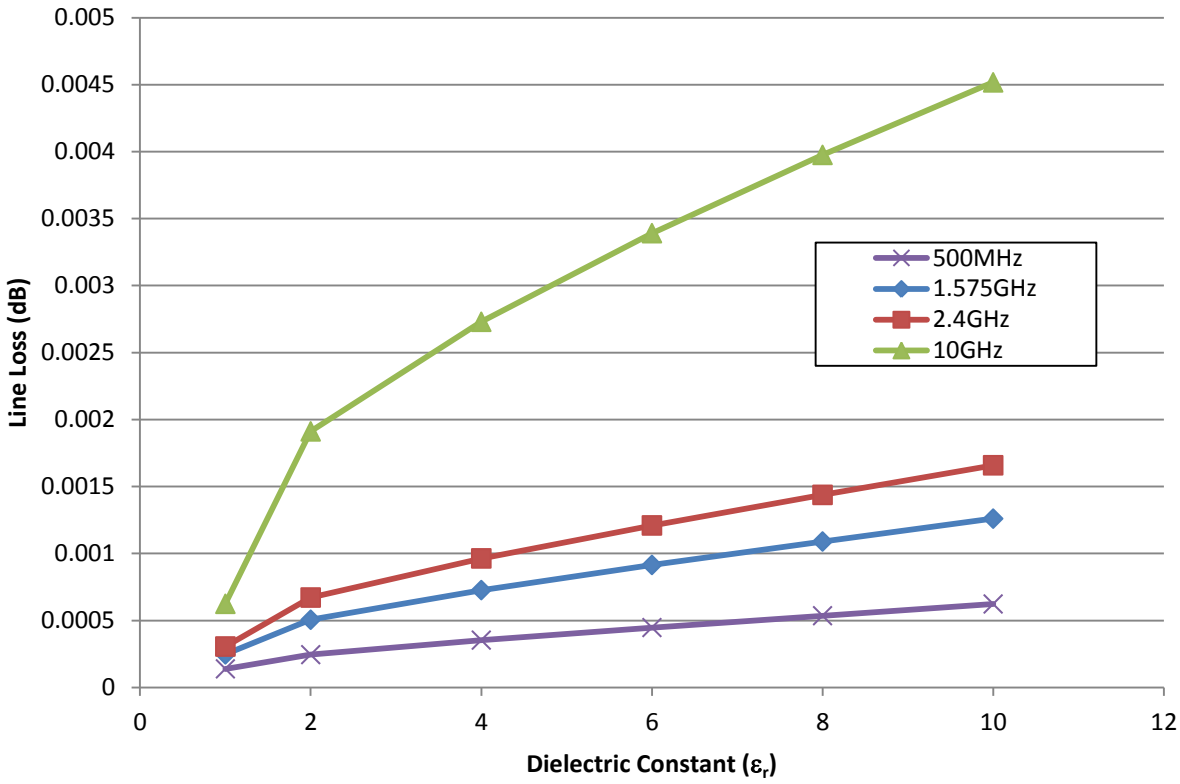

Figure 3:9: Transmission line loss against the dielectric constant for different frequencies

From Figure 3:9 it can be seen that lower dielectric constants are much more important at higher frequencies. Certainly at 10 GHz a dielectric constant of 2 or lower is desired to reduce losses. A high quality microwave substrate such as Duroid 5880 typically has a dielectric constant of 2.16 with a loss tangent of 0.001. At lower frequencies the dielectric constant follows a more linear relationship. Similarly from Equation 3:13 the dielectric loss tangent is also proportional to the loss in the transmission line and antenna so it is important to minimise these as much as possible.

3.4 Determining the Key Parameters for DW primary Printed Antennas

To maximise the efficiency of the antenna it is important to reduce the losses associated with the conductor and dielectric materials. From Equation 3:13 and Equation 3:14 it can be seen that as the frequency goes up so do the dielectric and conductor loss where the dielectric loss is proportional to frequency whereas conductor loss is proportional to the square root of frequency. This means at higher frequencies (>1Ghz) dielectric losses become more prominent.

From Equation 3:13 it can be seen that the dielectric loss can be reduced by having a low dielectric loss tangent. In general, at gigahertz frequencies a dielectric loss tangent below 0.005 is desirable although in some cases higher loss tangents may be acceptable [100]. The conductor losses in

Equation 3:14 can be minimised by increasing material conductivity and reducing the surface roughness of the conductor.

In general the dielectric thickness of the antenna is kept at a minimum to gain the low profile advantage of the micro-strip configuration. The minimum dielectric thickness that can be used must not be less than $\lambda/1000$, where λ is the wavelength. At thicknesses below this value the bandwidth of the antenna becomes so narrow that any temperature variation causes the resonance VSWR to rise rapidly causing reflection losses which reduce efficiency. Another by-product of having low dielectric thicknesses is that the Q of the antenna becomes so high that current losses become excessive and conductance across the cavity yields excessive dielectric losses.

The aim of the analysis conducted in this chapter is to put together a guideline for the general material and print parameters for a patch antenna a fabricated using DW. This guidelines has been put together so that it can be used independent of operating frequency or bandwidth (which is more to do with antenna design) although it is clear that as the frequency increases the losses increase. A summary of these parameters with target parameters is given in Table 3:1.

Table 3:1 can be used to select the most appropriate DW technology, materials and processing techniques for antenna fabrication. This can also be used to determine the key areas that are required for further development of the technology. It must be noted that this table only covers the primary device requirements for DW technology. For it to be implemented for real world applications a number of additional requirements need to be considered . This will be handled in Chapter 4.

Parameter	Antenna Parameter	Characteristic	Target parameters
Dielectric Loss Tangent, $\tan\delta$	• Antenna Efficiency • Antenna Bandwidth • Transmission line loss	Proportional to the dielectric loss in the antenna and transmission line. Low $\tan\delta$ increases antenna bandwidth	$\tan\delta_d < 0.005$ [100]
Dielectric Constant, ε_r	• Antenna efficiency • Antenna gain • Transmission line loss • Impedance	Dielectric constant is related to the speed at which an RF signal travels through a microstrip. Dielectric constant is proportional to transmission line loss and inversely proportional to line impedance	At 10GHz, < 2 At frequencies below 2.4GHz this should be minimised with a target value of $\varepsilon_r <$ 10 (inferred from Figure 3:9)
Dielectric height, h	• Antenna bandwidth • Antenna efficiency • Transmission line loss	Low dielectric height reduces antenna bandwidth and increases antenna and transmission line loss	h >1mm
Conductor thickness, t	• Antenna conductor loss	To reduce antenna loss α_{cr} from skin depth effect	$t=\delta_z*3$
Surface Roughness, R_a	• Antenna efficiency • Antenna gain • Transmission line loss	If the surface roughness is higher than the skin depth, z, RF transmission line losses can increase. For high conductivities the skin depth is smaller meaning the surface roughness of the conductor becomes more important.	$R_a < \delta_z$
Conductivity, σ_c	• Antenna efficiency • Antenna gain • Transmission line loss	Inversely proportional to skin depth, high conductivity reduces skin depth thereby decreasing antenna and transmission line loss	σ_c > 30% bulk conductivity of silver (inferred from Figure 3:8)
Conductor dimensions	• Impedance • Reflection loss • Resonant frequency	Impedance matching to connector interfaces between antenna, transmission line and power source reduces VSWR (power loss due to reflections)	Dimensions determined so that line has a 50Ω impedance and resonates at the correct centre frequency

Table 3:1: Summary of DW design guide for patch antenna

4 DW Requirements Capture and Analysis for the Production of High Frequency Communications

This previous chapter have so far introduced some of the basic science and concepts regarding the main area of interest of this thesis i.e. the production of low profile antennas on to aerospace components. The next step is to define the project and its objectives and translate the background understanding into a full set of system requirements.

When generating requirements it is not enough to rely solely on just the technical issues, all aspects of the system must be considered, without this understanding it is impossible to realise successful solutions. To enable a holistic viewpoint of the project a Systems Engineering (SE) approach is needed. This chapter introduces the SE process. By implementing SE processes and tools, DW specific requirements and solutions were generated for antenna fabrication.

4.1 Introduction to Systems Engineering

Modern day businesses are now under more internal and external pressures than ever before. Projects within the defence and aerospace industry for example are heterogeneous, cross disciplinary, involve large supply chains and need to be completed under tight time constraints at lower cost, whilst being able to adapt to the dynamic nature of the market. If the project involves some sort of physical 'deliverable' then there is the task of maintaining and managing the product's lifecycle after manufacture. These aspects must be considered when making decisions at the very start of a project. However, it is very difficult to define a 'best value' solution. Many requirements and design considerations cannot fully coexist in a single design step, there is, therefore, a need for a rigorous and iterative approach that addresses some of these issues.

To combat this, the problem can be considered as a 'system'. A system can be defined as a group of components that work together for a specific purpose [101]. It is important to define the nature of the system, its boundaries and interfaces. A 'systems point of view' should recognise that a problem and solution have many elements or components. The most important aspect of a system is often a function of how these components interact [102]. Whilst the SE perspective should examine the

specifics of the problem (i.e. the interactions between internal system components) the system boundaries must also be expanded to include interactions with the surrounding environment.

The International Counsel of System Engineers (INCOSE) defines SE as a comprehensive, iterative technical process to [103]:

A. Translate an operational need into a configured system meeting that need through a systematic, concurrent approach to integrated design of the product and its related manufacturing, test, and support processes
B. Integrate the technical inputs of the entire development community and all technical disciplines (including the concurrent engineering of manufacturing, logic, and test) into a coordinated effort that meets established program cost, schedule and performance objectives
C. Ensure the compatibility of all functional and physical interfaces (internal and external) and ensure that system definition and design reflect the requirements for all system elements (hardware, software, facilities, people, and data)
D. Characterise technical risks, develop risk abatement approaches, and reduce technical risk through early test and demonstration of system elements.

Similar definitions can also be found in the MIL-STD-499A and MIL-STD-499B documents [104].

4.1.1 Systems Engineering Process: The 'V-Model'

The SE process is essentially applied over the whole system lifecycle. There are a number of models that describe the SE process over the system lifecycle, the most widely used and accepted is the 'V' model.

The emphasis of the 'V-model' is on the flow down of requirements as the system detail is elaborated. The V-model of good practice illustrates each stage in the top-level SE process as a series of small loops or phases. A version of the V-model is given in Figure 4:1:

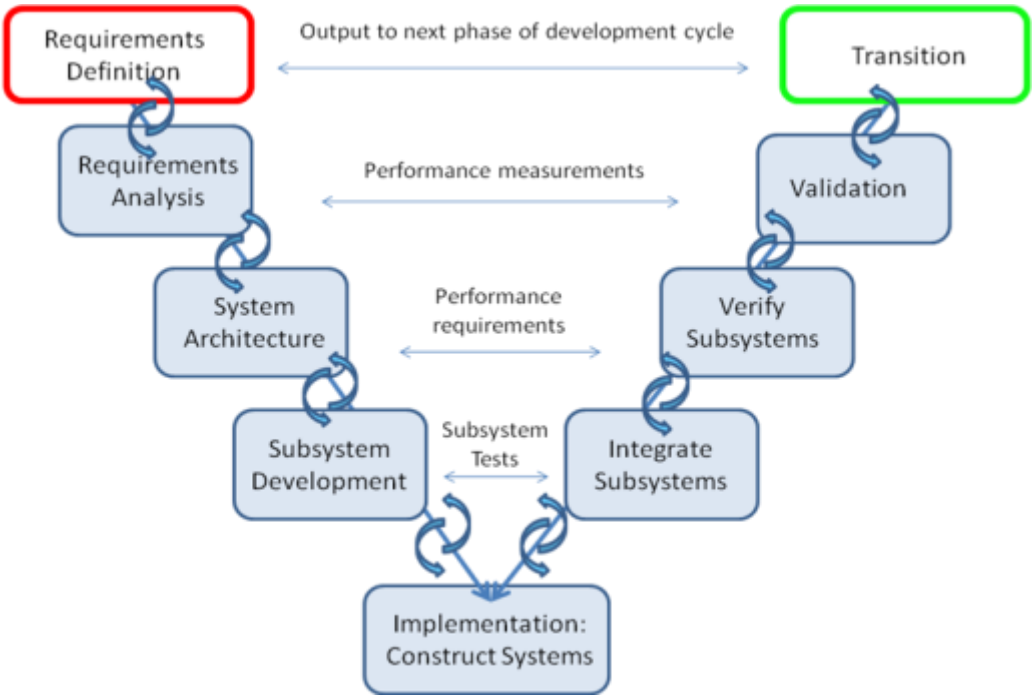

Figure 4:1: V-model (modified from Elliot, C [105])

The left leg of the 'V' describes system decomposition. This is defined as the hierarchical, functional and physical partitioning of the system into hardware, software or operational contexts [106] In the V-model, System decomposition involves:

- Problem definition: Identify the all relevant stakeholders, and together, collate information to define the problem to produce system/customer requirements

- Requirements Analysis: Translate the system requirements into functions. This will then prompt reconsideration of the requirements so that each identified function is traceable back to a requirement.

- Architecture: Design the system architecture in a way that all subsystems (hardware, software, human) are defined along with their relationships and interfaces.

- Subsystem development: Detail design of subsystems and how they work. Will prompt a revisit of both system requirements and architecture. Subsystems may also be considered as separate systems themselves.

The right leg of the V-model represents the integration, verification and validation of the system and its components. Verification ensures that the selected solution meets its specified technical or performance requirements and correctly integrates with interfacing components whereas validation ensures that the requirements are consistent with respect to higher level requirements (i.e. acceptance by the customer) [107].

At each decomposition phase there should be a direct correlation between activities on the left and right sides of the V-model. This is important as the verification and validation activities must be traceable to the system requirements. This ensures that when each requirement is generated it is done so in such a way that can be measured and verified. It must be noted that the V-model is not meant to be prescriptive and encourages re-visitation of each of the processes over the course of the lifecycle.

4.1.2 Systems Engineering Applied to Defence Research Projects

The work published in this report was conducted at BAE Systems, Advanced Technology Centre (ATC). This acts as corporate research centre with the emphasis of developing Low Technology Readiness Level (TRL) technologies for the benefit of the defence industry and/or integration within the different BAE Systems platforms (e.g. aircraft, ships, land vehicles, etc). TRL's are defined by the Ministry of Defence (MoD) in Figure 4:2, generally, research projects such as this aims at developing technologies that start at TRL 1-4.

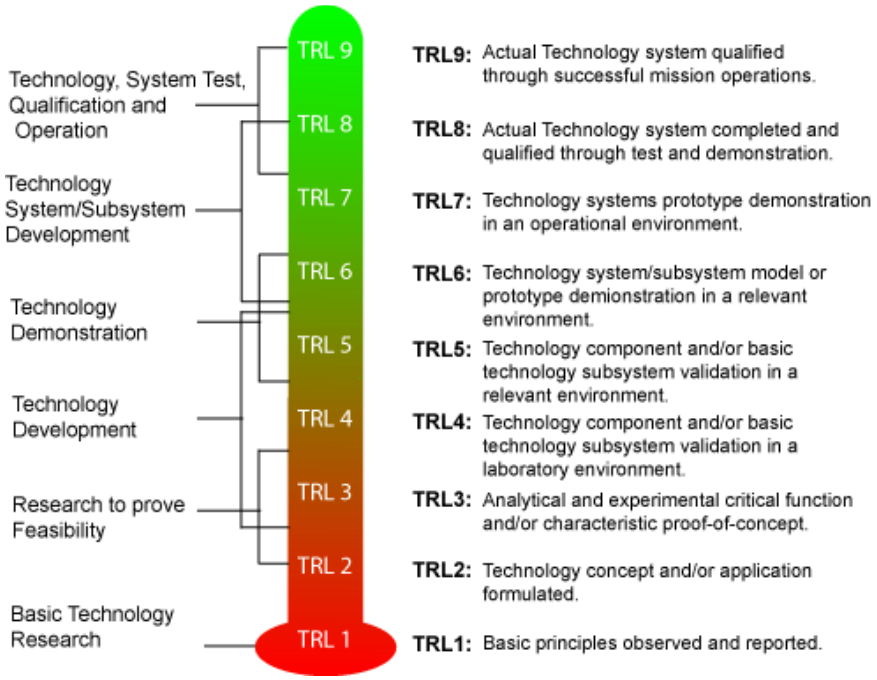

Figure 4:2: TRL defined by the Ministry of Defence, MOD [108]

Increasing TRL's involves developing not only the technical aspects of a system (its functionality) but also its ability to be seamlessly integrated within high legacy defence platforms. Integration requires in-depth knowledge of the platform technology and the environment it will operate in. This involves a multidisciplinary approach and understanding of the lifecycle issues with the development technology as well as the platform technology. The lifecycle of a product can be defined by the CADMID model given in Figure 4:3.

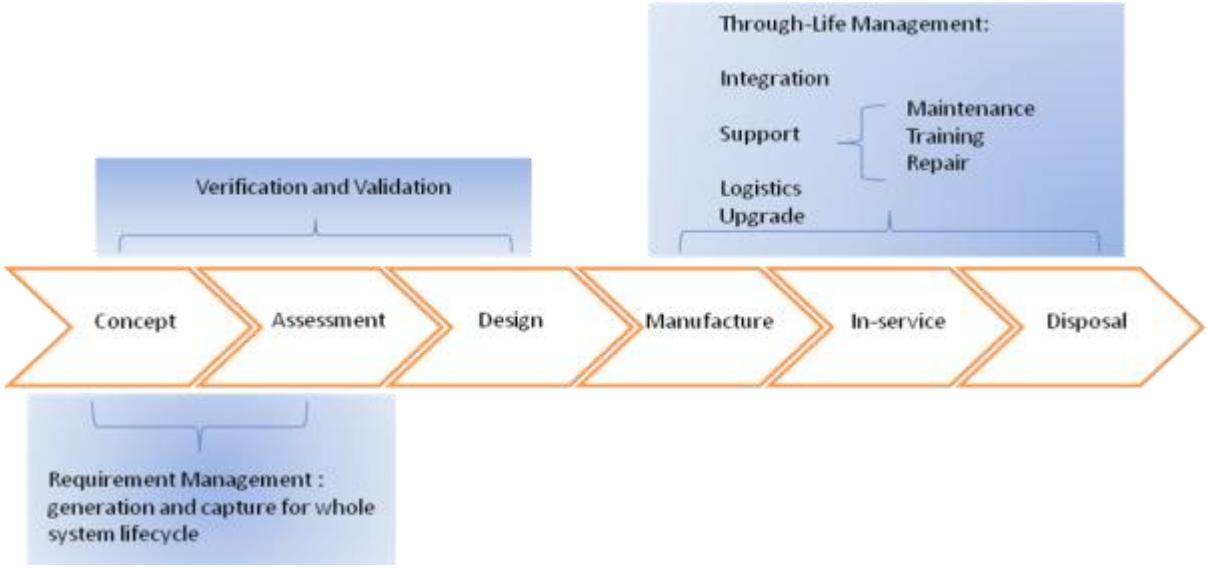

Figure 4:3: System lifecycle represented by the CADMID cycle (modified from Romero Rojo, F Jet al. [109])

Essentially the majority of research projects are conducted in the first three stages of the system lifecycle; Concept, Assessment, Demonstration and to some extent Manufacture. However, to have a full systems approach concept exploration and design must also incorporate through-life aspects such as deployment/integration within the environment, logistics, maintenance (through-life support) and disposal to ensure system acceptance and increasing TRL.

In defence projects the unique relationship between the MoD customer, industry and the end-user results in requirements that are often fluid and varied depending on origin. During the development cycle these requirements can also evolve and even become obsolete. This can be a real issue in research environments where development cycles are considered longer, often ranging over many different projects. Therefore, projects require a process which allows for adaptability and flexibility to be designed into the solution [110].

To manage these issues the SE process enables incremental development and a continual through-life technology refresh. Where research projects are concerned, SE documentation provides traceability to requirements, the customer and end-user which is invaluable for successive research

to quickly pickup on previous work, maintaining continuity and vision. In terms of integration, the process encourages the development of all Defence Lines of Development (DLoD) supporting equipment, training, personnel, doctrine, infrastructure and logistics and can be adapted to co-exist with other detailed defence specific architectural views such as MoDAF[2] [110].

4.2 Capturing the requirements for DW fabrication

SE is a discipline which uses a number of tools to capture and understand requirements. This can be useful as often key requirements can be missed when approaching the system or project problem for the first. Often these requirements are inter-related and have dependencies on each other. SE allows these dependencies to be fully understood so that the developed solution has the properties that were expected from the outset of the project.

The aim of this section will be to use a selection of SE tools to define the project problem and develop a set of requirements for antenna fabrication for aerospace and defence applications. From this a number of technical performance measures can be defined which can be used to assess the progress (w.r.t to the requirements) of the research conducted in this thesis.

4.2.1 Concept Phase: Stakeholder Analysis

The first task in the SE process from the V-model of best practice (described in Figure 4:1) is to identify all the stakeholders associated with the project and define their relationships. Stakeholder analysis allows the whole environment in which the system operates to be captured. It serves to identify people or organisations that interact with the system either directly or indirectly providing resources or information over the course of the system lifecycle. The majority of this information can be captured using a stakeholder context diagram [111]. The stakeholder context diagram for DW fabrication of an antenna structure is given in Figure 4:4.

[2] Ministry of Defence Architectural Framework (MODAF): Is a defence specific architectural framework, details can be found at http://www.modaf.org.uk/

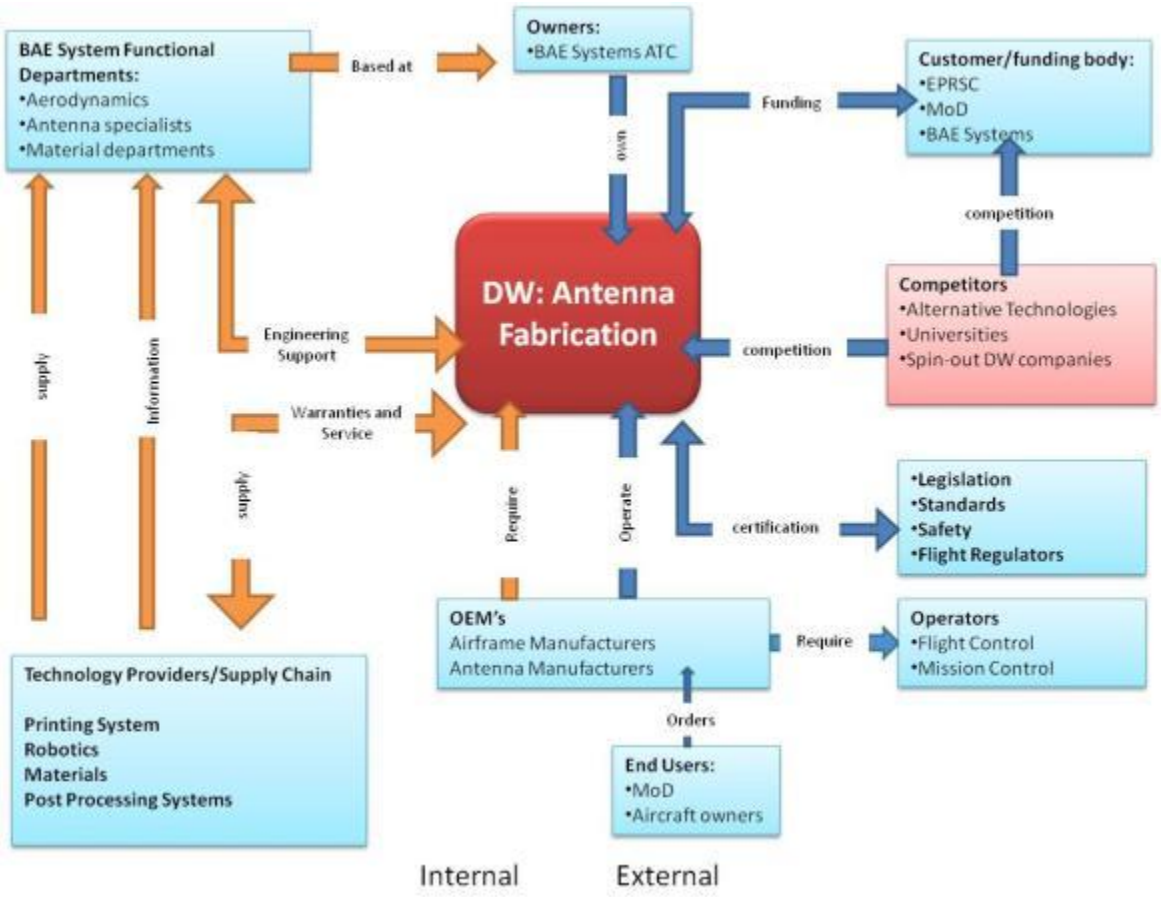

Figure 4:4: Stakeholder context diagram for DW antenna fabrication on to a wing component

The stakeholder diagram is segmented into two sections, internal (orange arrows) and external (blue arrows) stakeholders. Internal stakeholders act prominently within the project to help achieve system solutions. However, they also need to maintain awareness of external stakeholders which influence system requirements and constraints on the project. The external stakeholders form part of the environment the system operates in, therefore, some requirements may not become apparent until later in the system lifecycle. Some stakeholders have internal and external influences, such as end users and project owners which can determine requirements and act as technology providers.

The main requirements for this project originate from the end users. The end users can be categorised as the operators, (airframe) manufactures and users. In a UK defence project the main user would be the MoD and those associated with gathering data from the antenna will be the operators. The users and operators supply the airframe manufacturer or the platform owner with a set of requirements or specifications. Additional requirements will also originate from independent flight and safety regulators which may become more active later in the system lifecycle.

4.2.2 Concept Phase: Defining Customer Requirements

Now that the stakeholders have been identified the project goals and top level requirements can be clarified. For the purpose of this project, antenna design was not considered the main focus. Instead the criterion was to determine the technology gaps for DW antenna fabrication on to aerospace structures and find appropriate solutions. To capture all the customer requirements a Systemic Textual Analysis (STA) can be constructed. STA is useful as it decomposes the main customer requirements (non-functional statements) into a set of functional system requirements and defines each of these functions with a performance requirement [112].

This thesis aims to look at the general development and manufacturing requirements for conformal antenna fabrication. For simulation purposes a patch antenna (operating at GPS frequencies) was considered for fabrication onto the surface of an aircraft wing. Based on internal discussions at BAE systems a mock STA was developed for this application and is given in Figure 4:5.

Project				
DW Antenna Fabrication				
Context:				
To reduce weight and size conformal planar antennas can be used to replace conventional antennas in aerospace systems. A possible manufacturing method for conformal antennas is through the use of Direct Write technology				
Operational requirement:				
To demonstrate an operational DW antenna on to aerospace carbon fibre wing				
Non-functional customer requirements:				
Operational Antenna at GPS like frequencies				
Flexible positioning				
System must meet mil standards				
Integration within aircraft platform including all connectors and power sources with minimum signal loss (<10dBi across cable length)				
Functional requirement	**Performance requirements**			
Receive/Send signal	1.533 GHz	Bandwidth 100MHz	60° Patch coverage	50Ohm impedance
Fabricate on to carbon fibre wing component	Processing temperatures below 120°C	10° curvature	Wing component 1m long	
Print low profile antenna	Maximum height 2mm			
Operate in Aerospace Environment*	Max temperature (120°C)	Min Temperature (-40°C)	Solvent resistance: water, oil	Skydrol Resistance

Figure 4:5: Customer Requirements for mock antenna application captured by STA (template based on (Burge [112]))

The customer requirements were based on a project starting at TRL2/3 with the aim of increasing the technology closer to TRL5 or 6. To achieve TRL5 the system had to be demonstrable and validated in an operational environment (according to Mil standards). As can be seen these requirements are relatively vague and do not contain much detail. They also do not specify the DW or printing requirements that must be captured to determine the areas of development.

4.2.3 Systems Engineering Viewpoint of DW

To help in determining the DW requirements it is necessary to take a holistic outlook of the system and decompose it into its main components. A systems viewpoint diagram for DW technology is given in Figure 4:6, the arrows show which components have relationships between them.

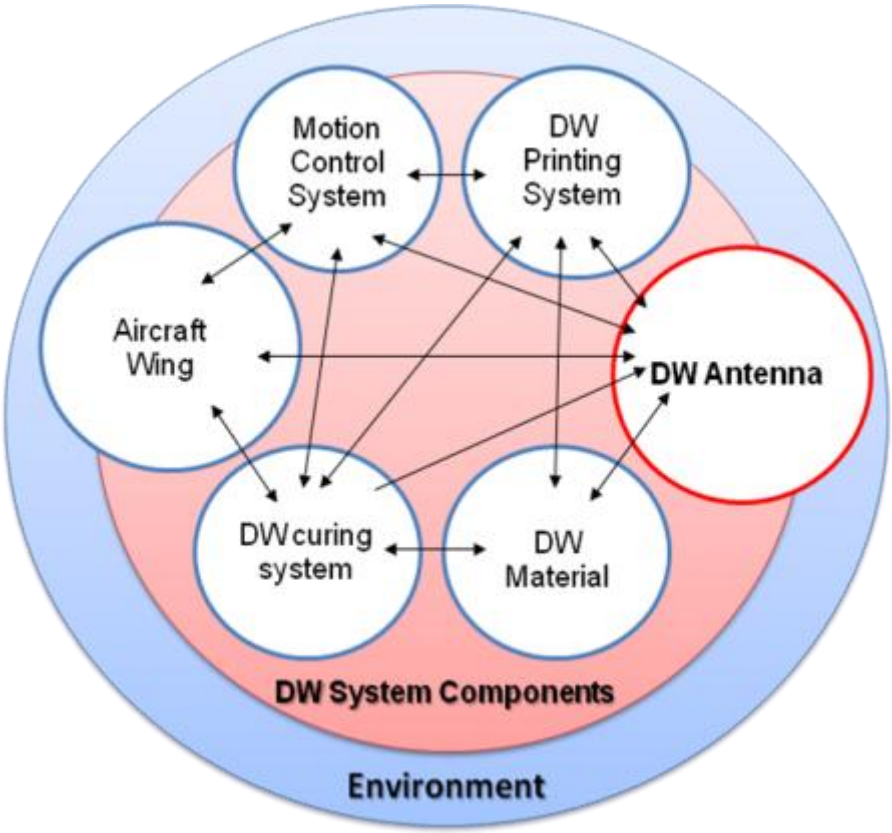

Figure 4:6: Systems Overview of DW components required to fabricate a conformal antenna

The high inter-relationship between the system components means that requirement allocation can become more complex. For example the antenna requirements (bandwidth, frequency, etc.) will determine the functionality that is required in the DW materials and also specify the accuracy of the DW printing. However, as seen in chapter 2, certain materials can only be printed with certain deposition technologies. This flow of requirements is an important factor in DW. If the DW antenna is fabricated on to an aerospace structure (an aircraft wing) then this will have consequences on the

conformal printing capability on the printing system, the durability of the DW material and the processing temperature of the DW curing system. Selecting material and processes which meet these requirements may then have consequences on the performance of the antenna. Essentially it is important to make sure that all system components are compatible, thereby reducing or preventing any unwanted emergent properties that could lead to system failures.

4.2.4 System Architecture: Capturing Technical Requirements

To transform the customer needs (see STA, Figure 4:5) into a set of meaningful technical and functional DW requirements an understanding of the antenna system is needed. Using the information collated from the background research conducted in chapter 3 and the SE viewpoint of DW all design constraints related to the antenna can be captured using systems architecture. There are many different tools that can be used to map the relationships and attributes between system components. This chapter is going to focus on using Unified Modelling language UML, tools to provide system description.

UML is used to describe Object Orientated Systems, where each object represents an entity of interest and can be described by its class, state, and its behaviour. UML has mainly been applied in software engineering however, there are some examples of its advantages in developing hardware systems [113]. One of the most widely used models of Object Orientated systems are class diagrams. Class diagrams are used to depict the attributes, operations and relationships between objects (system components) in a static phase (known as classes), it is also used to design or describe structures in the system. The class diagram therefore enables a very descriptive summary of the design and organisation and functional properties of the system in question [114]. A class diagram for a DW antenna system is given in Figure 4:7. A summary of the notations used in the class diagrams is given in appendix A [115].

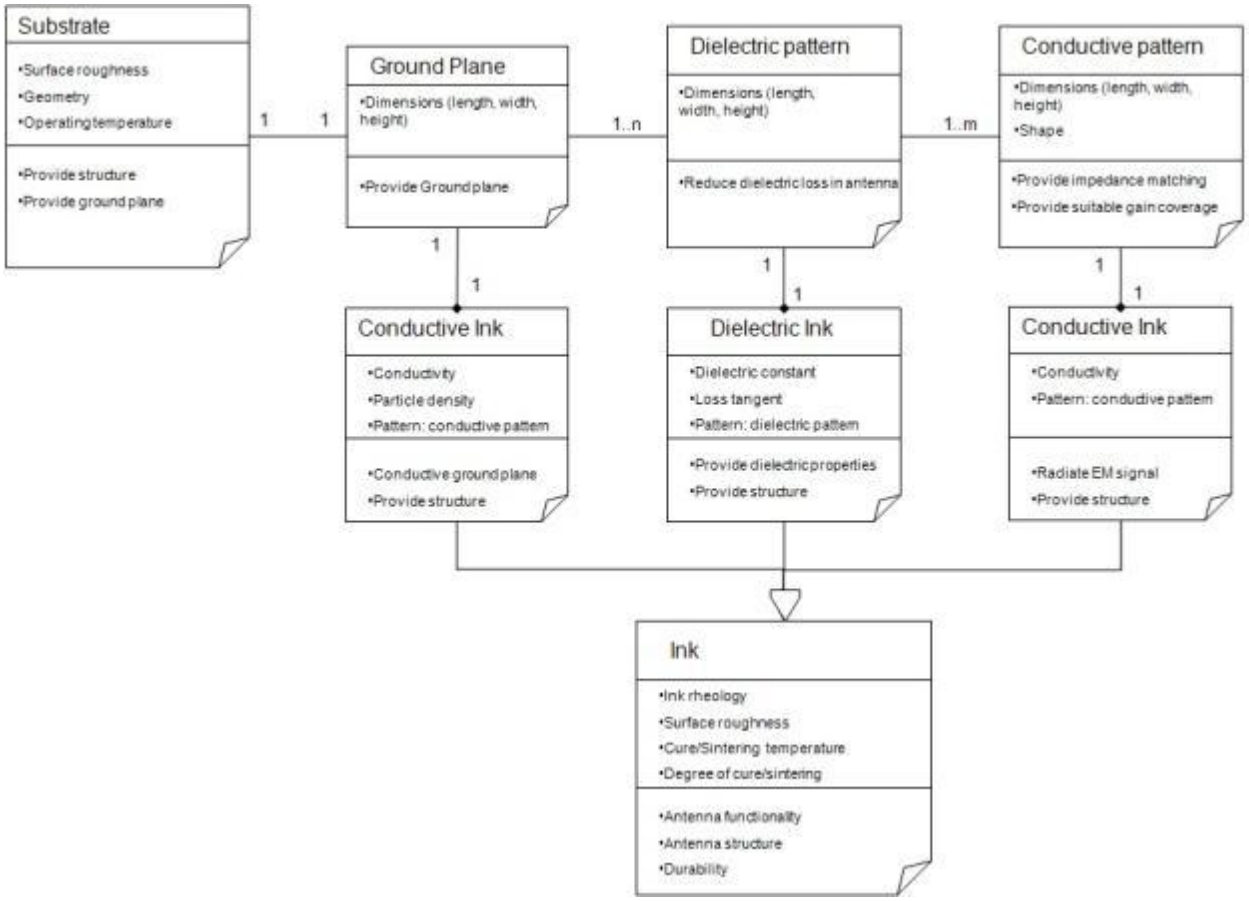

Figure 4:7: Class diagram for DW antenna ('n' and 'm' determine the number of dielectric and conductive patterns)

From the class diagram the structure of the DW antenna (the substrate and dielectric and conductive pattern) has been modelled. If produced by DW, each pattern or layer in the antenna is shown to be composed of DW ink. In this case, there are two types of ink, conductive and dielectric variants. These inks also share certain properties and this is captured using a generalisation 'ink' class. An important attribute of the ink is the degree of cure and how it affects the functional properties of the ink. For example the conductivity of the ink is determined by the conductive particles and the density (loading by weight) of particles defined in the conductive ink class and also by the degree of cure/sintering defined in the generalisation 'ink' class.

The biggest advantage of the class diagram is that it depicts all the attributes that determine antenna functionality from the structure, materials and patterns. The DW system can be built around this model by making sure that its meets all the necessary parameters.

The first goal is to provide patterning of the DW material using a suitable printing system. The class diagram for a DW printing system is given in Figure 4:8.

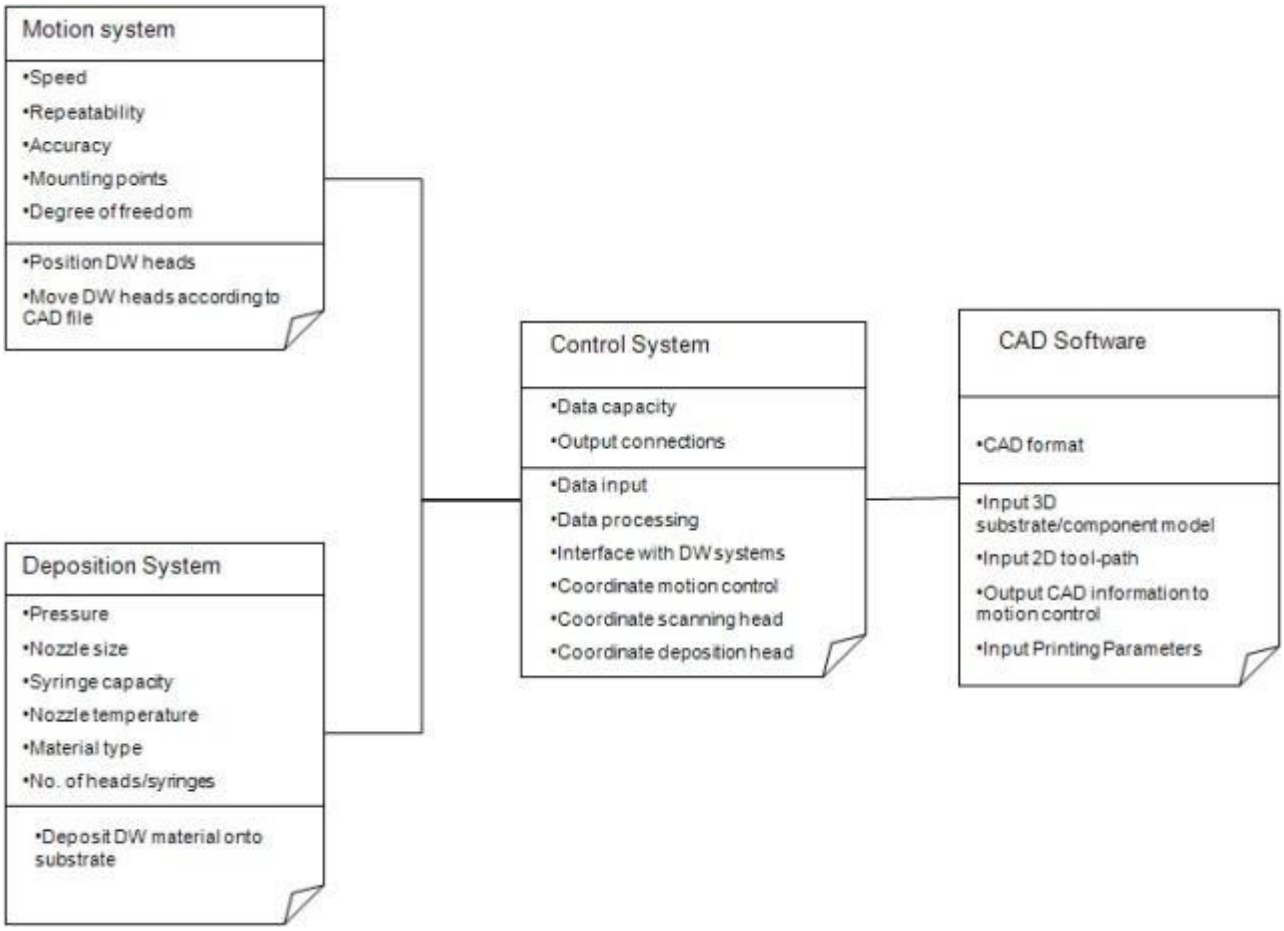

Figure 4:8: Class diagram for a general deposition system (scanning head remove CAD reference, motion system incorporates substrate).

Irrespective of DW technology employed, all the components are managed by a control system which co-ordinates the position of the deposition head with a suitable motion system. The tool paths for the DW system are entered by an operator. The tool paths must contain data detailing the DW pattern per layer, the DW structure (number of layers) as well as information on the geometry of substrate (which could be acquired through CAD data or a suitable scanning system). In this model it is assumed that all spatial co-ordinates for the DW system will be entered via suitable CAD software. This model shows that the objectives of the DW printing system match the required objects in the antenna architecture (i.e. patterning and structure of DW functional material). To accomplish these objectives each attribute in the printing system needs to be optimised.

From Chapter 2 it was shown that most DW ink materials require some form of post processing, such as curing in an oven, to solidify and functionalise the inks. Like the printing system, the post processing system needs to consider the structural properties and geometry of the substrate. From

the STA, it is known that the antenna requires printing onto large structures and so it is reasonable to assume that some form of localised heat treatment is required to cure the inks. The system architecture for this type of system is given in Figure 4:9.

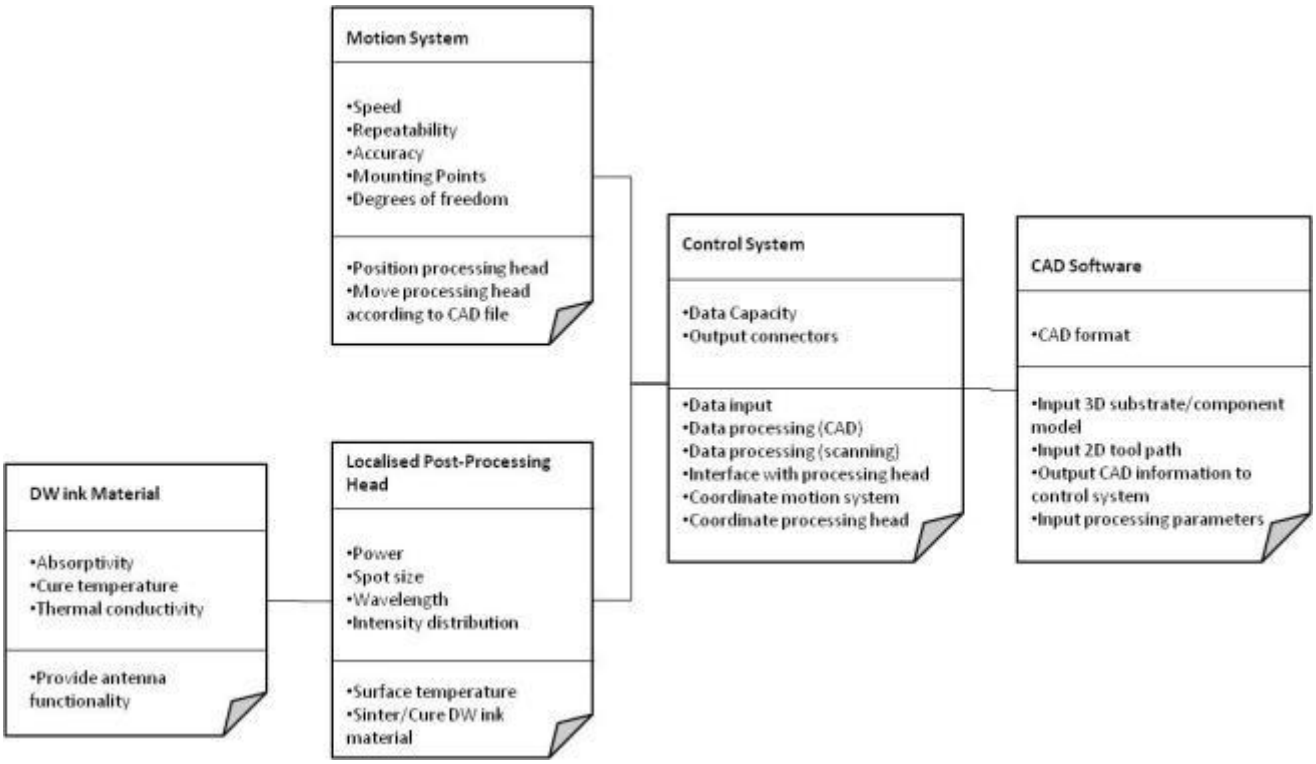

Figure 4:9: Localised processing system

It has been assumed that the localised post treatment will share many of the same type of components as the DW printing system (the motion system, motion control, and CAD implementation). This is useful as it means that the system solution can be designed so that the components are compatible and therefore easily integrated. As mentioned earlier in the antenna architecture the degree of cure is an important property in achieving DW material functionality, for the post processing system to achieve a high degree of cure it may require information on the curing, thermal and spectral properties of the ink material.

Each of these class diagrams represents the main DW sub-systems; in UML these are called packages. To summarise the whole system architecture a domain model can be produced. This shows the decomposition of the concept (known as the computational independent model, CIM) into the specific systems or packages, (the platform independent model, PIM) and finally into

possible solutions (Platform Specific Model, PSM). The domain model for the DW project is given in Figure 4:10.

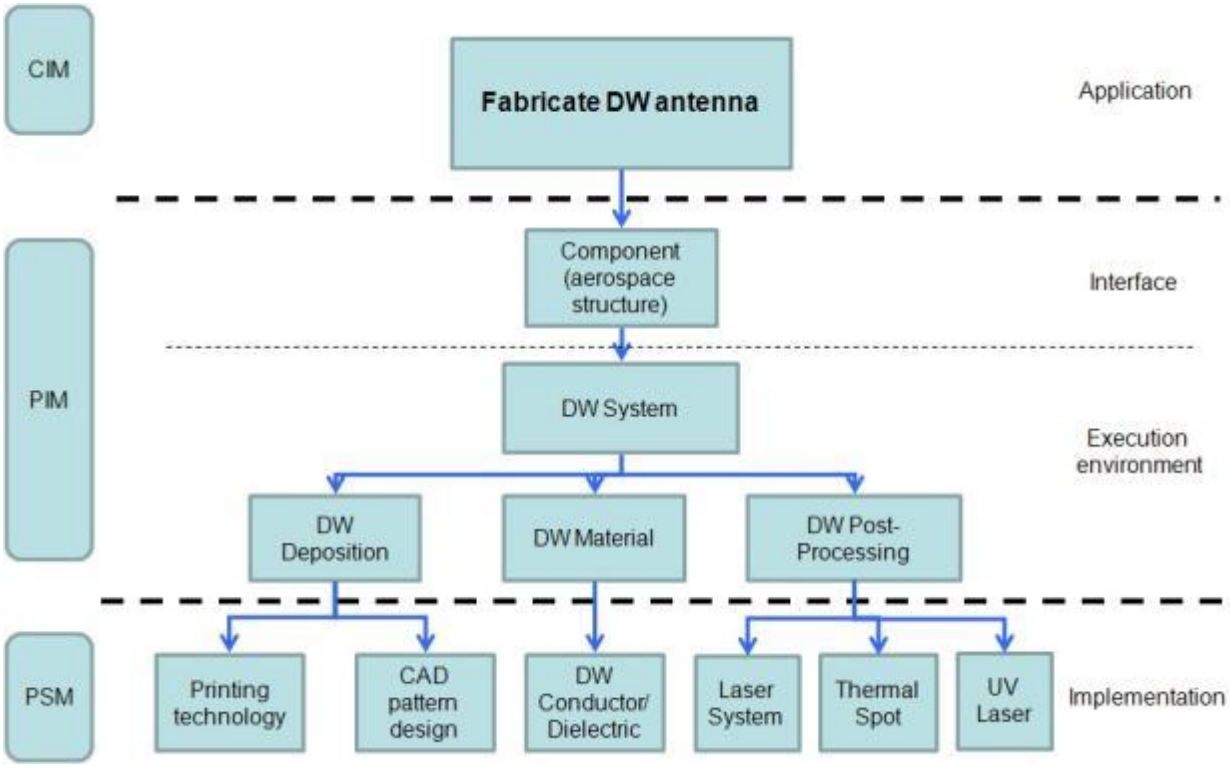

Figure 4:10: Overall System Architecture using Domain model

4.2.5 Through-Life considerations

One of the downsides of the class diagrams is that they fail to fully capture the through life requirements. Essentially there are two technologies in this project that have life-cycles, the DW system and the DW antenna. Through-life consideration focus on how the technology is deployed, supported and eventually disposed (i.e. the final three stages in the CADMID cycle). There are a number of methods which can aid the through-life process such as minimising the number of components and complexity of the system. Another important consideration is to make sure components are decoupled so that relationships are not critical, i.e. if there is a failure in a component it doesn't necessarily bring the whole system down.

One of the concerns with DW devices is how to support and maintain them. Assuming connectors, power sources etc. are ignored (for the purposes of this thesis) the critical components are the DW materials. Hence, the failure mechanisms are likely to be the behaviours and interactions between the DW materials. Factors such as material durability in harsh aerospace environments and ageing

will have consequences on the system functionality over the antenna lifetime. Repair of DW Antenna may require the use of the DW printing system, this may result in additional requirements which need to consider material removal, logistics (for in-situ on-site repair) and safety (localised processing/motion system). Solving these aspects of the problem is considered to be outside the scope of this research project but should still be included in the customer's requirements.

4.3 Requirement Analysis Solution Exploration

From the SE viewpoint of DW, the systems architecture developed in section 0 and the background information collated in chapter 2 a specific set of functional statements can be devised that will provide antenna capability using DW. It is essential that each functional statement is related to a system component and can deliver the relevant attribute/attributes and structure identified in the UML class diagrams.

Using Quality Functional Deployment (QFD) these functional statements or system 'how's' can be traced back to the original customer requirements, or 'wants'. The goal of QFD is to incorporate, engineering judgment and knowledge to provide organisation of the system functions and facilitate responsiveness to the customer requirements. The main body of the QFD matrix is used to assign relationship weightings between the customer and functional requirements. The 'roof' of the QFD (Figure 4:11) contains a further matrix which identifies the correlation between each of the system functions; some will have positive correlations whereas others may contradict each other. It is up to the systems engineer to determine what the tradeoffs and priorities are. This can be aided by providing additional weightings of importance against the customer requirements. This process helps to encourage identification of potential risks and issues at an early stage in the system lifecycle [102].

The bottom half of the QFD (Figure 4:11) determines what the target or optimum performance requirements are against each function and how difficult it may be to achieve the desired capability. Using this information combined with the customer weighing an importance value can be calculated against each function and subsystem highlighting key areas of development.

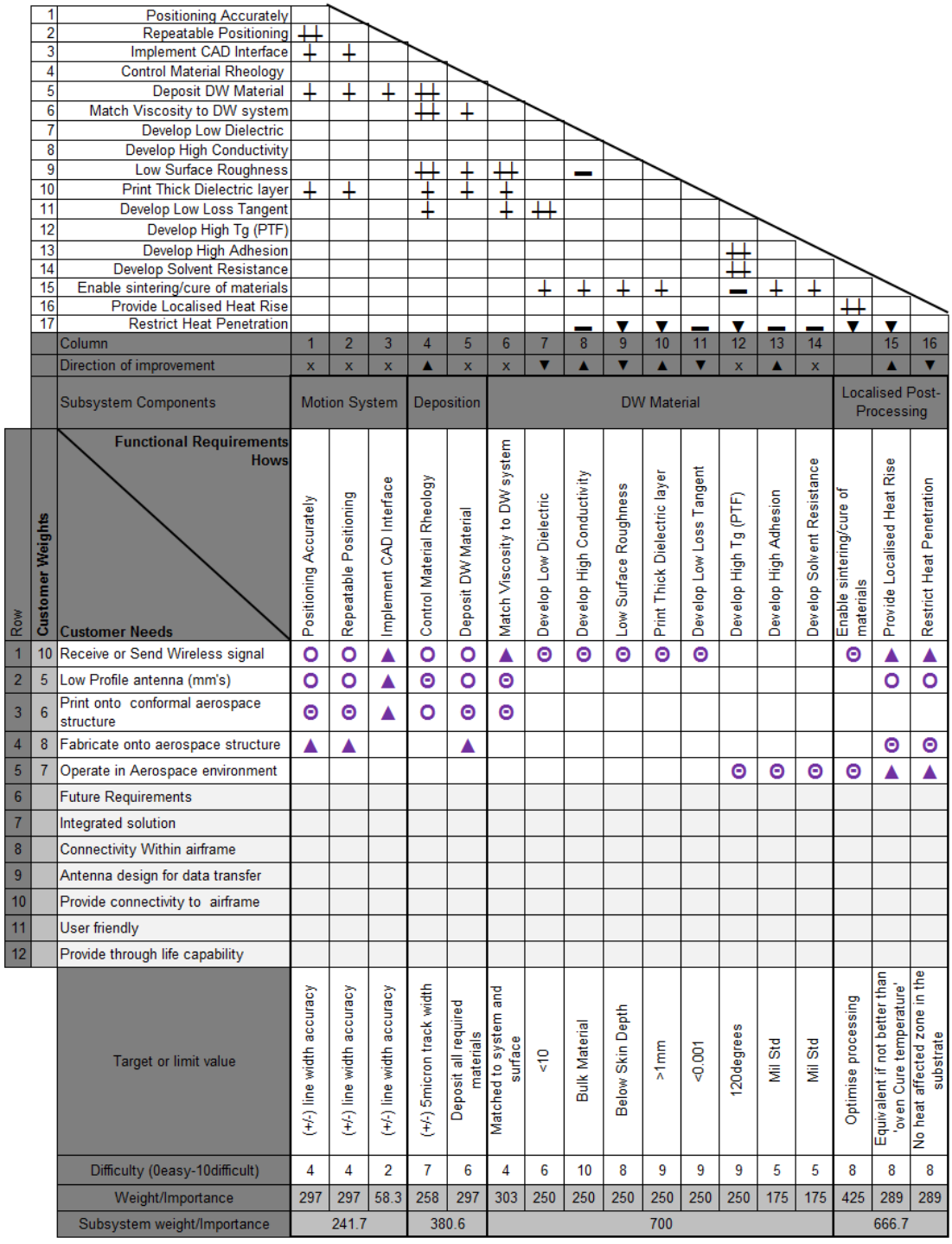

Key	Description	Relationship weight
Θ	Strong relationship	900
O	Moderate relationship	300
▲	weak relationship	100
++	Strong positive correlation	
+	Positive correlation	
−	Negative Correlation	
▼	Strong negative correlation	
▼	Minimise	
▲	Maximise	
x	Target requirement	

Figure 4:11: Quality Function Deployment (QFD) for DW: Conformal Antenna modified from [116]

The QFD in Figure 4:11 shows the relationships between the customer requirements and the systems solution as well as the priority/importance for each development. Customer weightings, relationships and difficulty ratings were derived through background reading and consulting with technical experts. The importance ratings were calculated using a combination of customer weights and their corresponding relationships (strong/moderate/weak) whereby:

Importance rating = (Σ(corresponding customer weight x relationship weight)) /total customer weight

The QFD identifies material development as the key research activity as it is highly related to two of the main customer 'wants', antenna functionality and durability. Related to high durability is the adhesion and solvent resistance of the material.

From the correlation matrix (QFD 'roof') it can be seen that there is high association between the localised post processing functions and each of the material functionalities. For example high curing temperatures may increase or improve the material functionality. However this may have consequences on other customer requirements such as being able to fabricate the antenna on to an aerospace structure such as carbon fibre which may be sensitive to high temperatures.

Where known, a number of target values have been set for the proposed functions, for example a target for the electrical conductivity of the DW material can be set based on the research conducted in Chapter 3. For some requirements it is more difficult to set a target parameter and it is better to keep it more open ended.

The future or customer requirements have also been included in the QFD. This allows the designer or research to develop the technology whilst keeping these requirements in mind. This can be important as eventually processing speed, repair and integration will all become very important if the technology is to be fully implemented.

4.4 System Verification: Technical Performance Measures

The verification phase of the SE lifecycle involves identifying measurable and tangible Technical Parameters, TP's, which can be assigned to the system performance or functional requirements in the QFD. To track, measure and verify each TP a Technical Performance Measure TPM is determined. This essentially defines the research methodology for this project. The TP and TPM's for this project

are documented in appendix B. Details of the measurement methodology and will be expanded further in Chapter 5 and in the subsequent technical Chapters.

Final system verification will be handled by demonstrating an operational antenna. Demonstration of the antenna will incorporate all of the system processes and material functions.

4.5 Conclusions

The SE process to this point has been used to define the stakeholders, the problem concept, and to elicit the project requirements. Using stakeholder knowledge and background research a System Architecture has been developed using UML class diagrams to model the Antenna device, DW printing and post processing systems. This information was directly used to determine a set of functional and performance statements that will enable the parameters in these models to be realised. Confidence in these function requirements was provided using QFD analysis which relates them back to the customer needs. QFD was also used to provide research focus by highlighting key functions, using customer importance and difficulty weightings. From the QFD analysis it was concluded that there are two key areas in DW that require developing:

- Material development to meet the functional requirements of the antenna system
- Curing techniques to enable DW materials to be fabricated on to large aerospace structures

To monitor the development of the system functions, TP's, have been assigned and methods to measure and track them (TPM's) have been identified. The SE is an iterative process, and over the course of the research programme the functions and requirements were revisited and refined. The verification process must also constantly update the customer with developments and attain constructive feedback to ensure success.

Depending on the success of this programme, further projects will need to transition DW technology into manufacturing environments. At this point the SE process will become more involved, and will have to consider human, manufacturing and lifecycle influences.

5 Experimental Methods

Chapter 5 introduces some of the main DW printing technologies that have been investigated in this thesis. A brief overview of some of the key experimental techniques used to measure the basic properties of the DW materials has been introduced. More specific measurement techniques will be introduced in further chapters as they arise.

5.1 DW printing methods

As discussed in chapter 2 a typical DW system consists of three main components, the printing system, the deposition material and, if needed, a post processing system. The design and selection of the DW system is determined by the device/application requirements as identified in Chapter 4. Figure 5:1 shows how the functional requirements of the device can affect the choice of DW system components.

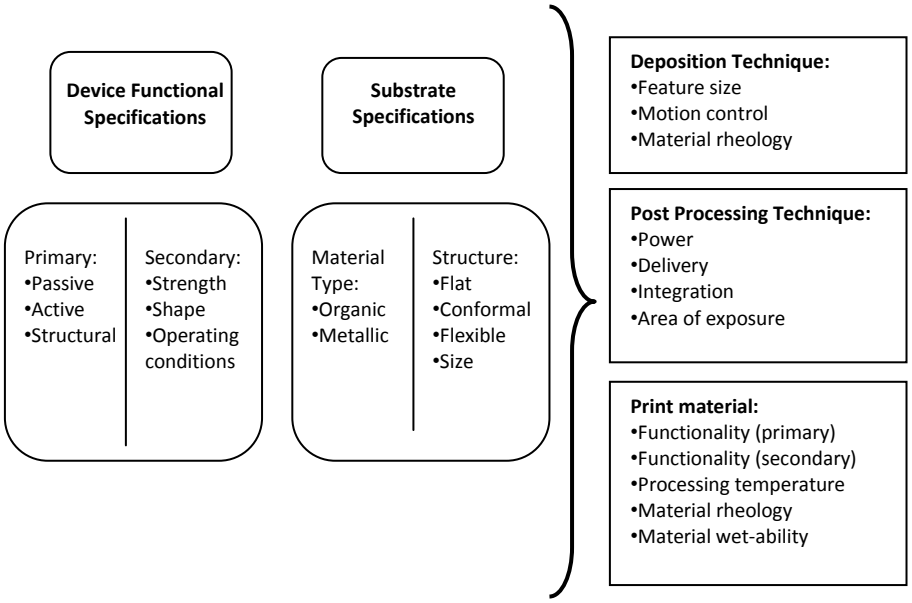

Figure 5:1: Factors for consideration when selecting a DW printing technology

As shown in Figure 5:1 the device and substrate determine which DW technologies are suitable for fabrication. In Chapter 2 it was discussed that the majority of DW technologies could offer conformal deposition if integrated with suitable robotics. The DW micro-nozzle system lends itself well to antenna fabrication due to its ability to use low temperature curable conductive and dielectric PTF inks. Inkjet systems are also particularly suitable for conformal printing as they require no direct

contact with the substrate. Inkjet systems are able to utilise high conductivity nano-particle ink solutions which can be sintered at relatively low temperatures. Both these systems were procured by BAE systems for the evaluation of DW in aerospace and defence applications.

5.1.1 Micro-nozzle system

The existing setup for the micro-nozzle system includes an Intertronics Digital Dispenser DK118, Keyence Lk-081 laser sensor, N-Scrypt Smart Z axis, two Naple Coombe (X and Y) motion control stages and a Servostep 1700 DMC motion controller. These components are interfaced and co-ordinated through LabView software specifically written for this system by N-Scrypt.

The micro-nozzle setup enables a 2D tool-path to be designed in AutoCad before being converted into .DMC format which can be uploaded to the DMC controller. Using the 2D tool patch the surface topography of the substrate is scanned using the Keyance laser displacement sensor. The data is then fed into the LabView software which is then used to control the smart z axis during printing. This step allows the offset distance between the micro-nozzle and substrate surface to be maintained within a +/-5μm accuracy. Once the surface has been mapped the LabView software initiates the printing procedure which involves activating the Intertronics Digital Dispenser and controlling the motion stages accordingly.

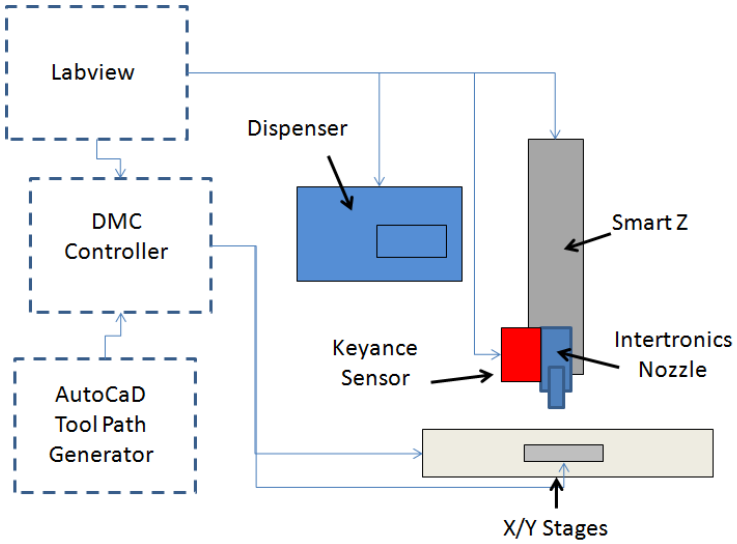

Block diagram of DW setup

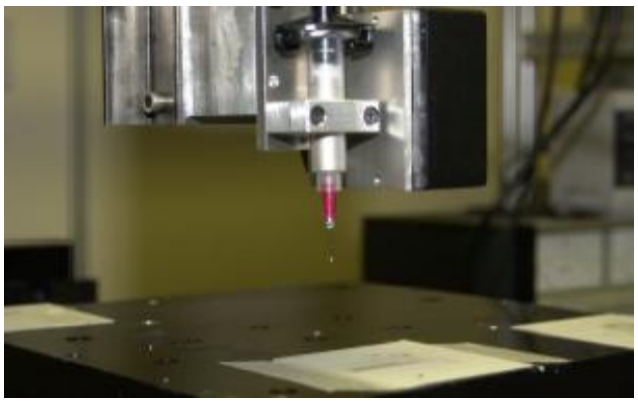

Micro-nozzle

Figure 5:2: Micro-nozzle system

The print resolution (height and width) of the micro-nozzle system is largely dependent on the deposition speed, pump pressure nozzle size and the contact angle the ink makes with the substrate system [16]. The Intertronics micro-nozzle system comes with variety of nozzle sizes, ranging from 0.2mm to 1.5mm (inner diameter). These nozzles allow ink viscosities between 7-15Pa.s to be deposited. Print accuracy is dependent on the accuracy of the motion stages and the calibration between the micro-nozzle system and laser displacement sensor. The process of calibration can lead to measurement errors and is limited by the size of the laser displacement sensor (70μm spot size) and measurement error (approximately +/-30μm).

One of the other problems that affect the deposition of ink through the micro-nozzle is the presence of air-gaps in the ink. This can lead to voids in the deposit which can be difficult to repair accurately. One method used to remove the air gaps in the ink is to completely de-gass it in a centrifugal mixer. For this an ARE-250 Thinky Mixing Machine was used. It was found mixing for 15mins removed air gaps in the ink completely as shown in Figure 5:3.

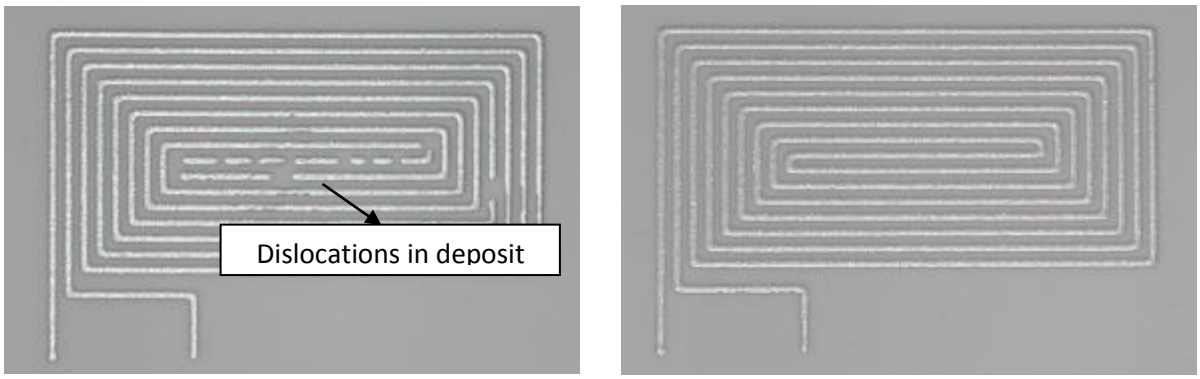

A. B.

Figure 5:3: (A) The effect of air gaps within the ink (B) Result after degassing for 15mins

5.1.2 Inkjet System

To conduct the inkjet prints a single 80µm Microfab MJ-ATP inkjet was used which was mounted on to a 5-axis Aerotech gantry system as shown in Figure 5:4. All tool paths for the 5-axis system were generated in Mastercam CAD/CAM software before being uploaded to the Aerotech controller. Whilst the Aerotech system allows for conformal DW, this capability was not used in this study and instead all elements were fabricated using only the x/y/z axis.

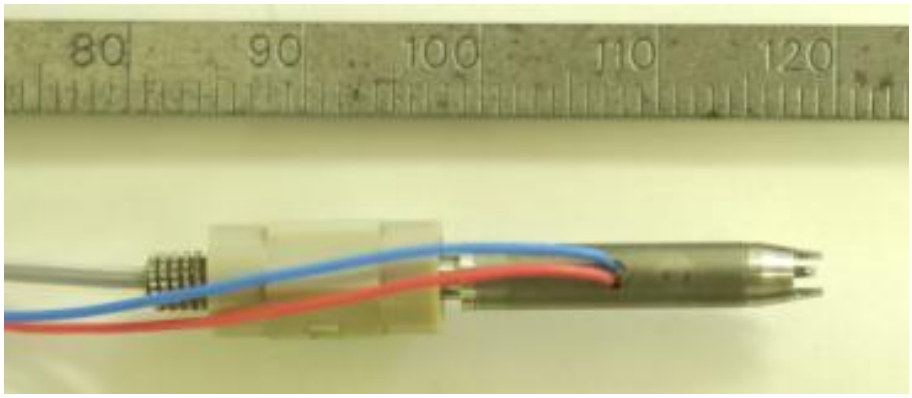

A.

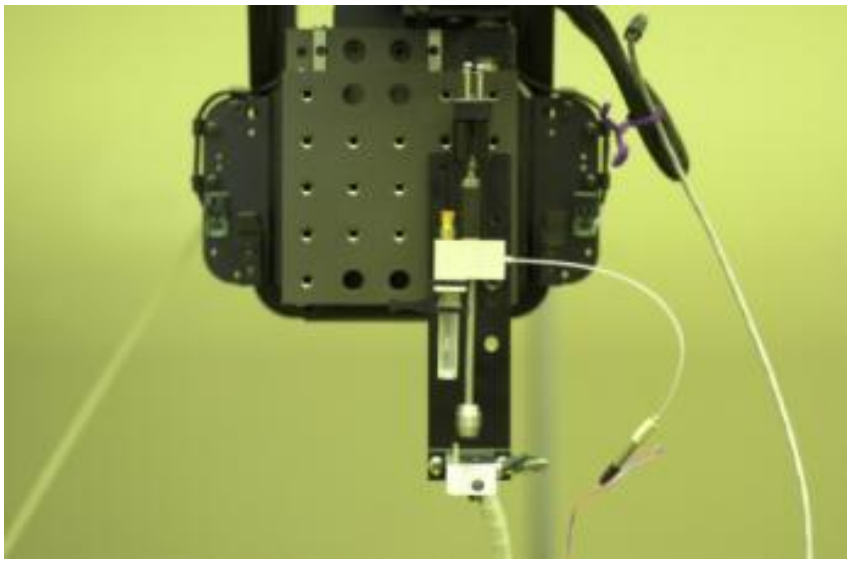

B.

Figure 5:4: (A) 80μm Microfab inkjet head (B) Inkjet head mounted on to 5-axis gantry system

The Microfab MJ APT jetting head is based on a squeeze mode piezoelectric design. In this setup a ceramic tube, with an electrode on its inner and outer surfaces, encloses a capillary where the ink flows. When a voltage pulse is applied, the transducer contracts and will eject ink out of the orifice. Ink is pushed both ways. However, due to the acoustic impedance of the tube's small bore and length considerably more material is ejected out of the nozzle. Conversely as the piezoelectric returns to its steady state (or expands due to negative voltage pulses) the negative pressure exhibited is not enough to overcome the surface tension of the ink at the orifice. This leads to ink being drawn into the device from its reservoir and not through the orifice.

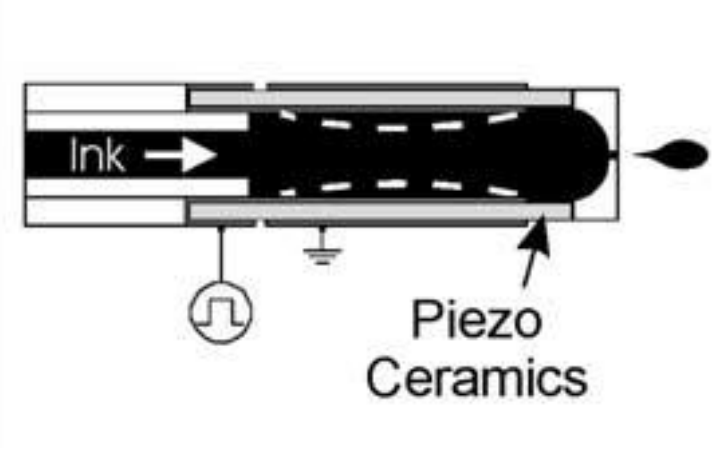

Figure 5:5: Squeeze mode piezoelectric design (Modified from Wijshoff, H [117])

The applied voltage or voltage waveform determines how the droplet is deposited from the jetting head. To monitor the droplet as it exits the jetting head a Prosilica GigE camera (model GE1350C) was used. To illuminate the droplets an LED source is used which pulses at the same frequency as the droplets exiting the nozzle. The droplets were captured by the camera by setting the exposure time to ~1 second to produce a stroboscopic image made up of thousands of droplets superimposed on each other. The repeatability of the process enables a clear, sharp and well defined image to be taken, mimicking a high speed camera. An image of a droplet (from a silver nano-particle ink) exiting the nozzle with a bipolar waveform is shown in Figure 5:6. This waveform setting allowed consistent and repeatable deposition of the silver nano-particle inks used in this thesis.

A.

B.

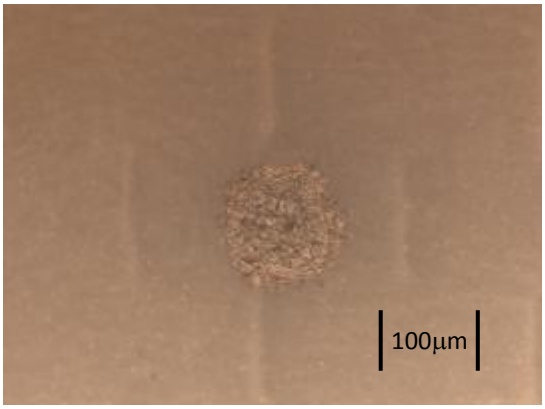

C.

Figure 5:6: (A) Waveform used to print silver nano-particle ink (B) Image of droplet exiting nozzle (C) Printed nano-particle ink on polyimide substrate using above waveform with a traverse speed of 100mms^{-1}

5.1.2 Tape Cast Printing

An additional way of depositing DW inks is to cast them using a mask or a tape. This is particularly useful when conducting material analysis because it isolates the ink material without influence of the printing method (which could affect surface roughness and functionality). This is also useful for depositing a large amount of material on to a flat substrate relatively quickly with a repeatable deposit thickness.

Figure 5:7 illustrates the tape cast process. Essentially a 40μm thick Tamiya masking tape was used to create a mask on to a flat substrate. Ink is applied into the channel created by the mask and a doctor blade is used to smooth the flow along the channel creating an even deposit. The ink can then be dried at low temperatures before removing the tape and curing.

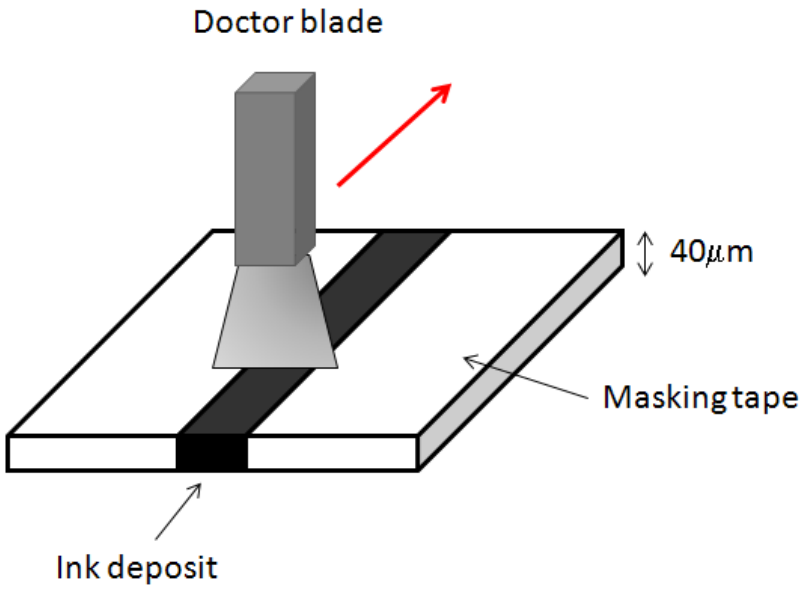

Figure 5:7: Tape cast method

5.2 Functional Measurements

Using the printing systems mentioned above the DW ink materials and processes were investigated for their durability, basic functional properties (such as adhesion, conductivity) and RF performance. As mentioned in Chapter 4 there are a number of key performance parameters which are linked to the performance of a DW antenna (see Appendix B), however, the main parameters that will be assessed throughout each chapter are:

- Ink Resistivity/Resistance (refer to Appendix B: DW/M/TP7, DW/M/TP8)
- Deposit Height (refer to Appendix B: DW/M/TP9)
- Surface roughness (refer to Appendix B: DW/M/TP9)
- Adhesion (refer to Appendix B: DW/M/TP12, DW/M/TP13)

This section will describe a number of standard methods used to measure these parameters for reference in later chapters.

5.2.3 Resistivity/Resistance Measurements

The basic equation for volume resistivity is given by [118]

$$R = \rho \frac{l}{A}$$ **Equation 5:1**

Where R is the resistance, ρ is the resistivity, l is the track length and A is the cross-section area of the conductor.

If the dimensions of the line or track are known (or can be measured accurately) then resistivity can be found by measuring the resistance of the track. To conduct the two wire resistance measurement a FLUKE 8845A digital multi-meter was used [119].

A multimeter can be used to measure the majority of resistances, however, for resistance in the milli or micro-ohm range a multimeter is not as accurate enough due to the effects of contact resistance [120]. Contact resistance is the additional resistance contribution from the wires, probes and leads used to measure the resistance of the device [120] [121]. A four-point probe can be used to eliminate contact resistance and is used to directly measure the sheet resistance of a thin film of uniform thickness. A schematic of the four-point probe is given in Figure 5:8.

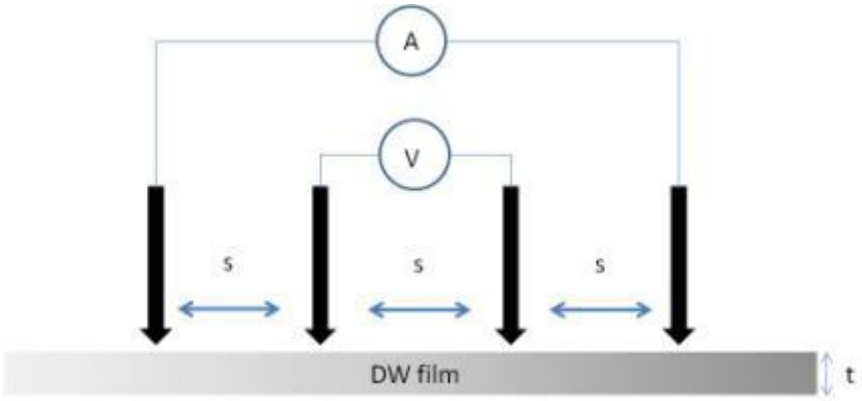

Figure 5:8: Schematic of four point probe measurement

In four-point probe measurement a fixed current, I, is injected into a film of thickness t, through the outer probes and the voltage V, is measured via the two inner probes similar to the four-wire resistance measurement. In this setup the probes are spaced equally by a distance S. The sheet resistance R_{sq}, can then be given by Equation 5:2 if the probe spacing is much greater than the thickness of the sample (s>>t) and much smaller that the diameter of the sample d (S<<d) [122].

$$R_{sq} = (\Omega / sq) = \frac{\rho}{t} = \frac{\pi}{\ln 2}\frac{V}{I} = 4.532\frac{V}{I}$$ **Equation 5:2**

To conduct the four-point measurements a Jandel Universal Probe station was used with a Keithly 220 programmable power source and a Kiethly 2000 power source. In this setup the current was set to 4.532mA so that the sheet resistance is simply the voltage reading (mV) on the multimeter in mΩ. The resistivity can then be found by measuring the thickness of the sample and multiplying it by the thickness.

5.2.4 Deposit Profilling

To measure the sample thicknesses and surfaces roughness values an Alphastep 200 step profiler was used. The Alphastep 200 comes with a programmable X-Y stage and a 9 inch monitor which displays a magnified view of the sample and stylus during the scan as well as the scan profiles and summary of the scan data. The Alphastep measures small steps with a 40nm horizontal resolution and has a vertical (height) resolution of 0.5nm. The maximum sample dimension is 16.5mm thickness with 162mm diameter [123].

Figure 5:9: Alphastep 200 (image from BSI Brumely South [124])

5.2.5 Adhesion Measurement

A number of methods can be used to measure the adhesion of the DW samples. The most simple and inexpensive test method is the peel test based on the ASTM D3359 standard. This method uses a semi-transparent, pressure sensitive tape, 2.5cm in width to test the adhesion of the coating. Qualitative assessment is carried out by creating an X-cut (method A) or cross-hatch pattern

(method B) in the coating with a carbide tool tip before applying and then removing the tape to see how much material is removed. In the method used in this thesis cuts were not created in the film and instead the adhesion was measured by measuring the resistance before and after applying the tape.

A more quantitative method of measuring the adhesion is the ASTM D4541 standard pull-off PATTI test. To conduct these measurements an Elcometer 110 PATTI tester was used. This system uses a pneumatically operated piston to apply a tensile force along the axis of a pull stub which has been glued to the coating. The size of pulling piston determines the maximum load that is applied to the coating. In most cases DW inks were tested using a F2 (max. load 2000Psi) or F4 (max. load 4000psi) piston. The PATTI tester measures the pressure in the piston during the test and records the pressure at the point of failure. This value can then be converted to bond strength in MPA [125].

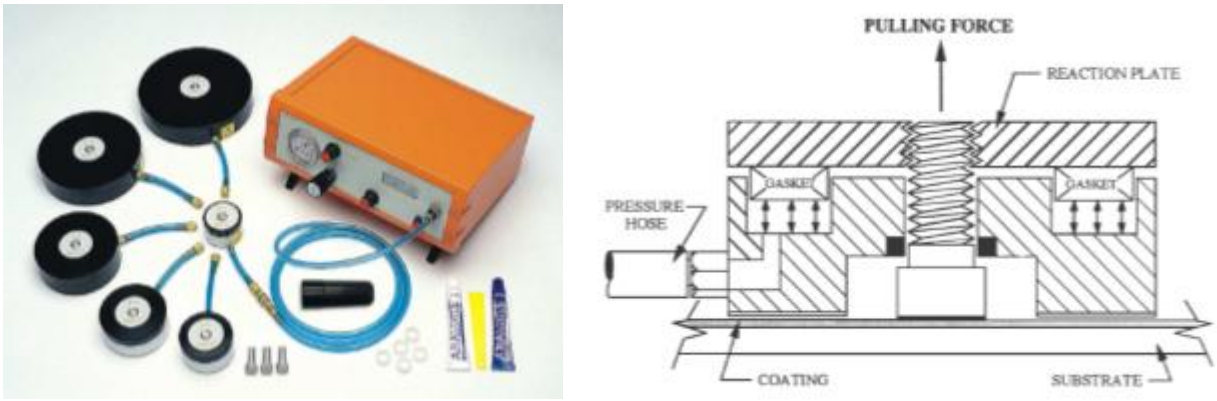

A. B.

Figure 5:10: (A) Elcometer 110 PATTI tester showing the different piston sizes (B) Schematic of operation (images from Elcometer [125])

5.3 Conclusions

This chapter has introduced the two main printing systems that will be investigated for antenna fabrication, the N-Scrypt DW micro-nozzle system and the Microfab inkjet system. Both these systems have been integrated on to suitable robotics to allow for deposition on to planar surfaces. Conformal printing was not investigated in this thesis but is an area of research which could form part of a further study.

A brief overview of the experimental techniques used to measure the basic functional properties of the DW materials has also been given. Further measurement methods will be introduced in their relevant chapters.

6 DW Material Characterisation for Aerospace applications

This chapter characterises a number of conductive DW materials based on the material requirements identified in Chapter Three. The DW materials selected in this study can be deposited using either inkjet or micro-nozzle printing systems (described in more detail in Chapter Four). Whilst most literature has investigated the main functional properties of DW deposits (such as conductivity and adhesion) this study will also asses the durability of the inks against known aerospace/defence requirements. A summary of the parameters investigated in this chapter is given in Table 6:1. The RF performance of these inks will be further investigated in chapter 10.

Functionality	Processing	Durability
• Adhesion • Conductivity • Surface Roughness	• Processing Temperature • Rheology	• Temperature range • Humidity • Corrosion • Fluid/solvent immersion

Table 6:1: DW material test parameters

6.1Project Material Overview

Table 6:2 gives an overview of the main conductive inks acquired for this project. These inks were based on three different carrier systems: a PTF thermoplastic resin, PTF thermosetting resin and inkjet solvent system. Both the inkjet silver and PTF thermoplastic inks were Commercial off The-Shelf (COTS) inks obtained from Sun Chemicals [126] and Electrodag [127] respectively. The PTF thermosetting silver inks (PTF Silver and PTF Silver Hybrid) were developed in conjunction with Gwent Electronic Materials (GEM) as part of the DW EASY project [128]. These inks were designed specifically to have high adhesion and durability on typical aerospace structures such as carbon fibre and primed metals (such as Aluminium 2024 and Steel).

Ink Type	PTF Silver	PTF Silver Hybrid	PTF Silver Thermoplastic	Inkjet Silver
Manufacturers code	GEM, C2050712D58	GEM, C2080929D6	Electrodag 725A	Suntronics U5714
Carrier	Thermosetting Polymer binder	Thermosetting Polymer binder	Thermoplastic Polymer Binder	Solvent
Silver Content (w.t. %)	Silver flakes, 58.8%	Silver Flakes, Silver soap, 61.29%	Silver Flakes 58.0 – 62.0%	Nano-Silver Particles 40%
Recommended Curing	130°C, 20mins	180°C 20mins	120°C, 15min	150°C-300°C, 30mins
Resistivity (Ω/sq) (where specified)			37.5	5-30
Viscosity (Cps)	7098	44050	11000-14000	10-14
Deposition technique	Screen Printable, Mico-nozzle	Screen Printable, Mico-nozzle	Screen Printable, Mico-nozzle	InkJet

Table 6:2: DW inks properties [129] [127] [126]

The silver and hybrid silver thermosetting conductive inks contain silver flakes (30μm diameter, 2μm thickness) dispersed (approximately 60% in volume) in a thermosetting epoxy based resin binder designed to cure at temperatures as low as 90°C. The recommended oven curing temperature for this resin, stated by the manufacturer, is 130°C for 20mins; this allows the composition to achieve high flexibility, good adhesion and electrical conductivity. The hybrid silver ink differs in that it contains an additional organo-metallic/silver salt component. At high temperatures (>160°C) the organo-metallic component decomposes into silver nano-particles which fuse, thereby increasing the electrical conductivity of the composition. This ink was developed to give the advantages of both PTF inks and nano-particle sintering in the same ink composition.

6.2 Conductivity and Adhesion Measurements

6.2.1 Comparison of ink conductivities

The inks identified in Table 6:2 were measured and compared for material conductivity based on their manufacturers stated cure. For comparisons these inks were also tested at the same elevated cure temperature of 200°C. This elevated curing temperature was selected as it enables all inks to be compared under the same processing conditions whilst also being sufficient enough to sinter the nano-particles in the Hybrid silver and inkjet silver ink (see Figure 6:10).

To prepare samples for conductivity measurements the inks were printed on to Alumina (96%, Al_2O_2) ceramic tiles. Alumina was used as it is able to withstand high temperatures and its low surface

roughness (0.19μm as measured by the alpha step) allows the height of the ink coating to be easily measured. DW PTF inks were applied to the ceramic using the tape-cast method described in Chapter Four. This method was used as it enables the conductivity of the material to be measured irrespective of the printing technique. Unfortunately the inkjet ink could not be applied using this method as the ink tended to seep under the tape due its low viscosity. Instead the inkjet silver ink was printed on to a polyimide substrate using an 80μm Microfab MJ-ATP inkjet head attached to an X/Y motion stage.

This gave a track width on the substrate of approximately 150μm when printed at 1000Hz (1000 drops per second) at a traverse speed of 80mms^{-1}. To increase the width of the deposit adjacent tracks were printed with an overlap of approximately 120μm. This overlap ensured that there were no pinholes in the deposit.

Conductivities were calculated using a four-point probe measurement technique described in Chapter 4. This method requires that the width and length of the conductive coating is much larger than the spacing between the probes on the measurement device (5mm). To comply with this the inks were printed with dimensions of approximately 30mmx60mm as shown Figure 6:1.

Figure 6:1: DW Silver hybrid ink sample applied to Alumina Tile for conductivity measurement.

The four-point probe measurement technique measures the sheet resistance of the ink. To convert this into bulk resistivity the height of the sample must be known. The height of the PTF inks coating were measured using an Alpha Step 200 touch probe. The conductivity results are shown in Table

6:3 . To allow for comparison these values were also plotted as a percentage of the bulk conductivity of silver ($1.6e^{-8}\Omega m$) in Figure 6:2.

	Cure Time (mins)	Cure Temperature (°C)	Height (μm)	Sheet Resistance (Ω/sq)	Resistivity (Ωm)	Conductivity (Sm^{-1})
PTF Silver Ink	20	130	52	0.0232	8.32E-07	1.20E+06
	20	200	50	0.0150	1.16E-06	8.62E+05
PTF Silver Hybrid Ink	20	160	30	0.0211	6.35E-07	1.57E+06
	20	200	28	0.0055	1.54E-07	6.49E+06
PTF Thermoplastic Silver Ink	20	120	32	0.0230	6.272E-07	1.59E+06
	20	200	27	0.0196	6.21E-07	1.61E+06
Inkjet Ink	20	200	~2	0.0963	1.926E-07	5.19E+06

Table 6:3: Comparison of coating heights and sheet resistance measurement for DW inks

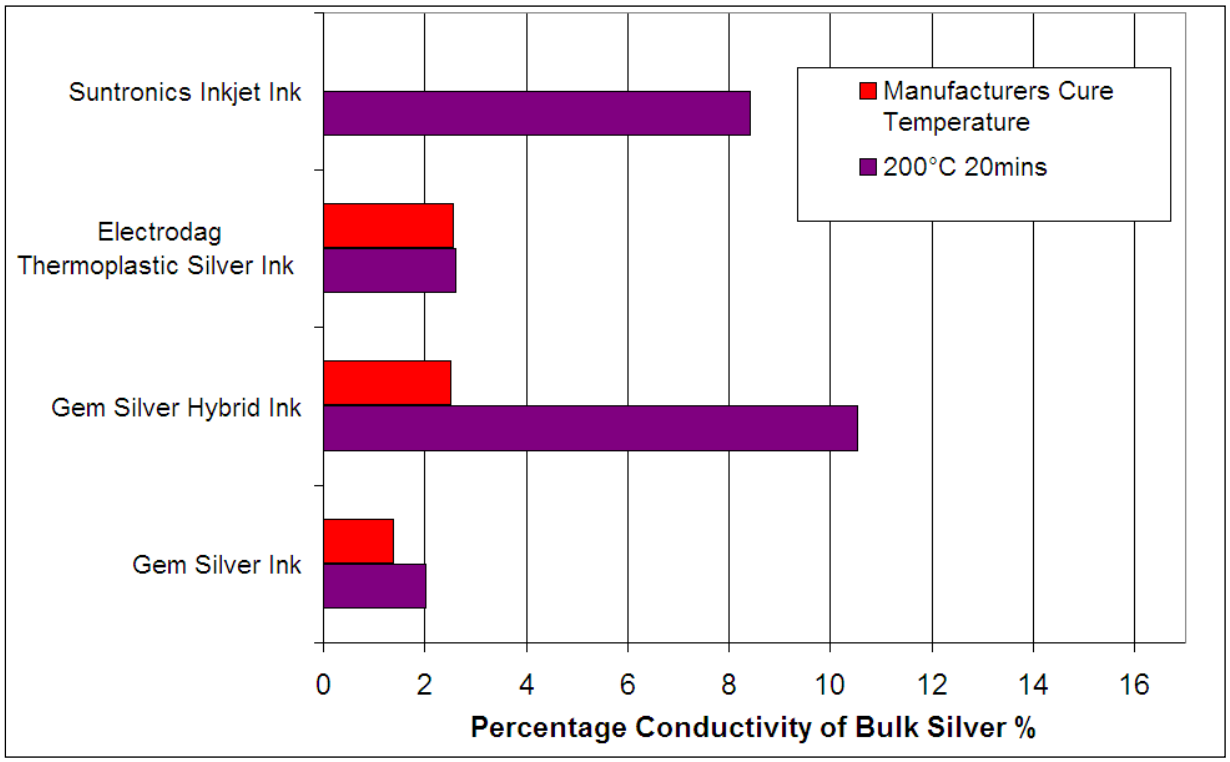

Figure 6:2: Conductivity of DW inks as a percentage of the bulk conductivity of silver when oven cured at 200°C for 20mins

The Results in Table 6:3 show that the inks exhibit higher conductivities when cured above the manufacture's stated temperature. For the Electrodag PTF thermoplastic ink the increase in conductivity is negligible. The PTF thermosetting silver ink on the other hand exhibits a 0.5% increase in bulk conductivity of silver whereas the Hybrid Silver ink increases by almost 8% bulk conductivity of silver. For the hybrid ink the rise in conductivity is down to the sintering of silver nano-particles within the ink composition according to the ink manufacturer [129].

Comparison of the DW inks when cured at 200°C for 20mins shows that the hybrid silver ink has the highest conductivity at just over 10% bulk silver. The thermoplastic and thermosetting inks have similar conductivities of approximately 2% bulk silver. The inkjet ink has 8% bulk conductivity of silver when cured at this temperature although the manufacturer has stated that greater conductivities can be achieved at higher processing temperatures (Table 6:2). To test this, a further inkjet track was printed on to a thin polyimide substrate with dimensions of approximately 100mmx3mmx2μm and cured at 350°C for 20mins. The track resistance was measured using a two-wire resistance method at 1.51Ω corresponding to a volume resistivity of $4.53 \times 10^{-8}\ \Omega m^{-1}$ which is 33% bulk conductivity of silver.

6.2.2 Adhesion of inks on to different Substrates

The adhesion of the DW inks was investigated on three different substrates of varying surface roughness, alumina ceramic, carbon fibre composite and primed aluminium (primed aluminium, was used to stop the conductive track from shorting with the substrate). The DW PTF inks were applied to the substrate using the tape-cast method and the inkjet ink was printed via the Microfab 80μm inkjet head MJ-ATP as described earlier. In most cases adhesion was also tested at two different cure temperatures (for 20mins); the manufacture's stated cure temperature and an elevated cure temperature of 200°C. At 200°C the carbon fibre composite begins to release unknown gasses which affect the adhesion of the ink. This is possibly due to solvent evaporation and/or decomposition of the resin used in the Carbon fibre. For this substrate an upper temperate limit of 180°C was used. Although this is still higher than the glass transition temperate of most carbon fibre resins there was no out-gassing from the substrate.

To measure the adhesion of the inks the ASTM D4541 standard pull-off PATTI test method was used. This technique has also been used in a similar experiment which investigated the adhesive strength of bonds in printed wiring boards before and after environmental exposure [130]. The glue (used to attach the PATTI stub to the coating) was also tested for adhesion on to these substrates to test its suitability. In addition to the PATTI test method a simple peel strength adhesion measurement was made (based on the ASTM D3359 standard but without cross hatching) using a 3M Pressure sensitive scotch tape. This method allowed a quick measurement to be made to see if the inks could meet a minimum standard.

Figure 6:3 shows two possible failure mechanisms after PATTI pull-off testing. Figure 6:3 A shows adhesive failure of ink to substrate whereas Figure 6:3 B shows cohesive failure of the ink. The

occurrence of cohesive failure shows that the bonding between the substrate and ink is greater than the molecular bonding in the ink itself.

A. B.

Figure 6:3: Removal of ink coating via pull-off adhesion test for (A) Adhesive failure of ink layer (B) Cohesive failure of ink layer

The results from the adhesive measurements are given in Figure 6:4 and Table 6:4. All results showed at least some form of failure indicating that the adhesive strength of the glue was stronger than the DW ink coating.

In general Table 6:4 demonstrates that the adhesion of the inks can be increased with increasing cure temperature. For the PTF thermosetting inks a higher cure temperature results in more adhesive failures. This trend can be attributed to the increased cross-link density with increasing cure temperature (this is discussed in section 5.3.3). The thermoplastic and inkjet inks have a much smaller increase in adhesion with cure temperature. The increased adhesion in these inks could be attributed to the densification of the ink as it is cured at higher temperatures. The silver particles in the inkjet ink will also undergo a greater degree of sintering at higher temperatures increasing the density of the ink.

Comparison of the ink coatings on different surfaces (Figure 6:4 and Table 6:4) shows that the adhesion increases with surface roughness. This is particularly evident with the inkjet ink which has low adhesion on alumina substrates but adhesion equivalent to the PTF inks on carbon fibre. In most inks the increased adhesion on rougher surfaces is better than the intermolecular bonding within the ink itself leading to more cohesive failures.

When cured at elevated temperatures (200°C, 20mins) the thermosetting PTF ink has the highest adhesion on all three substrates. At lower curing temperatures the thermoplastic PTF ink has better

adhesion. In each measurement Pull-off testing of the hybrid ink removed a small layer of ink resulting in cohesive failure. Although the hybrid ink is essentially based on the same resin system as the silver ink the silver particles do not seem to be as tightly bound.

Silver PTF thermosetting and thermoplastic inks passed the minimum adhesive requirement which was to withstand the tape peel test with no silver or resin removed. The inkjet also passed this standard on every substrate except the alumina substrate where the low surface roughness attributed to low adhesion. The hybrid failed the test on all substrates with a layer of silver removed after each test resulting in a measurable reduction in track resistance.

Ink	Substrate	Ra of Substrate (μm)	Cure Temperature (°C)	Adhesion (MPa)	Failure Type	Peel Test[3]
Silver	Alumina Ceramic	0.19	200	2.5	Adhesive	Pass
			130	0.98	Cohesive	Pass
	Primed Aluminium	1.18	200	4.33	Adhesive	Pass
			130	1.985	Cohesive	Pass
	Carbon Fibre	8.24	180	5.5	Cohesive	Pass
			130	4.9	Cohesive	Pass
Hybrid Silver	Alumina Ceramic	0.19	200	0.608	Cohesive	Fail
			180	0.55	Cohesive	Fail
			150	0.398	Cohesive	Fail
	Primed Aluminium	1.18	200	0.745	Cohesive	Fail
	Carbon Fibre	8.24	180	1.01	Cohesive	Fail
			150	0.603	Cohesive	Fail
Thermoplastic Silver	Alumina Ceramic	0.19	200	2.424	Adhesive	Pass
			120	2.23	Adhesive	Pass
	Primed Aluminium	1.18	200	3.95	Adhesive	Pass
			120	3.7	Cohesive	Pass
	Carbon Fibre	8.24	180	5.14	Cohesive	Pass
Inkjet	Alumina Ceramic	0.19	200	1.2	Adhesive	Fail
	Primed Aluminium	1.18	200	3.5	Cohesive	Pass
			150	3.2	Cohesive	Pass
	Carbon Fibre	8.24	180	5.33	Cohesive	Pass
Glue	Alumina Ceramic	0.19	24	3.6	Adhesive	Pass
	Primed Aluminium	1.18	24	5.4	Adhesive	Pass
	Carbon Fibre	8.24	24	5.8	Adhesive	Pass

Table 6:4: Adhesion of Silver and Hybrid Silver PTF thermosetting inks applied on different substrates of varying surface roughness and cured at different temperatures for 30mins

[3] ASTM D3359 standard but without cross hatching

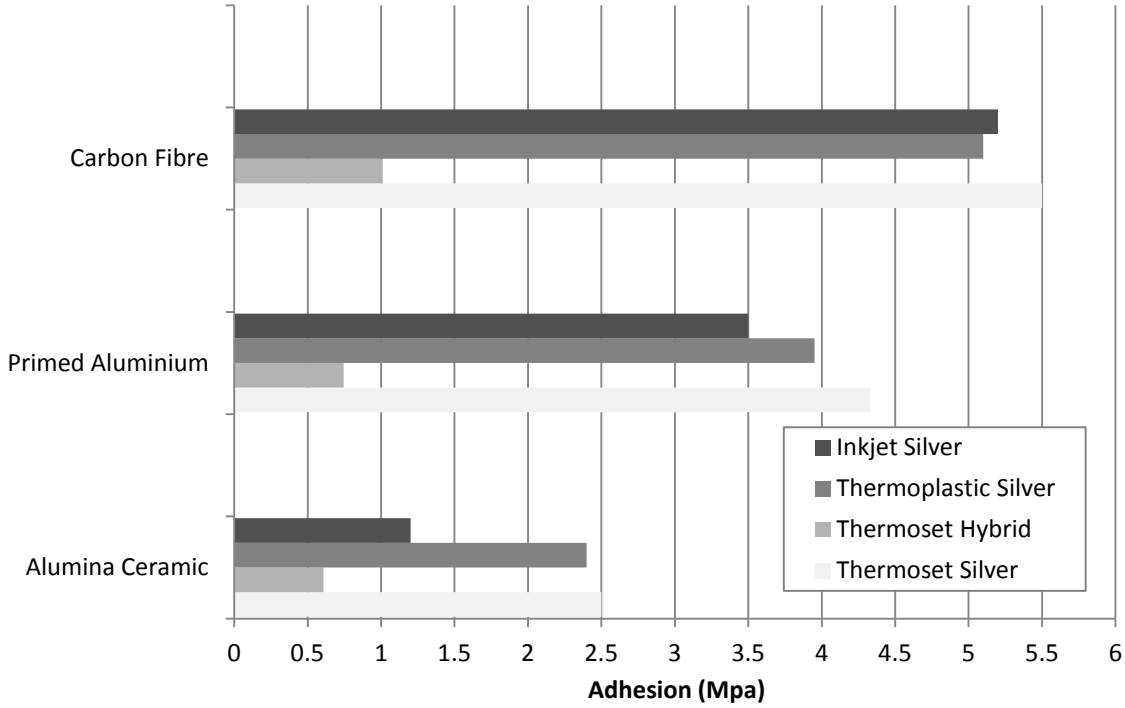

Figure 6:4: Adhesion of Silver Hybrid and Silver ink on aluminium and ceramic cured at 220°C for 30mins and carbon fibre cured at 180°C for 30mins

6.2.3 Discussion

The adhesion and conductivity of DW PTF and Solvent based inks have been investigated using different processing parameters. In both cases it has been shown that performance of PTF inks can be increased if higher cure temperatures are used. Inkjet inks also show improved conductivities at higher cure temperatures due to increased nano-particle sintering. As a result of these observations the optimisation of curing temperature and time on PTF inks will be investigated in more detail in section 5.4.

Material conductivity measurements showed that current DW inks are unable to meet the minimum 30% bulk conductivity requirement for RF applications when cured at 200°C (identified in chapter 3). Again conductivities may be increased with higher curing temperatures however higher processing temperatures may not be desirable for highly controlled aerospace structures. Alternative methods to improve the DW conductivities will be investigated in Chapter Seven and Chapter Eight.

The adhesion of all DW inks with the exception of the PTF Hybrid ink passes the minimum adhesion criteria. The Hybrid ink tended to have weak interlayer bonding resulting in a thin layer of silver being removed from the surface in all test methods. Whilst this ink has superior conductivity than the other PTF inks the poor adhesive properties make it less attractive for aerospace applications. As

expected the inkjet ink had poorer adhesive properties on the smooth Alumina substrate than the PTF inks but equivalent adhesion on the rougher surfaces. Results showed the thermosetting PTF Silver ink to have the best all round adhesion on all substrate types.

6.3 Surface morphology of printed PTF inks

This section characterises the parameters that affect the surface roughness of printed thermosetting PTF inks. The surface roughness of printed inks can be an important factor in both RF applications and multilayer prints. The exact morphology (and hence surface roughness) of a printed track is a function of both the rheology of the ink and surface energy of the substrate. Additional factors such as processing temperature can also play a part in the final structure.

The work presented in this section was in collaboration with Prof. Liang Hao and Dr Mike Sloan of Exeter University and was presented at the 36th MATADOR conference [131].

6.3.1 Viscosities of PTF Inks

The viscosities of the Hybrid and Silver Thermosetting PTF inks were measured at Exeter University using a rotational rheometer (TA Instruments AR2000) as a function of temperature. The results are given in Figure 6:5. At room temperature the viscosities of the silver and hybrid ink was measured at 25.27Pa.s and 81.58Pa.s respectively. As the hybrid ink has a higher viscosity it is more likely to be able to hold its printed profile with less spreading on the substrate. From a processing point of view the lower viscosity of the silver ink can be advantageous as it leads to reduced forces acting upon the print head and has less chance of clogging the nozzle head.

As the temperature increases the viscosity of the silver ink remains relatively constant up to 64°C when the onset of cure takes place and the viscosity rises sharply reaching undergoing a second transition where the viscosity rises less rapidly. The viscosity of the hybrid ink initially decreases with temperature reaching a minimum viscosity of 14.24 Pa.s at 68.7°C as opposed to the silver inks minimum of 20.01 Pa.s at 48.2°C. This suggests that printing at elevated temperatures then cooling/quenching the material on the substrate could be an approach to tailor the printing performance of the inks such as holding the shape of the tracks. Post 68.7°C the hybrid ink shows a steady increase in viscosity until around 90°C when the gradient becomes steeper. Note that the hybrid does not reach a plateau like the silver inks; this is due to its ideal cure temp being around 180°C.

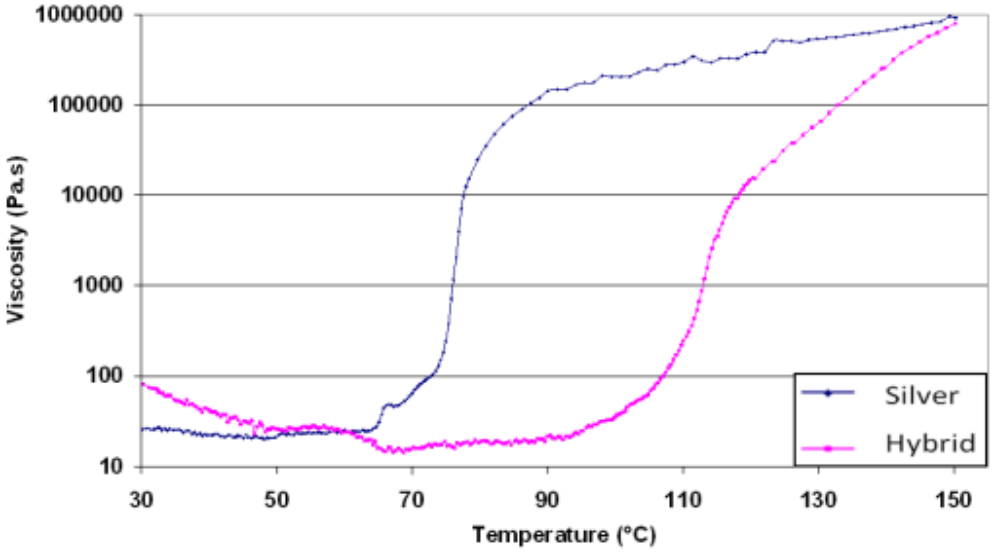

Figure 6:5: Viscosity of PTF thermosetting silver and hybrid inks as a function of temperature

6.3.2 Surface roughness of PTF inks on different substrates

Both the silver and hybrid PTF inks were deposited on alumina ceramic and carbon fibre substrates by the micro-nozzle DW process. The micro-nozzle system was configured with a nozzle of inner diameter 0.25mm and set with a deposition speed of 4mms^{-1} and dispensing pressure of 165kPa. Following DW deposition the PTF tracks were cured for 30mins, at 100°C, 130°C and 150°C and hybrid PTF tracks at 150°C, 180°C and 200°C in order to investigate the effect of curing above and below the supplier's recommended temperature.

The surface profile and roughness of the printed tracks and substrate were characterised using a Talyscan (Taylor Hobson) using a contact stylus. The average surface roughness of the alumina ceramic was measured at 0.24µm and the carbon fibre at 13.3 µm. The highest rough peak on the surface of the ceramic alumina is 8.5µm height and the coordinated weave of the carbon fibre substrate creates the highest surface peaks of 75µm height.

Figure 6:6 shows the track profile of the printed hybrid and silver ink tracks on the alumina and carbon fibre substrates cured at the manufacturer's recommended curing temperature (see Table 6:2). The track profiles for the hybrid ink are much higher than the silver ink; 40µm and 130µm for the former and 35µm and 83µm for the latter on alumina and carbon fibre substrates respectively. The hybrid ink also tends to keep its shape when deposited from the micro nozzle on both alumina and carbon fibre substrates. This is because the hybrid inks have a higher viscosity and therefore holds its printed profile, while the lower viscosity silver inks is likely flow outward, thus reducing the profile of the track.

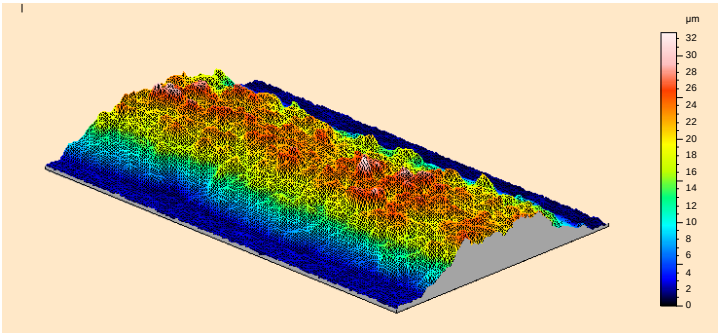

A

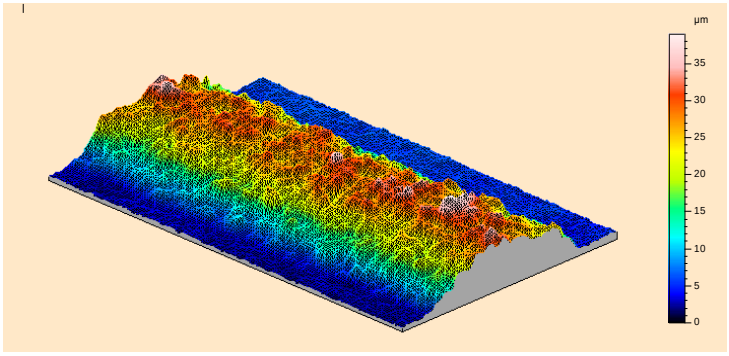

B

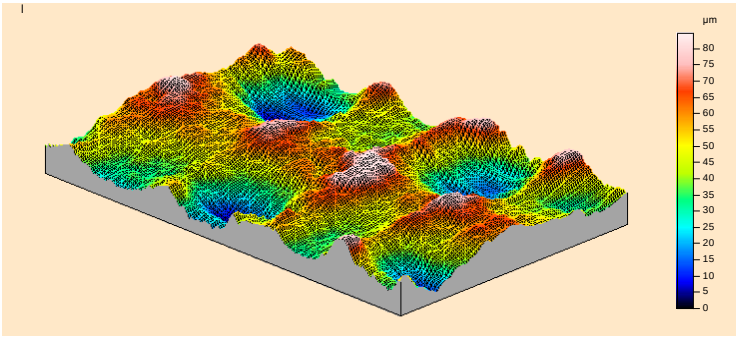

C

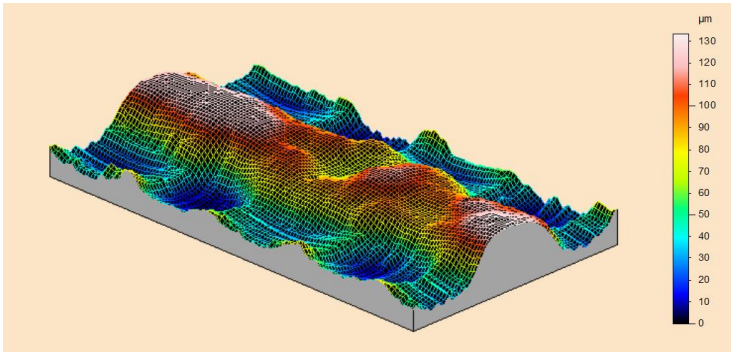

D

Figure 6:6: Surface profiles of (A) the printed silver ink on alumina, (B) the printed hybrid ink on alumina, (C) the printed silver track on carbon fibre, (D) the printed hybrid on carbon fibre

Figure 6:7 compares the average surface roughness R_a, of the hybrid and silver inks on both the alumina and carbon fibre substrates. The R_a of the cured silver tracks on the carbon fibre substrate (R_a 4.74) as more than double that on the alumina substrate (R_a 2.27); while for hybrid inks, the R_a of the cured tracks on the carbon fibre substrate (R_a 6.1) is nearly 3 times that on the alumina substrate (R_a 2.51). These results also show that the surface roughness of the cured tracks is correlated to, but not directly proportional to that of the substrate as the surface roughness is 31 times the difference between the alumina and carbon fibre substrates.

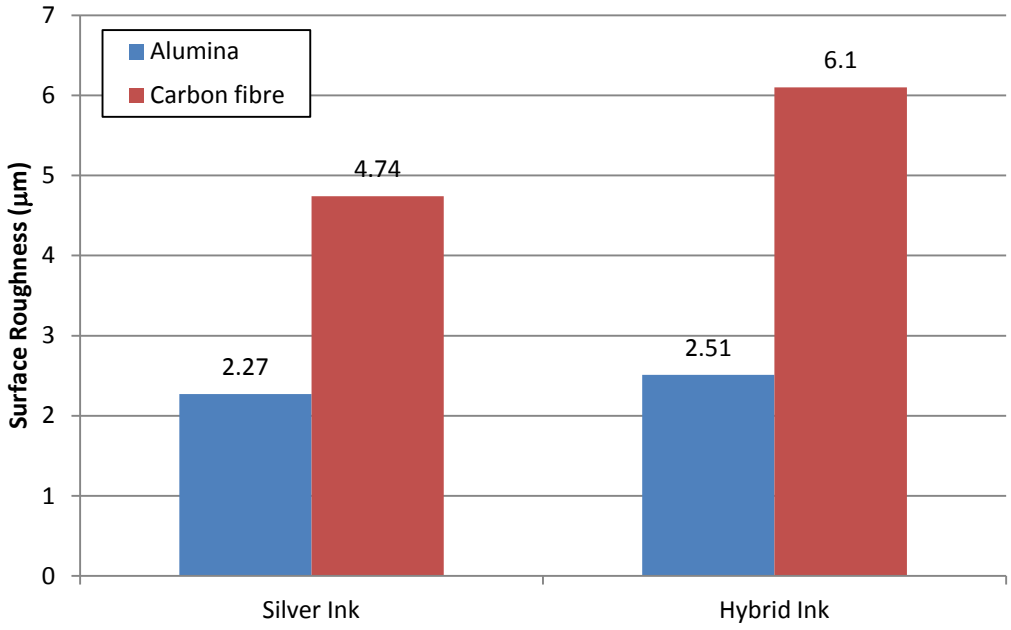

Figure 6:7: Surface roughness of micro-nozzle printed silver ink and hybrid ink tracks on Alumina and Carbon Fibre substrates.

6.3.3 Surface Roughness of PTF inks as a function of cure temperature

Figure 6:8 shows the effects of curing temperature on the surface roughness of silver and hybrid inks on alumina substrates. For this measurement the Talyscan measured the surface roughness over three different scanning areas 10mmx0.2mm, 5mmx0.2mm and 2.5mmx0.2mm. For hybrid tracks, the surface roughness decreased with increasing curing temperature, indicating that a higher degree of cure results in better surface quality. For the silver ink, the surface roughness of the tracks cured at 130°C is higher than that cured at 100°C, this is possibly because the track cured at 100°C was not completely cured and contained some solvents which may help to smooth the surface. When cured at 150°C the surface roughness of the ink begins to drop similar to the hybrid ink.

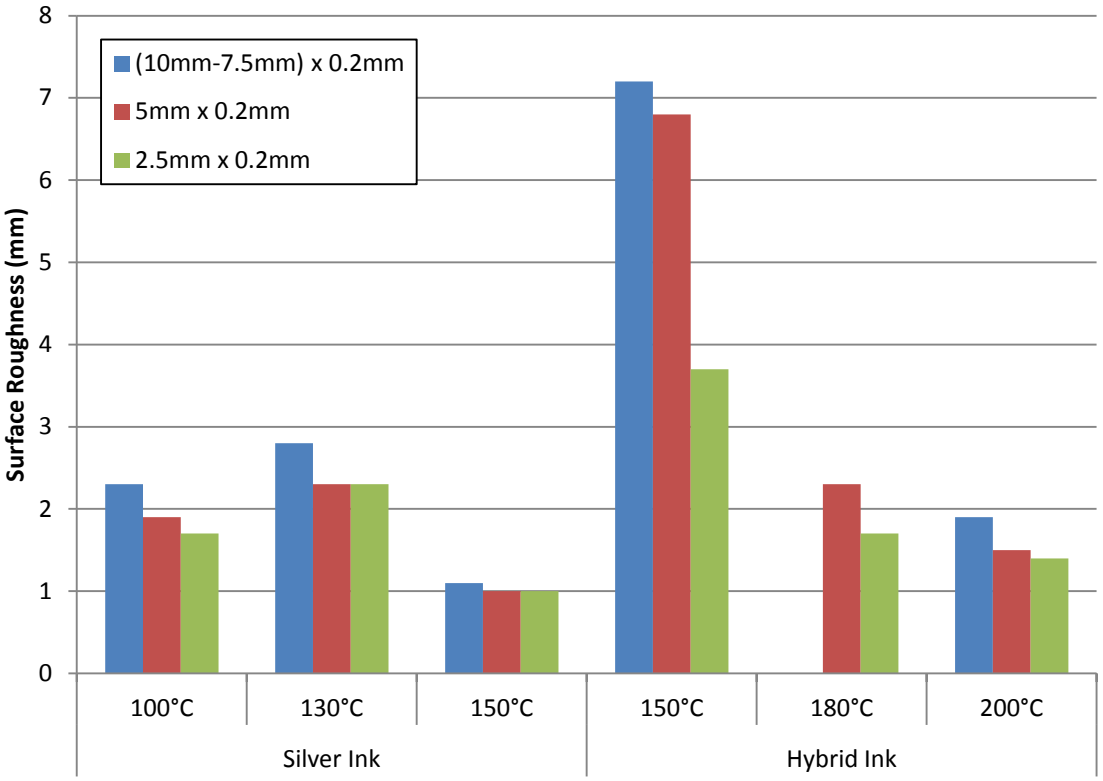

Figure 6:8: Surface roughness of silver and hybrid inks on alumina substrate cured at different temperatures

6.3.4 Discussion

This study shows that the surface roughness of PTF inks are primarily dictated by the properties of the substrate surface. However, surface roughness can be improved for inks with lower viscosity as this allows the ink flow into the surface filling voids and crevices. Additionally higher cure temperatures also seem to have a positive effect on surface roughness.

For RF applications such as micro-strip antennas the majority of the electrical signal travels at the bottom surface of the conductor (at the interface between the conductor and dielectric). This suggests that the surface roughness on the underside of the conductor is more important that the top surface of the conductor. At this interface the surface roughness of the conductor is highly dependent on the surface properties of the dielectric material. Whilst this study only covers improving the top surface of conductive PTF inks if, for example, the dielectric was fabricated from a PTF ink then the same rules could be applied.

6.4 Ink Processing: Optimisation of PTF inks by curing

The measurements from section 6.3 and 6.4 show a relationship between cure temperature and the final properties of the PTF ink material. Investigation of the curing kinetics of these inks can give an

indication of how to optimise the curing parameters, this is particularly important for localised curing, where the temperature dynamics will be very different from the traditional oven curing. To do this three thermodynamical analytical techniques were used, Thermogravimetric Analysis (TGA), Differential Scanning Calorimetry (DSC) and Dynamic Mechanical Analysis (DMA).

6.4.1 Thermogravemetric Analysis of PTF conductive Inks

To determine the makeup of the PTF inks in terms of functional (silver) particles, solvent content and polymeric content Thermogravemetric analysis (TGA) can be used. TGA will also determine at what temperature solvent evaporation takes place (which can be useful when curing the inks) and at what temperature degradation of the polymer matrix occurs.

TGA is an analytical technique which is used to determine a materials thermal stability by measuring the weight change of a sample as it is heated. Upon heating a polymer sample it undergoes a series of mass losses which contribute to the emission of volatile compounds (moisture, the emission of solvents), plasticizers, and the decomposition of the polymer resin [132]. After all the chemical reactions have taken place the remains will be ash and any filler (e.g. silver) that were incorporated into the sample.

TGA measurements were performed on a Netzech TG 209 Thermogravimetric Analysis (TGA) system. Air and Nitrogen purge gases were utilised at flow rates of 60ml/min. The liquid samples were placed inside an Al_20_3 crucible that had already been weighed and zeroed on a Mettler Toledo balance which was accurate to 0.1mg. The crucible was then placed inside the TGA where it was subjected to a constant rate of heating of 10°C/min from 20°C to 600°C. This process was repeated for the Silver and Hybrid thermosetting DW inks. The TGA displays the mass loss as a function of weight as given in Figure 6:9. The Netzech TGA software can also be used to give a first derivative of this plot thereby allowing the calculation of the point where each of the inks constituents decomposes. This can be used to calculate the percentage weight of each component as given in Table 6:2.

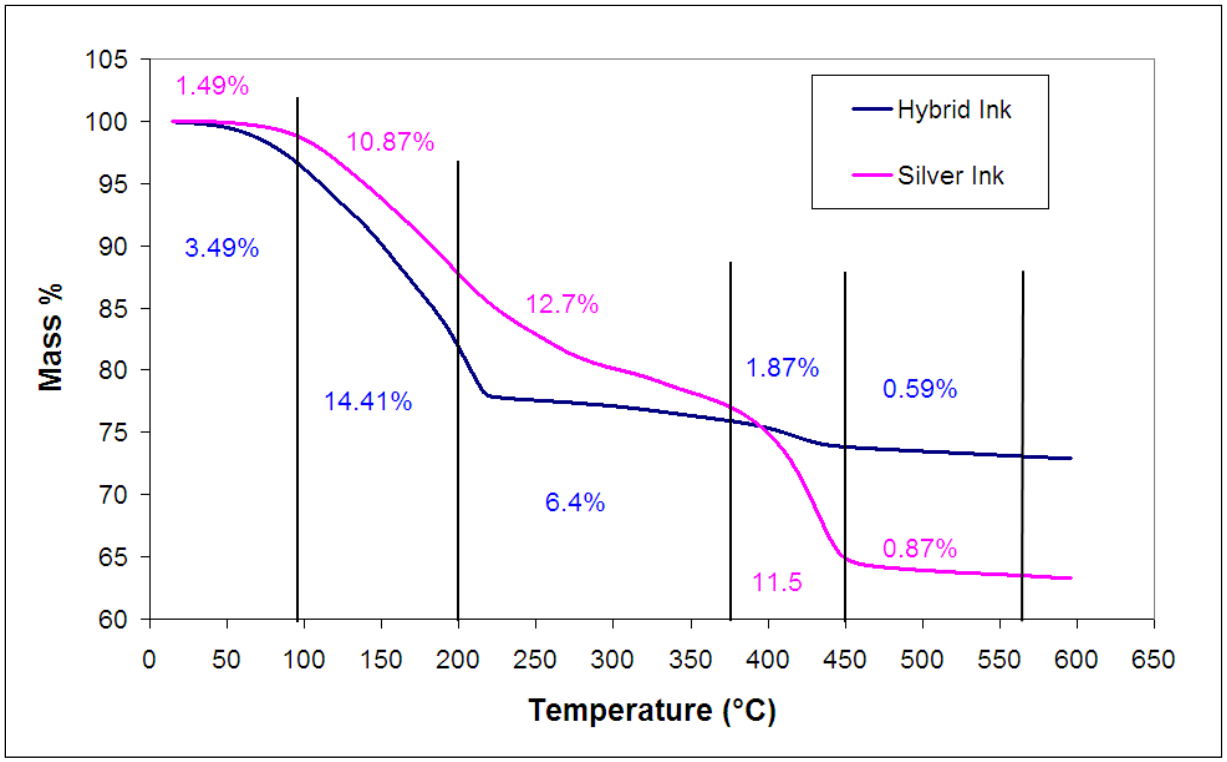

Figure 6:9: TGA analysis of DW Silver and Hybrid Thermosetting Inks

PTF Ink	% Volatile content	% Polymer	% Residue
Silver Ink	22.78	3.94	73.28
Hybrid Ink	19.87	16.56	63.57

Table 6:5: Percentage mass of constituents in DW Thermosetting Inks

The result from the TGA depicts the main decomposition events in the polymer compounds. The initial mass loss can be contributed to solvent loss (volatiles) within the inks. The volatile component in the Silver and Hybrid PTF ink make up nearly 20% of its mass. At the respective cure temperatures (130°C silver ink, 180°C hybrid ink) the inks still contain some element of moisture/solvent content. This is only completely volatised at temperatures above 200°C. The curing and hence the performance of the ink could be increased by removing all the solvent before or during cure. At temperatures above 300°C the both inks undergo degradation. Table 6:5 shows that there is indeed more solid content in the Hybrid ink than the Silver ink which could be due to the presence of silver nano-particles.

6.4.2 Differential Scanning Calorimetry (DSC) Analysis of PTF Conductive Inks.

The Dynamic Scanning Calorimetry (DSC) technique was used to measure the thermal events within the thermosetting PTF inks. DSC is a thermo-analytical technique in which the change in the heat flow required to raise or decrease the temperature of a sample encapsulated inside a crucible is

compared to a reference crucible. Heat flow is a transfer of power and as such is measured in milliwatts (mW). The energy that is transferred relates to the change in enthalpy of the sample. When the sample absorbs energy, the change in enthalpy is endothermic and likewise when the samples releases energy the change in enthalpy is exothermic. Analysis of the DSC results can accurately depict thermal events such as glass transition, T_g, crystallisation temperatures, T_c, melting temperatures, T_m and decomposition temperatures, T_d [133].

Figure 6:10 shows the DSC profile obtained using a Mettler Toledo DSC821 for thermosetting silver and silver hybrid inks. The ink samples were placed in a 40µl aluminium crucible. All measurements were made using an empty 40µl aluminium crucible as a reference. When preparing samples it was important to have only a small amount of ink in the pan to ensure the sample will heat up uniformly. The lid of the pan was also perforated so that any solvent evaporation could escape without affecting the measurement. The DSC was set to heat the samples from 25°C to 400°C at 10°C/min.

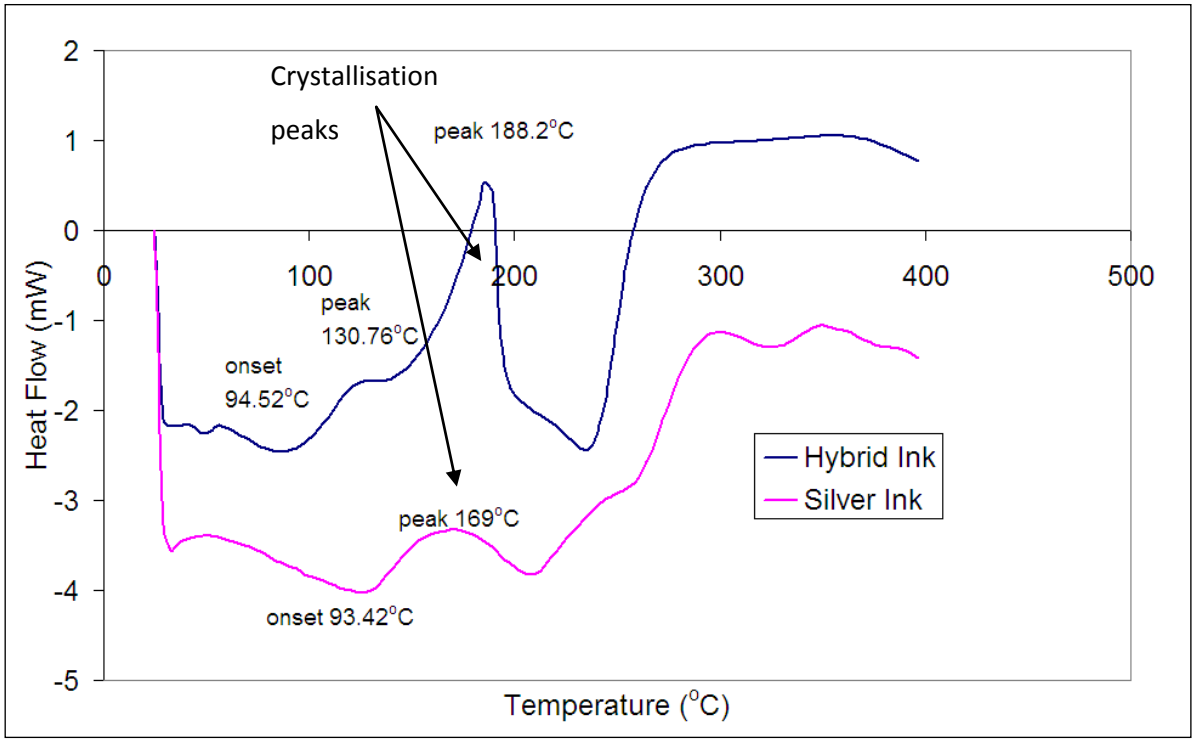

Figure 6:10: DSC measurement of thermosetting silver and hybrid ink.

Analysis of the DSC scans was carried out by the Mettler Toledo DSC821 software. From this analysis one can get the extrapolated onset temperature of all thermal events measured by the DSC. The onset temperature is defined as the temperature of intersection between the extrapolated initial base line and the tangent or line through the linear section of the leading edge of the peak [134]. It

is this temperature as opposed to the peak maximum temperature that was used to characterise endothermic and exothermic peaks as it is less affected by the heating rate and the samples mass.

Upon inspection of Figure 6:10 both the Silver and Hybrid crystallisation peaks can be observed. These peaks correspond to curing events within the inks. It can be seen that the Hybrid silver ink undergoes two separate crystallisation peaks. The first occurs at very a similar onset temperature as the regular Silver ink sample. As both share the same resin backbone it is not surprising that they cure at the same onset temperature. The second crystallisation peak in the Hybrid ink corresponds to the sintering of the silver nano-particles within the ink composition. The degradation peaks can also be viewed using the DSC. Both the thermosetting inks begin to degrade at approximately 250^{o}C.

6.4.3 Dynamical Mechanical Analysis (DMA) of PTF conductive inks

DMA is a measurement technique which measures the storage modulus (elastic modulus) and loss modulus (viscous modulus) of a polymer material as a function of time and frequency. The storage and loss modulus can be related to Young's modulus using Equation 6:1 [133].

$$E = E' + iE'' \qquad \textbf{Equation 6:1}$$

Where E is the complex Young's modulus, E' is the storage modulus, and E'' is the loss modulus. The storage modulus measures the stored energy and the loss modulus measures the energy dissipated as heat. The ratio between the storage and loss modulus gives the mechanical loss tangent, tanδ, or the damping of the system. This damping is essentially a measure of how good the material is at absorbing energy.

DMA is an important technique in polymer analysis as it can be used to measure the glass transition temperature, T_g. The T_g is an important phenomena in polymer materials. It marks the reversible change at which a polymer goes from an amorphous solid state to a melt state [133]. In the amorphous state the polymer can have high tensile strength due to the random cross-linking of the polymer chains. In the melt phase thermal energy is sufficiently high enough for the polymer chains to move in random micro-Brownian motion leading to a decrease in structural properties. This could also lead to degradation in electrical functionality and resistance to environmental effects. The glass transition temperature is related to the crosslink density or degree of cure of the polymer material. The relationship between T_g, and crosslink density is given by the Fox-Loshaek equation [133]:

$$T_g = T_{g,\infty} - K_c \rho_c$$ **Equation 6:2**

Where $T_{g,\infty}$ is the maximum glass transition temperature that can be achieved at a theoretical infinite weight, K_c is a polymer specific constant and ρ_c represents the number of cross-links per gram.

The glass transition temperature can be seen as a large drop in the storage modulus when measured using a DMA. The lower storage modulus indicates the more rubbery amorphous state of the polymer material. A more accurate measure of the glass transition temperature can be found by measuring the peak maximum in the loss tangent when plotted as a function of temperature.

To reduce the number of tests DMA analysis was conducted on just the silver ink as the hybrid ink is based on the same resin system. To prepare the samples steel coupons were coated with approximately 40μm of the silver ink before being cured in an oven at different temperatures for 20mins. Steel coupons were used as they are unaffected by DMA and therefore isolate the ink layer for testing. Once cured the samples were placed in a Netzsch DMA 242 and heated at a rate of 10°C/min from 25°C to 170°C at an oscillating frequency of 5Hz. The results from the DMA were analysed on the Netzch DMA 242 software which can plot the storage modulus, loss modulus and tanδ as a function of temperature. This software can also be used to resolve the peak maxima in the tanδ plots.

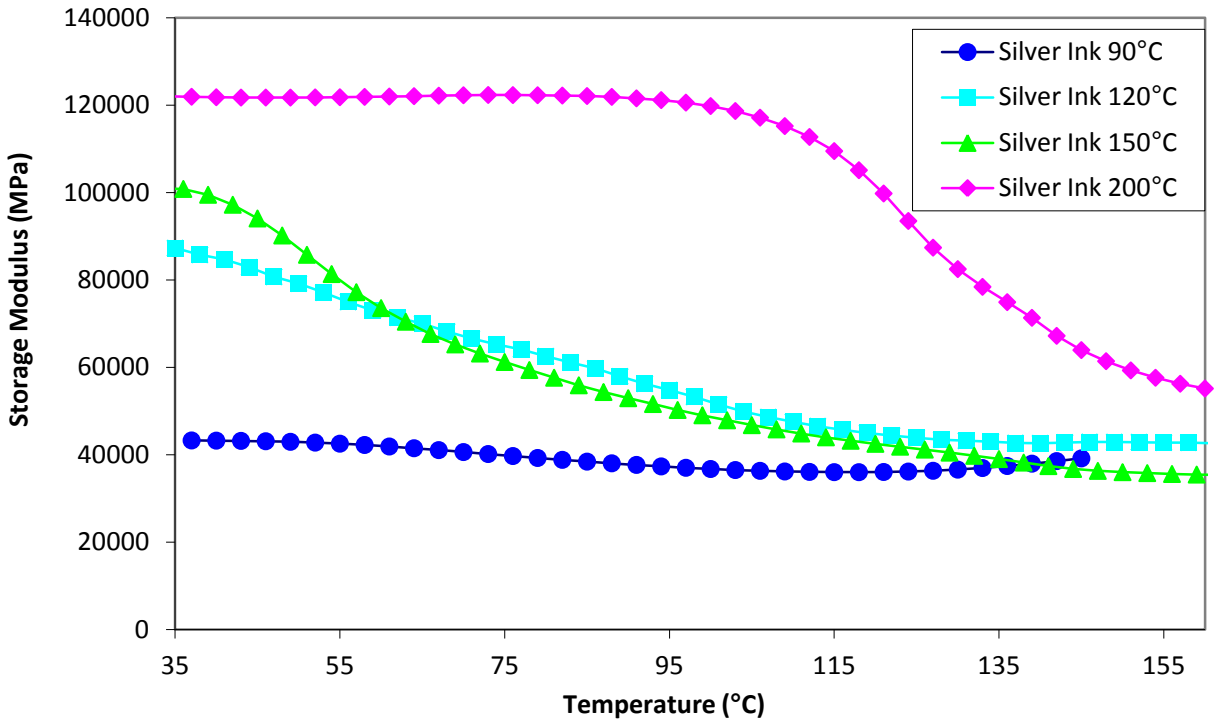

Figure 6:11: Storage Modulus as a function of temperature of PTF silver ink cured at 90°, 120°, 150° and 220°C for 20mins.

Figure 6:11 shows the storage modulus of the combined steel and PTF thermosetting silver ink cured at different temperatures for 20mins. This shows that an increase in cure temperature results in a higher storage modulus or stiffness when at room temperature. Conversely lowering the cure temperature lowers the storage modulus indicating more flexural properties. When the material is cured at 200°C the storage modulus of the material is also more stable when heated. Whilst this measurement is useful to show the trend in storage modulus with cure temperature it is less useful for measuring the absolute tensile properties of the ink due to the presence of the steel substrate.

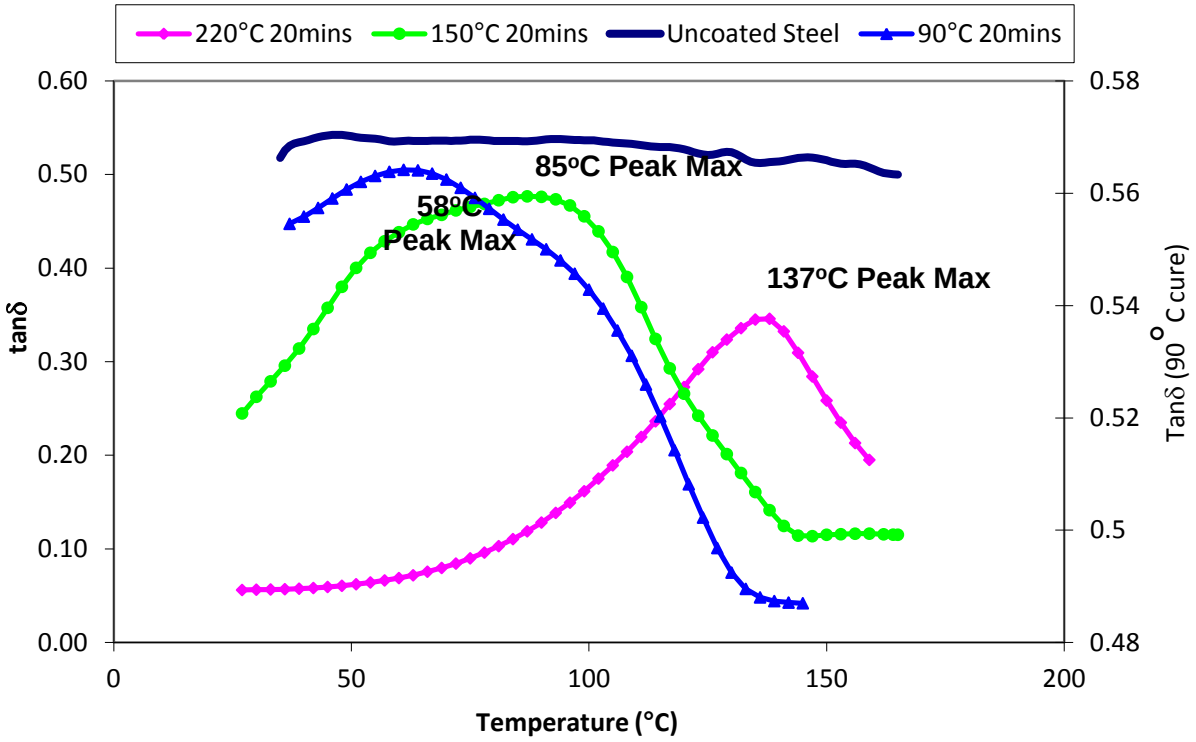

Figure 6:12: tanδ measured as a function of temperature for the silver ink cured at 90°C, 150°C and 220°C for 20mins.

The relationship between the loss tangent (peak maxima) and cure temperature can be seen in Figure 6:12. As the cure temperature increases the peak maxima in the loss tangent shifts to the right (indicating an increase in T_g) and becomes narrower and better defined (indicating an increasing degree of cure). It must be noted that any further increase in cure temperature after 220°C results in very minimal increase in T_g. Therefore at this cure temperature the ink is said to be fully cured and will achieve its greatest physical and electrical properties. Figure 6:12 also shows the tanδ for the uncoated steel coupon which remains constant as a function of temperature indicating no measurable effect on the results.

The glass transition temperature (peak maxima in tanδ curve) can also be plotted as a function of cure temperature (at a constant cure time of 20mins) as shown in Figure 6:13. As the temperature of cure increases there is an exponential rise in T_g up to a cure temperature of 180°C where the curve begins to flatten indicating optimum cross-link density.

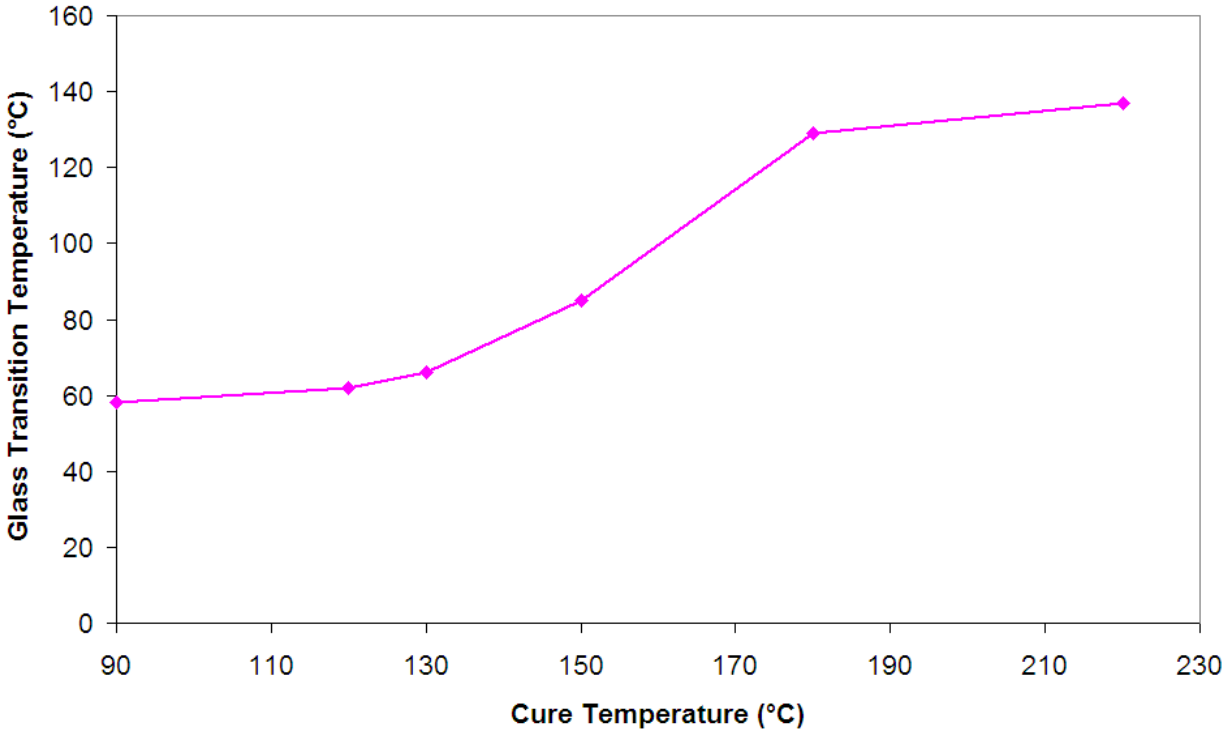

Figure 6:13: Glass Transition temperature as a function of cure temperature

Table 6:6 compares the peak maximum in the tanδ curves as a function of curing time for cure temperatures of 120°C and 220°C respectively. A glass transition temperature of approximately 90°C can be achieved by curing the resin at 220°C for 5mins, compared to curing at 120°C for an hour. This result shows that curing temperature is more influential than cure time when curing DW inks. This can have important consequences on processing parameters as high bursts of heat energy at short exposures could be used to cure DW material. This will be investigated in more detail in Chapter 8.

Cure Temperature (°C)	Cure Time (mins)	tanδ Peak Maximum (°C)
120	5	Insufficient Curing
120	20	73
120	60	93.2
220	1	68
220	5	98
220	20	136

Table 6:6: Comparison of peak tanδ against cure time for 120°C and 220°C

6.4.4 Discussion

TGA and DSC analysis of the PTF thermosetting Silver and Hybrid inks have indicated the main thermal events within the inks such as the onset of solvent evaporation, curing and decomposition. Decomposition temperatures are particularly useful as they determine the maximum temperature of

operation before failure. DSC analysis also shows the onset of sintering (second crystallisation peak) within the hybrid ink which occurs at a higher temperature than curing.

The results from the DMA are perhaps more useful as they show how the cure temperature can be used to tailor the mechanical properties of the ink. For example low cure temperatures can enable the ink to have more flexural properties whereas high cure temperatures increase the stiffness of the material. Importantly DMA shows that increased cure temperatures increase the glass transition temperature, T_g, of the polymer resin which leads to more stable mechanical properties at higher temperatures.

The glass transition temperature is an important phenomenon in polymer materials, above this temperature the properties within the ink will change which could have an effect on the adhesion and conductivity of the ink. It is important then that the T_g is above the required operating temperature of the device. Military standards for example conventionally require components to maintain performance over a temperature range between -55°C and 125°C. This temperature range accounts for extreme aircraft climates as well as heat originating from aircraft components [135]. In some cases, depending on the location of the devices, industrial standards can be used with a more relaxed temperature range of, -40° to 85°C. Assuming full military temperature requirements a T_g of 125°C would be needed which would require a processing temperature of approximately 180°C for 20mins (according to Figure 6:13). To meet industrial temperature requirements (85°C) a processing temperature of approximately 155°C for 20mins would be needed.

Whilst the T_g of DW PTF materials can be increased by curing at higher temperatures it is not desirable when processing on highly specified aerospace materials, where the designs have been set on very specific material properties. For example in the case of metal alloys such as Aluminium 2024, the cure temperature may not be high enough to cause melting or softening of the metal but could induce annealing and age hardening effects [136] [137] which may require the airframe to be recertified. Whilst the duration of age hardening is much longer than the durations required to cure the heat effects should be minimised.

Aerospace components are also manufactured out of Carbon Fibre composites. These materials commonly contain epoxy resins which can have a T_g of 120°C or lower. This dramatically limits the processing temperature of any materials printed on to the surface of such components. A number of techniques can be used to minimise the thermal impact on the substrate when processing DW

material. This includes reducing the temperature of cure by increasing cure durations or by implementing localised processing techniques thereby minimising the heat input into the substrate. Interestingly DMA measurements showed that cure temperature is the predominant factor when curing polymer inks. This suggests that localised curing techniques which have a high heat input at short exposures could be used to cure these inks.

6.5 Environmental Durability of PTF inks

Military based environmental standards can be found in the MIL-STD-810G document [135]. This document acts as a guideline for the requirements and environmental test procedures necessary for military grade components. A selection of the most relevant standards was used to test the DW PTF thermosetting conductive inks to increase confidence that these materials could be used for military and aerospace applications. A summary of these standards are given in Table 6:7. The majority of these tests were conducted at Airbus UK as part of the DW: EASY project. As such the duration of some these test methods could not be divulged for commercial reasons. Skydrol hydraulic fluid immersion testing was conducted as this is one of the most severe conditions a material would have to withstand in aircraft system. Although this fluid is mainly used within hydraulic machinery it can often also be used as a lubricant and can therefore come into contact with aircraft surfaces where a DW sensor may be placed. To measure the survivability of the DW materials under these test conditions both the track resistance and adhesion were monitored before and after each test. This complies with the Technical Performance measures identified in the requirements study.

Requirement	**Procedure**	**Test Method**	**Test Provider**
Severe Low Temperature Resistant	Environmental Chamber	Cyclic temperature ramping from 23 -65°C	Airbus UK
Severe High Temperature Resistant	Environmental Chamber	Cyclic temperature ramping from 23-110°C.	Airbus UK
Constant High Humidity Resistant	Environmental Chamber	95% Relative Humidity at 70°C	Airbus UK
Resistant to Fluid Immersion	Solution immersion	Skydrol (Phosphate ester based hydraulic fluid) Immersion	Airbus UK
Corrosion Resistant	Salt Fog Chamber	Prohesion Solution 3.5% ammonia sulphate. 0.5% NACl. 35°C alternating wet and dry cycle over a minimum of 24 hours	BAE Systems

Table 6:7: Durability standards tested for DW components on Aircraft

6.5.1 Airbus Environmental Testing

For Airbus durability measurements only the thermosetting PTF silver ink was considered. This was mainly because the hybrid thermosetting ink exhibited poor adhesion on aerospace substrates in previous experiments (section 6.3.2).

To prepare the samples, the thermosetting PTF silver ink was applied to primed Aluminium coupons before being cured at the manufacturers recommended cure temperature of 130°C for 20mins. Primed Aluminium was chosen as it represents a material commonly used in aerospace applications. Each coupon consisted of a spiral pattern and two identical rectangular geometries. The rectangular geometries were printed with the tape-cast (as described in Chapter 5) and micro-nozzle deposition methods for comparison. The rectangular geometries were designed to comply with sheet resistance (four-point probe technique) and adhesion (PATTI pull-off technique) measurements procedures. The spiral pattern was designed to allow a large line length (700mm) to be incorporated within the test coupon so that the resistance of the track could be easily measured using a standard two wire ohmmeter.

For micro-nozzle printing, the system was configured with a 0.25mm inner-diameter nozzle using a deposition pressure of 165kPa at a traverse speed of $4mms^{-1}$ relative to the substrate. This resulted in printed tracks with width of approximately 0.5mm with a height of 0.045mm. Tracks were printed adjacent to one another with an overlap of 30% to increase the track width. This overlap was selected by trial and error as the optimum for producing wide tracks with minimum pinholes and surface ripple across the track.

The Alpha step probe (described in Chapter 4) was used to measure the height of the printed ink tracks. The micro-nozzle and tape cast rectangular geometries measured approximately 0.05mm and 0.04mm respectively after curing. The spiral geometry was printed with a single line width using the micro-nozzle system resulting in a track height of approximately 0.045mm. Figure 6:14 shows a schematic and photographic image of one of the test coupons used in the experiment.

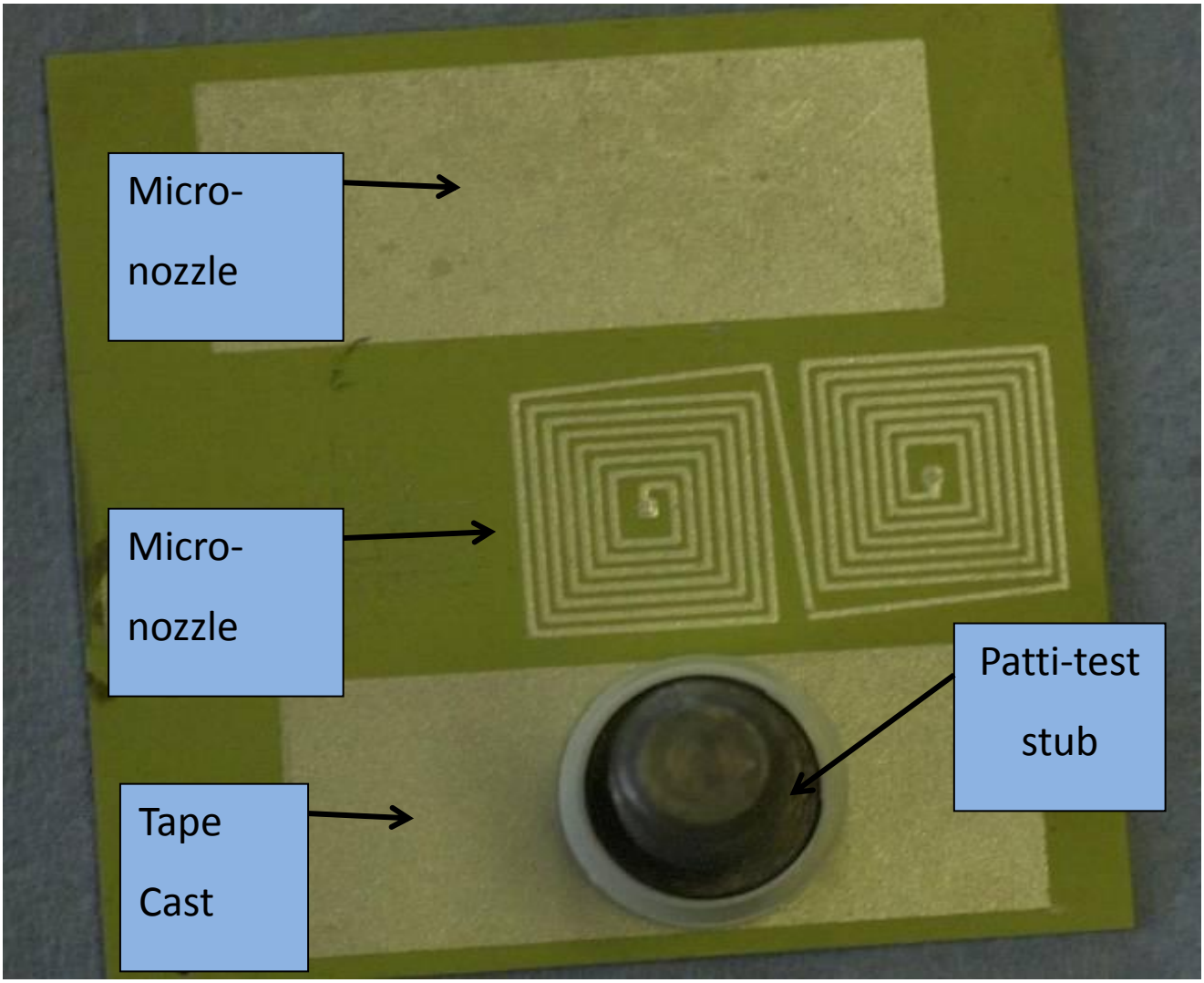

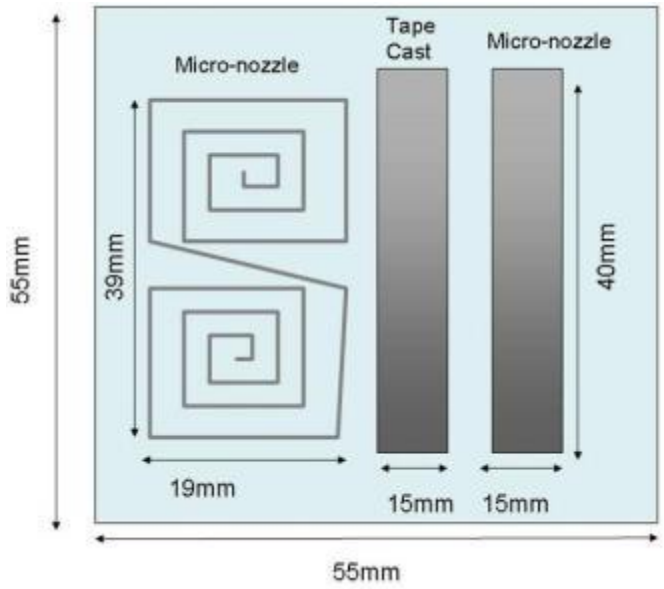

Figure 6:14: Coupon used for environmental testing

The adhesion results from the durability tests are given in Table 6:8 and Figure 6:15. Two coupons were used per test with the mean adhesion recorded after environmental exposure. These measurements were compared with a control coupon manufactured using the same conditions as the other samples but left at room temperature without any additional exposure. All measurements were made at the same time which was approximately four months after initial fabrication of the samples.

Test Method	Print Method	Mean Adhesion (MPa)	Failure
Control	Tape Cast	1.723 +/- 0.02	Cohesive
	Micro-Nozzle	1.575 +/- 0.02	Cohesive
Humidity 60°C 95%RH	Tape Cast	2.703 +/- 0.02	Adhesive
	Micro-Nozzle	2.5 +/- 0.02	Adhesive
Skydrol	Tape Cast	0.643 +/- 0.09	Cohesive
	Micro-Nozzle	0.75 +/- 0.12	Cohesive
Low temperature (-40°C)	Tape Cast	1.797 +/- 0.02	Cohesive
	Micro-Nozzle	1.85 +/- 0.02	Cohesive
High temperature (-110°C)	Tape Cast	3.5 +/- 0.02	Adhesive
	Micro-Nozzle	3.42 +/- 0.02	Adhesive

Table 6:8: Adhesion of DW samples after environmental testing

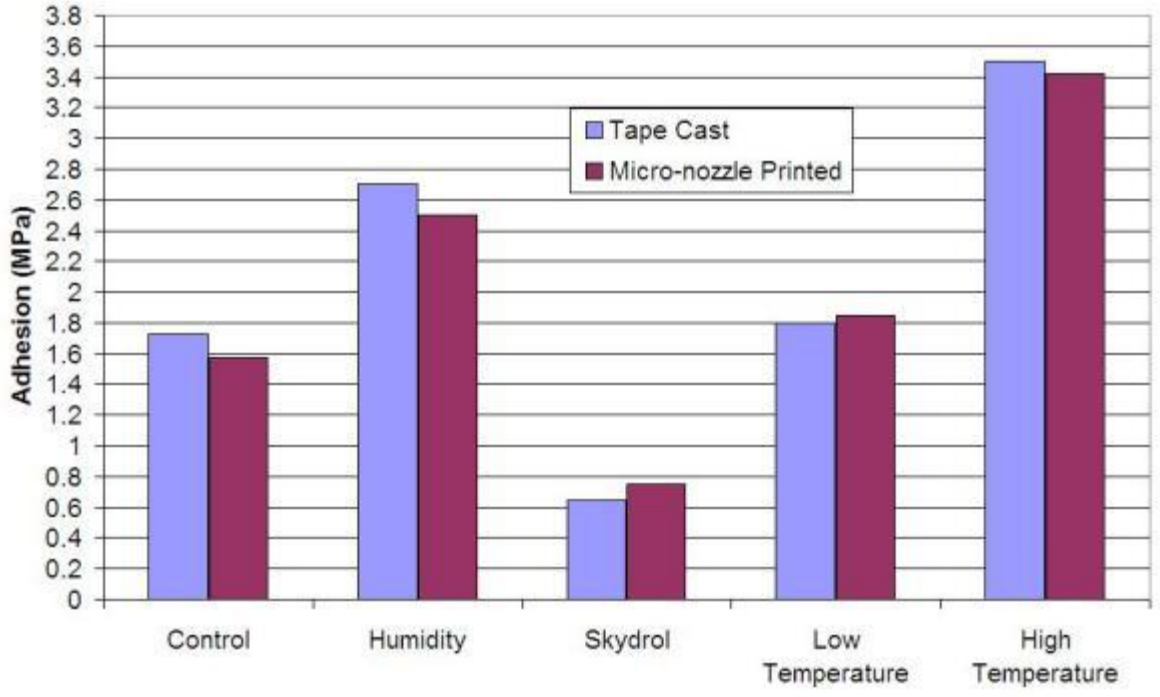

Figure 6:15: Comparison of adhesion between Tape-cast and Micro-nozzle printed DW silver tracks after environmental exposure

The adhesion tests show there is little difference between the micro-nozzle and tape cast deposited prints. Exposure to high temperature environments increased the adhesion of the inks to the substrate. As the failures were adhesive in nature this could be attributed to greater crosslink density in the ink deposit as a result of further curing in these environmental conditions. This is possible as the inks were not fully cured (at 220°C for 20mins) for these experimental trials. Skydrol immersion significantly degraded the adhesion of the track. Sala, G., also found that Skydrol immersion can significantly degrade the structural properties of composite materials [138]. In this report degradation was attributed to the plasticising effect of the Skydrol fluid on the resin within the composite [138].

		Track Resistance Spiral (Ω)		Sheet Resistance (Ω/sq)	
Test Method	**Print Method**	**Before**	**After**	**Before**	**After**
Control	Tape Cast	N/A	N/A	0.01835	0.0182
	Micro-Nozzle	36	35.7	0.0323	0.0322
Humidity 60°C 95%RH	Tape Cast	N/A	N/A	0.019	0.0163
	Micro-Nozzle	37.9	41.2	0.0351	0.0372
Skydrol Immersion	Tape Cast	N/A	N/A	0.0167	∞
	Micro-Nozzle	37.5	∞	0.0324	∞
Low temperature (-40°C)	Tape Cast	N/A	N/A	0.0252	0.0257
	Micro-Nozzle	35.8	36.3	0.0321	0.0326
High temperature (-110°C)	Tape Cast	N/A	N/A	0.0201	0.018
	Micro-Nozzle	43.32	36.85	0.033	0.0286

Table 6:9: Resistance of DW silver ink before and after environmental exposure

Table 6:9 shows the resistance of the track before and after exposure to environmental exposure. The control sample shows no significant change in resistance after four months at room temperature. Similarly severe low temperature exposure had no significant impact on resistance. When exposed to humidity the samples show a 6% increase in sheet resistance. The increase in resistance does not follow the same trend as the adhesion measurements which improved when exposed to humid and hot conditions due to possible increased cross-linking. Inspection of this sample shows a discolouration of the silver (Figure 6:16) when compared to the control sample. This discolouration could be caused by oxidisation of the silver flakes within the binder. As the conductivity of the ink relies on contact between the silver flakes a thin layer of oxidisation around the particles could cause an increase in resistance.

Skydrol immersion severely degraded the electrical conductivity of the silver ink with no measurable signal measured with the four point probe or two-wire resistance method. Figure 6:16 also shows a darkening of the ink coating when compared to the relatively silvery colour of the control sample. One reason for the loss in conductivity of the sample could be the absorption of the Skydrol fluid by the resin. It has previously been reported that Skydrol can cause softening of polymer resin and reduction in cross-link density (hence the reduction in adhesion and conductivity) [139].

The resistance of the track was also affected by exposure to high temperatures. In this case the resistance reduced by approximately 15%. This is perhaps not surprising as the ink was only cured at 130°C and therefore not fully cross-linked. The ink resistance has since been measured at room temperature two months after the experiment and the resistance has held constant. This experiment shows that it is better to fully cure the ink in order to control the final resistance.

This investigation acknowledges that a more conclusive experiment of environmental durability would have been to monitor the resistance of the DW material during environmental testing. This would have allowed a better understanding of how properties such as the glass transition temperature affects material properties as the temperature of the environment increases.

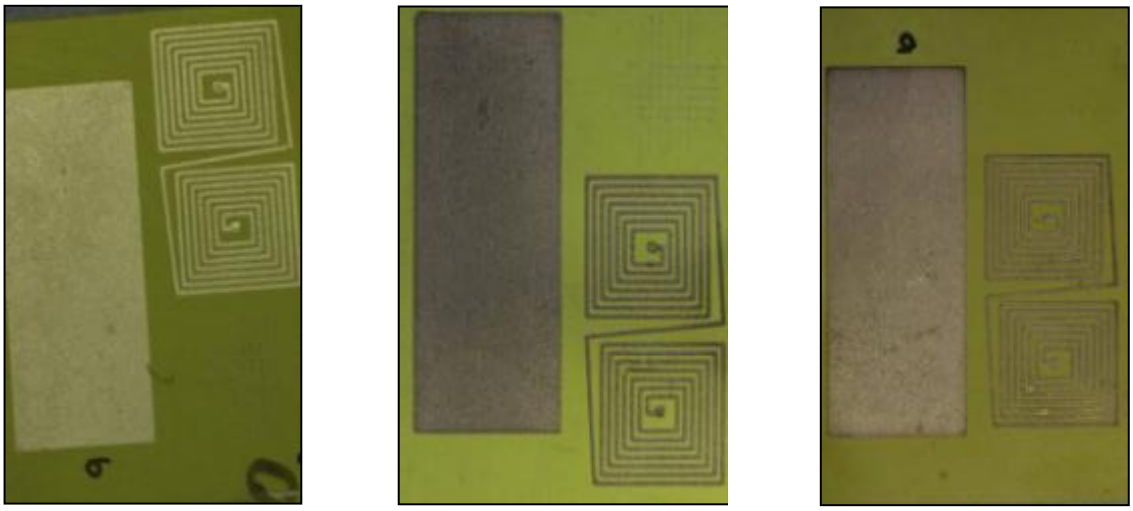

A B C

Figure 6:16: DW silver ink samples (A) Control (B) After exposure to humidity (C) After immersion in Skydrol

6.5.2 Corrosion Resistance of DW inks

Corrosion effects can have a detrimental effect on the material properties of metals. In the past the corrosion of silver in accelerated environments has been investigated for electrical [140] and structural [141] properties.

The corrosion resistance of the conductive PTF DW ink tracks was investigated using the Prohesion ASTM G85–A5 accelerated test standard. This Prohesion test method represents a real world environment by exposing the samples to continuous wet and dry cycle for a fixed number of hours. Each cycle consist of spaying the sample with the Prohesion solution (0.35% Ammonia Sulphate, 0.5% Sodium Chloride) at 24°C for one hour before undergoing a drying cycle of one hour for 35°C. There is no set standard for the duration of accelerated salt fog testing however military standards suggest that a minimum exposure of 24 hours should be used for alternating wet and dry testing (Prohesion method). For this investigation a test period of approximately 260 hours was used. This prolonged exposure was used to test the long term durability of the ink tracks.

Corrosion was monitored by measuring the resistance of the tracks in-situ with the test. Samples were prepared by tape casting primed 2024 Aluminium substrates with PTF thermosetting silver and hybrid inks with dimensions of approximately 0.05x0.5x100mm. Wires were attached to these samples using a two-part epoxy conductive glue which was subsequently coated with a protective sealant (PPG aerospace sealant PR 1422). To check the durability of the wires and coating one of the printed tracks was coated completely with the sealant. Figure 6:17 shows one of the test samples with three bare PTF Silver ink tracks and one PTF ink track coated with the sealant.

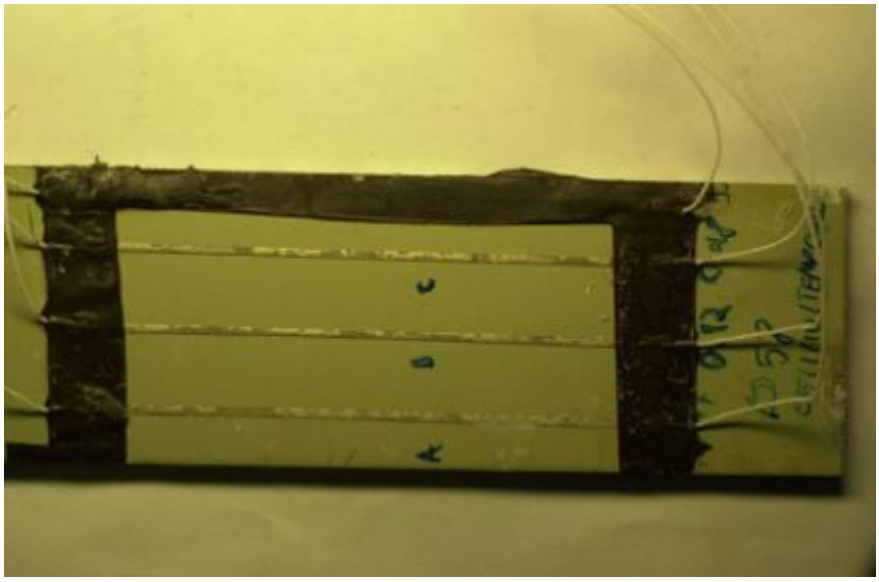

Figure 6:17: Example of sample for corrosion testing

The resistance was monitored by connecting the wires from the sample to a National Instruments multi-meter module which logged the resistance as a function of time every 10 seconds. A sample of

the results over a 20 hour period is given for both inks in Figure 6:18. Essentially the results show there is a periodic change in resistance every 2hours. This can be directly attributed to the change in temperature in the Prohesion chamber as it cycles from the wet and drying temperatures.

The initial and final (after corrosion testing) resistance of the hybrid silver ink track (1.34Ω to 1.27Ω) and silver ink track (1.732Ω to 1.703Ω) showed no significant change after salt fog exposure. Inspection under a microscope showed also showed no indication of corrosion. The corrosive resistance of silver PTF inks is perhaps not surprising as the silver particles are encased in the resin binder effectively protecting it from corrosive effects. However, to eliminate any doubt of corrosion EDX could be used to investigate the sample for oxidisation of the silver. This was not conducted due to restrictions on time but should be followed as a further study.

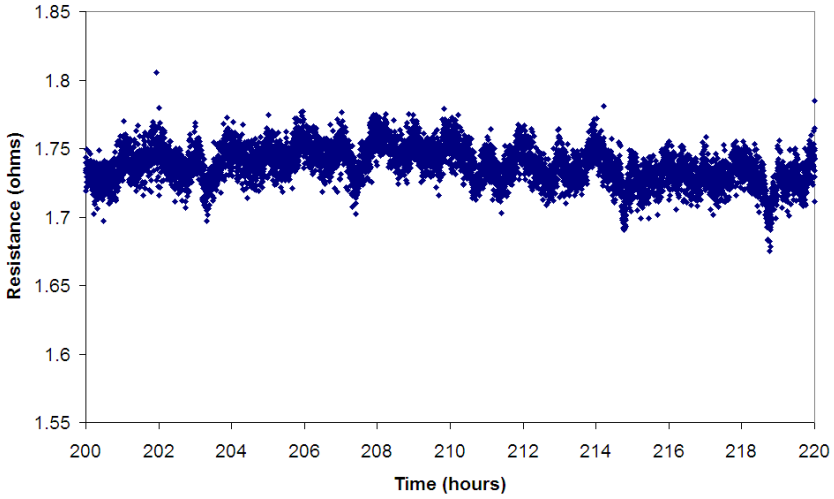

A.

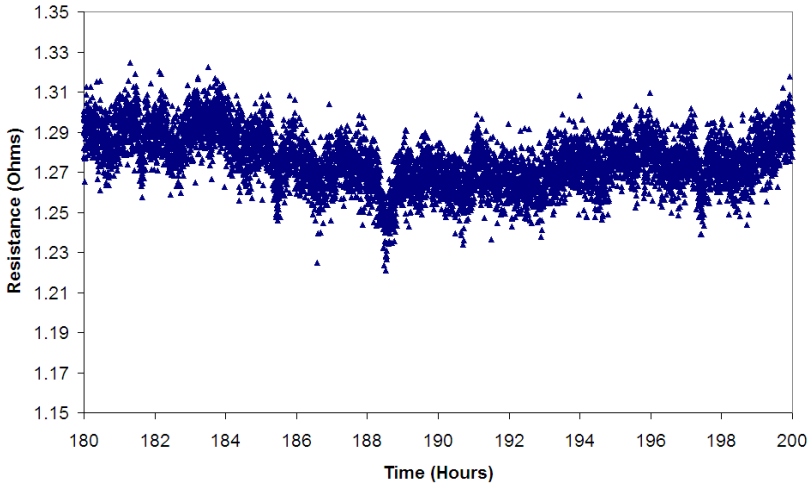

B.

Figure 6:18: Resistance of thermosetting PTF ink track during Prohesion durability testing (A) Silver Ink (B) Hybrid Ink

6.5.3 Discussion

The results from this section show that the PTF conductive inks have good durability when exposed to humid, high temperature and low temperature conditions with fairly minor changes in ink resistance and adhesion. As discussed previously greater immunity to temperature effects can be achieved with higher cure temperatures (so that material T_g is increased). Salt spray measurement also show high stability and resistance to corrosive effects. Unfortunately Skydrol immersion shows complete breakdown of both adhesion and conductivity within the inks.

6.6 Conclusion

Conductive PTF and Inkjet ink compositions have been characterised in terms of their conductivity and adhesion. When all inks are cured at the same temperature of 200°C for 20mins the hybrid ink exhibits the highest conductivity, however, this composition also has the poorest adhesion. The opposite is true for the thermoplastic and thermosetting silver inks which have low conductivity but relatively high adhesion on all substrate types. Inkjet inks on the other hand can have high conductivity but the strength of adhesion is highly dependent on the surface roughness of the substrate. In all cases it was shown that the adhesive and conductive properties could be improved by higher degrees of curing specifically through increased curing temperatures although this may be undesirable when processing on aerospace components. For antenna applications it can be concluded that conventional curing at temperatures below 200°C result in ink conductivities that are below the desired 30% bulk conductivity requirement identified in Chapter 3.

Curing kinetics of DW thermosetting inks were investigated to optimise the curing parameters of DW inks. Both TGA and DSC analysis gave an overview of the significant thermal events occurring within the ink when heated (i.e. onset of curing/sintering and polymer decomposition). DMA analysis was used to show how the mechanical properties of PTF inks could be tailored with curing temperature. Lower curing temperatures, for example, could be used to derive more flexural properties within the ink. This could be useful for applications involving highly flexible substrate materials although there is the risk that at lower temperature the inks are not fully cured and therefore functional and adhesive properties could suffer. Significantly, DMA showed that as the curing temperature increases so does the glass transition temperature, T_g. A high T_g indicates greater mechanical stability at higher temperatures. Mechanical stability is important as it has a knock-on effect on the adhesion and conductivity of the ink. Comparison between cure temperature and time indicated that higher T_g can be achieved by using high temperatures at short exposures times. This suggests that localised curing techniques, such as laser processes, could be used to cure the inks. Laser

processing is highly advantageous as heat penetration in the substrate is restricted which can be advantageous when processing on temperature sensitive materials.

Conductive PTF inks were investigated for their durability in harsh environments using a selection of military standards. It was found that the majority of samples exhibited small changes in adhesion and conductivity when exposed to temperature changes. The primary reason for this was down to the low curing temperature used to prepare samples. In order to reduce creep in material properties the T_g needs to be increased with higher curing temperatures as described above. In general however, it was found that the PTF silver inks were resistant to high and low temperature, humidity and salt fog environments. However, Skydrol immersion severely degraded the conductive and adhesive performance of PTF inks. It remains to be seen whether PTF inks could be modified in order to meet this requirement. It may, for example, be necessary to coat a protective layer over the top of the DW material to prevent Skydrol degradation. Unfortunately due to time constraints the environmental durability of inkjet and thermoplastic PTF inks were not investigated. Whilst there is literature on the durability of polymeric resins, such as those used for coatings, there is currently no data on the durability of DW specific materials. It is important therefore to build on this work in future studies to enable DW to be adopted in aerospace and defence industry sectors.

7 Improving Direct Write Material Conductivity Using Localised Electroplating

Experimental data from Chapter Five highlighted the large discrepancy between the conductivities of current DW inks and the conductivities required for RF applications. PTF silver inks for example exhibit electrical conductivities in between 1-3% of bulk silver. As shown in the Chapter Three conductivities below 30% bulk silver result in high transmission losses at radio frequencies.

A number of methods could be used to try and improve the electrical properties of DW ink materials. The most obvious solution would be to increase the silver content within the ink composition. This however could have a number of consequences on the other ink properties such as the adhesion, rheology and durability [16].

Another method of increasing ink conductivity is to try and sinter the silver particles after deposition. By heating the metallic particles sufficiently high enough bonding can occur, causing densification and hence higher electrical conductivity [142]. Unfortunately the melting temperature of silver (961°C [143]) requires high sintering temperatures that would completely burn off the resin binder in PTF inks and would significantly damage the underlying aerospace structure. Sintering temperature can be reduced by using silver nano-particles rather than silver flakes used in PTF ink compositions [144]. As shown in Chapter Five manufacturers have successfully combined silver nano-particles with inkjet printable solutions. The silver particles in these inks begin to sinter at temperatures as low as 200°C resulting in ink conductivities close to 10% bulk silver whilst sintering temperature of 350°C result in ink conductivities closer to 30%. To achieve the desired ink conductivities these temperatures are still too high when processing on to aerospace components which involve composite materials.

This chapter aims to investigate an alternative technique for increasing the conductivity of DW ink coatings. This method involves an additional processing step whereby the DW ink material is locally electroplated with copper after it is deposited and cured.

7.1 Introduction to Electroplating

Electroplating (EP) is the application of a metallic coating to a metallic or other conductive surface by an electrochemical process. EP can be used to enhance the protective, surface, structural or electrical properties of a conductive material [145] [146]. In traditional EP methods the workpiece (the article to be plated) is immersed in an electrolyte solution containing metallic ions. The workpiece acts as a cathode (negative electrode) and is connected across a terminal to a sacrificial or permanent anode (positive electrode). Essentially the ions in the electrolyte complete the circuit. According to Faradays law of electrolysis, upon application of a current the positive ions from the electrolyte move towards the cathode and the negatively charged ions move towards the anode [145]:

At cathode $M^{z+}(aq) + ze^- \rightarrow M(s)$ **Equation 7:1**

At anode $M(s) \rightarrow M^{z+}(aq) + ze^-$ **Equation 7:2**

Where M, is the metal work piece, M^{z+} metal ions with z number of electrons involved in the reaction.

The cathode provides the positively charged metallic ions with electrons thereby allowing them to form a metallic layer on the work piece. As long as the sacrificial anode is made from the metal to be deposited on the work piece it can provide a fresh source of metal to the electrolyte solution before completely dissolving. A schematic of the EP process is given in Figure 7:1.

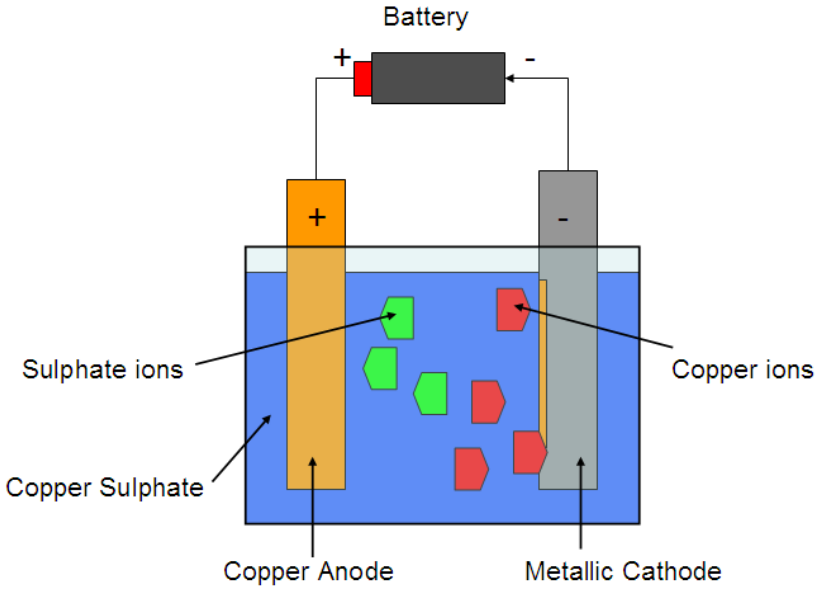

Figure 7:1: Schematic of copper EP process

The amount or mass, m, of the plating material transferred to the cathode is proportional to the quantity of electric charge Q_c, passed through an electrochemical cell. This is Faraday's law of electrolysis which follows Equation 7:3.

$$m = \left(\frac{Q_c}{F}\right) * \left(\frac{M}{n}\right) \qquad \textbf{Equation 7:3}$$

Where, F, is the Faraday constant (96,485 $Cmol^{-1}$), M, is the molar mass of the plating material and n, is the valence number of the plating material.

7.1.1 Electroless Plating

Plating of metallic material can also be achieved without the need for an electrolytic solution. The process, called electroless plating does not require an external power source but instead relies on simultaneous chemical reactions in an aqueous solution. The plating mechanism is similar to EP but the source of electrons originates from a chemical reducing agent. Electroless plating offers a number of advantages over electodeposition process such as more uniform plating and better metallurgical properties.

Equation 7:4 shows the chemical reaction for elecroless plating of copper (Cu^{2+}) in the presence of a palladium catalyst [145]. In this reaction electrons are obtained from the reducing agent formaldehyde (HCHO).

$$Cu^{2+} + 2HCHO + 4OH^- \longrightarrow Cu + 2HCOO^- + 2H_2O + H_2 \qquad \textbf{Equation 7:4}$$

Where $HCOO^-$ (formic acid) is the oxidation product of the reducing agent.

The chemical reaction in Equation 7:4 highlights some of the disadvantages of electroless plating in that formaldehyde is a particularly toxic and volatile chemical with particular risk to human health [147]. Furthermore, in order for the reaction to progress the correct ratios of each of the chemical must be maintained which can be difficult as their lifespan is particularly short [147].

7.1.2 Electroless plating of plastics

Electroless plating can also be used to coat non-conductive materials such as plastics. At first this seems an attractive alternative to DW processes for patterning conductive medium on structural

surfaces, however, this process involves a number of steps not suitable for DW applications. The first step requires etching the plastic surface with an aggressive chromic/sulphuric acid solution to create microscopic holes or pits. The plastic part is then placed in a palladium chloride bath which deposits palladium in the previously etched pits. The palladium acts as a catalyst for the deposition of copper or nickel via the electroless plating process [148].

7.2 Electroplating of DW materials

Plating of DW material for high frequency applications has previously been investigated using the electroless plating technique. In this process an inkjet silver ink was used as a seed layer for copper plating [73]. Results showed that the plated copper on the inkjet track had 50% bulk copper conductivity. The adhesion between the copper to silver seed layer also passed scotch adhesion tests (ASTM D3359 standard). Whilst the results from this investigation are promising the electroless plating process does not lend itself well to applications involving large structural system. The presence of formaldehyde as a reducing agent may also restrict its use in uncontrolled manufacturing environments.

A more localised approach to electroplating seed layers can be found by using a brush plating approach. Brush plating is particularly attractive as it does not require the use of large chemical baths. The brush plating tool consists of a handheld stylus, whereby a metallic anode is wrapped with an absorbent material dipped in the electrolyte solution. The anode is connected to the positive part of a DC power source and the workpiece or cathode (item to be plated) is connected to the negative side. As the brush is applied to the workpiece its deposits the plating material. Brush plating has been used in a number of different applications such as providing wear and or corrosion resistance [149]. A schematic of a brush plating tool is given in Figure 7:2.

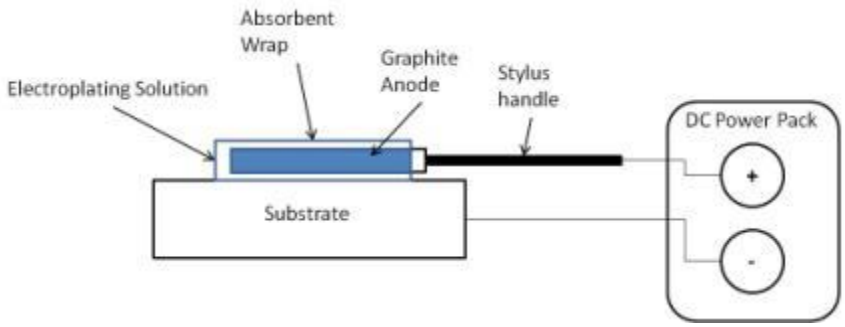

Figure 7:2: Schematic of Brush plating tool [149]

One of the main issues with brush plating can be inconsistent application of the electrolyte solution to the part due to drying effects in the tool. In manual operation uneven contact pressure between the tool and the workpiece can also be an issue. Any discontinuous plating results in uneven laminar structure of coatings, which significantly affects the coating performance [150]. An automatic brush plating system has since been developed to alleviate these problems by providing machine control and automated provision of the electrolyte solution [150]. This system showed much better plating consistency when compared to manual brush plating (Figure 7:3).

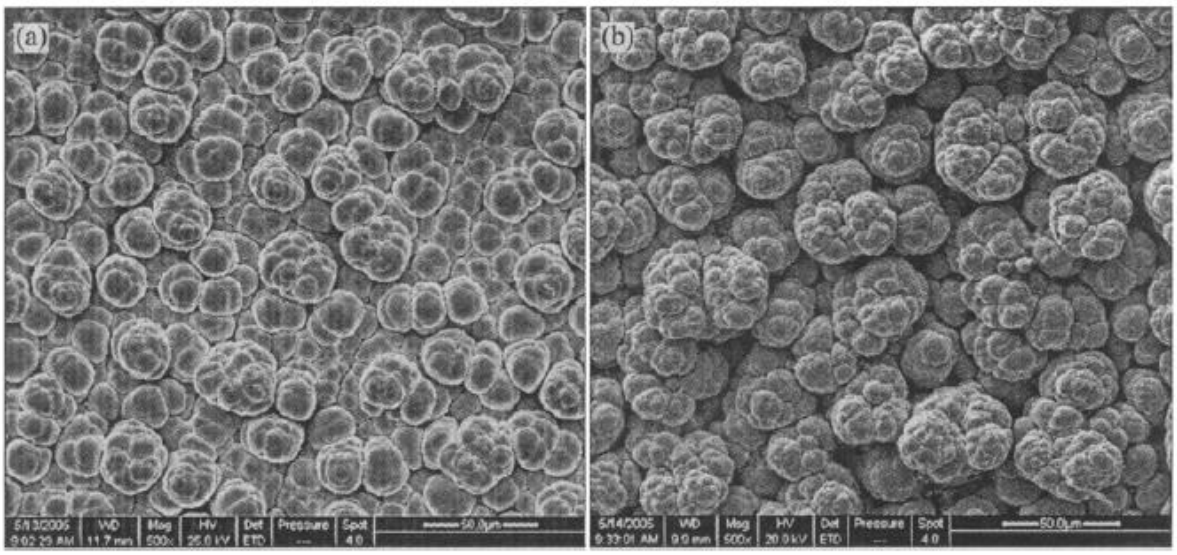

(A) (B)

Figure 7:3: SEM surface morphologies of automatically plated coating (A) and manually plated coating (B) (images obtained from Bin, WU et al. [150])

7.3 Development of a Brush Plating Tool for DW Applications

Working in collaboration with Additive Process Technologies (APT) Ltd [151] a new electroplating tool was designed specifically for DW applications. The first iteration of this tool (developed by APT) was based on the brush plating method described in section 7.2. This system consisted of a wick soaked in copper sulphate solution wrapped round a copper wire anode as shown in Figure 7:4.

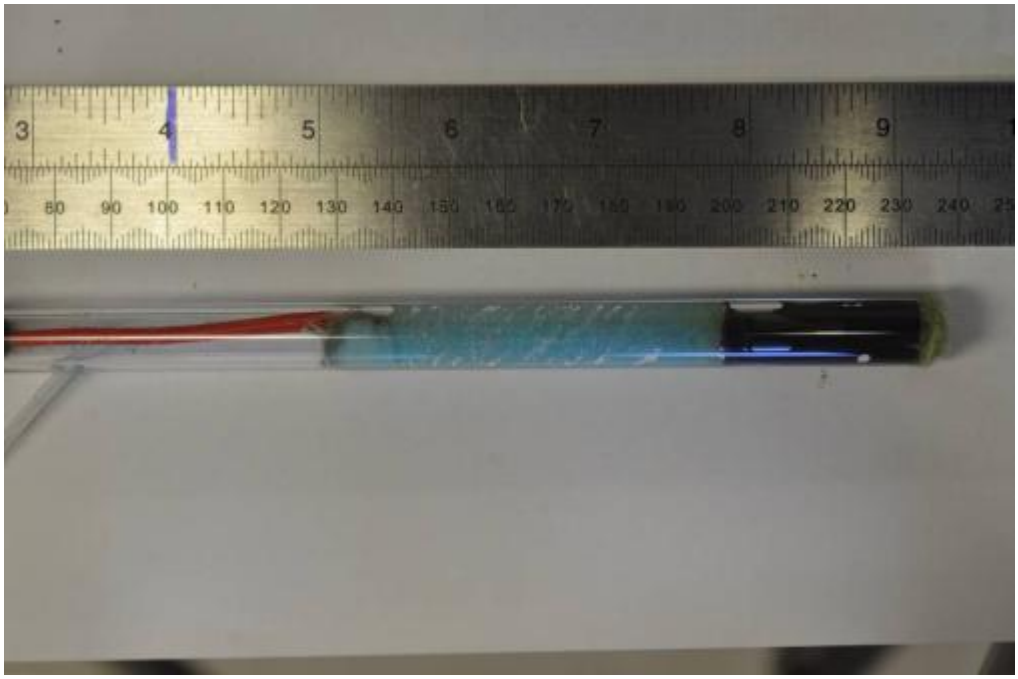

Figure 7:4: Copper plating tool developed by APT

The tool head shown in Figure 7:4 was attached to a 3-axis motion control system to allow for automated copper plating. Copper sulphate had to be applied manually to the wick from the top of the tool using a syringe. The brush plating tool was investigated for copper plating on to the silver based PTF thermoplastic, thermosetting and inkjet silver DW ink materials introduced in Chapter 5. The Hybrid ink was not considered for this test as it showed poor adhesion on a number of different substrate materials (see Chapter 5). To prepare the test samples all inks were printed on to single sided copper clad FR4 substrates with dimension of approximately 100x3x0.04mm for the PTF inks and 100x3x0.002mm for the inkjet samples. FR4 dielectric was chosen so that the samples could be tested for their RF properties at a later date. A 3mm track width was used so that each line would have an impedance of approximately 50Ω (calculated using linecalc software). For the inkjet inks an isola FR-370 substrate was used as this has a higher T_g (180°C) than regular FR4 (130°C) allowing the inkjet inks to be cured appropriately. The isola FR-370 was chosen as it also had similar dielectric properties to the FR4 substrate. Before plating the PTF inks were cured at 130°C for 30mins and the inkjet ink at 180°C for 30mins in an oven.

7.3.1 Initial Trials Using Copper Brush Plating of DW Seed Layers

Before plating the DW seed layers were connected to the negative side of a DC power supply and the brush tool to the positive side of the power supply. For these tests the current was limited to 0.1A on the power supply. APT recommended that the current density should be limited to no more

than 0.5A. Although higher current densities can increase plating efficiency (Equation 7:3) it also increases the rate at which the copper anode deteriorates. For these trials a robotic traverse speed of 20mms^{-1} was used at 10V of power. It was found that this gave adequate plating results for all inks (i.e. a measurable drop in resistance). At these settings the current tended to fluctuate between 0.05-0.09Amps for all ink samples (as long as the copper sulphate solution was regularly replenished). Plating efficiencies could be improved through optimisation of these parameters (e.g. higher voltages or slower traverse speeds) however this was not conducted as part of this study.

To build up the thickness of the plated copper multiple scans with the brush plating tool were used. Figure 7:5 shows microscope images of the DW seed layers before plating, after 6 plating scans and after 20 plating scans. After 6 scans all DW seed layers show partial plating however, there are far more silver voids in the PTF inks than the inkjet ink. Increased plating efficiency in the inkjet ink can be attributed to a much smoother surface layer and increased surface area of silver to plate to due to the absence of a resin binder. After 20 scans a continuous layer of copper forms on both the thermoplastic PTF silver and inkjet silver inks. This suggests that in the first few scans copper islands tend to form on the ink surface. Increasing the copper thickness allows these copper islands to eventually coalesce. The thermosetting PTF silver ink had the highest number of silver voids visible after 20 scans. This is perhaps not surprising considering the greater resin content within the ink layer. Any resin that remains part of the surface essentially inhibits plating. Conversations with APT suggested that higher current densities could be used to burn off any surface resin allowing more exposure to the silver particles within the ink.

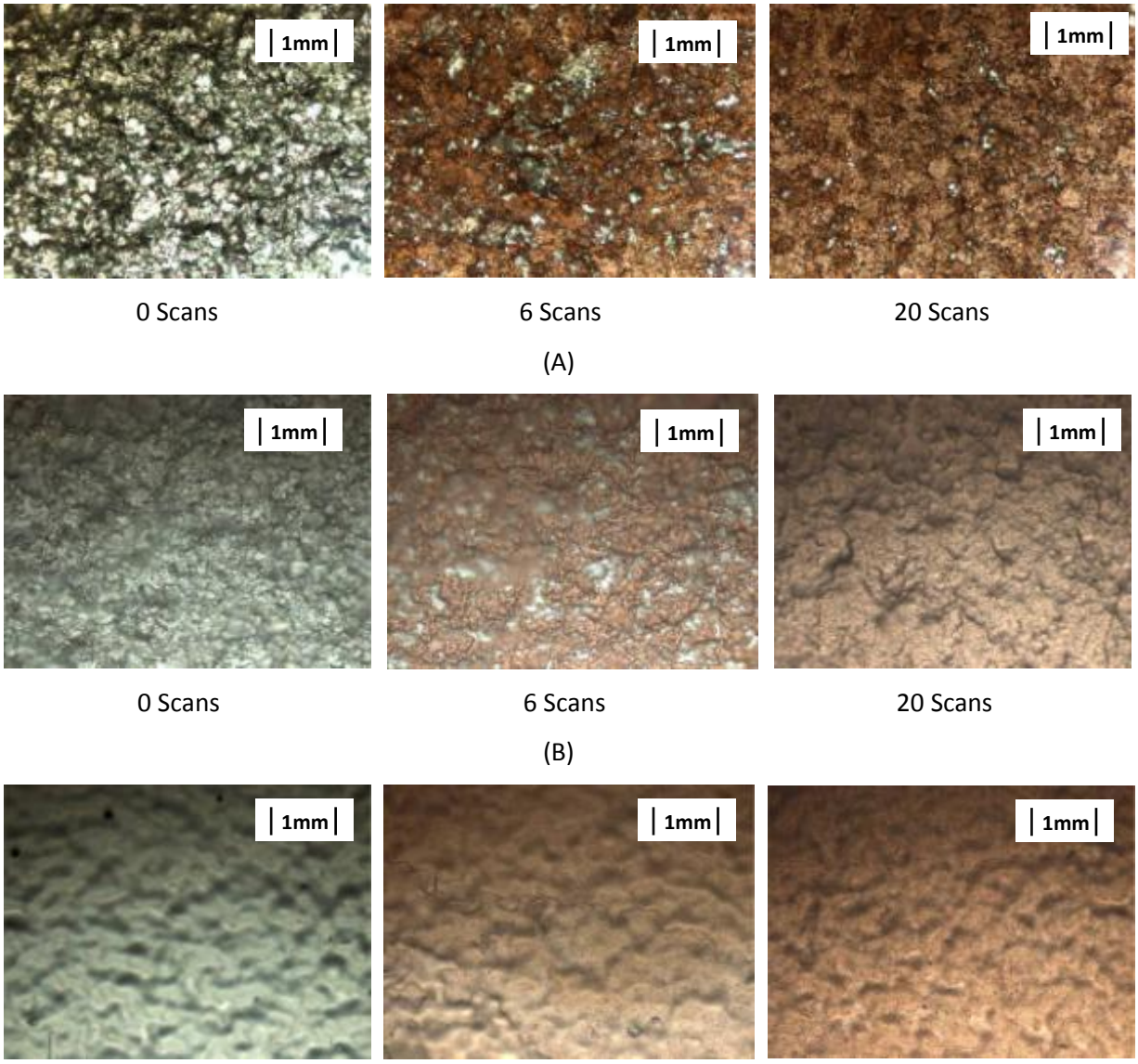

Figure 7:5: microscope images after brush plating for (A) thermosetting silver ink 20x magnification (B) thermoplastic silver ink 50x magnification (C) inkjet silver ink 50x magnification

Figure 7:6 shows the profile of the inkjet ink before and after copper plating using the Alpha-step touch probe. The profile of the ink before plating, Figure 7:6 (A), shows higher material content around the edge of the silver ink track. This phenomenon is caused by preferential drying of a droplet at the droplet's edge which subsequently creates an internal migration of solid material to the boundary of a droplet to compensate for material loss due to evaporation [152]. Figure 7:6 (B) shows how this 'coffee staining' effect can result in preferential plating around the edges of the inkjet track after brush plating due to higher silver content. Around the edges of the inkjet track the alpha step measure approximately 14-28μm of copper whereas in the middle of the track only 5-

6µm of copper was measured (assuming a 2µm inkjet layer). There are a number of ways to combat coffee staining such as substrate heating to stimulate solvent evaporation [153] and combining high and low boiling point solvents, which reduce the high evaporation rate at the droplets boundary [154].

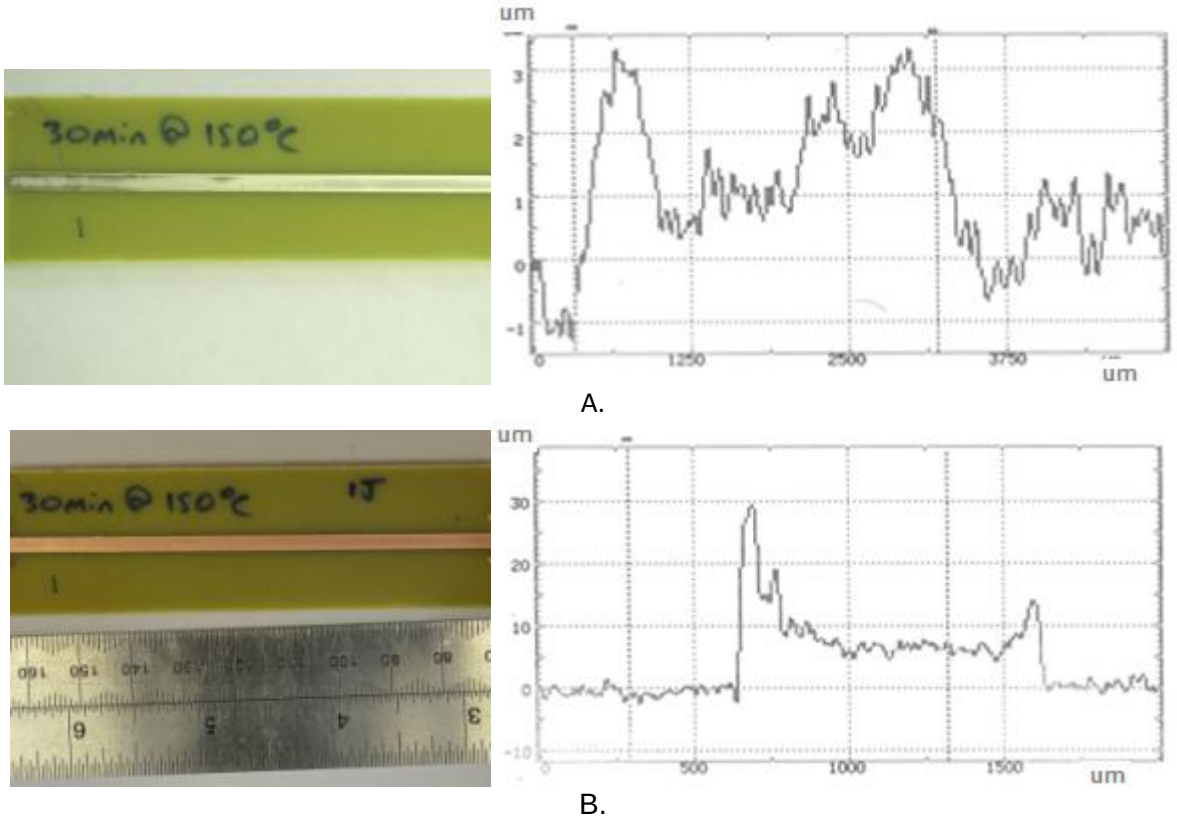

Figure 7:6: Inkjet DW seed layer on FR4 (A) before plating, (B) after brush plating (C) Alpha Step measurement of copper plated inkjet track, (after 40 EP scans)

7.3.2 Copper Brush Plating Resistance Measurements

To measure the resistances of the DW tracks before and after brush plating the two wire probe method was implemented (see Chapter 4). To calculate the bulk resistivity of the tracks accurate height and widths were required which were measured using the Alpha-step touch probe. The plating efficiency can be calculated in two ways, either by comparing the mass of copper expected from Faraday's law of electroplating (Equation 7:3) to the measured mass of copper obtained on the sample (requiring very accurate scales) or by measuring the resistance of the plated copper (isolated from the DW seed layer) and comparing it with bulk copper. The resistance of the plated copper can be calculated from Equation 7:5.

$$\frac{1}{R_{track}} = \frac{1}{R_{seed}} + \frac{1}{R_{copper}}$$ **Equation 7:5**

Where, R_{track} is the total resistance of the track after electroplating, R_{seed} is the resistance of the track before electroplating and R_{copper} is the resistance of the plated copper.

The thickness of plated copper can be calculated by measuring the difference in track height before and after plating. For the inkjet track the average track thickness was used to calculate the height and resistivity of the track.

A plot of the total resistance of the track, R_{track}, and plated copper, R_{copper}, as a function of successive scans with the brush plating tool is given in Figure 7:7 and Figure 7:8 respectively.

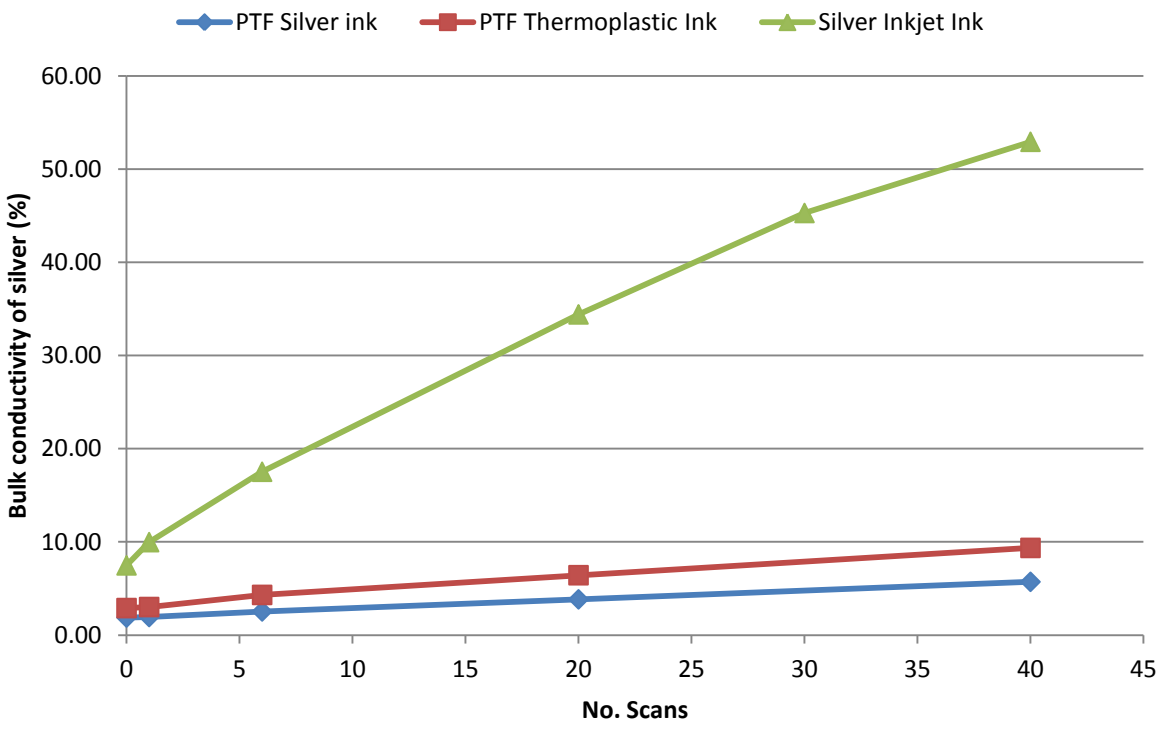

Figure 7:7: Bulk Conductivity (as a percentage of bulk silver conductivity) of copper plated DW deposits as a function of electroplated scans

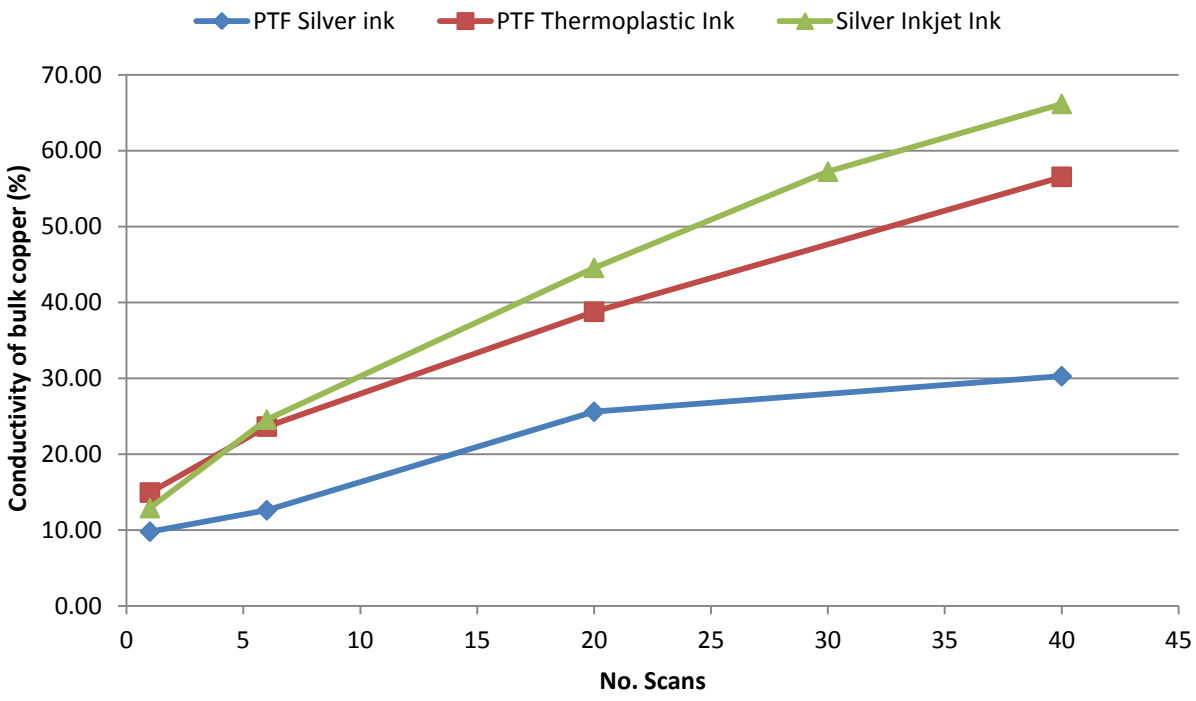

Figure 7:8: Calculated conductivity (as a percentage of bulk copper) of the plated copper layer as function of electroplated scans

The results show that as the number of plating scans increase the track resistance decreases. This is a consequence of both an increase in plating thickness and an increase in the amount of copper that is deposited per scan. This result is supported by the results obtained in Figure 7:5 where copper plating eventually covers the surface area of the DW seed layer. It is also noticeable that after 20 scans the rate at which the conductivity increases begins to tail off suggesting that there will be a maximum copper plating conductivity that can be achieved with these parameters. Increasing the voltage or reducing the scan speed may increase the efficiency and hence the conductivity of the copper that is plated on to the DW seed layer.

Comparison between the DW seed layers shows that the plating of the inkjet material gave the greatest increase in bulk conductivity. The conductivity of the plated copper (as a percentage of bulk copper) after 40 scans was calculated at approximately 66.2%. As suggested earlier the plating efficiency of this ink may be improved further by reducing the coffee staining effect. Interestingly the brush plating technique gave a higher copper conductivity than the results reported from studies on electroless plating of inkjet tracks which quoted copper conductivities of $(2.5–3)\times10^{7}$ Sm^{-1}, approximately 50% the bulk conductivity of copper [73] [155].

The thermosetting PTF ink was plated with copper with the lowest conductivity of only 30.29% bulk conductivity of copper. This is not surprising when considering the microscope images in Figure 7:5 which showed large silver voids in the thermosetting ink after 40 scans. All samples also passed ASTM D3359 adhesion measurements with a 3M pressure sensitive scotch tape with no change to material conductivity.

7.4 Development of a localised Electroplating tool

One of the potential difficulties of using the brush plating tool can arise when trying to make a connection between the DW seed layers and the power supply. If the DW seed layer is particularly large it can act as a large resistor in the circuit reducing the current density and efficiency of the EP process. In addition to this for certain applications there may not be a suitable way of connecting the seed layer effectively to a power supply during the fabrication process.

To overcome this, APT in collaboration with BAE Systems, investigated alternative ways to provide localised EP connection to the DW seed layer. One potential solution was developed that consisted of a spring mounted steel ring on the bottom of the brush plating tool which was connected directly to the negative terminal on the power supply. When the steel ring is in contact with the DW seed layer an electrical connection can be made through the DW seed layer to the copper anode (via the electrolyte solution) resulting in plating.

A schematic of the localised brush plating tool is shown in Figure 7:9. To help the ring move smoothly over the seed layer the underside was chamfered and polished. The diameter of the steel ring was approximately 20mm, which meant that this was the minimum feature size that could be plated using this tool.

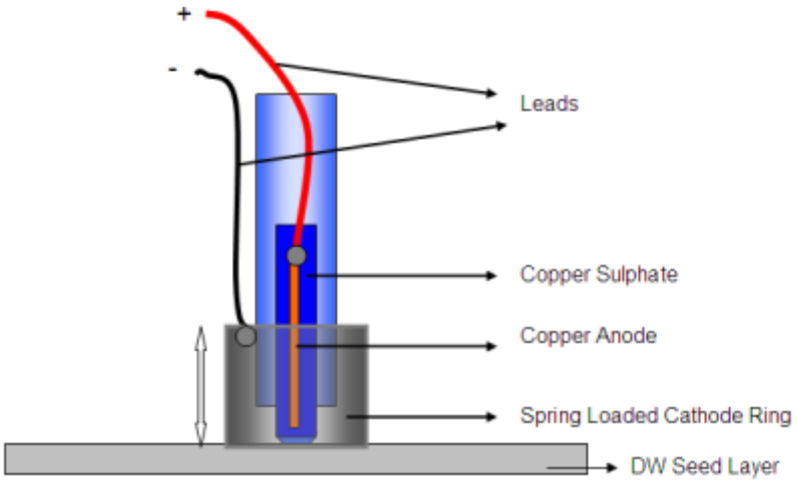

A.

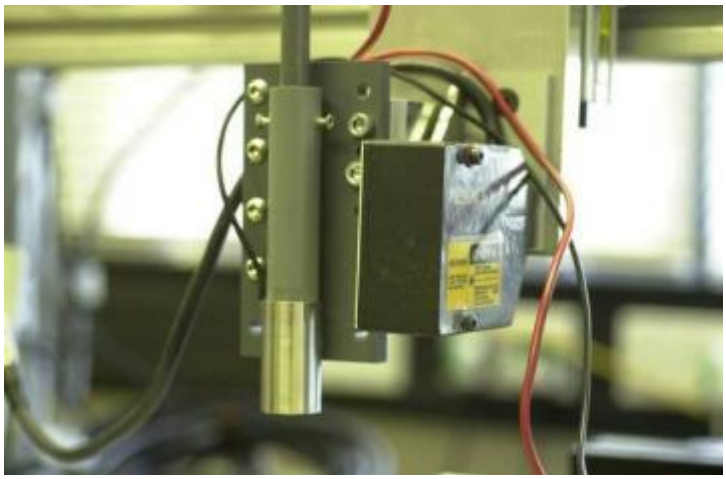

B.

Figure 7:9: (A) schematic of localised brush plating tool (B) Image of brush plating tool on 3-axis motion system

Copper plating using the localised brush plating tool was investigated for the inkjet and PTF inks using the same parameters described in section 7.3.2. Figure 7:10 shows microscope images of the results. These images show that whilst copper plating is achievable the steel ring causes streaks and scratches on the surface of the track where copper has effectively been stripped from the seed layer. It was also found that the resistance of locally plated copper deposits were much higher than the brush plating method used in section 6.3.2. Poor copper plating was primarily down to preferential plating of the steel cathode ring as opposed to the DW seed layer. This occurred because excess copper sulphate was wetting the steel ring during the plating process essentially bypassing the DW seed layer. In turn copper deposits on the steel ring would roughen the surface thereby scratching the surface of the DW seed layer (as observed Figure 7:10).

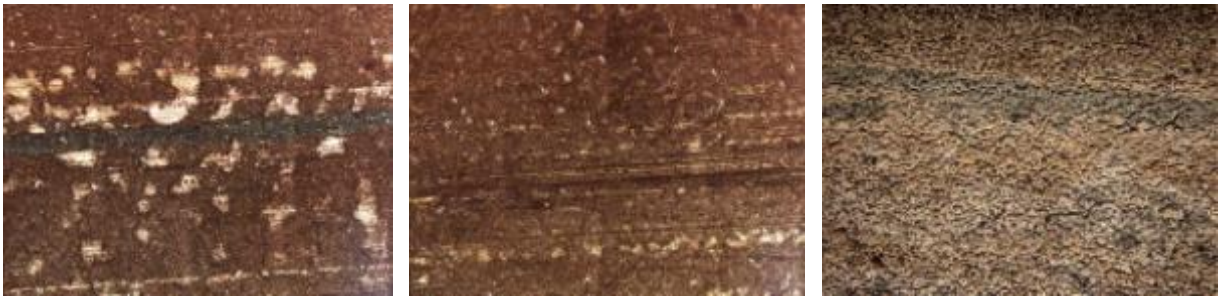

A. B. C.

Figure 7:10: 20x Microscopic images of locally plated DW Seed layers (A) PTF Thermosetting Silver ink (B) PTF thermosetting silver ink (C) Inkjet silver ink

7.5 Conclusions

This chapter has presented a novel method of electroplating DW seed layers for improving the conductivity of DW ink tracks. Previous studies have used electroless plating techniques to plate copper on DW seed layers [73]. However, this type of process uses aggressive chemicals and is not suitable when applying DW to large structural systems [145]. Brush plating on the other hand can locally plate DW deposits and can be automated using suitable robotics [150].

Brush plating was used to add copper to PTF and inkjet inks which were printed on to FR4 substrates. Results showed that the thermosetting PTF ink system was not as suitable for brush plating as inkjet and thermoplastic inks due to large pockets of resin on the top surface of the conductor. Plating on both the inkjet and thermoplastic PTF inks resulted in conductivities of 66.3% and 56.6% bulk copper respectively. It was noted that the plating efficiency of the inkjet ink could be further improved by removing or reducing the coffee staining effect. This would allow the inkjet inks to be printed with a uniform distribution of silver nano particles across the track profile thereby increasing the surface area that can be deposited onto by the localised plating head.

For this technology to become useful for printing onto larger structural components further developments are also needed to increase the plating efficiency of the localised brush plating tool. Results showed that the current design scratches the top surface of the plated track thereby reducing conductivities.

8 Localised curing of DW deposits

Improvements in DW ink conductivity can be achieved via the application of localised electroplating as described in Chapter Six. This technique requires the DW ink material to be thermally processed which is conventionally done in an oven beforehand. For applications of interest to this project, oven curing is either not practical or not desirable.

A number of investigations have explored ways to overcome these issues by using a laser source to process DW ink materials [156] [68]. One of the biggest advantages of laser processing is that heat can be restricted to a localised area thereby minimising thermal penetration into the substrate surface. Furthermore, it enables easy integration with the DW system so that curing can take place in-situ with printing. This enables DW processing on to large structures without the restriction of an oven and also removes re-registration problems that could occur when printing devices with multiple material layers.

This chapter aims to identify a suitable method for localised processing of DW ink materials. This study will include spectral analysis of the DW material and experimental trials with a laser diode and broadband spot curing system.

8.1 Introduction to Localised Curing

As mentioned the main localised curing techniques that have been used for DW applications have tended to use a laser source to impart heat into the material. Past experiments have shown localised curing using Nd:YAG, CO_2 and diode lasers for localised curing of both polymeric, PTF and inkjet materials [156] [68] [157]. Induction heating could also be used to process DW material although it may be difficult to localise the heat treatment especially if other conductors (such as the substrate) are nearby, or there is a requirement to cure non-conductive DW elements (such as dielectric inks) [158].

Optimum optical processing relies on generating sufficient heat rise within the material which is distributed evenly throughout the material layer. The heat rise in the material for a given laser power will be dependent on the heat capacity of the composition, its reflectance and absorptivity. According to the Beer-Lambert law (Equation 8:1), the amount of energy that can be coupled into a

material is dependent on the absorption coefficient which can change as a function of the wavelength of incident radiation and the material composition.

$$T = \frac{I}{I_0} = e^{-\alpha l}$$ **Equation 8:1**

Where T is the transmission, I_0 and I is the intensity of the incident light and the transmitted light respectively, L is the distance the light travels in the material and α, is the absorption coefficient.

Absorption of electromagnetic radiation by DW ink materials can be complex. Conductive PTF inks for example are composed of multiple materials including a polymeric resin, high and low boiling point solvents and metallic silver particles. At wavelengths greater than 400nm (above the UV spectrum) the polymeric resin component will become more transparent to electromagnetic radiation compared to the silver which is highly reflective [159]. Taku, et al [156] described absorbance as being a combination of three processes, primary absorbance by the polymeric resin, secondary absorbance by the silver particles and tertiary absorbance in both the resin and silver through multiple reflections by the silver particles within the ink composition.

Even distribution of the heat energy within the material will rely on having a high penetration depth of incident radiation and high thermal conductivity. The penetration depth is defined as the depth at which the radiation inside a material falls to 1/e (~37%) of its original value within the material. The penetration depth is given by Equation 8:2.

$$\delta_p = \frac{1}{\alpha}$$ **Equation 8:2**

Where δ_p is the penetration depth and α, is the absorption coefficient.

As the material is heated the thermal conductivity could also change. For example, during the first phase of heating the ink will be wet due to high solvent content. Upon heating the solvent will evaporate changing the thermal conductivity of the material. Further heating will initiate curing (through cross-linking, sintering or higher boiling point solvent release) bringing the silver particles into greater contact with one another thereby increasing material thermal conductivity.

When determining the thermal distribution within the DW material it is also important to consider the influence of the substrate. A thermally conductive substrate will act as a heat sink dissipating heat from the ink which could lead to uneven curing. Conversely, an insulating substrate material will enable the majority of the heat to be encapsulated within the ink deposit.

One of the biggest challenges with laser curing is trying to achieve the required heat rise and distribution with the short dwell times needed to make laser curing a viable alternative to oven curing. This requires optimising the processing parameters and thermodynamic and curing properties of the ink material whilst taking into account the thermodynamic properties of the substrate.

8.2 Investigation of curing mechanics of DW PTF inks.

The curing mechanics of DW inks can be an important factor in determining whether they are suitable for localised curing. DMA was used to measure the glass transition temperature, T_g, as a function of cure temperature and time for the PTF silver ink. This work follows on from the DMA experiments conducted in Chapter 5 showed how tanδ (and hence crosslink density) increases with cure temperature. A similar graph to the one shown in Chapter 5 is given in Figure 8:1.

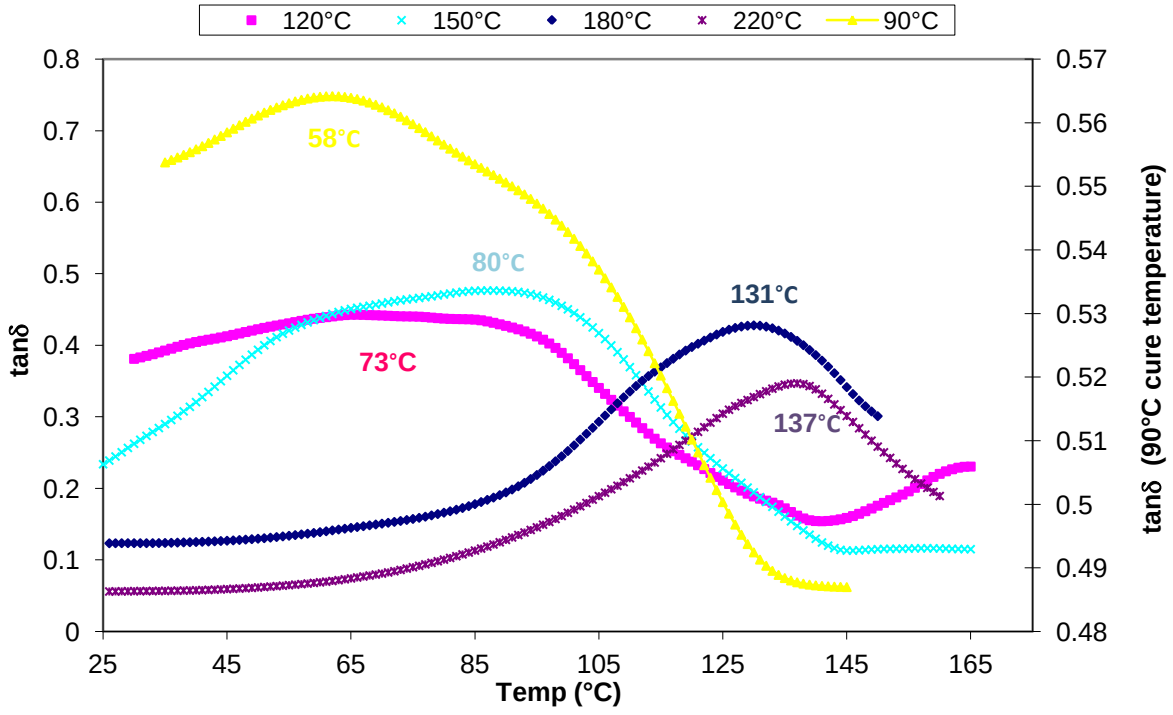

Figure 8:1: tanδ measured as a function of temperature for the silver ink cured at 90°C, 120°C, 150°C and 220°C for 20mins. Peak maxima are shown in figure indicating T_g.

A further set of experiments were performed using the DMA to see the effects of cure time at constant cure temperature. As before approximately 40μm thick silver ink was coated on to a steel substrate using the tape cast method before being cured in an oven. The inks were cured at 120°C and 220°C at varying cure times before undergoing DMA analysis. Once cured the samples were placed in the DMA and heated at a rate of 10°C/min from 25°C to 170°C at an oscillating frequency of 5Hz. The results from this analysis are shown in Figure 8:2, Figure 8:3, and Table 8:1.

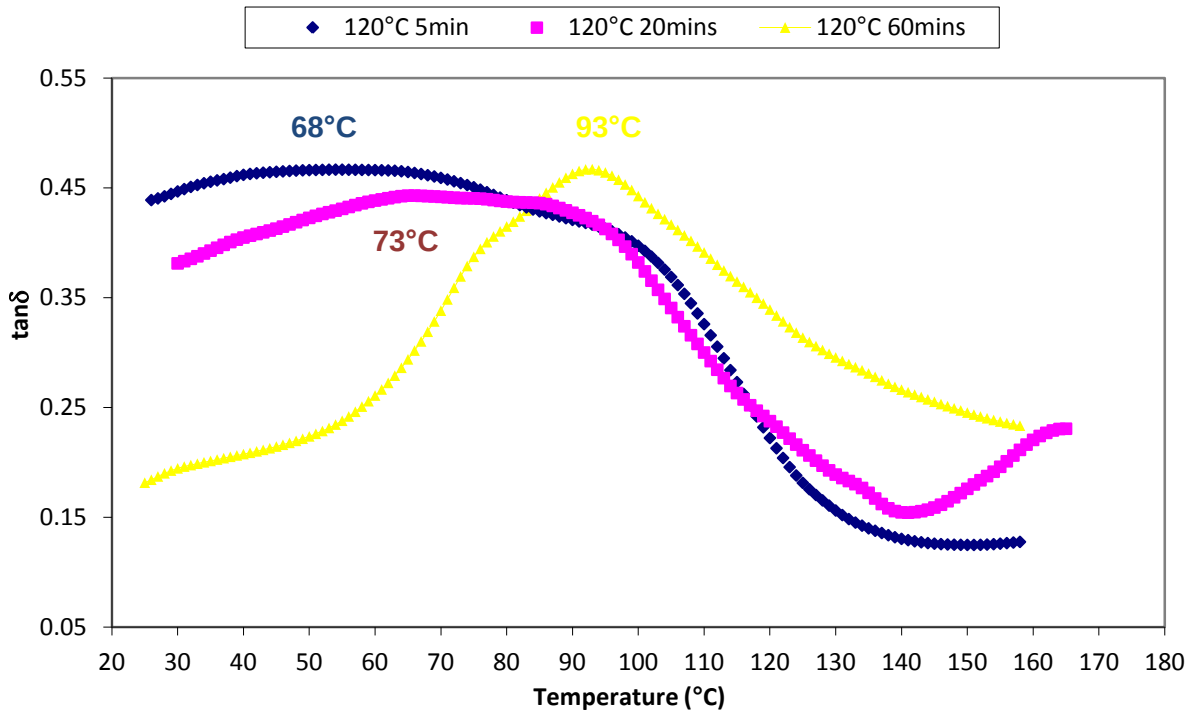

Figure 8:2: tanδ measured as a function of temperature for the silver ink cured at 120°C for 5, 20 and 60mins. Peak maxima is shown in figure indicating T_g

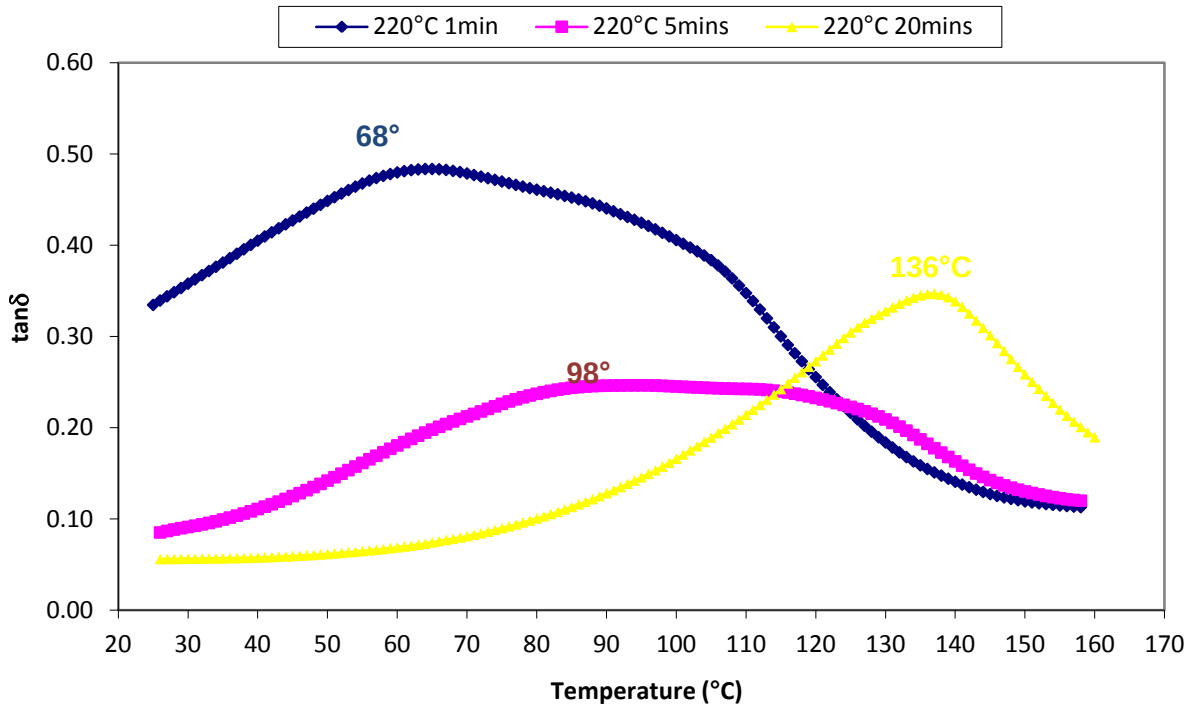

Figure 8:3: tanδ measured as a function of temperature for the silver ink cured at 220°C for 1, 5 and 20mins. Peak maxima is shown in figure indicating T_g

Cure Temperature (°C)	Cure Time (mins)	Tanδ Peak Maximum (°C)
120	5	Insufficient Curing
120	20	73
120	60	93.2
220	1	68
220	5	98
220	20	136

Table 8:1: Summary of results DMA results

The results show that as curing time increases so does the T_g. Comparison between curing at 120°C and 220°C shows that much shorter curing times can be used if a high enough temperature is used. For example, a T_g of approximately 90°C can be achieved by curing the resin at 120°C for 60mins whereas a similar T_g can be achieved for a much shorter cure time of 5mins when cured at 220°C. Whilst this experiment cannot mimic the kind of temperatures and exposure times used in laser curing it does suggest the curing mechanism is more dependant of temperature than time and hence that theses ink may be suitable for laser curing.

8.3 Spectral Analysis of DW PTF inks

The efficiency of the laser curing process is reliant on the absorption and penetration depth of laser irradiation. To measure these properties absorption spectroscopy can be used. The spectrophotometer is made up of a light source, a holder for the sample, a diffraction grating to separate the different wavelengths of light and a detector. The light source determines the wavelength range over which the sample can be measured [160].

The spectral properties of the DW PTF inks were measured with a Varian Cary 5000 UV/Vis spectrometer over the wavelength range of 300nm to 3300nm. This wavelength range covers a range of laser such as diode, ND:YAG and fibre lasers. These lasers can be delivered through a fibre which has many advantages for DW such as ease of integration and increased accessibility to difficult to reach areas. To measure the spectral properties at longer wavelengths (mid to long IR) Fourier Transform Infrared Spectroscopy (FTIR) can be used.

To calculate the absorption percentage the reflectance and transmission was measured with the UV/Vis spectrometer. Reflection measurements were made by coating a white alumina tile with approximately 40μm of ink before placing it in an integrated sphere. The integrated sphere essentially acts as a light collector which helps to increase the signal-to-noise (SNR) ratio. A schematic of the integrated sphere is given in Figure 8:4.

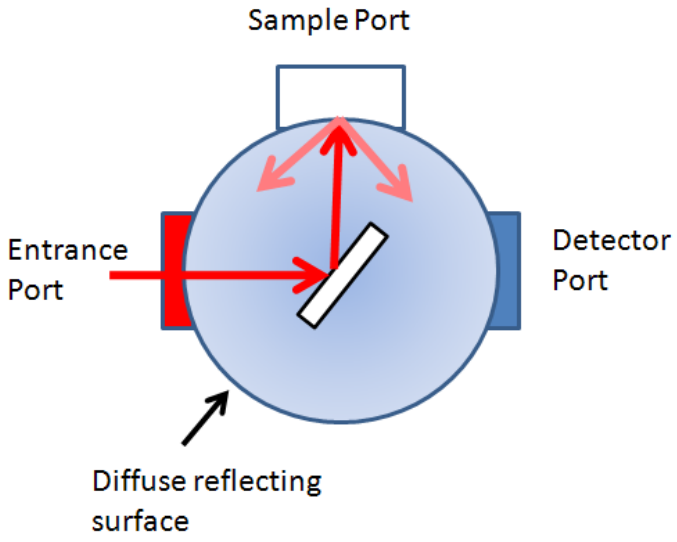

Figure 8:4: Schematic of Integrated sphere

Transmission was measured by coating a glass slide with approximately 40μm of ink (as with the reflectivity measurements) using the tape cast method. All results were recorded by removing

background radiation and reflection/transmission from the substrate material (e.g. absorption by the glass slide).

The absorption percentage was calculated as the percentage of incident radiation I_o, minus the reflected I_r, and transmitted radiation I_t, as shown in Equation 8:3.

$$I_A=I_0-I_t-I_r \qquad \textbf{Equation 8:3}$$

The absorption percentage can be related to the penetration depth to give an indication of how the sample is heated. The penetration depth was calculated from Equation 8:1 where I_0, is the incident radiation percentage minus the percentage reflected and I, is the transmitted radiation. Spectral analysis was conducted for five different inks:

- Silver hybrid [161]
- Silver PTF ink [161]
- Carbon doped silver ink [161]
- PTF thermosetting resin binder [127]
- low cure (90°C) thermoplastic dielectric ink [161]

The carbon doped silver ink is a version of the PTF silver ink loaded with additional carbon black particles. Carbon black was chosen to increase IR absorptivity of the ink material. To minimise any significant effect on the electrical conductivity and mechanical (adhesion etc.) only a small amount of carbon was used (approximately 0.75% by weight). To investigate the spectral properties of the inks without any silver present a further ink was formulated which contained only the resin binder. In addition to the PTF silver inks, a low cure thermoplastic dielectric ink was also analysed for comparison. The absorption percentage for the silver inks is shown in Figure 8:5.

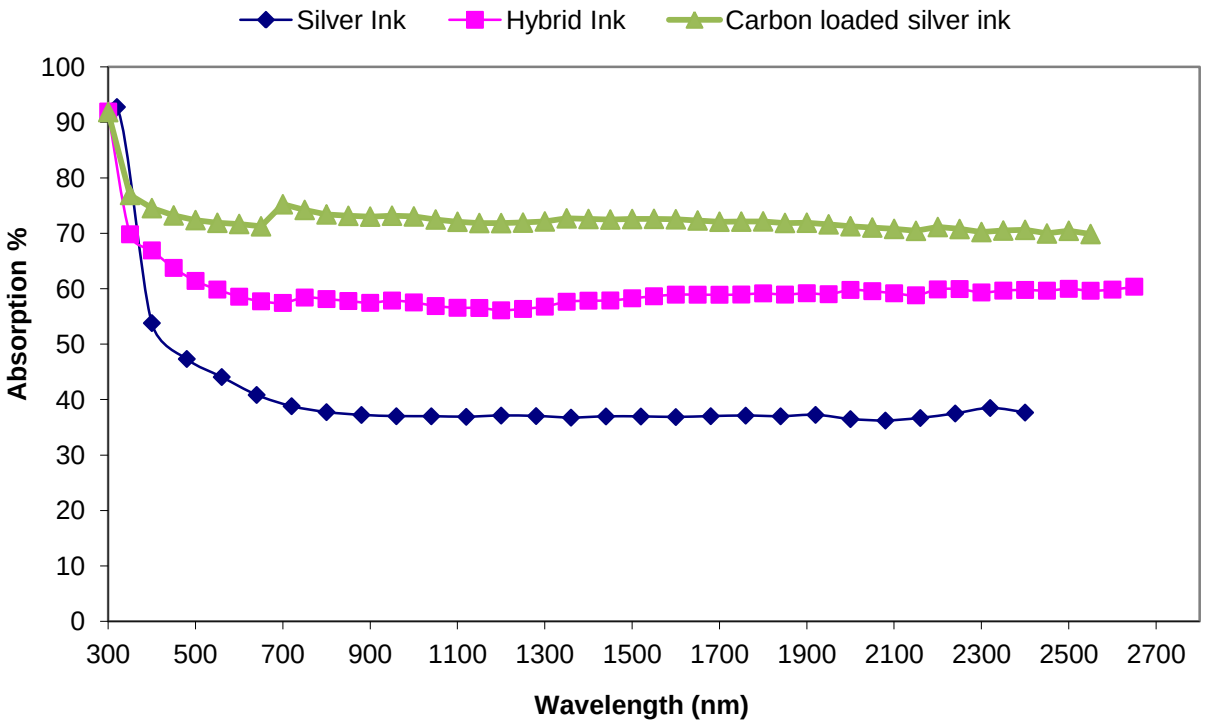

Figure 8:5: Absorption spectra of silver, Carbon doped silver and Hybrid inks.

Figure 8:5 shows that at wavelengths greater than 350nm the absorption for the silver inks remains relatively constant. As expected the carbon doped silver ink has the highest absorption at approximately 70%, nearly 20% better than the original silver ink composition which stands closer to 40%. The hybrid ink also has a higher absorption than the silver ink at 60% (above 350nm).

Figure 8:6 shows the average reflection (between 350nm to 2700nm) of the hybrid and silver inks after drying at room temperature and heat treatment in an oven for 30mins. After heat treatment at 160°C the reflectivity of the hybrid ink reduces from 52% to approximately 43% (after 350nm) whereas the reflectivity of the silver ink changes only marginally from 65% to 63%. This outcome could be of particular importance when laser curing the hybrid ink as it suggests the first laser scan will impart the most amount of heat energy within the ink.

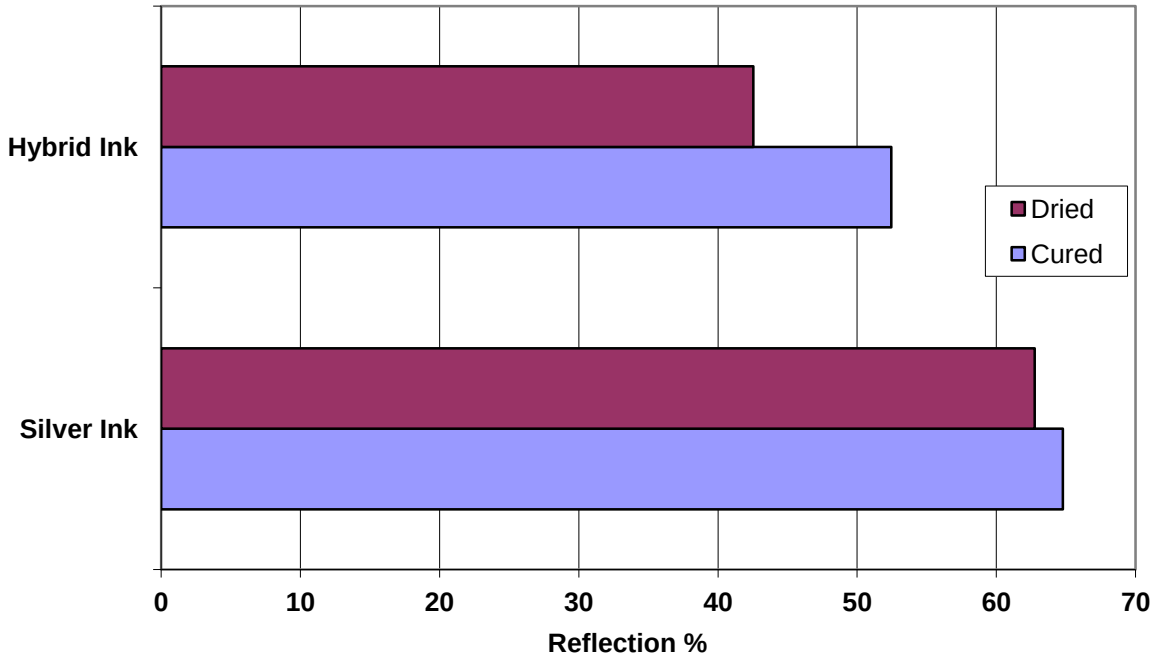

Figure 8:6: Average reflection of silver and hybrid inks (between 350nm to 2500nm) after room drying and oven curing at 120°C and 160°C respectively

The calculated penetration depth in Figure 8:7 shows that the IR radiation only penetrates 10μm into the ink layer for all inks (approx. 25% of the 40μm film thickness). The penetration of the incident radiation is important as it will have an effect on the distribution of heat energy within the deposit. For thin film deposits (in the region of 40μm) the low penetration depth of the incident radiation is compensated by the relatively high thermal conductivity of the silver particles (compared to the polymer resin) which will allow the majority of the heat to distributed evenly across the deposit (as demonstrated by the laser cure results in section 8.4).

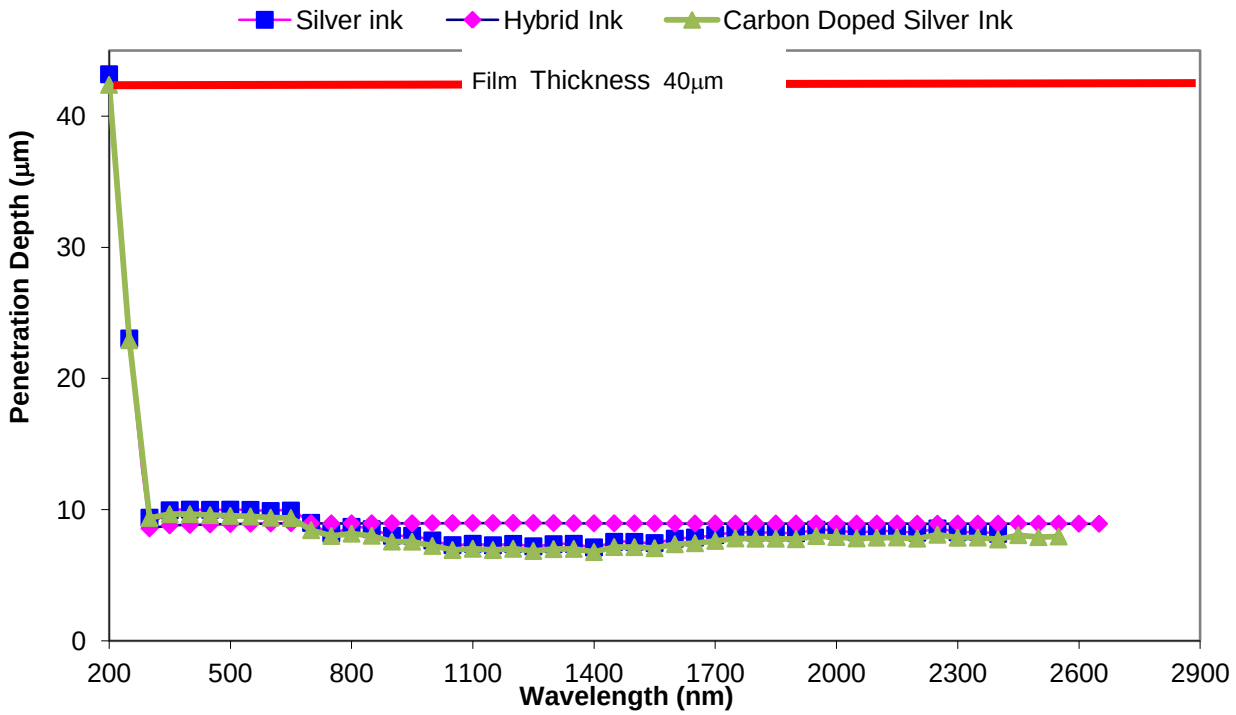

Figure 8:7: Penetration depth as a function of wavelength for silver, carbon doped silver and hybrid inks.

Figure 8:8 (A) shows the absorption percentage for the PTF resin binder and thermoplastic resin binder. The resin binder has a number of discrete absorption bands primarily in the UV and the mid infra-red (above 2700nm) wavelengths when compared to the silver inks. Between these wavelengths most of the radiation will transmit straight through the resin with no absorption (Figure 8:8, (B)). At certain wavelengths it can be seen that the resin has high absorption and can be heated uniformly with penetration depths greater or equal to the 40 μm film thickness. The dielectric ink also contains a number of absorption bands almost identical to the resin system but with lower greater absorption. For radiation which is transmitted through the sample there could be additional absorption by the underlying substrate material. Whilst this could aid the curing process by transferring heat to the ink via heat conduction, it may be undesirable for temperature sensitive substrates.

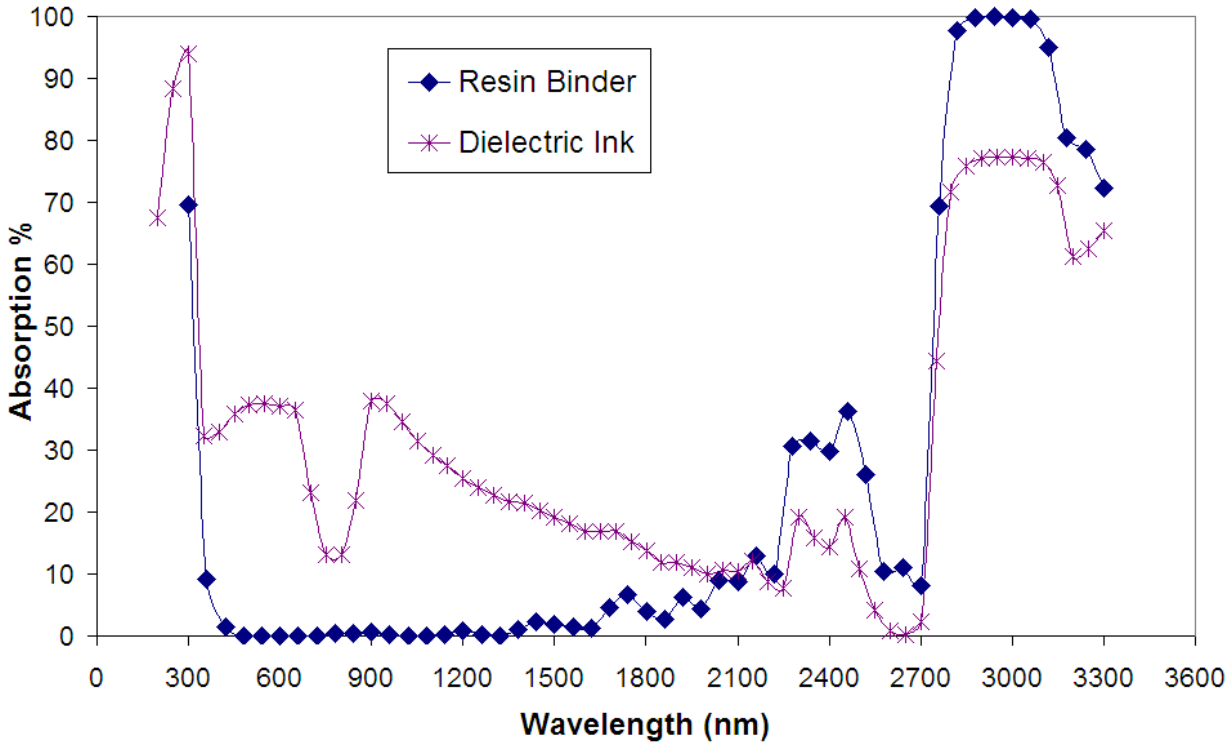

(A)

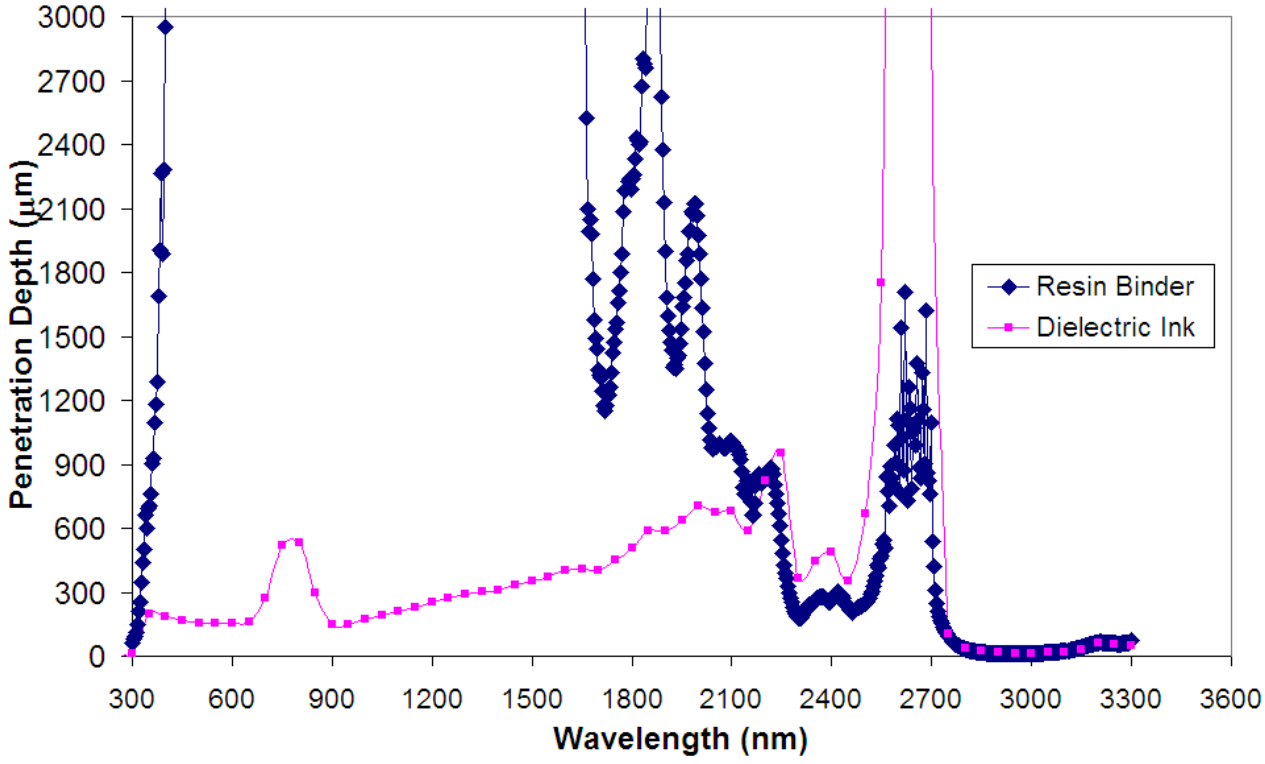

(B)

Figure 8:8: (A) Absorption spectra unloaded resin binder and dielectric ink (B) Penetration depth as a function of wavelength in resin binder and dielectric inks.

8.3.1 Discussion

The spectroscopy results show the resin binder acts as the primary absorber for IR radiation within the ink composition. It is unclear how much of this radiation will actually be absorbed by the ink due to the high reflectivity of the silver particles. It may be possible to optimise the curing process by choosing a radiation source that matches the peak absorption bands within the resin system to get the highest possible heat rise within the ink. Carbon black particles can also increase IR absorptivity of the conductive silver inks.

Tailoring of the laser source can be particularly useful for materials with low thermal conductivity where it is difficult to heat the ink uniformly. For example a particularly large dielectric film thickness may require higher penetration depths. Typically ND:Yag (1.064μm wavelength) and $C0_2$ lasers (10.2μm) have been used for material processing applications such as welding and cutting [162]. As can be seen from the spectroscopy results at 1.064μm the polymer resin tend to be transparent with low absorption, however, the dielectric ink will absorb at these wavelengths. Whilst C02 lasers are currently being used there are proving to be more unpopular due to their large size and inability to be fibre delivered. For this reason, high power, highly stable and more compact fibre lasers such Erbium doped fibre laser are being used with an output wavelength of 1550nm. As DW inks only require very low temperature for curing lower power laser sources such as diode lasers can be used. Diode lasers can range between wavelengths of 370nm-3300nm and so can be selected depending on the applications and power required. Other laser sources such as Excimer lasers can be used at UV frequencies from 193nm-351nm's where the DW silver inks have been shown to have higher absorption [163].

An alternative solution to using different laser sources would be to use a broadband or white-light source to process the inks. A broadband system would be able to take advantage of all the absorption bands within the ink composition.

8.4 Localised curing trials

Localised curing of DW inks was investigated using two different systems, an 808nm fibre delivered diode laser and a broadband thermal spot curing system. The primary objective of these investigations was to determine the minimum energy density required to cure the inks to obtain results equivalent to fully cured inks processed in an oven. Energy density was calculated using Equation 8:4 [164].

$$E_l = \frac{P}{\pi D_{sp}{}^2 / 4_s} \frac{D}{V_s} = \frac{4P}{\pi V_s D_{sp}}$$ **Equation 8:4**

Where, P, is the power, D_{sp}, is the spot diameter and V_s is the scanning rate of the localised curing system.

8.4.1 Laser Processing Setup

Laser curing trials using a fibre delivered 808nm laser diode system were conducted on the silver PTF and carbon doped silver PTF inks. The laser diode was selected for its ease of integration with the DW system, and relatively high powers for processing. The laser is delivered from a fibre bundle consisting of several multimode fibres. In this experiment a 10-times microscope objective was used in conjunction with a 100 mm focal length spherical lens to acquire a beam waist $1/e^2$ diameter of approximately 450 μm (the beam profile was measured using a 4222-2000 Cohu CCD camera). With the optical arrangement used, the beam-waist was formed at approximately the focal point of the lens, giving the far-field beam profile which was somewhere between a Gaussian and a top-hat profile. This setup is illustrated in Figure 8:9.

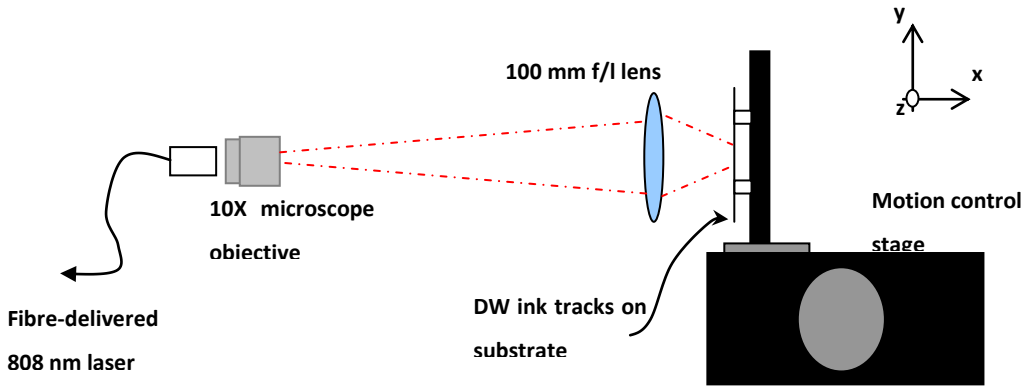

Figure 8:9: Experimental configuration for laser curing of DW PTF inks

For these trials the silver PTF and carbon doped PTF inks were tape-cast printed on to a carbon fibre substrate. The carbon fibre substrate consisted of a HexPly 8552 [165] resin system which has a maximum operating temperature of 120°C. This material was selected as it is used in a number of different military and aerospace applications. Before applying the silver ink to the substrate it was first coated with approximately 30-40μm of PTF dielectric ink [161] before curing for 100°C for 30mins in an oven. The dielectric ink layer was used to further protect the carbon fibre substrate from damage and to prevent electrical shorts between successive conductive tracks. The silver and

carbon doped silver were printed on to the substrate with dimensions of approximately 100x0.5mm with a film thickness of approximately 40μm. The track width was selected to be similar to the diameter of the laser beam. Resistance measurements were made by placing multi-meter probes at either ends of the printed tracks after each traversed laser pass. After each pass the sample was allowed to cool down for 5mins before the next scan was initiated.

All measurements were normalised against an equivalent 220°C oven cured silver PTF ink track (where a value of '1' is equal to the resistance of the oven cured track) which was tape cast on to a alumina ceramic substrate, this gave a resistance value of approximately 6.38Ω. Oven curing at this temperature and time allows the ink to reach maximum cross-link density (Chapter Five section 5.5.3 figure 5). It should be noted that the oven cured resistance of the carbon doped silver track was much higher at 10.4Ω.

8.4.2 Laser diode curing results

Curing was investigated by varying the laser power at a constant laser traverse speed of 1mms^{-1}. Results were only recorded at laser powers which resulted in no visual damage to the substrate material. At powers greater than 3W burning marks could be seen in the dielectric layer. The results for the silver PTF and carbon doped silver PTF ink are shown in Figure 8:10 and Figure 8:11.

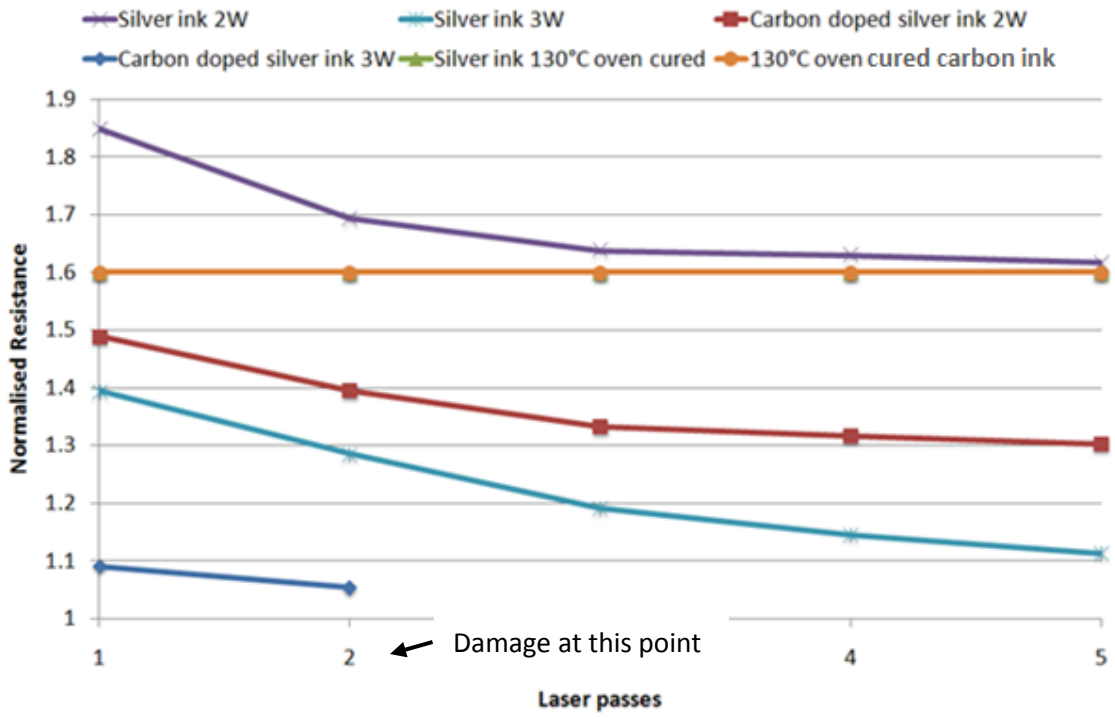

Figure 8:10: Normalised resistance (DW silver ink 220°C, 30min cure) against successive laser passes for the DW silver and DW carbon doped silver ink.

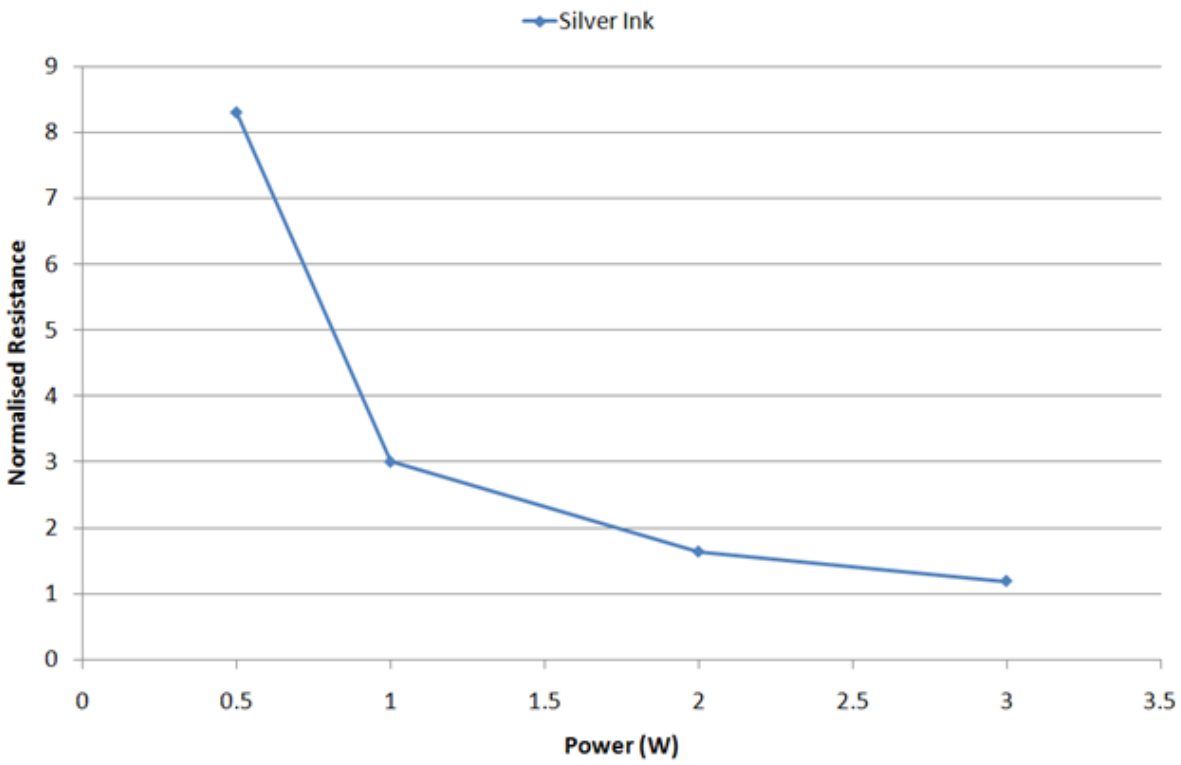

Figure 8:11: Normalised resistance of silver ink after three passes at different powers with a traverse speed of 1mms^{-1}

Figure 8:10 shows that the resistance follows an asymptotic relationship as the numbers of scans are increased. After a certain number of scans any further increase has little effect on the resistance of the material. An increase in laser power was shown to lower resistances for the same number of laser passes (Figure 8:11). The relationship between laser power and number of scans is consistent with previous DMA results (Table 8:1) which suggested that temperature (laser power) had a greater effect on curing than processing time (number of laser scans). The optimum resistance using this setup was obtained with 3W of laser power after 5 laser scans resulting in a normalised resistance of 1.2. Increasing the laser power above 3W resulted in visible damage to the dielectric and substrate material.

It was shown that the resistance could also be reduced by using a carbon doped silver ink. Whilst the oven cured resistance of the carbon doped silver ink was higher than the oven cured silver ink, laser cured samples showed an improvement in both resistance and processing times. With a laser power of 3W and processing speed of 1mms^{-1} a normalised resistance of approximately 1.05 was achieved after only two laser scans. This result could be explained by greater absorption of the laser energy. It was noticed that a greater amount of smoke was being ejected from the ink material as it was processed. It could also be seen that after one or two passes the under-lying dielectric ink became

burnt and black. In fact after 3 passes with the laser the carbon doped silver ink and substrate became so damaged that the resistance was impossible to measure.

Figure 8:11 shows how the resistance drops asymptotically with power for a given speed and laser scan. It is likely that the initial drop in resistance is a consequence of high solvent loss and reaching the activation energy for curing. Upon initiation of curing any further drop in resistance (caused by crosslinking of the resin binder) could be proportional to the increase in energy density shown by the flattening of the graph in Figure 8:11. Degradation would occur at larger powers and may hinder the functionality of the ink causing an increase in resistance.

One of the key observations made when laser curing both the silver and carbon doped silver ink materials was the increased surface roughness when compared to oven cured silver ink tracks. Figure 8:12 shows a photographic image of a laser cured silver ink track next to a 130°C oven cured silver ink track. A higher oven cured temperature was not used due to the maximum operating temperature of the carbon fibre substrate [165].

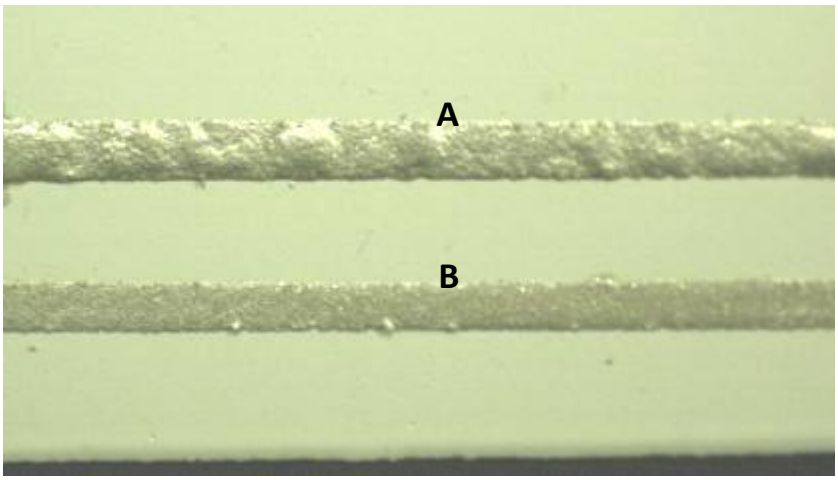

Figure 8:12: Printed silver ink track onto a dielectric coating on carbon fibre which were (A) Laser cured (B) 130°C oven cured.

To measure the surface roughness of the ink tracks a Wyko NT1100 white-light interferometer was used[4]. Using this technique the surface roughness, Ra, of the oven cured silver ink track was measured at approximately 4.2μm whereas the surface roughness of the laser cured silver ink was measured at 9μm. The white light interferometer results for the laser cured silver ink are shown in

[4] These Measurements were made by Taku Sato and Sandeep Raja in Collaboration with the Laser Group, Dept of Engineering, University of Liverpool

Figure 8:13. This technique was particularly limited as it could only capture a small area of the deposit (approximately 3mmx3mm area). The measurement was also made on a particularly smooth part of the track and therefore does not take into account some of the large blisters that are present in the material. It was hypothesised that the main reason for the high surface roughness and blistering of the ink track was the fast evaporation of the volatile solvents within the ink.

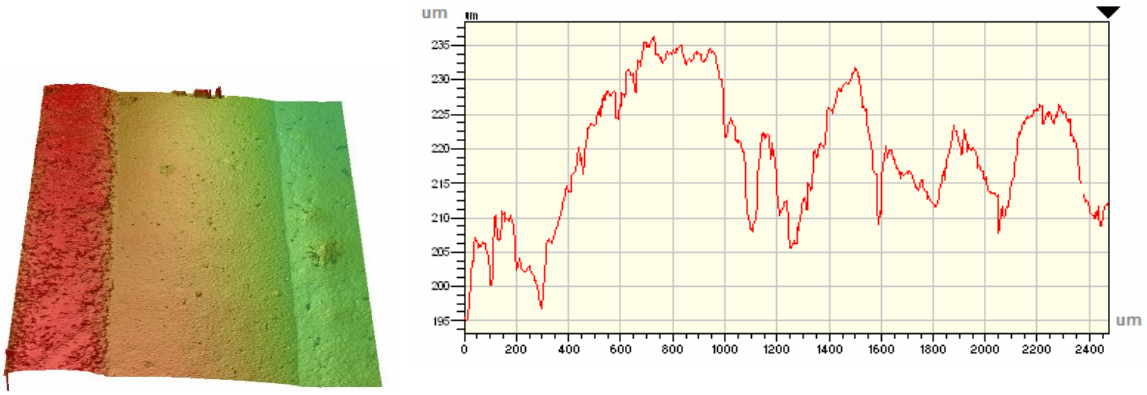

Figure 8:13: White light interferometer measurement of laser cured silver ink track (profile measured in µm).

A number of methods could be used to reduce the surface roughness of laser cured deposits. The inks for example could be modified to contain quick drying solvents which could be driven off at room temperature before processing. One disadvantage of changing the solvents within the inks is that it can have a knock-on effect on the rheology of the ink and how long it could be kept within the nozzle before drying. Alternatively pre-heating methods could be used to drive off the solvent before processing. Unfortunately due to the subsequent unavailability of the 808nm diode system this could not be investigated any further.

8.4.3 Broadband Spot Curing

Results from section 7.3 suggested that as the DW inks can absorb infrared radiation at different wavelengths and a broadband source may be better suited for curing than a laser source. To investigate broadband curing of DW inks the IR Photonics AS200 iCure^{tm} thermal spot curing system was used. This system uses an optical fiber to deliver broadband (300nm to 3500nm) thermal energy from a 200W mercury vapour lamp over a localised area [166]. The Full Width Half Maximum (FWHM) spot diameter from the fiber is 2.4mm when the standoff height is 9mm from the surface of the ink track. Like the 808nm diode laser, fiber delivery allows the iCure^{tm} system to be easily integrated with DW print head on a 3-axis motion control system. The iCure^{tm} system is shown in Figure 8:14.

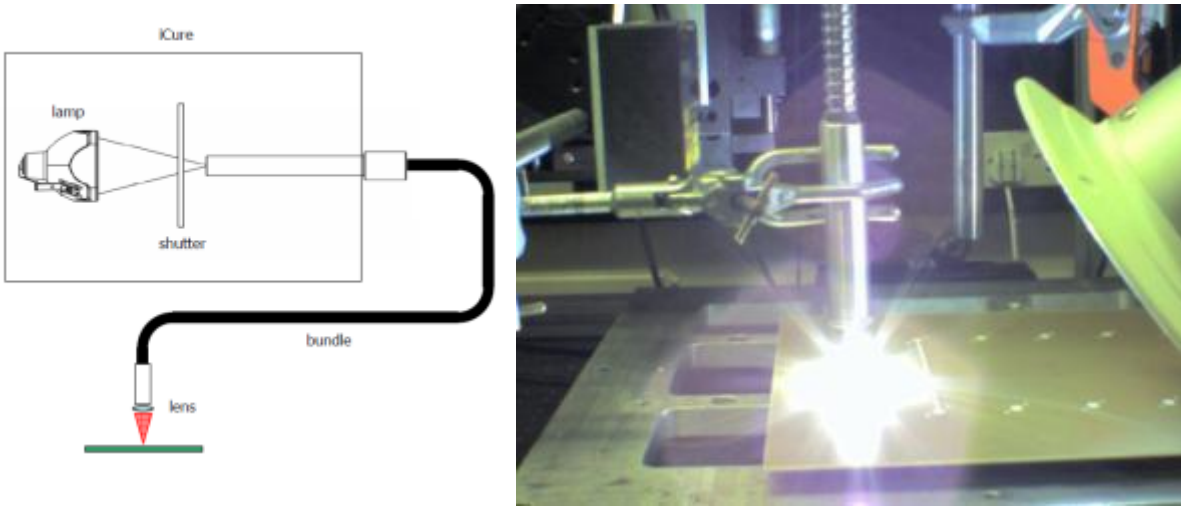

Schematic of the iCure[tm] system [166] iCure[tm] system used to process DW ink material

Figure 8:14: The iCure[tm] system (courtesy of Photonics, IR [166])

The normalised intensity output from the iCure[tm] system is plotted as a function of wavelength in Figure 8:15. This shows that the system compliments the absorption bands in the PTF inks by delivering power in both the UV and low to mid IR regions.

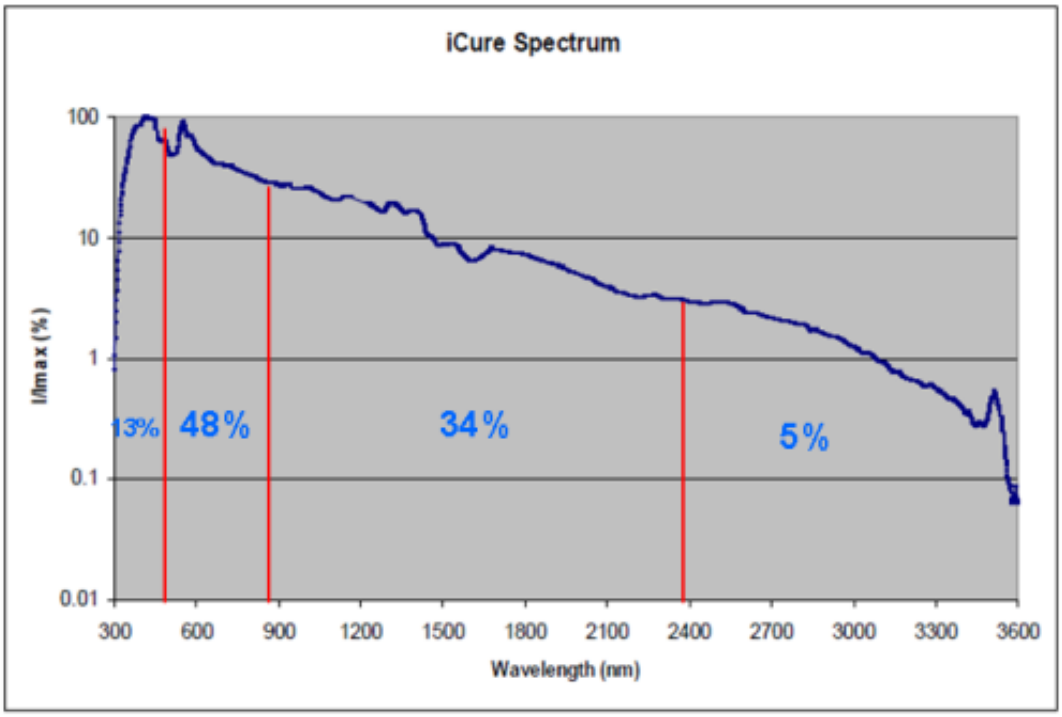

Figure 8:15: Output spectrum from iCure[tm] system normalised to the maximum intensity of the system (I/Imax) the distributed power from the iCure[tm] is also indicated as a percentage of the total power (courtesy of IR Photonics [166])

Broadband localised curing using the iCure[tm] system was investigated for the following inks:

- PTF silver ink [161]
- PTF carbon doped silver ink [161]
- PTF hybrid ink [161]
- Silver inkjet ink [126]
- Thermoplastic silver ink [127].

To prepare the PTF ink samples the inks were tape cast printed with consistent dimensions (100x1.5x 0.04mm) on to composite (single side copper clad) FR4 substrates [167]. Print thicknesses were estimated to be equivalent to the height of the tape (approximately 40μm). As the viscosity of the silver Inkjet ink was too low to be applied via the tape cast method, samples were printed via a Microfab MJ-ATP 80μm head attached to an X/Y motion stage. The droplet size was approximately 150μm in diameter when printed at 1000 Hz at 80mm/s. To build a track width of 1.5mm an overlap of 120μm was used between each inkjet track. On alumina ceramic substrates the film thickness of the inkjet ink was measured to be approximately 2μm after curing (see Chapter 5).

FR4 was used as a substitute for the carbon fibre material as it was no longer available for this investigation. FR4 has similar thermal properties to carbon fibre and it is not electrically conductive which allows the inks to be directly applied to the surface of the substrate without the need for an insulating coating. As the FR4 is a dielectric material it also enables the microwave properties of the inks to be analysed (see Chapter Eight for these results). It is also important to note the FR4 uses an epoxy resin with a T_g of 135°C which effectively determines the maximum operating temperature of the material.

For consistency the speed of the iCure[tm] system was kept constant and track resistance was investigated for different processing powers. Initial experimentation suggested that a traverse speed of 4mms^{-1} gave the most consistent curing results. Track resistance measurements were made after successive passes with the system and normalised against equivalent oven cured samples. All the PTF inks were cured in an oven at 220°C for 20mins to achieve maximum crosslink density and cure. DSC analysis (see Chapter 5) showed that this temperature will also be sufficient enough to cause nano-particles in the hybrid ink to sinter. For comparison, resistance value for PTF ink tracks cured at the manufacturers recommended cure temperature was also included in the results.

For inkjet inks sintering of the silver nano-particles starts to occur at 150°C, however, results showed that lower resistances could be achieved at elevated temperatures up to 330°C for 30mins. For the PTF inks oven cured measurements were conducted on alumina ceramic substrates since FR4 has a operating temperature dictated by its T_g which is 130°C. The benchmark inkjet tests were carried out on polyimide substrates as this gave the optimum print conditions for the silver inkjet ink.

DW Material	Cure Temperature (°C)	Cure Time (mins)	Resistance (Ω)
PTF Silver Ink	220	20	1.01
PTF Carbon doped silver ink	220	20	1.63
PTF Hybrid Ink	220	20	0.77
PTF Thermosetting silver ink	220	20	0.75
Inkjet silver ink	330	30	2.7

Table 8:2: Oven cured track resistances for the DW inks

8.4.4 Broadband Spot Curing of Thermosetting Silver PTF Inks

Average resistance measurements for iCure[tm] silver and hybrid ink tracks were normalised against their respective oven cured values and plotted as a function of the number of iCure[tm] passes over the track (Figure 8:16 and Figure 8:17). At first all ink tracks were processed with the iCure[tm] system whilst wet. When the power was kept constant the resistance of these tracks decreased asymptotically with the number of passes.

Similar to the laser cured results it was found that the surface roughness of these tracks was significantly higher than their oven cured counterparts (Table 8:3). High surface roughness can be problematic for high frequency application, such as transmission lines and antennas [72]. It was hypothesised that the main reason for the high surface roughness was the fast evaporation of the volatile solvents within the ink. In order to remove these solvents without curing the ink a number of processes were employed. These included air drying the sample for 24 hours, pre-treating samples in an oven at 60°C for 3 hours and finally vacuum oven drying under 1000mbar at 70°C for 2 hours. The resistance measurements for these samples after iCure[tm] processing is shown in Figures 5 A and B and the resulting surface roughness measurements are given in Table 8:3.

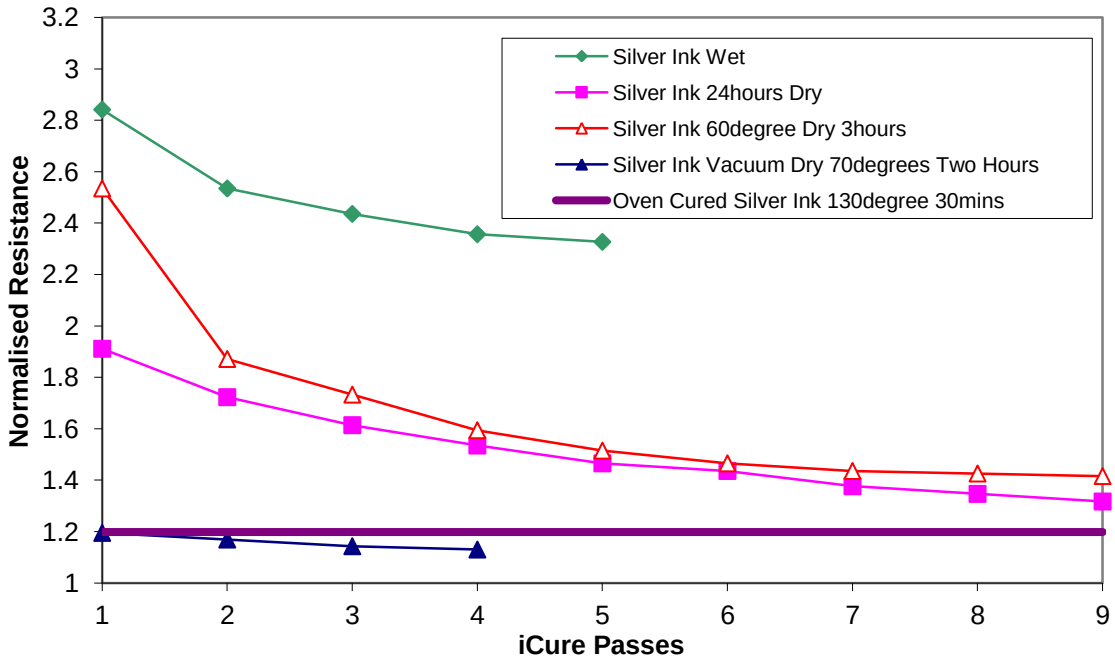

Figure 8:16: Normalised resistance (against 220°C 20min oven cured silver inks) for successive iCure^{tm} passes at 4mms^{-1} traverse speed, 5W power for Silver inks using different pre-treatment methods

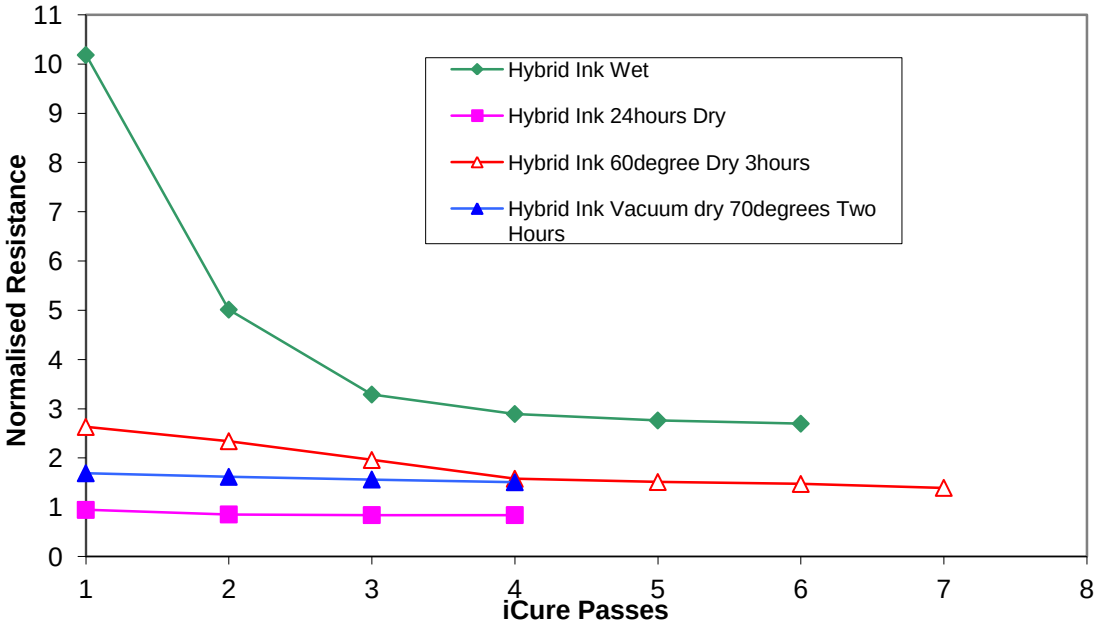

Figure 8:17: Normalised resistance (against 220°C 20min oven cured hybrid inks) for successive iCure^{tm} passes at 4mms^{-1} traverse speed, 5W power for Hybrid inks using different pre-treatment methods

	Silver ink		Hybrid Ink	
Process	**Ra (mm)**	**Feature Size (mm)**	**Ra (mm)**	**Feature Size (mm)**
Oven Cured 200°C 30mins	2.57	N/A	1.53	N/A
iCured 5W Wet	26.47	N/A	15.11	N/A
iCured 5W 24 hour dry	12.60	30	5.11	N/A
iCured 60°C 3hr Oven Dry	43.55	120	22.30	40
iCured 5W 70°C 2hr Vacuum Oven Dry	2.84	N/A	1.65	N/A

Table 8:3: Comparison of silver and hybrid track surface roughness, Ra, after iCure^{tm} treatment for different pre-treatment methods. If blistering is present then average height of blisters is also included.

Figure 8:17 shows that when wet, the resistance of the silver and hybrid inks is the highest when iCure[tm] processing. Resistance is improved if the samples are air dried or vacuum dried in an oven at 70°C for two hours. Similarly, the surface roughness of the ink samples reduces when air dried or vacuum dried (Table 8:3). Air and oven drying can also cause the formation of blisters in the ink track (Figure 8:18). Blistering could be a result of trapped solvent within the ink due to preferential drying at the top surface of the ink layer. Blistering can have adverse effects on both the resistance and adhesion of the ink. The cross-section micrograph and Alpha-step image of the DW ink track clearly shows the size and nature of the blisters (Figure 8:18). Cross-section samples were prepared by mounting the DW ink track and substrate in a Struers Epofix Resin before grinding the sample down to the area of interest.

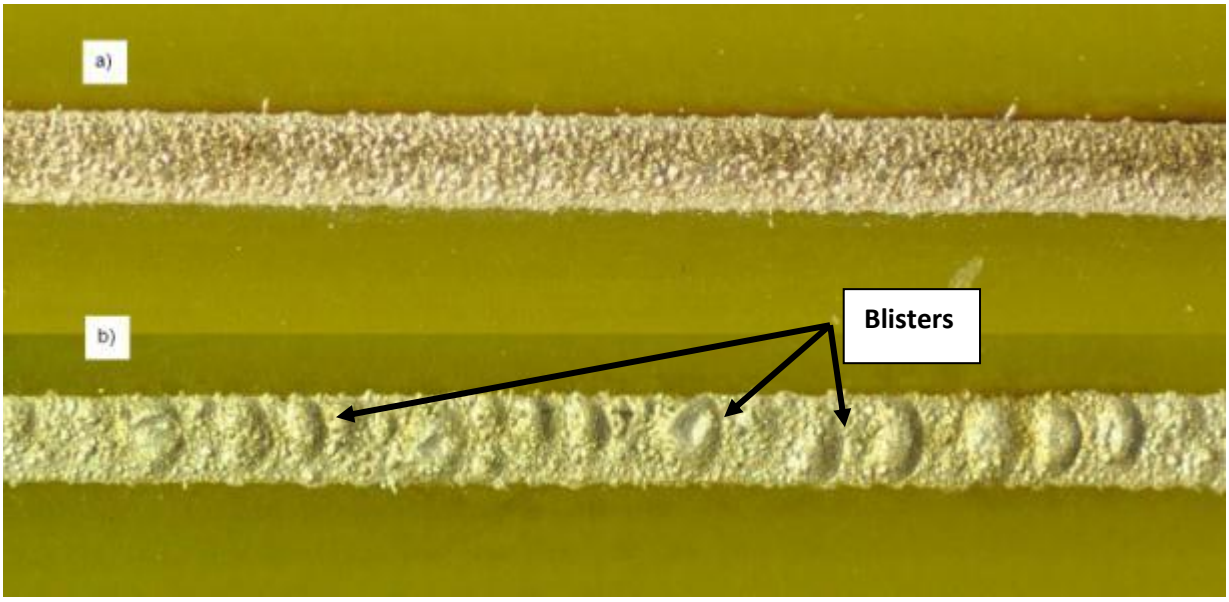

Figure 8:18: A) Wet silver ink track processed with the iCure[tm] system B) 24hr air dried silver ink track processes with the iCure[tm] system.

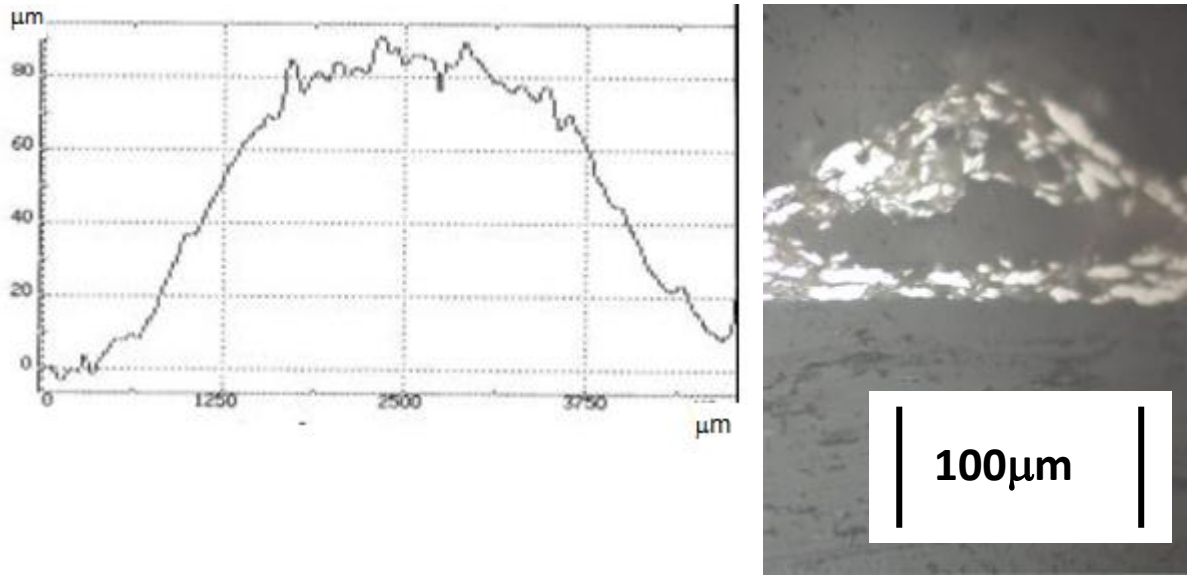

A B

Figure 8:19: (A) Alpha-step image of surface defect present on an iCure^{tm} silver track which is pre-treated in an oven at 60^{o}C for 3hours (B) Cross-section (X 20 magnification) micrograph image of silver ink track which is pre-treated in an oven at 60^{o}C for 3hours

The vacuum drying approach seemed to be a much more effective process at removing the high boiling point solvents within the ink material. This is reflected in near oven cured surface roughness values for vacuum treated iCure^{tm} ink tracks. The removal of solvent also aids the curing process as both silver and hybrid inks exhibit much lower resistance values than wet or oven dried ink tracks. For hybrid inks the lowest resistances were achieved when air drying for 24hrs rather than vacuum drying. One possible explanation for this could be due to the formation of small air gaps between the nano-particles as solvent is removed via the vacuum thereby hindering their ability to sinter efficiently although this has yet to be validated experimentally.

Figure 8:20 shows ink tracks that were pre-treated in a vacuum oven and processed with the iCure^{tm} at different powers. Similar to the results obtained with the laser diode, higher processing powers were shown to be much more effective at reducing track resistance than increasing the number of processing scans. When vacuum dried, the silver inks are able to achieve equivalent oven cured ink resistances after four passes at 6.5W. The resistance of the hybrid ink on the other hand was approximately 4% higher than oven cured tracks after 4 passes, however, this value was achieved at a lower power of 6W.

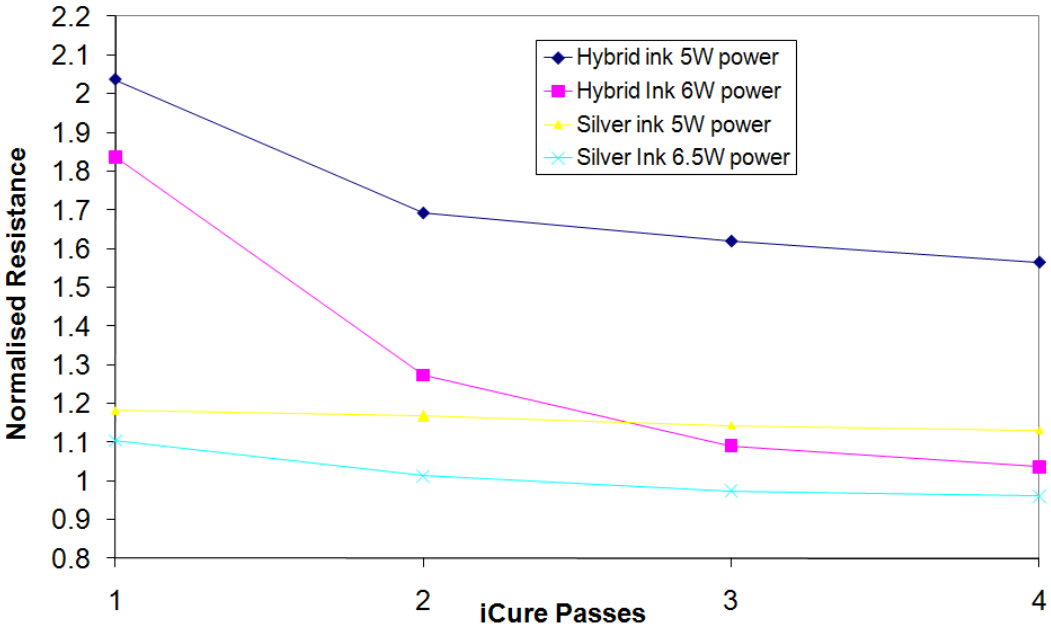

Figure 8:20: Normalised resistance of vacuum dried silver and hybrid ink tracks cured at different iCure[tm] powers

8.4.5 Broadband Spot Curing of Thermosetting Carbon doped silver ink

Using the same parameters as the vacuum dried silver PTF ink (at 5W of power) the carbon doped silver ink was processed with the iCure[tm] system (Figure 8:21). Initially after the first scan the resistance of the carbon doped silver ink is higher than the conventional silver ink track. However, subsequent passes show that the resistance drops below the silver ink similar to the measurements obtained with the laser diode system. After 5 passes the normalised resistance is 0.94 with a surface roughness of 3.1µm. At powers greater than 5W the higher absorption of the carbon ink caused the substrate to blacken and burn. Because of this the ink was not investigated for higher power processing.

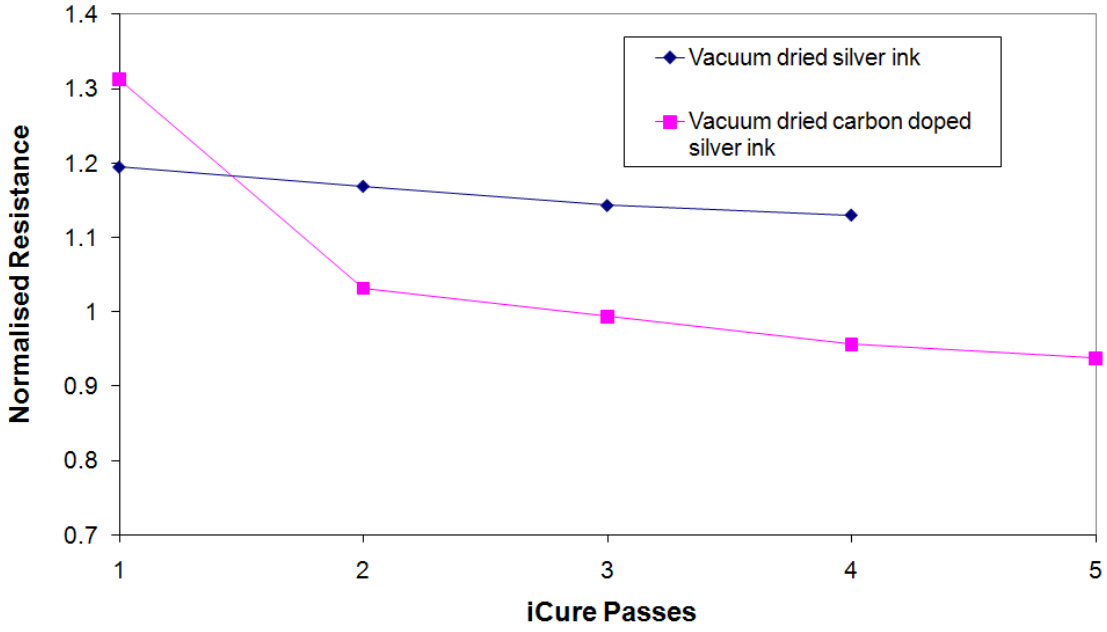

Figure 8:21: Normalised resistance (against 220°C 20min oven cured thermosetting carbon doped silver ink) against iCure^{tm} passes for vacuum dried PTF silver and carbon doped silver ink processes at 5W power at 4mms^{-1} traverse speed.

8.4.6 Broadband Spot Curing of Thermoplastic Silver PTF Ink

As with the PTF thermosetting inks the surface roughness of the thermoplastic ink is higher when processed whilst wet. It was found that the surface roughness of the thermoplastic ink could be reduced by either air drying the sample for three hours or heating at 60^{o}C for 60mins. Normalised resistance (0.75Ohms for oven cured Thermoplastic silver ink) measurements against successive iCure^{tm} passes for the oven dried thermoplastic silver ink are given Figure 8:22.

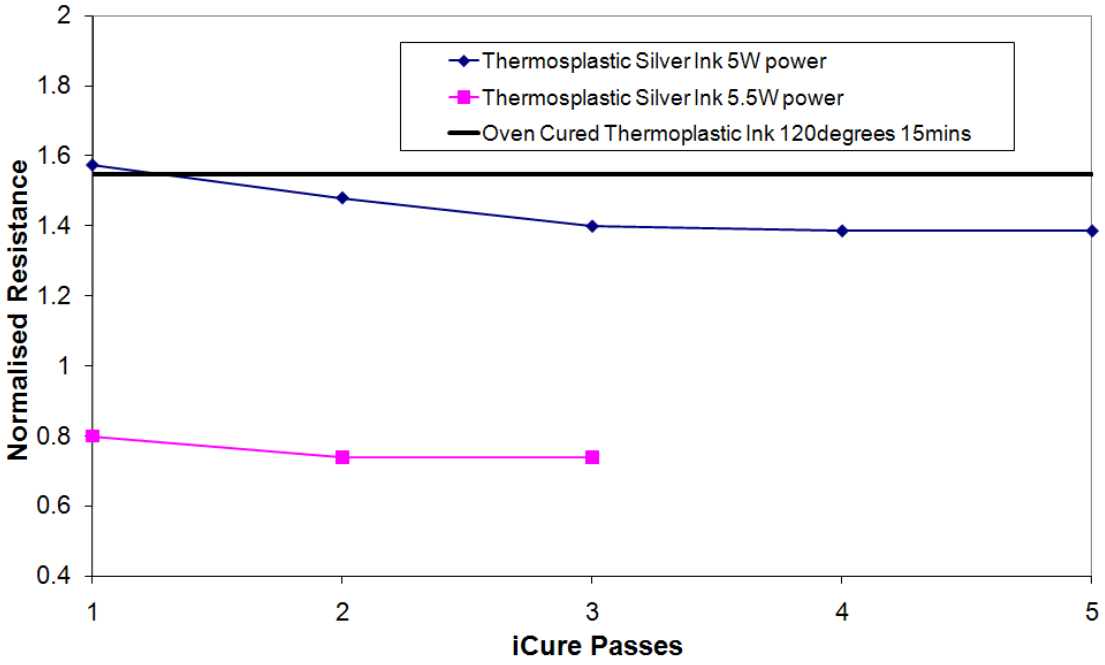

Figure 8:22: Normalised Resistance (against oven cured tracks, 220°C 20min tracks, 0.75Ohms) of pre-treated (oven, 60°C 1hour) silver thermoplastic ink tracks against successive iCure[tm] passes for different powers

The results show that at 5.5W only a single pass is needed to reduce the resistance of the thermoplastic silver ink to a value 20% lower than 220°C oven cured tracks. Using these parameters the resulting surface roughness of the track was measured at 1.45µm. This is better than both the oven cured and iCure[tm] processed silver and hybrid inks.

8.4.7 Broadband spot curing of inkjet ink

Initial processing of the inkjet ink with the iCure[tm] system showed poor adhesion to the substrate surface often resulting in de-lamination of the sintered ink track. This effect was attributed to the fast evaporation of the high boiling point solvents within the ink. A number of pre-drying methods were investigated to try and remove the solvents from the ink before processing. The most successful results were achieved when the inkjet ink was dried in an oven at minimum drying temperatures of 120°C for 20mins. As this drying temperature was close to the maximum operating temperature of the FR4 material (130°C) a compromise drying temperature of 100°C for 120mins was used instead. The results for these tracks are given in Figure 8:23.

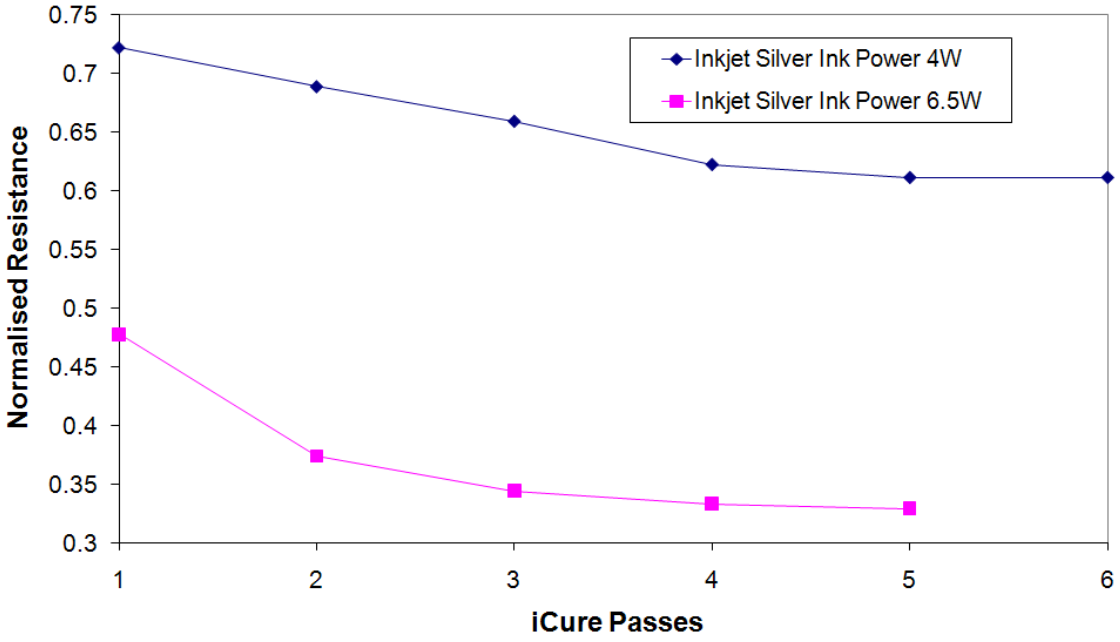

Figure 8:23: Normalised Resistance (against oven cured track 330°C 30min tracks, 2.7Ohms) of pre-treated (oven, 60°C 1hour) silver inkjet ink tracks against successive iCure^{tm} passes for different powers

The resistance of the iCure^{tm} processed inkjet inks are far superior than their oven cured counterparts when pre-dried in an oven. At 4W only one pass was needed to obtain a track resistance nearly 25% lower that a sample cured in an oven at 330°C for 30mins. Even lower resistances could be obtained at 6.5W resulting in a resistance almost 75% better than an oven cured sample after 3 passes. The resistivity of this ink track equates to approximately $2.67 \times 10^{-8} \Omega m$ or 60% bulk conductivity of silver. These results demonstrate that unlike the PTF inks, the inkjet materials used here are not hindered by the presence of a resin binder and so if processing temperatures are high enough a high density of sintered silver nano-particles can be achieved. The surface roughness of the inkjet track processed at 6.5W was measured at 0.630μm this was also lower than the surface roughness obtained with the PTF silver inks.

As an alternative to oven drying the inkjet inks the iCure^{tm} system itself was investigated as a means for drying the inkjet inks. It was found that the majority of the solvent was removed after 20 scans at a power of 2.5W. Once the majority of the solvent was removed from the ink track (indicated by a change in colour from a dark to silvery ink track) a processing power was used to sinter the ink.

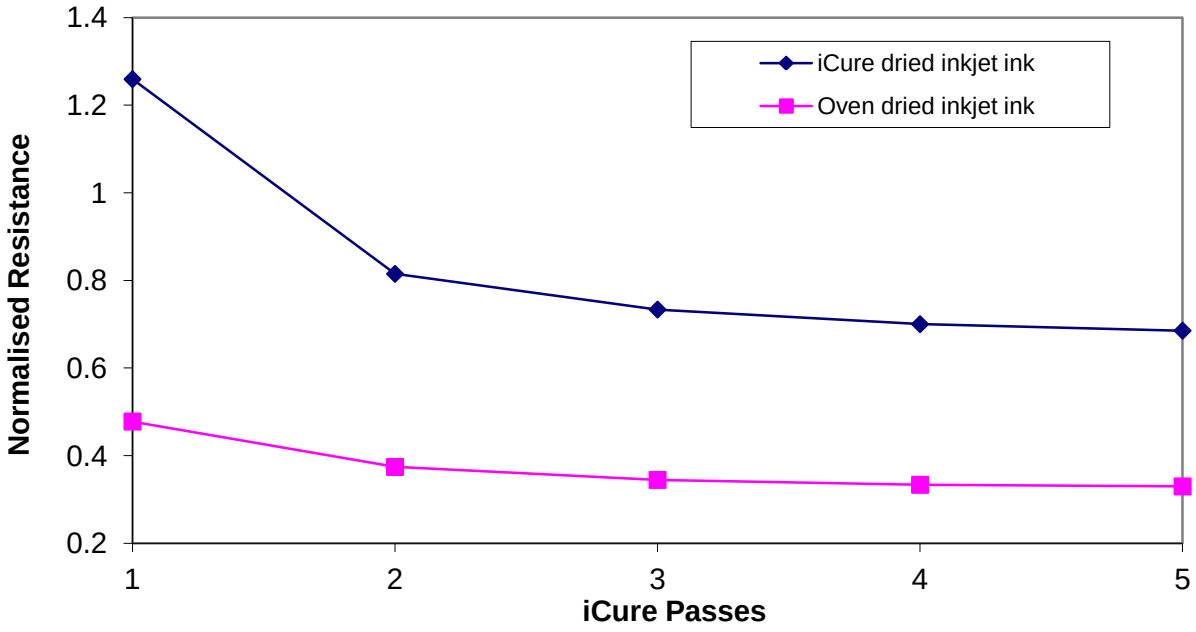

Figure 8:24: Comparison between oven dried (100°C 120mins) and iCure[tm] dried (3W 22 scans) inkjet ink tracks when processed with the iCure[tm] system at 6.5W of power

Although processed at the same power (6.5W) the iCure[tm] dried inkjet ink tracks have a resistance approximately 30% higher than the oven dried inkjet ink tracks. The adhesion of these tracks also seems poorer with a number of samples showing de-lamination over the space of a few days (Figure 8:25).

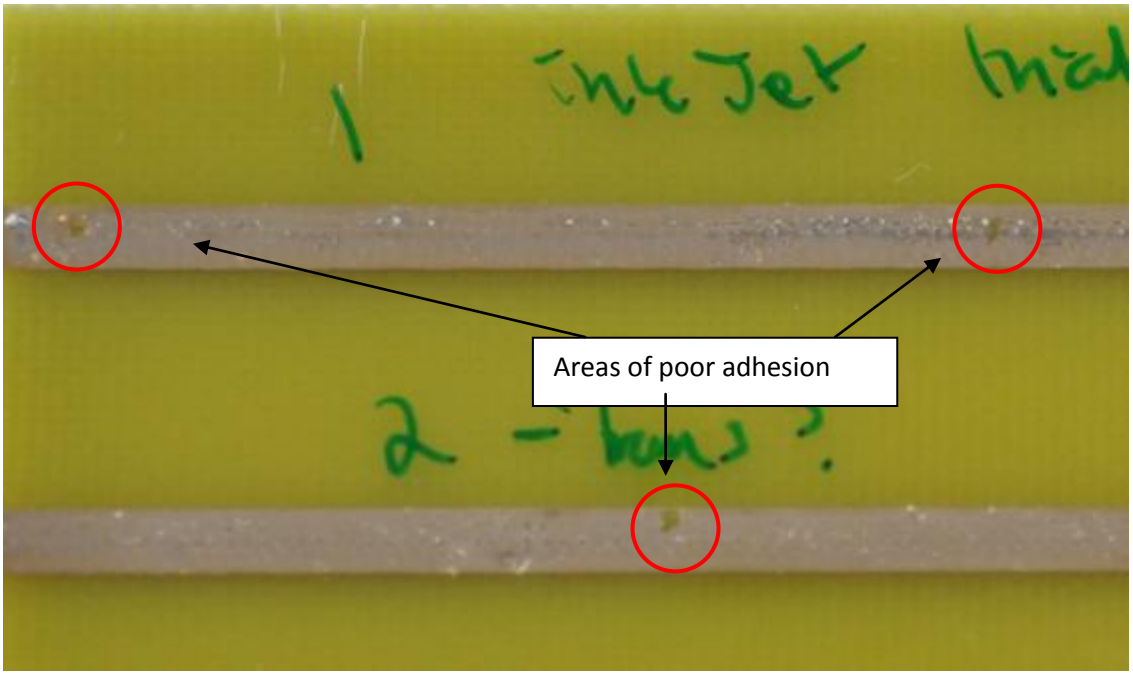

Figure 8:25: iCure[tm] dried inkjet inks that show areas of de-lamination (circled) over time

To investigate the difference between the oven dried and iCure[tm] dried samples they were placed in an SEM microscope for investigation (see Figure 8:26). The SEM microscope images show that the iCure[tm] dried inkjet ink tracks have a number of fine cracks in them which could contribute to their higher resistance and poorer adhesion. The origination of these defects could be from insufficient removal of the solvent before processing or high local thermal gradients.

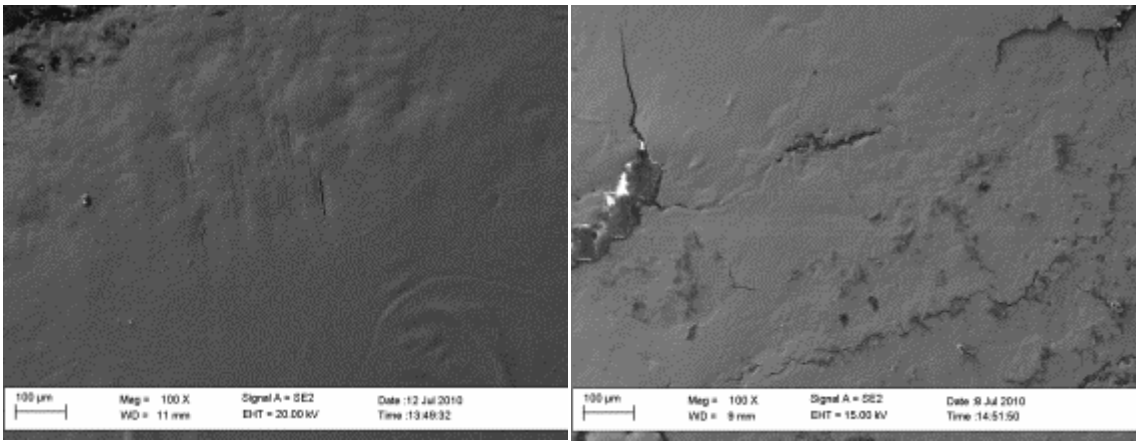

A. B.

Figure 8:26: 100x SEM microscopy image of (A) oven dried (100°C 120min) inkjet ink track processed with the iCure[tm] system. (B) iCure[tm] dried (20 passes, 3W) inkjet ink track before processing with higher powers (2 passes 6.5W).

8.4.8 Substrate Heat Affected Zone(HAZ) analysis

One of the benefits of localised curing is the restriction of heat into the substrate material. However, if high powers are required to process the inks than damage could still occur at the interface between the substrate and ink material. One method for investigating the Heat Affected Zone (HAZ) is to scrape off the ink coating and investigate the surface of the substrate. This method is limited as it is difficult to see how far the HAZ penetrates into the surface and scraping of coatings can often result in scratching of the substrate surface. It was noticed that certain samples such as the hybrid and thermoplastic silver ink suffer from reduced adhesion when processed at powers greater than 6W. An example of the thermoplastic silver ink processed at 6W is shown in Figure 8:27.

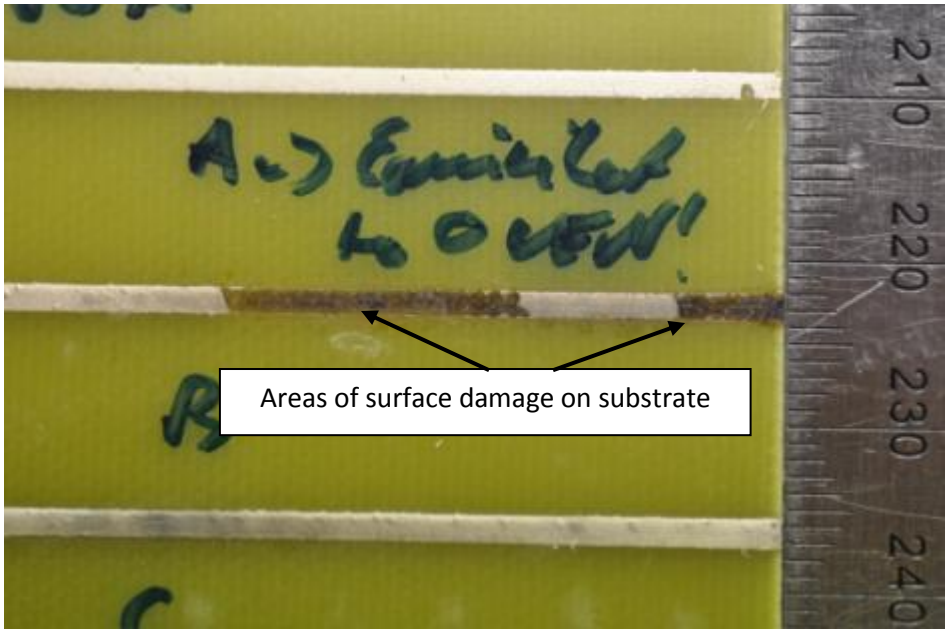

Figure 8:27: Surface damage caused by processing the Thermosetting silver ink with the iCure^{tm} system at 6W at a traverse speed of 4mms^{-1}

In Figure 8:27 the damage caused by the curing system is clearly visible on the surface of the substrate. To investigate the HAZ more clearly cross-section images were taken of each of the DW materials when processed with the iCure^{tm} system using their optimum curing parameters (i.e. lowest resistance achieved shown in Figure 8:21, Figure 8:22, Figure 8:23, Figure 8:24). To prepare the samples they were sliced (from the middle of the track) using a guillotine before being mounted in an epoxy resin for grinding. To ensure the integrity of the coating during the mounting and grinding process an additional FR4 substrate was placed on top of the coating. The cross-section samples were then investigated using optical microscopy. The support substrate always appears on the left hand side of the image.

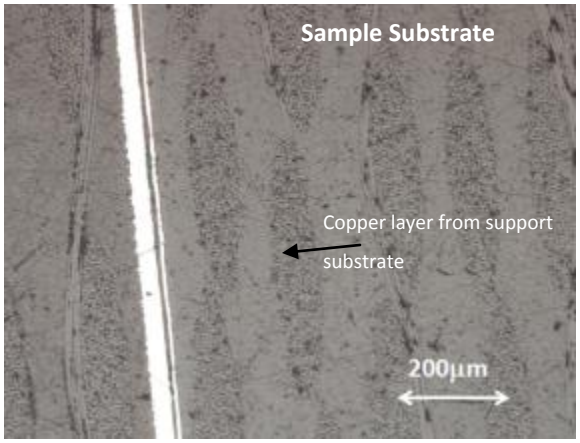

A.

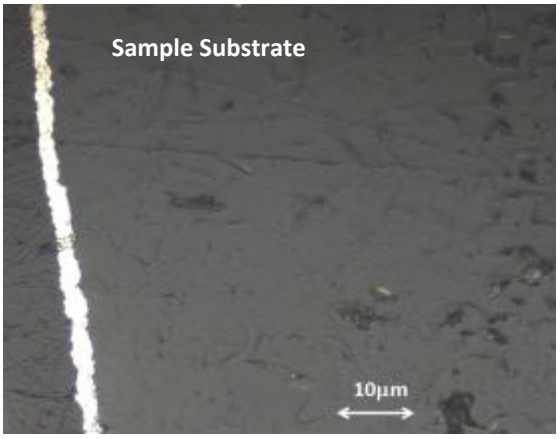

B.

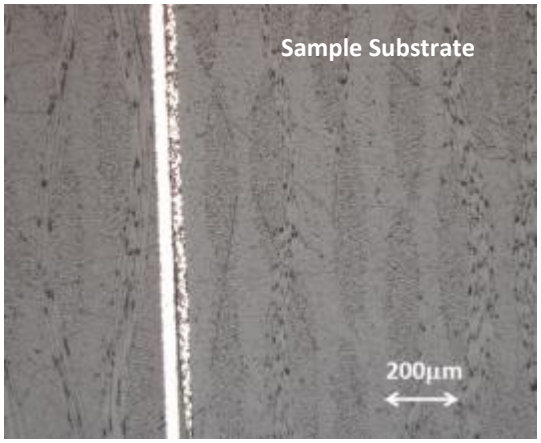

C.

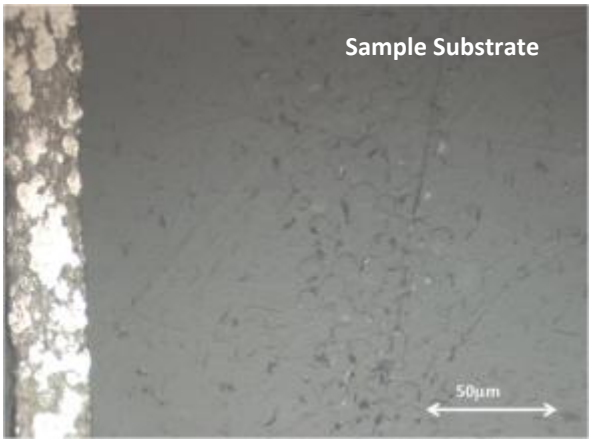

D.

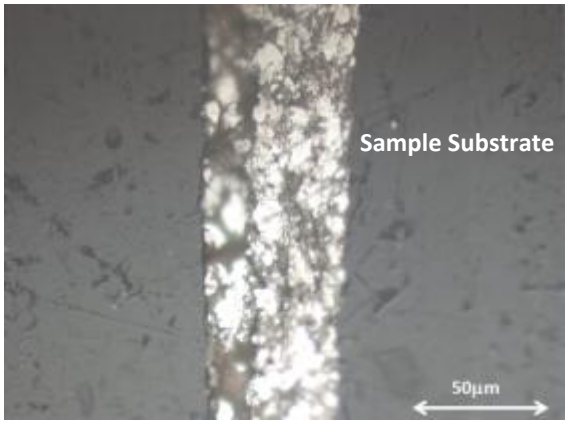

E.

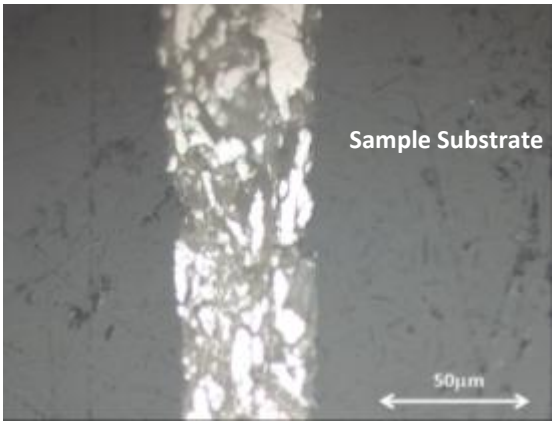

F.

Figure 8:28: Cross-section micrographs (A) 5x inkjet ink processed at 6.5W. (B) 50x inkjet ink processed at 6.5W. C) 5x PTF hybrid silver ink processed at 6W. (D) 50x Hybrid silver ink processed at 6W. (E) 50x PTF thermoplastic silver ink processed at 5.5W. (F) 50x PTF silver ink processed at 6.5W.

The cross-section images do not show any significant damage to the substrate material. It is clear from the images that iCure^{tm} processing has not affected the fibre-glass weave of the FR4 material. It is more difficult to tell if there is any damage to the epoxy resin binder used within the FR4

composite. Breakdown or decomposition of the resin will affect the chemical and environmental performance as well mechanical and electrical properties of the substrate. These properties would have to be investigated individually to determine if they have been affected. Alternatively if the temperature within the substrate could be measured or modelled then it may be possible to determine if the resin would theoretically degrade. Thermodynamical modelling of the localised curing process is conducted in Chapter Eight.

Apart from the HAZ analysis the cross-section images also give an indication on the density of silver within each ink composition. To quantify the density of silver within the DW ink materials Struers SCENTIS software was used. The SCENTIS software can approximate the density of silver particles within the ink using the contrast tool. This method requires setting the contrast so that only the silver particles are present within the image (see Figure 8:29). Whilst this type of measurement can be subjective (depending on how the user sets the contrast) is does give an indication of the density of silver within each composition.

From Table 8:4 it can be seen that although the inkjet ink is much thinner that the PTF inks the density of silver is much higher. Comparison between the thermoplastic and thermosetting silver inks shows that the silver particles are finer and closer together in the PTF thermosetting silver ink (Figure 8:28). This results in the thermoplastic ink having a density nearly 10% greater than the PTF silver ink. These observations correlate with the resistance measurements made with each ink.

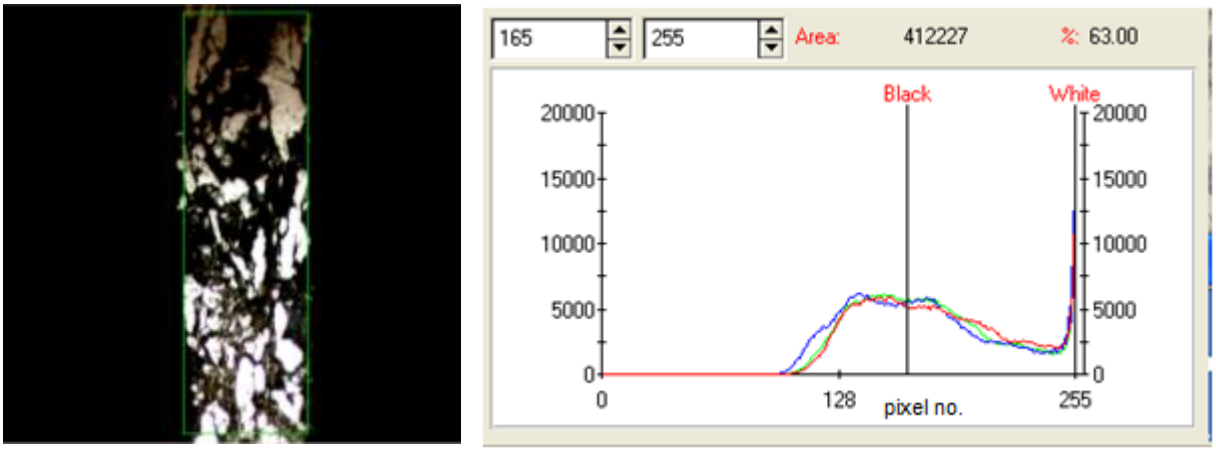

A. B.

Figure 8:29: (A) Binary image of DW ink track. (B) Contrast measurement used to determine the percentage density of silver particles within the DW inks.

DW Ink Material	Density of Silver (%)
PTF Silver	63.0
Hybrid Silver	71.1
Thermoplastic Silver	73.7
Inkjet Silver	94.2

Table 8:4: Summary of density measurements using the SCENTIS contrast tool

It is also evident from the cross-section images that the silver particles within the PTF inks do not form a continuous layer on the surface of the substrate. This could contribute to higher transmission losses in high frequency applications. The inkjet ink on the other hand forms a continuous conductive layer on the substrate surface which could give it an advantage for these types of applications.

8.4.9 Comparison between laser and broadband curing

Table 8:5 summarises the localised curing results with both the broadband light source and the 808nm laser diode system. The total energy density was calculated using Equation 8:4.

	Laser Diode		**iCure^{tm}**	
Ink Material	Energy Density (j/cm^2)	Normalised Resistance	Energy Density (j/cm^2)	Normalised Resistance
Silver Ink	848.83	1.11	86.21	0.96
Carbon Doped Silver ink	848.83	1.05	66.31	0.94
Hybrid Silver ink			79.58	1.04
Thermoplastic silver ink			72.95	0.74
Inkjet ink			86.21	0.33
			53.05	0.61

Table 8:5: Normalised resistance and energy density comparison between laser diode and iCure^{tm} processing

Although the resistance for the silver and carbon doped silver ink are lower with the iCure^{tm} System it must be noted that these inks were pre-dried before processing. It was shown that pre-drying can enhance the resistance of the silver inks when using the broadband curing system. Significantly the results show that the laser diode system requires almost ten times the energy density to cure the inks. It is evident from this that the additional absorption of the resin binder is indeed important when curing the inks.

Table 8:5 also shows that the PTF silver and hybrid silver inks require the highest energy density when processing with the iCure[tm] system. Low energy densities can be used to process the inkjet ink, however, this could primarily due to the low thickness of the film. The thermosetting silver ink can be processed with low energy densities whilst offering lower resistances than the PTF silver and hybrid inks.

ASTM D3359 peel test measurements showed that all the inks pass the minimum standard apart from the hybrid ink which had cohesive failure. This was not as expected considering the hybrid ink also failed in a similar fashion when oven cured.

8.5 Conclusion

This chapter builds on previous literature on laser curing of DW ink materials. Past experiments have shown that $C0_2$, Nd:YAG and diode lasers can be used to process DW ink materials [156] [68] [157]. It was shown, however, that DW materials can have different absorption characteristics at different wavelengths. Silver inks for example are particularly reflective at IR wavelengths whereas dielectric inks can have multiple absorption bands at both UV and IR wavelengths. One method of increasing the absorption in the IR range can be to dope DW inks with carbon black particles but this may not be possible for all ink compositions (such as inkjet inks or dielectrics).

This thesis presents an alternative method for curing DW inks using a localised broadband light source which delivers light radiation in UV and low to mid IR wavelengths (300-3600nm). Curing of UV curable polymers using a variety of (non-laser) light sources has been demonstrated, particular for dental applications [168] [169]. However, to the knowledge of this author curing of DW inks (polymer or inkjet composition containing functional particles) has not been conducted over a wider wavelength range using a localised source.

It was evident from the results that curing with a broadband light source can significantly decrease the energy density required to cure the silver PTF inks when compared to laser curing with an 808nm diode laser. For PTF inks broadband curing does not result in better resistances as they have maximum cross-link density limit before degradation occurs. Once this limit is reached the resistance cannot be reduced any further. However, the nano-particles within the inkjet ink are able to sinter without restriction of a resin binder. This enabled a conductivity of approximately 60% bulk silver to be obtained with the broadband white light source.

Whilst localised curing offers a number of advantages over conventional curing methods there are still a number of barriers to overcome. One of the most prominent problems is the effect of blistering and high surface roughness caused by the volatile evaporation of the solvents within the inks as they are processed. This affect can also cause higher track resistances and may affect the high frequency performance of the conductor. Whilst pre-drying methods have been shown to eradicate this problem they add an extra processing step. For the PTF silver and hybrid inks it also not viable to pre-dry them in a vacuum oven as this removes the benefits of localised curing. The high temperatures required to dry the inkjet inks is also un-feasible for processing on temperature sensitive substrates. For inkjet inks the broadband light source itself could be used to remove the solvents within the inks although this requires a high number of scans and increases processing time considerably. The thermosetting silver ink lends itself well to localised processing as the solvents can be easily removed by air drying or low temperature drying (in an oven or using a heat gun).

Cross-section micrographs were used to investigate the HAZ in the substrate after the DW inks were cured with the broadband white light source. The micrographs revealed no obvious damage to the substrate although it was inconclusive as to whether the properties of the material were affected by the heat treatment. To determine the temperature within the substrate thermodynamic modelling techniques can be employed. This information can then be used to determine if the substrate would theoretically deteriorate. The cross-section micrographs also show that the silver particles within the PTF inks do not form a continuous layer across the surface of the substrate due to the presence of the resin binder. It would be useful to measure the effective surface roughness of the silver particles within the resin binder at the interface between the substrate and ink. When cured, the silver nano-particles within the inkjet ink form a continuous conductive layer on the surface of the substrate. It is thought that this may improve the high frequency signal carrying properties of the inkjet ink.

In this Chapter the processing speed, power and drying methods have not been optimised. Further investigation of these parameters would verify the practicality of implementing localised processing in a manufacturing environment.

9 Thermodynamical Modelling of Localised Curing Process

In the case of the thermally cured inks, Localised processing of DW inks requires generating a significant heat rise within the material in a relatively short period of time [170]. With the optimised exposure parameters and the right choice of source and inks heat affected zone (HAZ) in the substrate can be restricted, there is still a requirement to determine the extent of the HAZ and thus estimate the effect it may have on the substrate. Thermodynamic modelling can assist with this by revealing the temperature rise and its dynamics in the substrate.

Accurate modelling requires the input of all material thermodynamic constants. As the DW inks are complex materials their heat capacity and thermal conductivity is generally unknown. It can be particularly difficult to measure the thermodynamic properties of these ink materials as they are relatively thin coatings which are difficult to isolate from a substrate when cured.

Chapter 9 introduces a method for measuring the thermal conductivity and heat capacity of DW materials using this information the localised curing process was simulated in a computational model.

9.1 Estimating the thermodynamic properties of DW inks

Conventional thermal conductivity measurements are made using the standard Guarded-Comparative-Longitudinal Heat Flow Technique (cut-bar technique) [171]. In this technique a sample is sandwiched between two pieces of material with known thermal conductivity using a thermal grease and pliable metal foil to eliminate interfacial thermal contact resistance between the materials. Thermocouples placed along the lengths of the three materials yield information of the heat flow through the materials. The heat flow can be used to determine the thermal conductivity using the one-dimensional Fourier conduction equation:

$$\frac{dQ}{dt} = -kA\frac{dT}{dx} \qquad \textbf{Equation 9:1}$$

Where dQ/dt is the rate of heat flow, k, is the thermal conductivity, A is the cross-sectional area through which the heat flows, and dT/dx is the temperature gradient. Experimentally, dT is the finite temperature difference and dx is approximated by the distance over which the temperature difference is measured.

This technique is not suitable for measuring samples which are not easily separated from a substrate layer such as coatings and inks. Furthermore the accuracy is diminished for sample thicknesses less than 150μm [172].

A steady-state method of measuring the thermal conductivity of plasma spray coatings has been demonstrated by implementing an infrared red microscope [172]. This measurement technique requires mounting and polishing of the sample surface so that it is both smooth and flat.

An alternative method for measuring the thermodynamic properties of coatings is presented in this chapter. This process involves matching the temperature profile of a sample measured experimentally with those predicted with Finite Element, thermodynamical modelling.

Experimental measurements consisted of coating DW material on to a substrate with known thermal properties. By exposing the material to a short period of heat energy the temperature rise and subsequent cooling can be measured as a function of time. The rate of cooling is a function of the thermal conductivity of the DW sample and the substrate material. The heat rise (or peak temperature) is dependent on the specific heat capacity of the coating, which is given by Equation 9:2.

$$\Delta Q_h = mc\Delta T$$ **Equation 9:2**

Where Q_h is the heat supplied to the sample, m, is the mass of the sample being heated, c, is the specific heat capacity of the sample, and T is the heat rise.

Experimental measurements of the heat rise and subsequent cooling can be compared to a computational simulation of the process. By altering the thermal conductivity and heat capacity coefficients in the model the peak temperature and cooling curve can be matched to experimental data. This process requires an iterative process as described in the flow diagram in Figure 9:1.

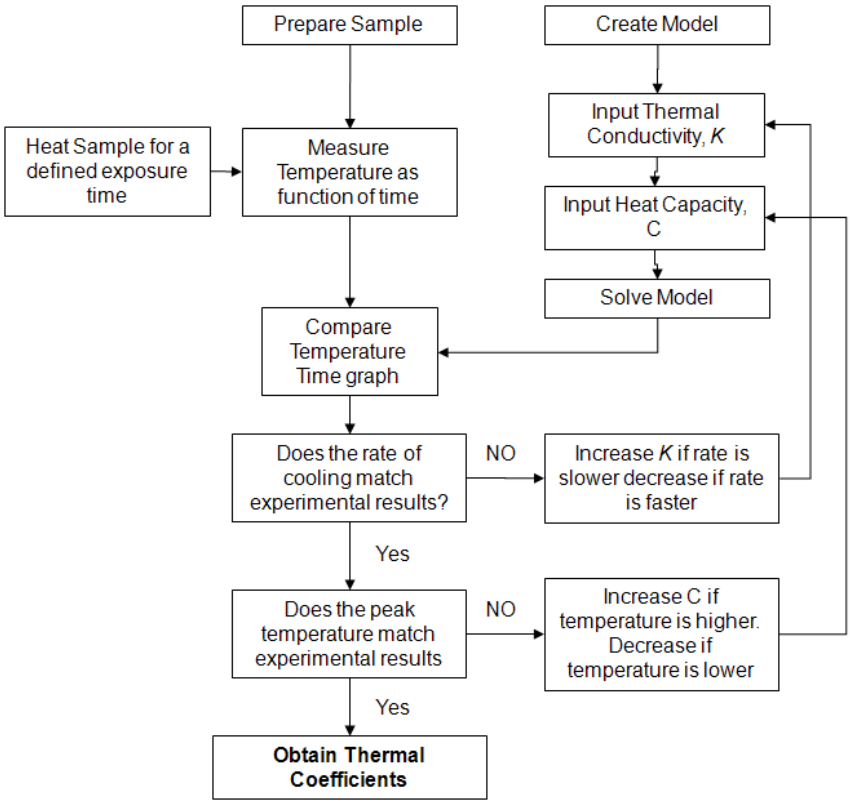

Figure 9:1: Flow diagram detailing experimental method.

9.1.1 Experimental Setup

The most practical way of heating the sample is to use a heat spot such as a laser source. This provides an efficient non-contact source to heat the sample. In this experiment a white-light thermal heat spot system [166], the iCure^{tm}, was used to heat the sample. This system has a spot diameter of 2.4mm with a near Gaussian distribution. To increase the coupling efficiency from the heat source to the coating , the samples were spray coated with a thin layer of black carbon/acrylic paint.

To measure the heat radiation from the sample a FLIR Thermacam P620 was used, this system has a measurement accuracy of +/- 2°C. As the samples were coated with black carbon/acrylic paint the thermal emissivity of the sample could be defined as approximately 95% [173]. To increase the accuracy of the results it was important to make sure that the ambient temperature remained constant and was smaller than the temperature measured in the material. To monitor the ambient temperature additional thermocouples were used and placed around the apparatus. A schematic of the experimental apparatus is given in Figure 9:2.

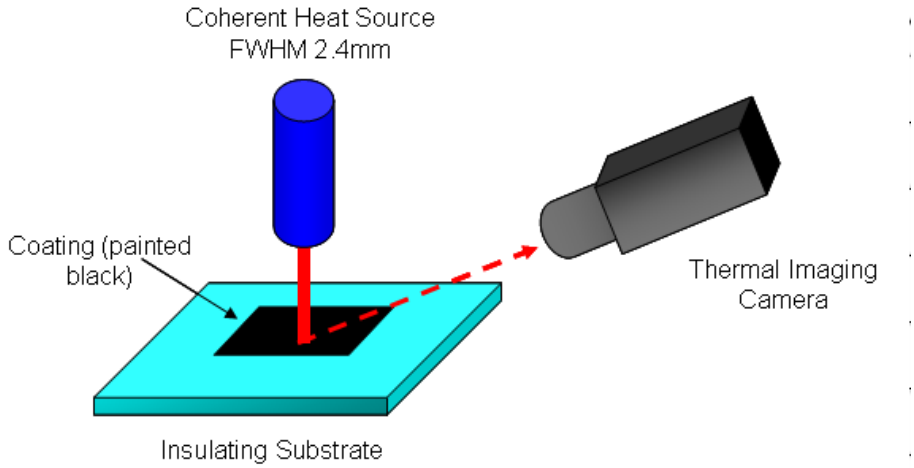

Figure 9:2: Schematic of experimental setup (thermocouples used to monitor ambient temperature is not shown)

This setup was used to measure the thermal conductivity of the PTF silver ink [161]. Samples were prepared by tape cast printing an FR4 substrate with approximately 35mmx35mmx0.060mm of the PTF ink. FR4 was used as it is acts as an insulator; this allows the ink to heat up to a measurable temperature. When Aluminium was used as the substrate material the rate of cooling was too fast to be accurately measured with the thermal imaging camera. Once the inks were applied to the substrate they were cured in an oven at 130°C for 30mins before being spray coated black.

9.1.2 Model Setup

COMSOL Multiphysics 3.5a was used to model the experimental setup using the same dimensions as the physical experiment. COMSOL has previously been used to investigate temperature effects due to laser heating [174].

When setting up the model only heat loss due to thermal conduction was considered, thermal loss due to radiation/convection was not included in the model. As the size of the coating was much larger than the spot size of the heat source it was assumed that edge effects could be ignored i.e. the heat energy has dissipated into the bulk before lateral conduction to the edge of the ink layer.

The intensity profile from the iCure[tm] system follows a 3D super Gaussian type distribution. This can be described using equation 3 [175].

$$f(x,y) = N.A_{amp} \exp\left(-\left(\frac{|x|}{\sigma_b}\right)^{\gamma} + \left(\frac{|y|}{\sigma_b}\right)^{\gamma}\right) \qquad \textbf{Equation 9:3}$$

Where A_{amp} is the amplitude, N is a normalisation factor, σ_b, is a constant relating to the width of the beam and γ, is the Gaussian factor. When γ is equal to 2 the beam profile resorts to a normal Gaussian function. The normalization factor was calculated from the integral of the super Gaussian function. This integral was solved numerically using MathCAD.

Both the γ function and width factor were found by matching the Super Gaussian function to the measured intensity distribution from the heat source. Figure 9:3 shows the intensity distribution from the iCure[tm] system (as measured by the manufacturer) overlaid with the intensity distribution obtained using the Gaussian function (Equation 9:**3**). It was found that a width factor of 1.5mm and a Gaussian Factor of 2.5 gave the closest match to the output from the iCure[tm] system.

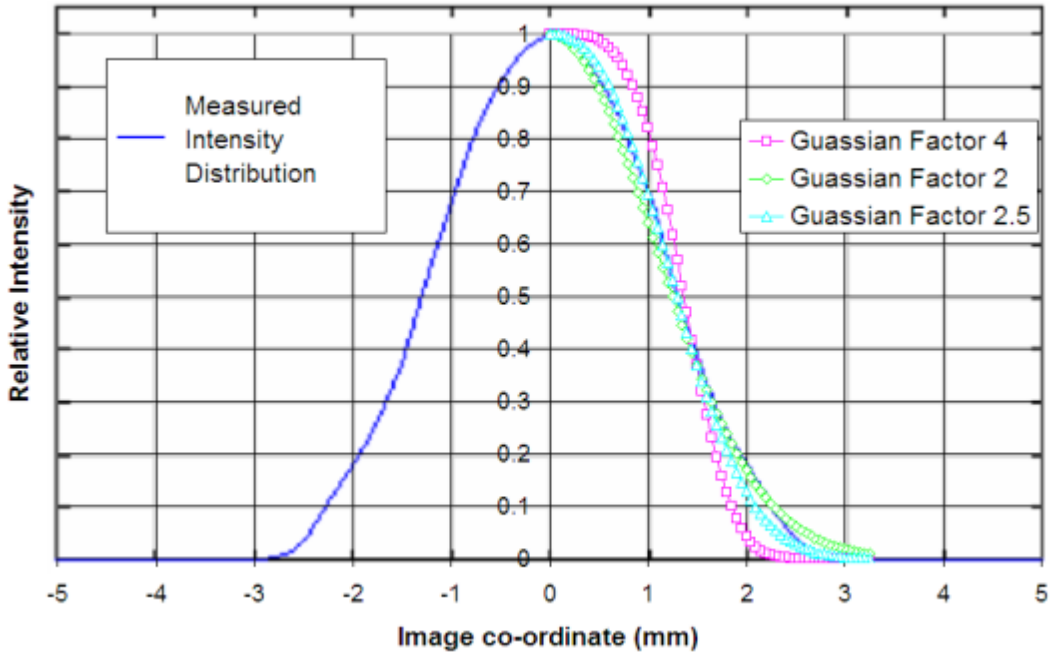

Figure 9:3: Normalised Super Gaussian function overlaid on to measured intensity distribution from iCure[tm] system for a width factor of 1.5(mm) for different Gaussian factors.

In the COMSOL model the mathematical formulation of the problem is described by the volume equation of heat conduction as given in Equation 9:**4**.

$$\rho_d C_p \frac{\partial T}{\partial t} - \nabla(k \nabla T) = Q_h \qquad \textbf{Equation 9:4}$$

Where ρ_d is material density, C_p the specific heat capacity, T is the temperature, t is the time and k thermal conductivity. Q_h is the heat source distribution in depth (z).

The surface boundary condition for the radiated part of the model (the DW coating, Figure 9:2) is described by Equation 9:5.

$$\vec{n}.(k\nabla T) = q_0 + h(T_{\inf} - T) \qquad \textbf{Equation 9:5}$$

Where $\vec{n}$ is the normal vector, q_o is the inward heat flux (distributed with the super Gaussian function described in Equation 9:3), h is the heat transfer coefficient and T_{inf} the external temperature.

The unheated areas (the substrate boundaries) are treated as thermally insulating (adiabatic conditions) such that:

$$\vec{n}.(k\nabla T) = 0 \qquad \textbf{Equation 9:6}$$

The Global constants used in the model can be found in Appendix C.

9.1.4 Model Validity

To test the validity of the proposed process the temperature profile of a material with known thermal properties was measured and compared to the model. An alumina tile (99.6%Al_2O_3) was selected for this measurement as it has a relatively low thermal conductivity which allows for a measurable heat rise to be obtained after a short exposure to the heat spot. The dimension of the tile was approximately 80x80x0.5mm and was coated with black acrylic/carbon paint.

The model for the ceramic tile is shown in Figure 9:4 A. The meshing parameters used in the model have a large consequence on the accuracy of the solution. However, using a fine mesh requires large processing times and memory usage. To optimise the mesh size the free-mesh option was used in COMSOL. This allowed the mesh size to be highly defined at the location of the heat source and coarse at the boundary edges of the alumina tile (Figure 9:4 B). Figure 9:4 C and D show the tile as it is being exposed to the heat spot in both the model and thermal imaging camera respectively.

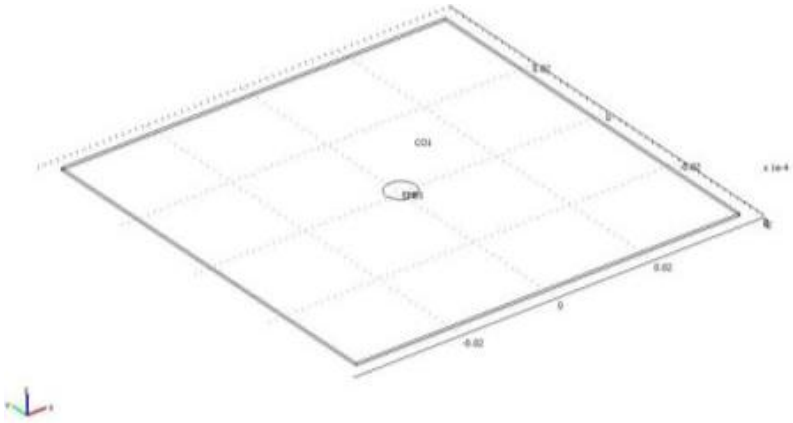

A

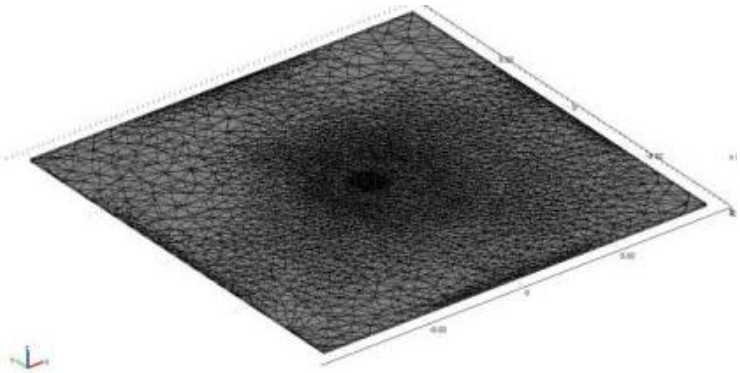

B

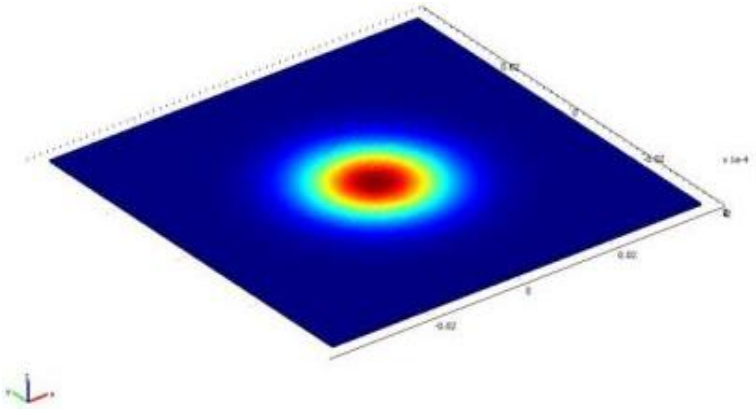

C

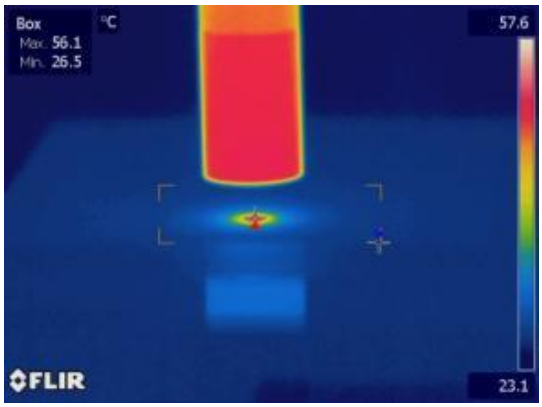

D

Figure 9:4: (A) Model of ceramic tile in COMSOL Multiphysics. (B) Mesh of ceramic. (C) Solution for ceramic tile as it is being heated by a heat spot. (D) Temperature measured by thermal imaging camera.

The ceramic tile was heated at three different heating profiles using the iCure^{tm} system, 2W for 0.5 second, 2W for 1 second and 5W for 1 second. The thermal imaging camera was used to monitor the peak temperature in the sample as the tile was heated and allowed to cool as a function of time. During this time the ambient temperature remained constant at approximately 25°C. The measurements from the thermal imaging camera were then compared to the simulation.

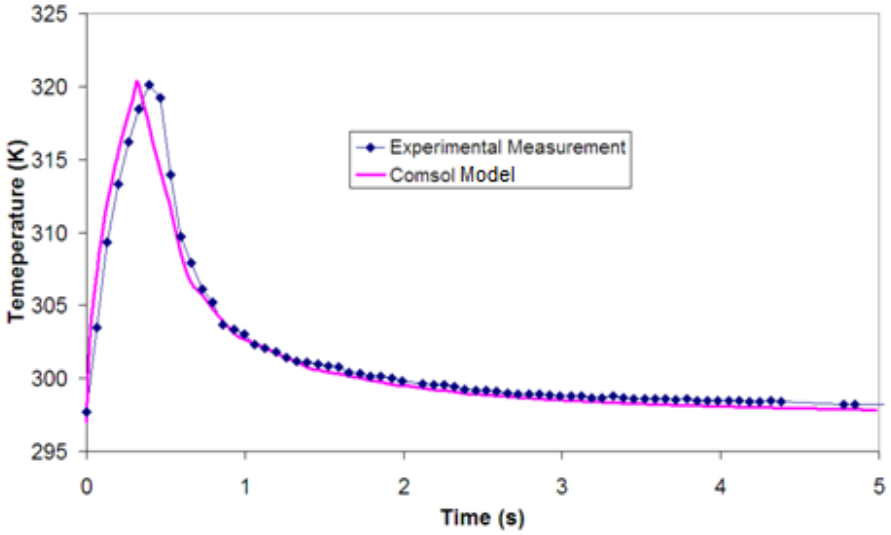

A.

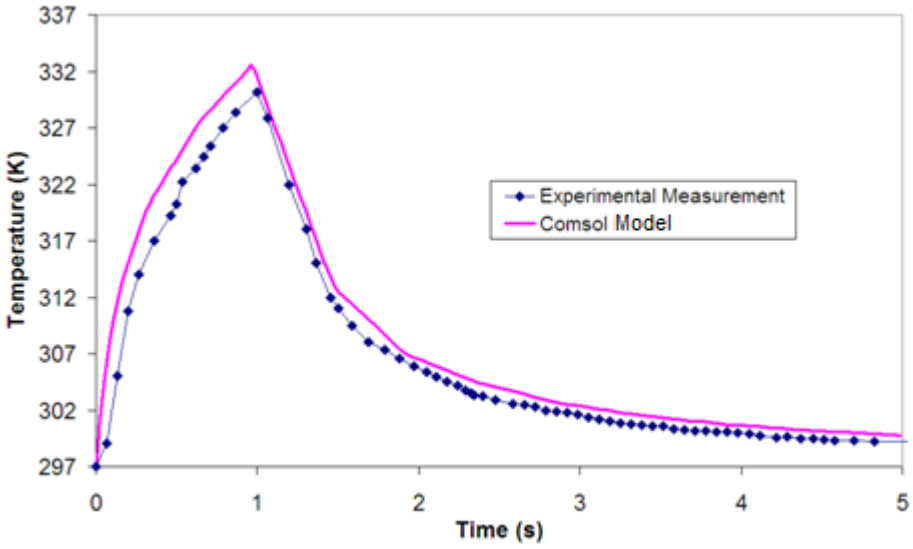

B.

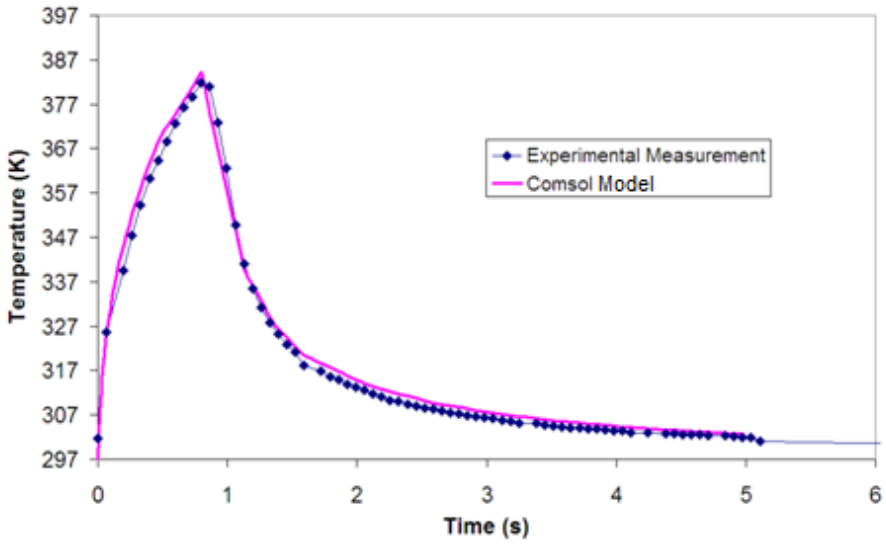

C.

Figure 9:5: Comparison between simulated and experimental measurement of temperature (K) against time (s) for a ceramic time heated at (A) 2W for 0.5seconds (B) 2W for 1second (C) 5W for 1 second.

The correlation between the measured and predicted data points in Figure 9:5 (A), (B) and (C) is within 10K. The peak temperature also shows close comparison between the model and measured values (approximately 2-3K).

9.1.5 Silver Ink Measurements: Thermal Conductivity

To measure the thermal properties of the DW silver ink the model was modified to contain both an FR4 substrate and DW coating layer (Figure 9:6). This model requires known physical and thermal properties for the FR4 substrate. The density of the DW coating was measured by weighing the substrate before and after application and curing of the DW coating and using the alpha step to measure the thickness of the coating. The density of the DW ink after curing was calculated at approximately 2600kg/m^3.

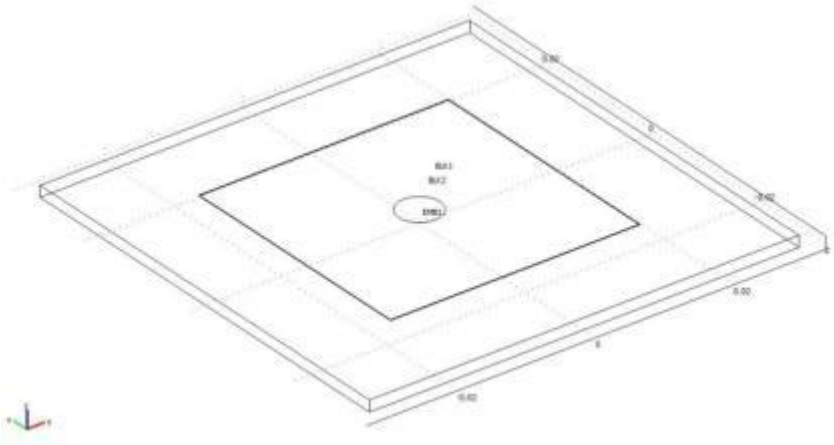

A.

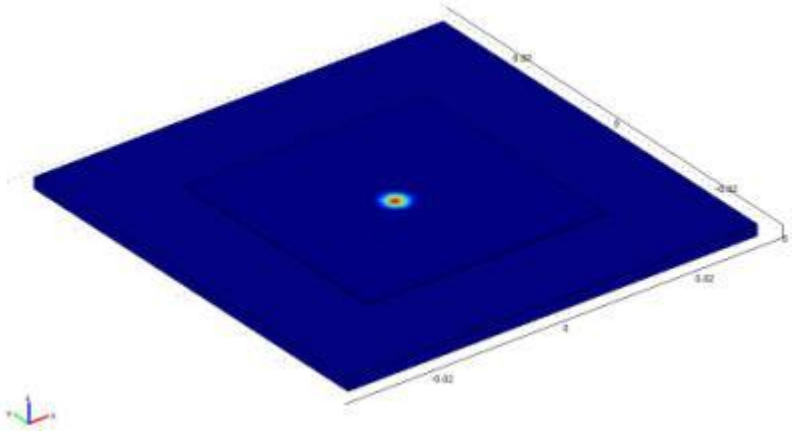

B.

Figure 9:6: (A) Multilayer model to measure the thermal conductivity of Silver Direct Write ink coated on to an FR4 substrate. (B) Model Solution

The methodology outlined in Figure 9:1 was used to measure the thermal coefficients for the DW coating. Essentially this process involves finding the coefficient of thermal conductivity from the rate of cooling after heating before finding the specific heat capacity from the peak temperature. The order of this process is important because the rate of cooling is dependent on one variable (the thermal conductivity) whereas the peak temperature is dependent on both variables (specific heat capacity and thermal conductivity). This effect can be seen in Figure 9:7 where the peak temperature varies with thermal conductivity at a constant heat capacity of 500J/kg.K when heated at a power of 0.5W for 0.5s.

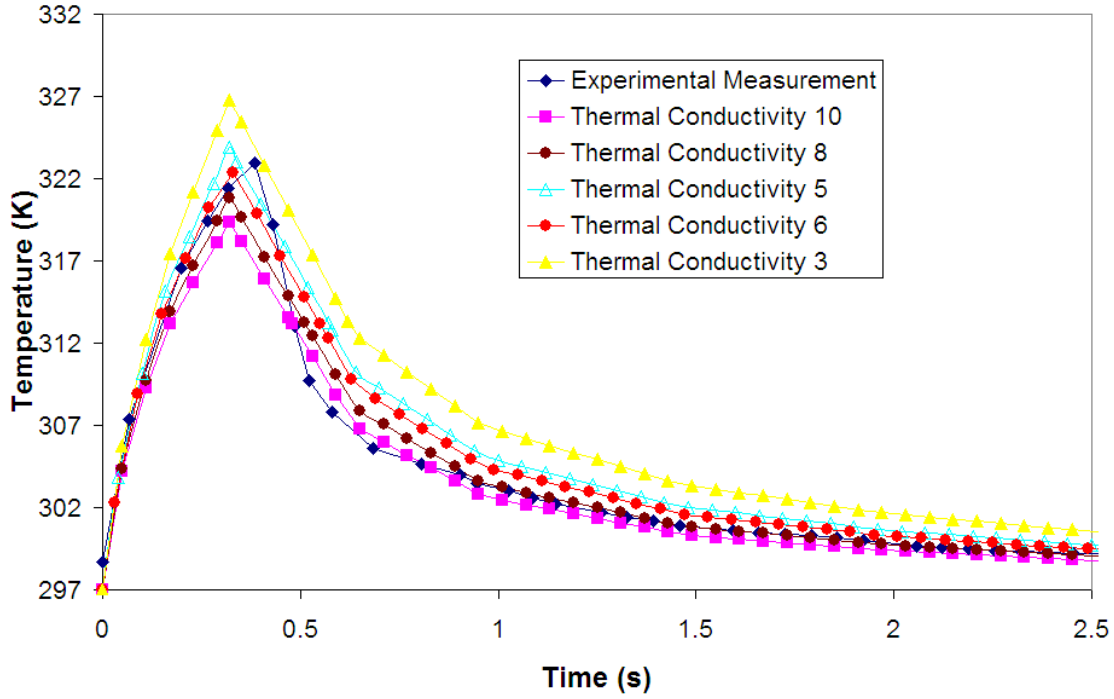

Figure 9:7: Simulated measurement of temperature profile for silver DW ink coated on to an FR4 substrate exposed to spot heating of 0.5W for 0.5seconds for different thermal conductivities for a constant heat capacity of 500(J/kg.K) compared to experimentally measured temperature profile..

Figure 9:7 shows that by decreasing the thermal conductivity of the coating the peak temperature increases after heating. As expected the rate of cooling is also directly proportional to the thermal conductivity. Figure 9:8 isolates the cooling curve when the sample is allowed to cool (at room temperature) from the same starting temperature for different thermal conductivities.

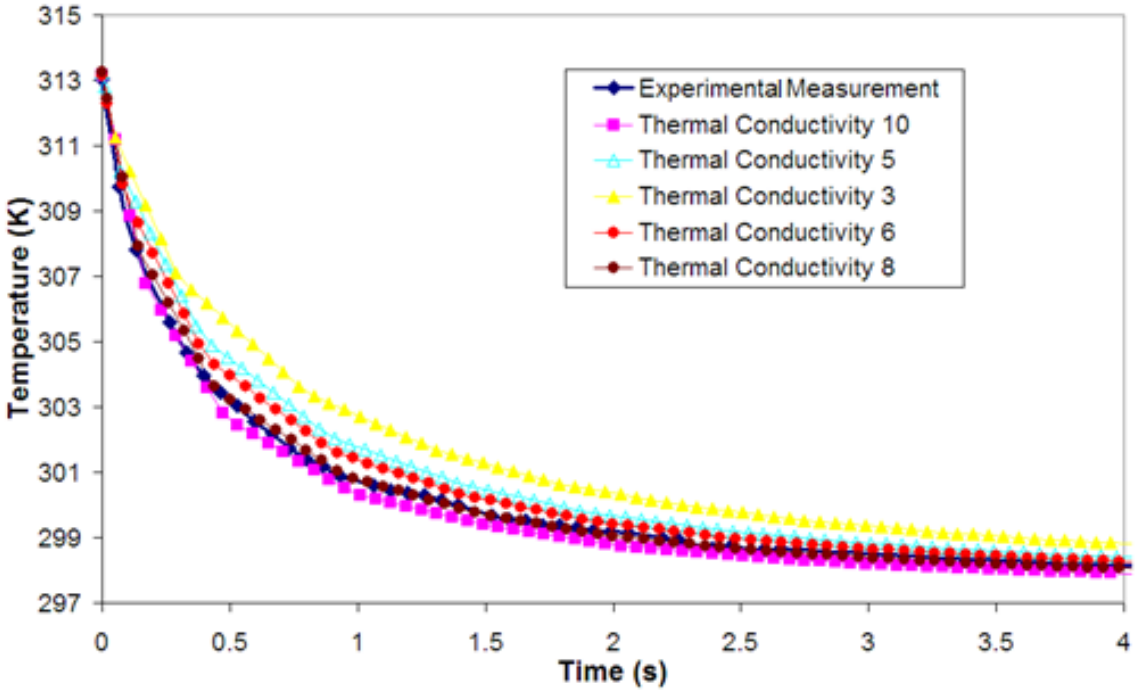

Figure 9:8: Simulated and experimental temperature profiles for a silver DW coating cooling from 313K modelled with different thermal conductivities with a heat capacity of 500J/kg.K.

The model shows a very close approximation to experimental measurements can be obtained when the coefficient of thermal conductivity is set to $8Wm^{-1}K^{-1}$. To explain this value it is necessary to identify the components that make up the ink composition. The DW ink, once cured, primarily contains silver and an unnamed epoxy resin component. The thermal conductivity of silver is $428Wm^{-1}K^{-1}$ and the thermal conductivity of a typical epoxy cast resin is $0.17\text{-}0.2Wm^{-1}K^{-1}$ [176]. The DW ink is loaded with approximately 60% of silver by weight however; this does not correlate to 60% of the thermal conductivity of bulk silver. A better indication of thermal conductivity can be found by measuring the electrical conductivity of the DW silver coating. According to the Weidemann Franz law [177] the thermal conductivity of a material (specifically a metal) is directly proportional to its electrical conductivity as described in Equation 9:7.

$$k = LT\sigma$$ **Equation 9:7**

Where k, is the thermal conductivity, T is the temperature (Kelvin), σ is the electrical conductivity and L is the Lorenz number ($2.44e^{-8}$ $W\Omega K^{-2}$).

Using a four-point probe the volume resistivity of the DW silver coating was measured at $9.4x10^{-7}\Omega m^{-1}$ or approximately 1.72% bulk conductivity of silver. This compares well with the calculated

thermal conductivity which is 1.896% of bulk silver. Using Equation 9:7 the thermal conductivity can be calculated at room temperature (273K) as 7.12$Wm^{-1}K^{-1}$. It must be noted the Weidmann Franz law is only really valid for metals (the DW ink is a composite material) [178]. However, this result does indicate a good relationship between thermodynamic theory, the model and experimental measurements.

9.1.6 Silver Ink Measurements: Specific Heat Capacity

To determine the specific heat capacity of the DW coating the model was modified so that the thermal conductivity was set constant at 8$Wm^{-1}K^{-1}$ and the specific heat capacity was changed instead. The peak temperature was then measured as the sample was heated at 0.5W for 0.5 seconds and compared to the simulated results (Table 9:1).

Heat Capacity ($jKg^{-1}K^{-1}$)	Peak Temperature after spot heating at 0.5W for 0.5s (K)
Experimental measurement	322.96
220	323.00
235	322.87
250	322.75
300	322.35
500	320.85

Table 9:1: Peak Temperature in DW coating after heating with heat spot at 0.5W for 0.5s modelled with different heat capacities.

The measured and modelled peak temperatures match when the heat capacity is approximately 220$J.kg^{-1}K^{-1}$. However, the difference in peak temperature with a heat capacity of 220$J.kg^{-1}K^{-1}$ when compared to 300$J.kg^{-1}K^{-1}$ is less than a 1K and so the accuracy of this measurement is very much dependant on the accuracy and resolution of the physical experiment. The FLIR thermal imaging camera has a stated accuracy of +/-2°C. According to the model, variation in the measured peak temperature could change the heat capacity by almost +/- 250$J.kg^{-1}K^{-1}$. The camera records the temperature at an interval of 0.066 seconds and so there is a possibility that the actual peak temperature may not be recorded accurately.

The heat capacity of silver is 235$J.kg^{-1}K^{-1}$ and that for a typical epoxy resin is 1110 $J.kg^{-1}K^{-1}$ [176]. The value from the model (220$J.kg^{-1}K^{-1}$) therefore suggests that the heat capacity may be dominated by the silver component rather than the resin binder.

The overall temperature profiles, as predicted by the model, using the thermodynamic coefficients obtained from this method are presented in Figure 9:9 for different heating profiles. These profiles were compared with the temperature profiles obtained from experimental measurements.

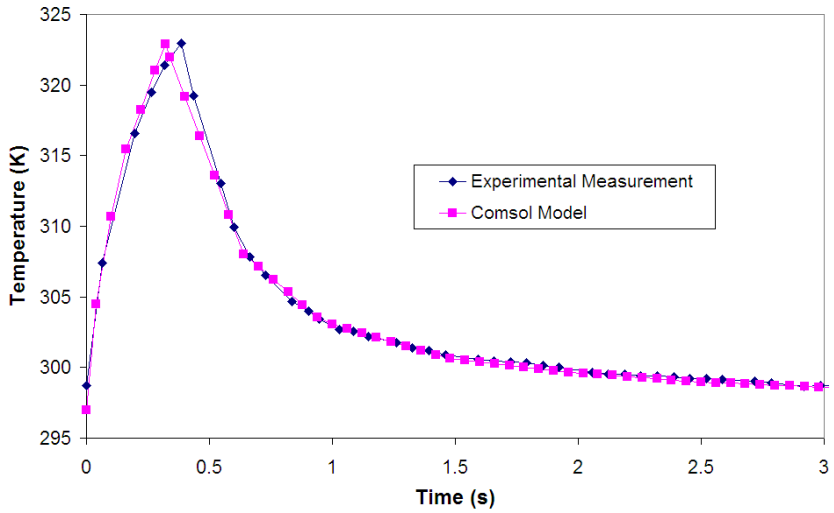

A.

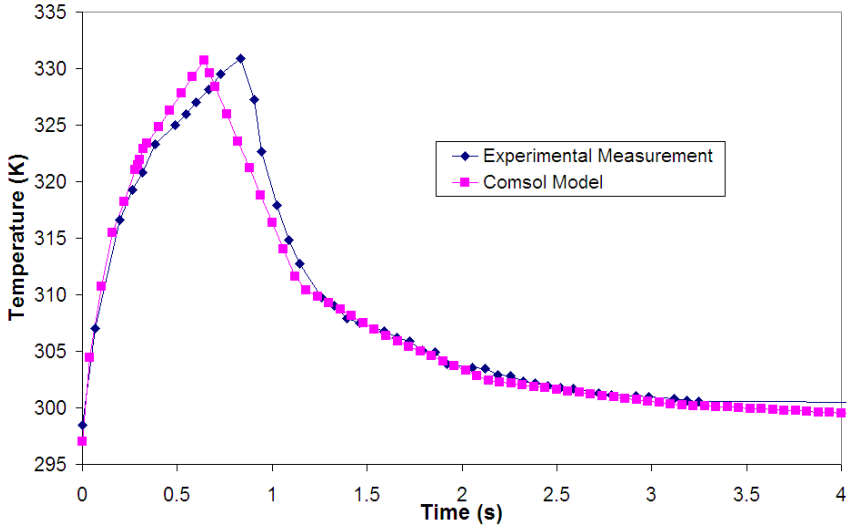

B.

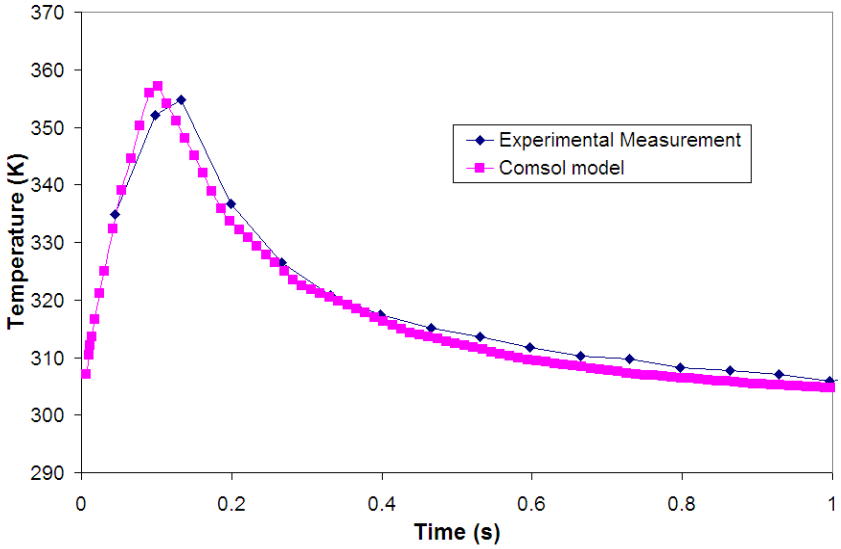

C.

Figure 9:9: Full temperature profile of DW coating as it is being spot heated for (A) 0.5W for 0.5seconds (B) 0.5W for 1second (C) 2W for 0.1second

In general the model compares favourably to the measured temperature profile obtained from the thermal imaging camera. The results show that there is a small time delay between the peak temperatures obtained in the model to the peak temperatures in the thermal imaging camera. Figure 9:9 C shows a disparity (~7K) between the experimentally measured peak temperature and the simulated peak temperature. The main reason for this is the lack of data points measured with the thermal imaging camera when compared to the heat exposure time. As data was taken every 0.066 seconds for a 0.1 second exposure to heat energy meaning the likelihood of measuring the exact peak temperature was low. Although this contributed to an error of approximately 2% it does highlight that this method is dependent on the accuracy and resolution of the physical experimental technique.

9.1.7 Discussion

The methodology presented in this chapter outlines a process whereby the coefficients of thermal conductivity and specific heat capacity can be estimated for thin film coatings which cannot be easily isolated from a substrate. This process compares the temperature profiles of a sample as it is heated with a spot heat source measured using a thermal imaging camera to those simulated in the COMSOL software. By implementing an iterative technique it was found that the thermal conductivity could be measured by comparing the rate of cooling with experimental data and the specific heat capacity by comparing peak temperatures.

To validate the model the technique was first implemented with a material of known thermodynamic properties. The results showed that there was close approximation between the peak temperatures and cooling rates in the model and thermal imaging camera. The process was then used to investigate the thermal properties of a PTF silver ink used for DW applications. It was found that the model gave credible measurements for the thermal conductivity of the DW ink which was related to the electrical conductivity of the ink. Measurements for the specific heat capacity could not be found as accurately due to the limitations in the thermal imaging camera.

9.2 Modelling Localised Curing Process

Using the thermodynamic constants for the DW silver ink determined in section 8.1 the localised curing process was simulated in COMSOL using equivalent parameters to those obtained in Chapter 7. The model consisted of an FR4 substrate with dimensions of 100x50x1.6mm with a DW track with dimensions of 100x1.5x0.04mm. The heat spot was applied with a diameter of 2.4mm and traverse speed of 4mms^{-1} with the equivalent intensity distribution as the iCure^{tm} system. Spectroscopy

measurements of the PTF silver ink conducted in Chapter 7 showed that approximately 60% of the incident radiation is lost to reflection. For the basis of this investigation it was therefore assumed that only 40% of the incident power was absorbed by the ink material. The transient model is shown in Figure 9:10.

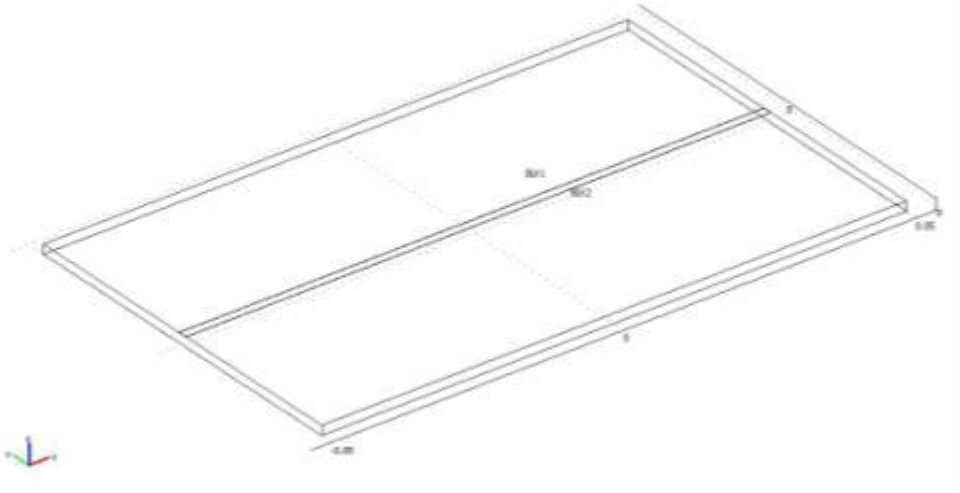

A.

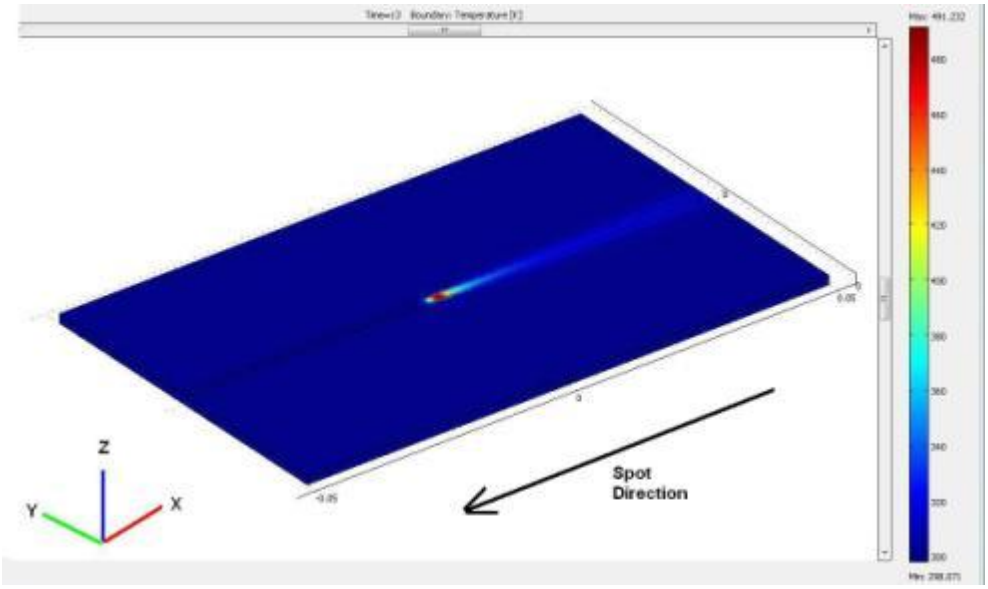

B.

Figure 9:10: (A) Model of localised broadband curing process. (B) Example model Solution

9.2.1 Simulation Results

Curing was simulated at 5W and 6.5W of power representing the experimental results obtained in Chapter 7. Temperature isotherms were taken in both the z-plane (the penetration into the substrate) and the x-plane (across the sample length) where the heat spot was located close to the middle of the track (see Figure 9:10).

The results for the temperature profiles in the z-plane are shown in Figure 9:11. In the figures the distance x = 0 represents the middle of the heat spot, positive values of x are in the forward facing direction of the beam as it traverses across the length of the DW ink track. The penetration depth, z = 0, is located at the boundary between the DW ink track and the FR4 substrate.

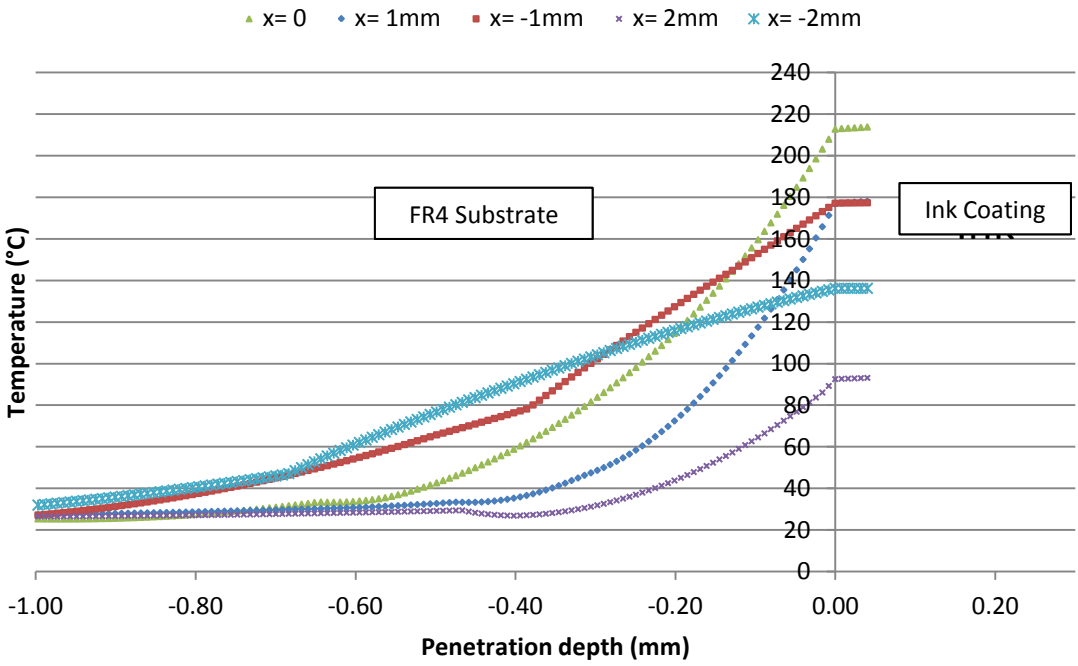

A.

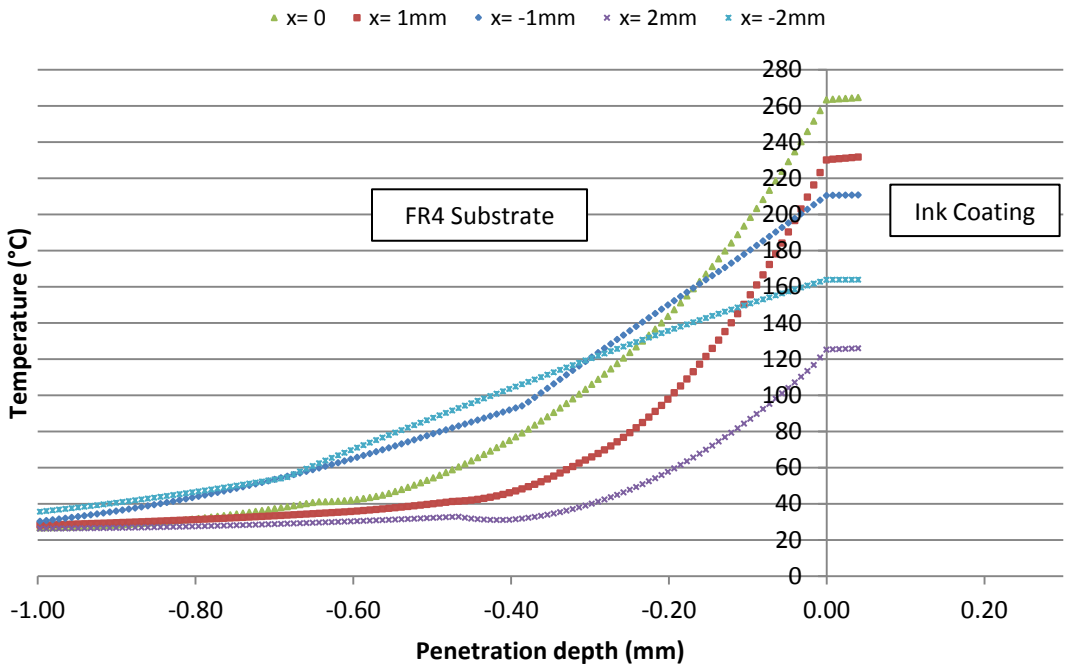

B.

Figure 9:11: Temperature against penetration depth taken in the z-plane at a traverse speed of 4mm^{s-1} (A) Incident power 5W (B) Incident power 6.5W

The model shows that the temperature within the ink coating directly underneath the heat spot is approximately 218°C and 260°C when processed at a power of 5W and 6.5W respectively. This temperature does not vary too much across the ink coating due to the relatively high thermal conductivity of the silver particles. The temperature from the ink coating is transmitted to the substrate by thermal conduction. It can be seen that directly underneath the beam the heat penetrates approximately 160μm (at 5W) to 200μm (at 6.5W) into the substrate before the temperature is below the manufacturer's recommended operating temperature (135°C). To determine how long the substrate is subjected to heat above 135°C the temperature profile was measured in the x-plane. The results are shown in Figure 9:12.

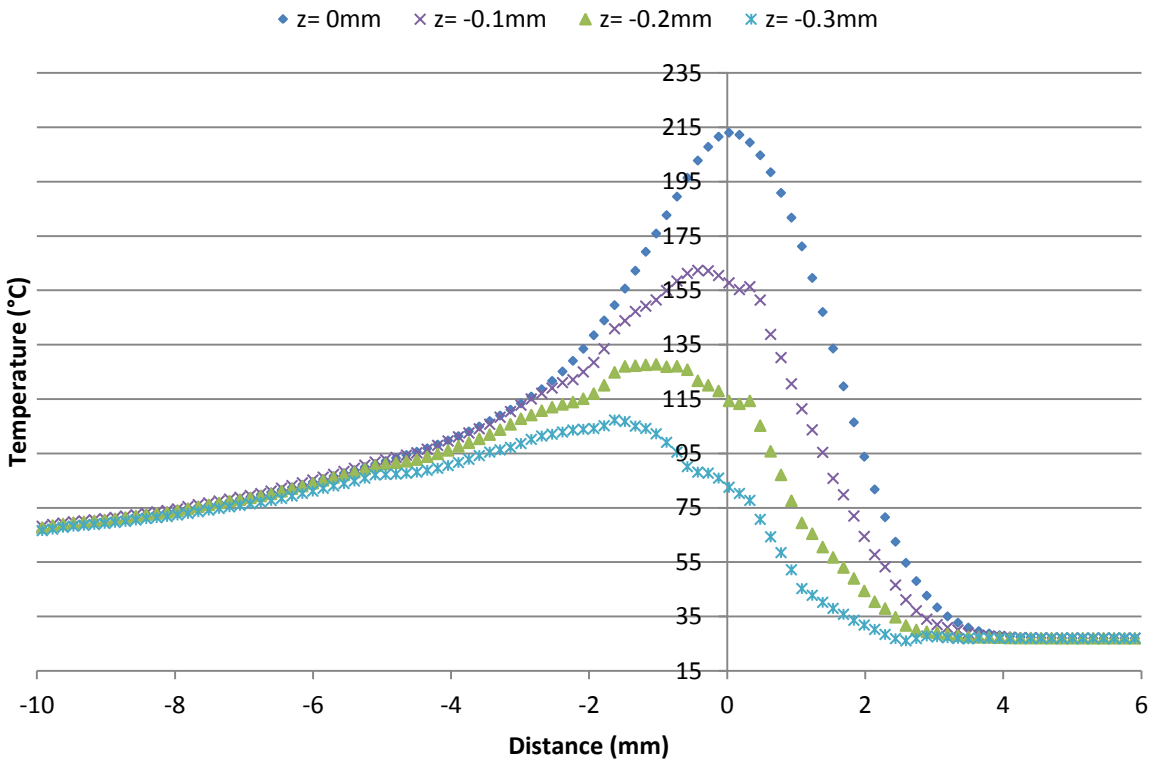

A.

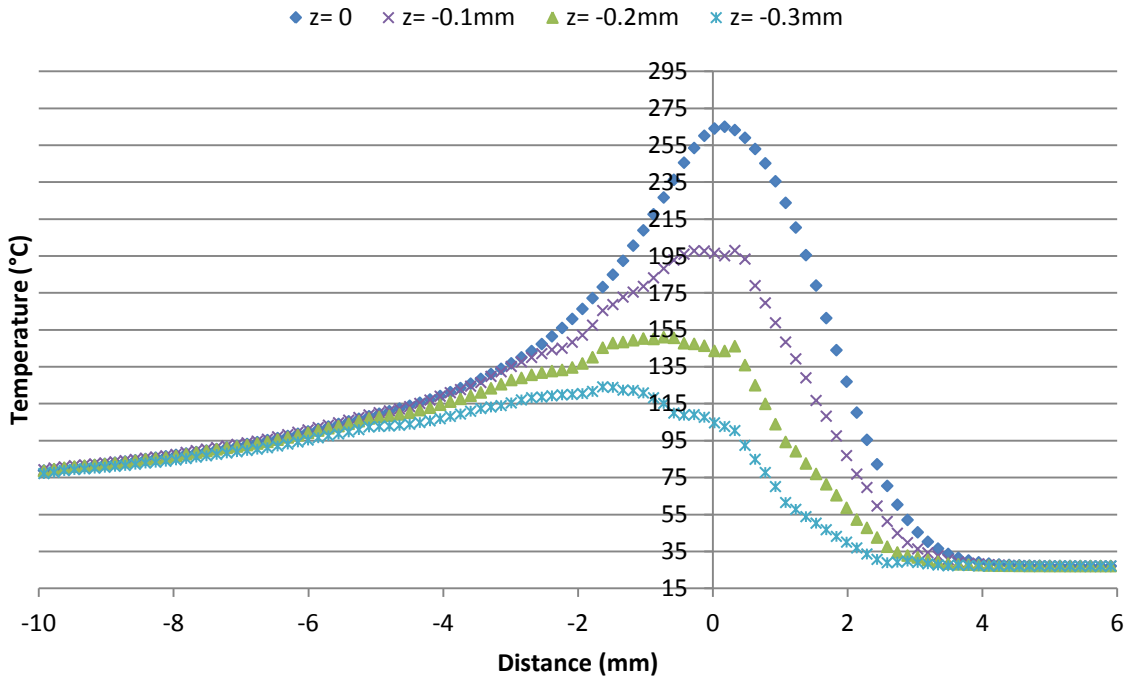

B.

Figure 9:12: Temperature against distance taken in the x-plane at a traverse speed of 4mms^{-1} (A) Incident power 5W (B) Incident power 6.5W

The temperature profiles from Figure 9:12 show the rate of cooling in the substrate is slower at the trailing edge of the beam than the front of the beam. As the beam traverses across the sample it

takes approximately 0.5 seconds at 5W and 0.6 seconds at 6.5W for the temperature to cool to below 135°C at a depth of z=0mm (the interface between the substrate and ink). Similarly at 5W, z=0.16 mm the temperature is above 135°C for approximately 0.3s and at 6W z=0.2mm, the temperature is above 135°C for approximately 0.5seconds. It takes between 7 and 8 seconds before the temperature in the substrate reaches room temperature.

9.2.2 Discussion

The simulation results show the relatively high temperatures required to locally cure the DW inks. Although there is high heat penetration into the substrate material (higher than the operational temperature of the material) this is restricted to only a few hundred micro-meters into the substrate and last less than 1 second. Further analysis is needed to determine if this would be sufficient enough time to affect the performance of the FR4 material.

9.3 Conclusion

Localised processing with a heat spot has been shown to adequately cure DW ink material. To determine if localised curing imparts any significant heat into the substrate material thermodynamical modelling techniques were employed. This required detail on the thermal coefficients of the DW material which were unknown. This is difficult to measure using conventional techniques (such as the cut bar [171] method) as the ink coatings are below 150μm and cannot be isolated from their parent substrate material.

To determine the coefficient of thermal conductivity and specific heat capacity for the DW material a methodology was presented which compared the temperature profile of a heated sample measured with a thermal imaging camera to those simulated in a COMSOL model. By implementing an iterative technique it was found that the process gave credible measurements for the thermal conductivity of the DW ink which could be related to the electrical conductivity of the material. Measurements for the specific heat capacity could not be found as accurately due to the limitations in resolution and accuracy of the thermal imaging camera.

Using the measured values for the thermal conductivity and specific heat capacity of the PTF silver ink the localised curing process was simulated in the model using the experimental parameters determined in Chapter 7. Although the isotherms from the model showed high heat penetration (above the operating temperature of the FR4) into the substrate this was restricted to a localised

area near the surface of the material (by a few hundred microns). The interaction time at this temperature was also very low measuring at sub one second durations.

Further analysis is needed to determine if the penetration depths and heat interaction times from the localised curing process is enough to degrade the performance of the substrate material. This is potentially a key requirement in determining whether heat radiation is a viable means of locally curing DW inks on composite type structures.

10 The Microwave and RF Characteristics of DW Materials

In Chapter 3 the key DW requirements required to fabricate an antenna on to the surface of an aerospace or military platform was discussed. The performance of the antenna is dependent on the signal carrying capability of the DW ink material and the accuracy at which the material can be deposited.

So far the majority of the work presented in this thesis has focused primarily on the development, characterisation and processing of conductive PTF and Inkjet DW ink material. One of the key developments was the improvement in conductivity that can be achieved when electroplating these inks with a brush plating tool.

In this chapter the developments made in this thesis will be brought together to test the RF and microwave properties of the DW conductive inks. Comparisons will be made between oven cured and broadband cured deposits as well as those electroplated with the brush plating tool.

10.1 DW Transmission Lines

Transmission lines are specialised cables used to connect antennas with their radio transmitters and receivers. Transmission lines are used to carry alternating currents in the radio frequency (microwave) range where the wavelength approaches the length of the cable used. At these frequencies ordinary cables would suffer from large power losses from radiating radio waves. Radio frequency currents also tend to reflect from discontinuities in the cable (such as connectors) which prevent the signal from reaching its destination. To overcome these problems transmission lines are designed with high quality dielectric material to insulate the signal and impedance matched to prevent reflections at connector interfaces.

Early microwave systems relied on waveguide or coaxial lines for signal transmission. Waveguide have the advantage of high power handling but are bulky and expensive whereas co-axial lines have high bandwidth but are a difficult medium in which to fabricate complex microwave components [95]. Planar transmission lines on the other hand are low cost, compact and able to be easily integrated with other devices particularly patch antennas. Planar transmission lines come in a number of different designs but the simplest structure to fabricate using DW is the micro-strip. This is because only a single conductive track is needed to form the waveguide. The micro-strip consists

of a conductor of width, w, printed on to a grounded dielectric substrate of thickness, *d*, and relative permeability ε_r (see Figure 10:1).

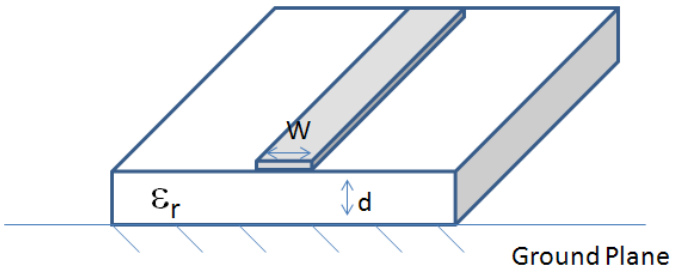

Figure 10:1: Microstrip transmission line geometry

In Chapter 3 the main DW design requirements for effective transmission line and antenna design were discussed. It is useful to recap here that the transmission loss in a microstrip line is attributed to the dissipative losses from the conductor, α_c (Equation 10:1), and dielectric material, α_d (Equation 10:2).

$$\alpha_d = \frac{\omega}{2}(\mu\varepsilon_0\varepsilon_r)^{\frac{1}{2}} \tan\delta_d \qquad \textbf{Equation 10:1}$$

$$\alpha_c = 8.68 * \frac{R_s}{wZ_m} \quad \text{where,} \quad R_s = \left(\frac{\omega\mu_o}{2\sigma_c}\right)^{\frac{1}{2}} \qquad \textbf{Equation 10:2}$$

Where, $\tan\delta_d$, is the loss tangent of the dielectric, ε_0, is the free space permittivity, w, is the width of the conductor, Z_m, is the characteristic impedance of the micro-strip, R_s is the surface resistivity, ω, is the angular frequency and, σ_c, is the conductivity of the micro-strip.

The equations show that at a given frequency the transmission line loss is dependent on both the loss tangent of the dielectric and the conductivity and width of the conductor material. In addition to this it is important to minimise reflections in the line by matching the characteristic impedance of the line to the antenna and power source. The impedance of a microstrip line varies as a function of the frequency of operation, the height above ground (the dielectric height), and the width and height of the conductor [100].

The skin effect can also contribute to RF losses especially if the surface roughness of the conductor is greater than the skin depth. The skin depth determines the penetration of the current in the conductor as a function of frequency.

$$\delta_z = \sqrt{\frac{1}{\pi f \mu \sigma}}$$ **Equation 10:3**

Where f is the frequency of the signal.

At high frequencies the current is restricted to the surface of a conductor. It was shown from simulations in Chapter 3 and previous work [179] that at high frequencies the majority of the current travels at the bottom of the conductor, whereas at lower frequencies (below 3-2Ghz) the current is more evenly distributed between the top and bottom surface of the conductor. This has important consequences for the localised electroplating technique which only plates the top surface of the DW ink coating with high conductive copper.

10.1.1 Microstrip Fabrication

Transmission line loss measurements were conducted for both oven cured, localised broadband spot cured and electroplated ink tracks. DW microstrip lines were constructed on to one sided copper clad FR4 dielectric substrates. Whilst FR4 is not considered to be an effective dielectric at frequencies above 1GHz because of its high loss tangent [100] industry standard microwave substrates such as Duriod can be extremely expensive to purchase. The dielectric properties of FR4 can also vary from batch to batch. Where appropriate microstrip lines were fabricated from the same batch of FR4 to avoid variable material properties. The only exception to this was when fabricating the oven cured inkjet micro-strip line. The inkjet ink requires processing at temperatures above 150°C and so an Isola FR-370 substrate was used. The Isola FR-370 has a higher T_g (180°C) than regular FR4 (T_g, 130°C) allowing the inkjet inks to be cured appropriately. According to the manufacturer the FR-370 substrate has a permittivity of 4.4 and loss tangent 0.016. This is similar to the regular FR4 substrate which has permittivity of 4.7 and loss tangent 0.014. For comparison a copper etched microstrip was also made from the same FR4 substrate. Whilst at high frequencies the loss in the FR4 would be high the copper etched sample can still act as a benchmark for the DW samples. The DW microstrip lines were fabricated from the following inks:

- PTF silver ink [129]
- PTF thermosetting silver ink [127]
- Inkjet silver ink [126]

The hybrid ink was not investigated in this experiment as it was felt the slight increase in conductivity was offset by poor adhesion.

The inks were deposited to give a track dimension of approximately 3 x 100mm. The length and width of the conductive track was calculated using AWR TX-LINE^{tm} Transmission line calculator to give 50Ω impedance.

The height of the ink layer can be an important factor when fabricating the DW micro-strip lines. For very thin strip lines (<skin depth) conductor losses can be high due to high surface resistivity. It has been suggested that the optimum thickness of the conductor strip is two or three times the skin depth [179, 8]. As the measurements would be made over a range of frequencies (with varying skin depths) it was decided that the maximum thickness of the DW microstrip line would be equivalent to or above to the skin depth at the minimum measurement frequency (500MHz).

Localised curing of the inks was conducted using the iCure^{tm} broadband spot curing system using the parameters determined in Chapter 7. Unfortunately due to print-head problems there was not enough time to process the inkjet ink with the iCure^{tm} system and test them for their RF properties using the facilities at BAE Systems. The parameters used to print and cure the inks and are given in Table 10:1. Table 10:1 also shows the skin depths for each ink layer calculated from Equation 10:3 using the measured track resistances. From the skin depth calculations it could be seen that the inkjet ink required three deposition layers to reach the required height. After each layer was printed the ink was cured before subsequent deposition.

Material	**Fabrication Method**	**Cure Method**	**Cure Parameters**	**Track Resistance (Ω)**	**Calculated Skin Depth at 500 MHz (μm)**	**Track Height (μm)**
PTF Silver	Micro-Nozzle	Oven	130°C, 20mins	0.74	20.78	38.4
	Micro-Nozzle	iCure	6.5W, 4mms^{-1} 3 scans	0.64	19.53	39.2
	Micro-Nozzle, Brush Plating (40 scans)	Oven	130°C, 20mins	0.22	12.23	44.75
PTF Thermosetting silver	Micro-Nozzle	Oven	130°C, 20mins	0.55	16.75	33.56
	Micro-Nozzle	iCure	5.5W, 4mms^{-1} 3 scans	0.46	15.49	34.33
	Micro-Nozzle, Brush Plating (40 scans)	Oven	130°C, 20mins	0.15	9.16	38.82
Inkjet Silver	Microfab inkjet Nozzle (3 layers)	Oven	3 x 180°C 30mins	0.41	6.55	6.88
	Microfab inkjet nozzle, Brush plating (40 scans)	Oven	180°C 30mins	0.077	4.17	14.86
Copper Track	Etched	N/A	N/A	0.015	2.92	30

Table 10:1: Curing parameters for DW ink tracks.

Once the DW micro-strip lines were fabricated two end launch SMA connectors were attached to either end of the line using a Circuit Works two part conductive epoxy adhesive which was dried at room temperature for 24 hours. The conductive adhesive was used to ensure electrical connection between the line and SMA connector. This method was preferred over soldering to avoid any potential damage to the DW ink material.

10.1.2 Loss Measurements

The transmission line loss was measured using a 2-port Vector Network Analyser (VNA) calibrated over a 0.13-20GHz range. The two port (denoted as 'S21') frequency domain data was used to extract the line loss. The VNA measures the loss of the transmission line in decibels, dB. The decibel describes is logarithmic unit which describes the ratio of two power levels, P_1 and P_2, as expressed by Equation 10:4.

$$dB = 10\log_{10}\frac{P_1}{P_2} \qquad \textbf{Equation 10:4}$$

The S21 data was recorded at a discrete number of frequency points by BAE Systems, Great Baddow. The data is obtained by visual inspection of the VNA display. It must be noted that there is some degree of subjectivity is introduced in this measurement due to the fast ripple (or fluctuations) in the data, this can be caused by poor connection in the line. Figure 10:2 shows the DW micro-strip line as connected to the VNA.

Figure 10:2: Two port S21 measurement of DW microstrip line

The characteristic impedance Z_m was measured using the single port (denoted as 'S11') measurement on the VNA. Again the measurements were conducted by BAE Systems, Great Baddow. The equation for Characteristic Impedance is given in Chapter 3 Equation 3:12.

10.1.3 Impedance and transmission line loss measurments

Before making the measurements a full two port calibration was conducted with VNA. An S21 measurement was also made with just the 50Ω connectors and cables to remove any signal attenuation from these components. The frequency S21 line loss measurements were made over a frequency range of 0.5GHz to 4GHz for each of the DW micro-strip lines. It was found at frequencies above 6GHz the substrate became very lossy making the results more difficult to interpret because of greater fluctuations in the VNA reading. The loss measurements for the oven cured DW micro-strip lines are given in Figure 10:3.

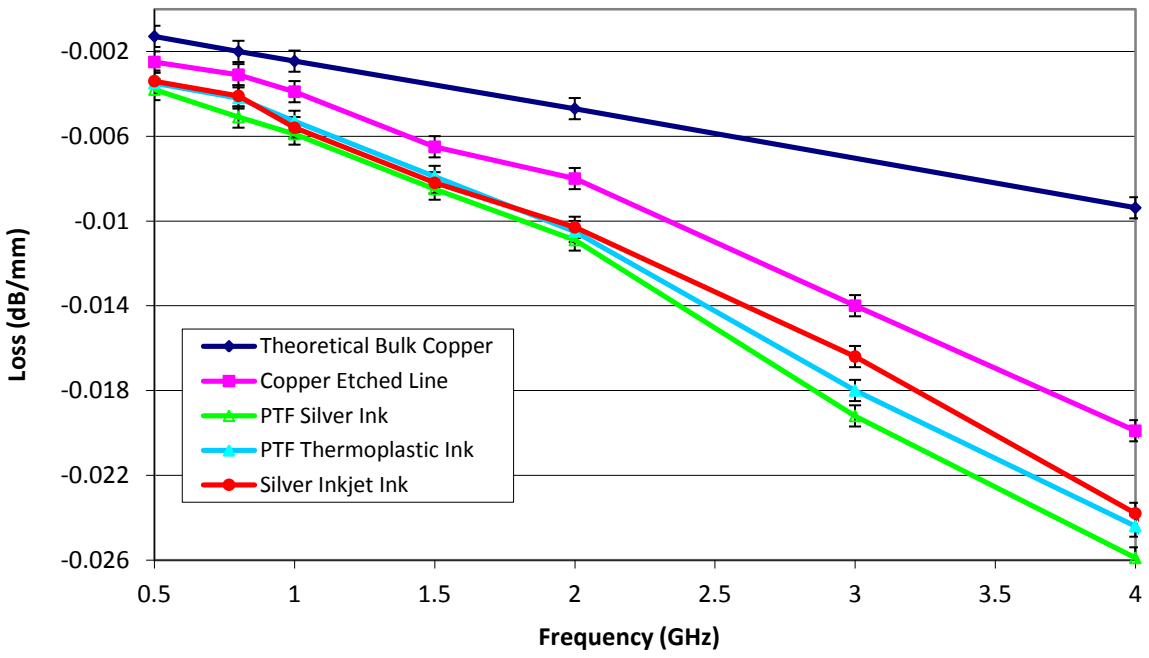

Figure 10:3: S21 transmission line loss for oven cured DW micro-strip lines from 0.5GHz to 4GHz

As expected the attenuation of the signal in the copper etched line differs significantly from the predicted loss at the frequency of the signal is increased. This effect is mainly caused by high loss tangent of the dielectric material. Other factors which may increase the signal loss in the DW micro-strip line are poor connection to the SMA connectors and reflection of the signal due to impedance mismatch. It can be seen that this trend is also evident in the oven cured DW micro-strip lines which suggests that the loss mechanisms are the same for all samples. Again as expected the lower

conductivity of the DW ink materials increase signal attenuation when compared to the copper etched tracks. A similar result was found in a study conducted by Z. Radivojevic et al. which found that the return loss of a silver nano-particle ink also gave a worse performance than an equivalent copper transmission line as a result of lower conductivity and track thickness [180].

Figure 10:4 shows the signal loss measured in a micro-strip line fabricated from the PTF silver ink when oven cured, broadband spot cured and copper plated. The results for the PTF silver ink and silver inkjet ink are given in Appendix D as the trends are similar.

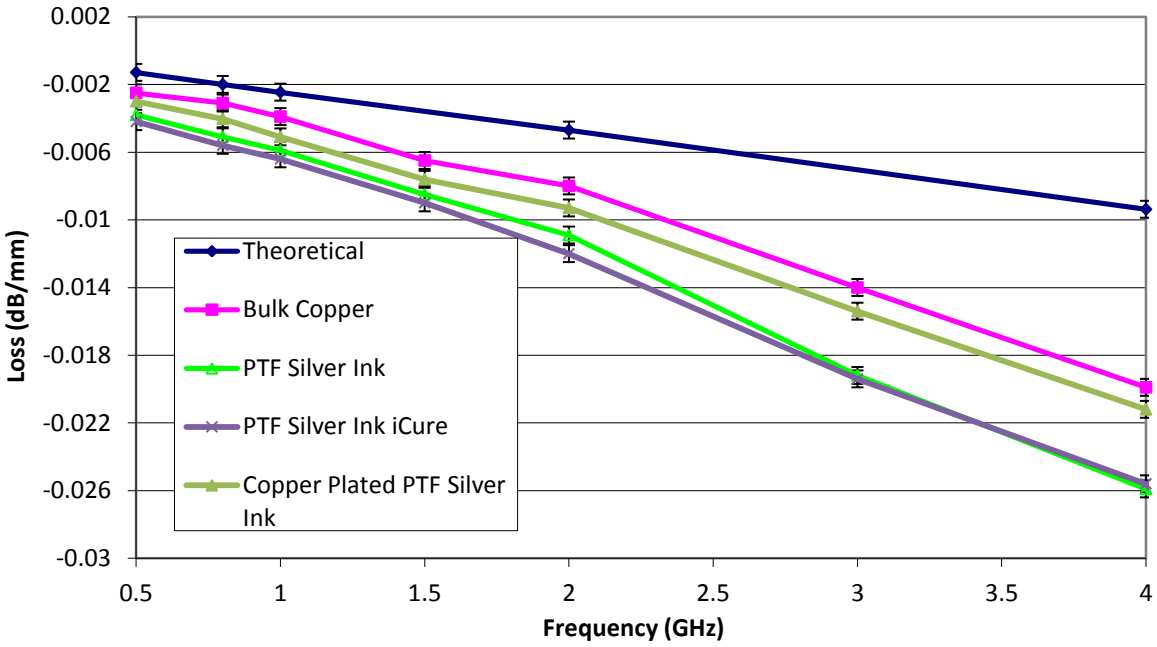

Figure 10:4: S21 transmission line loss against frequency for PTF silver ink micro-strip lines

It can be seen that from the results that the oven cured and iCure^{tm} processed DW inks have similar transmission line losses. This suggests that heat input from the iCure^{tm} source has not caused any degradation of the dielectric properties of the FR4 substrate. One of the key observations from these results is the decreased line loss of the copper plated PTF ink. This is because the signal is travelling through the path of least resistance which is in this case is through the copper layer. A comparison of all the copper plated DW transmission line is given in Figure 10:5.

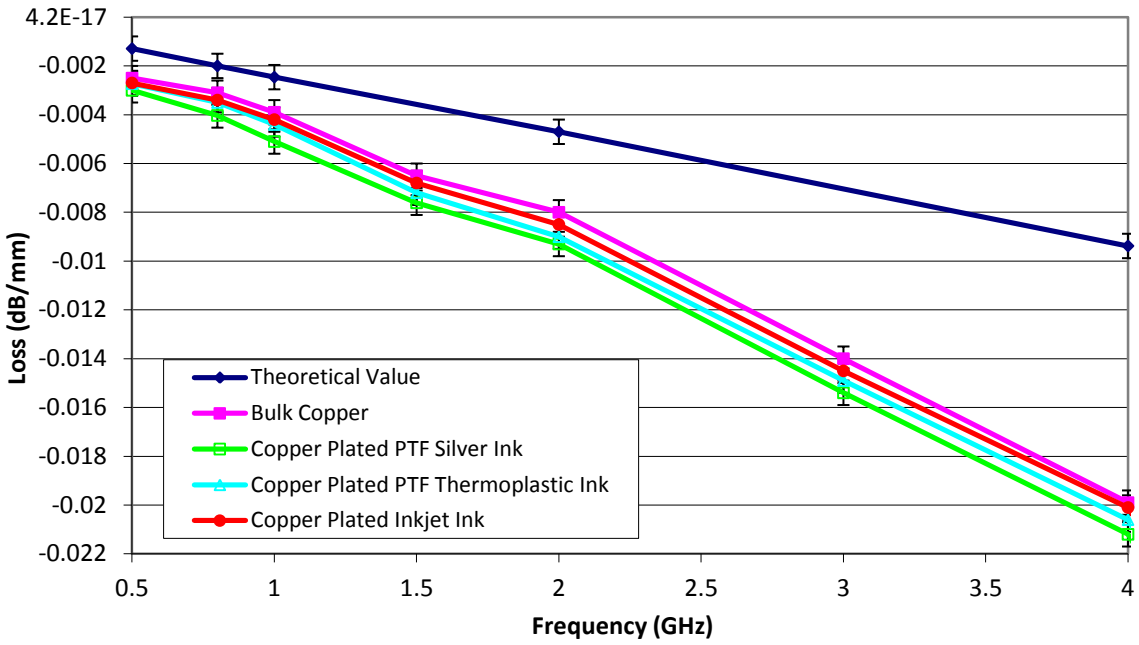

Figure 10:5: S21 transmission line loss against frequency for copper plated micro-strip lines

It can be seen from Figure 10:5 the copper plated inkjet ink has the lowest signal attenuation when compared to the copper plated PTF inks. The resistivity of the copper layer on the inkjet ink was calculated at approximately $2.03 \times 10^{-8} \Omega m^{-1}$ (or 85% bulk conductivity of copper) whereas the conductivity of the copper layer in the thermoplastic and silver PTF inks were $2.5 \times 10^{-8} \Omega m^{-1}$ (68% bulk conductivity of copper) and $7.5 \times 10^{-8} \Omega m^{-1}$ (23% bulk conductivity of copper) respectively. The higher plating efficiency on the inkjet ink therefore attributes to the lower signal loss.

Cross-section micrographs of the copper plated DW transmission lines are given in Figure 10:6. It can be seen that the inkjet plated line has a uniform layer of copper deposited onto it which correlates to the results given in Chapter 7.

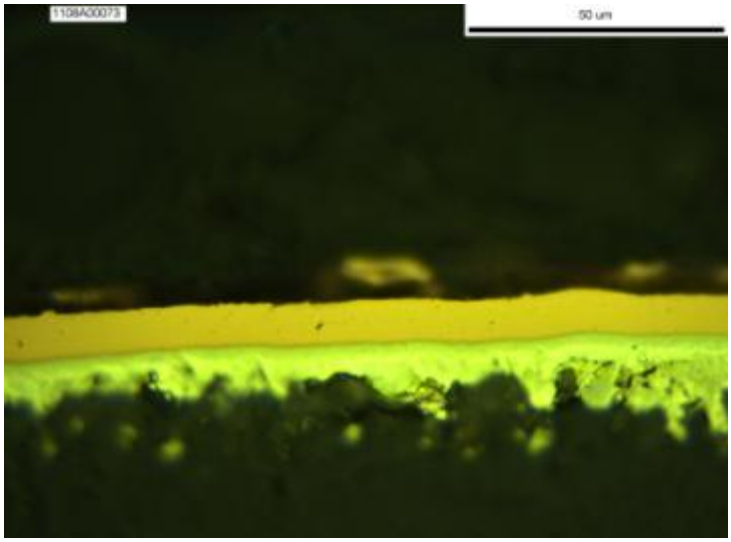

A

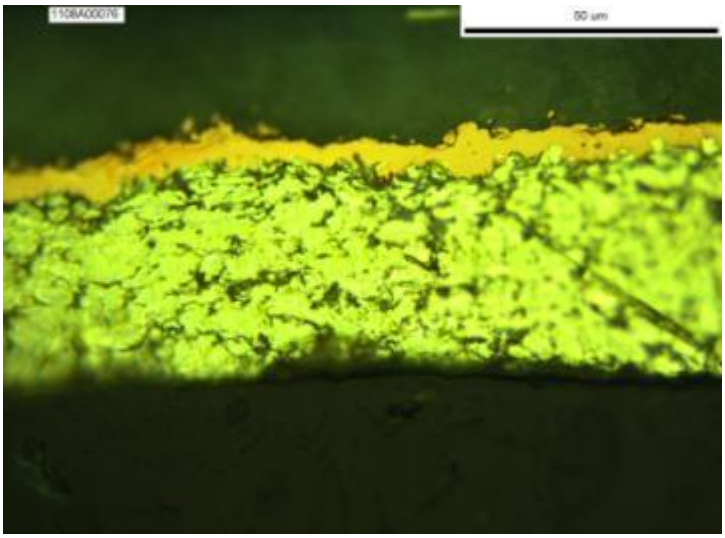

B.

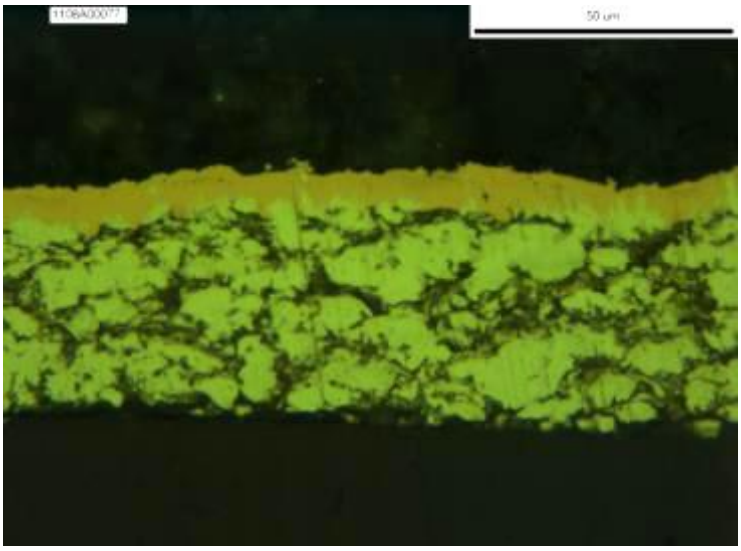

C.

Figure 10:6: Cross-section micrographs of copper plated DW micro-strip lines A. Inkjet ink B. PTF silver thermoplastic ink C. PTF silver ink

Table 10:2 shows the measured S11 line impedance for each of the DW micro-strip lines. The relatively small impedance mismatch (from 50Ω) of the DW samples is primarily caused by a difference in the required and printed dimensions of the printed ink tracks. Further work could have been done to modify the print parameters so that exact dimensions were achieved however the impedance values were deemed suitable for this experiment. Using TX line calc [98] it can be seen that an increase in impedance of 5Ω causes the loss of the line to increase by approximately $3.07x10^{-5}$dB/mm so the effect is negligible. It must be noted that the copper etched line also has a slight impedance mismatch which could be attributed to over etching of the copper track.

Micro-strip Sample	Characteristic Impedance $IZ_m I$ (Ω)
Copper Etched	54
Oven Cured Silver Ink	54.4
iCure Silver Ink	52.5
Electroplated Silver Ink	54.7
Oven Cured Thermoplastic Silver Ink	54.3
iCure Thermoplastic Silver Ink	54.8
Electroplated Thermoplastic Silver Ink	53.1
Oven Cured Inkjet Ink	52.3
Electroplated Inkjet Ink	52.2

Table 10:2: S11 measurements of micro-strip line impedance at 2GHz

10.1.3 Discussion

From the transmission line loss measurements it has been shown that localised electroplating of DW ink material can improve the signal carrying properties of DW ink materials. The loss measurements of broadband spot cured ink tracks were equivalent to those oven cured inks tracks. This demonstrates that the heat input from the curing process has not degraded the dielectric properties of the FR4 material. This strengthens the case for this process to be used to process DW ink material.

10.2 DW GPS Patch Antenna

A simple patch antenna was designed to further test the RF properties of the conductive DW ink materials. The antenna was designed by BAE System, Great Baddow to operate at the GPS frequency of 1575MHz based on a 1.6mm thick FR4 substrate. The design consists of a gridded patch with a 50Ω microstrip feed as shown in Figure 10:7. The patch was designed with a grid design to try to reduce the amount of material deposited with the DW process. This type of design has been investigated before for inkjet printing and transparent patch antenna design [181] [182].

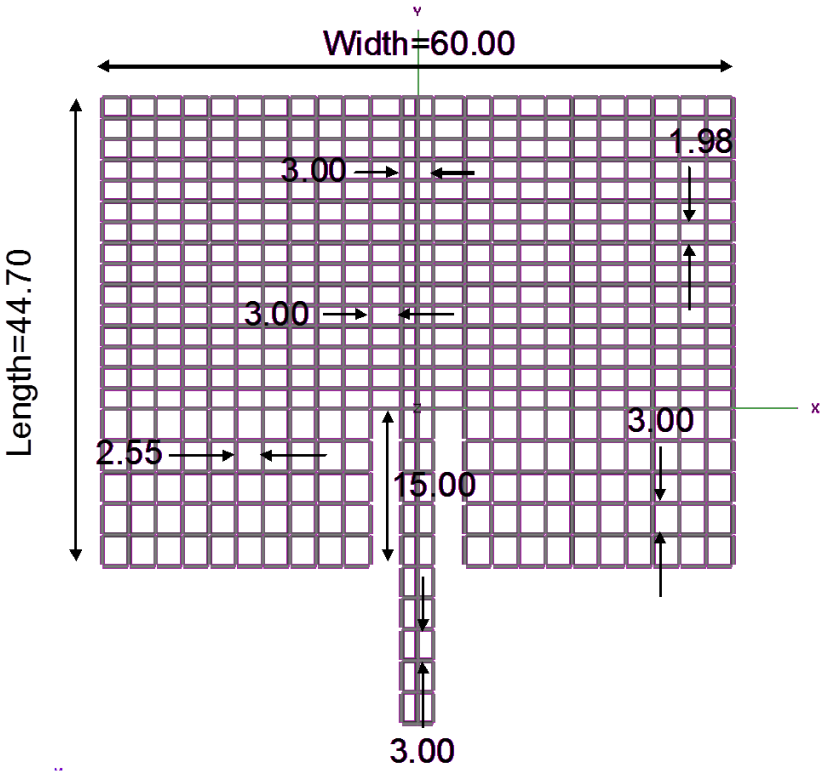

Figure 10:7: Gridded GPS patch antenna design with 50Ω feed line (all dimensions are in mm)

The GPS antenna was printed using the same inks used to fabricate the DW micro-strip lines in section 9.1. Due to equipment problems with the microfab inkjet nozzle the fabrication of the inkjet patch antenna was outsourced to a company called Printed Electronics Ltd [183]. To print the patch antenna Printed Electronics used a Xaar 126 print head with a 309dpi resolution. Unfortunately this system deposits a much finer layer of ink on to the surface of the substrate. This meant that after multiple deposits a height of only ~0.5μm was achieved in the DW antenna as opposed to the Microfab printed inkjet transmission line which had a height of 6.88μm (see Table 10:1). All DW inks were cured using the parameters detailed in Table 10:1 using both oven and iCure^{tm} processing.

To reduce the number of samples only patch antennas fabricated using the PTF thermoplastic and inkjet ink were electroplated with the brush plating tool using the parameters described in section 9.1. It was decided that the PTF silver ink was not included in this test as previous results has shown that this ink exhibits poorer plating efficiency when compared to the inkjet and PTF thermoplastic ink. The height of the copper plated inkjet antenna was smaller than the equivalent transmission line in section 9.1 measuring approximately 3.82μm as opposed to 8.86μm in height. Again this was due to thinner inkjet seed layer achieved with the Xaar print head. Figure 10:8 shows an example of a DW printed patch antenna with and without copper electroplating.

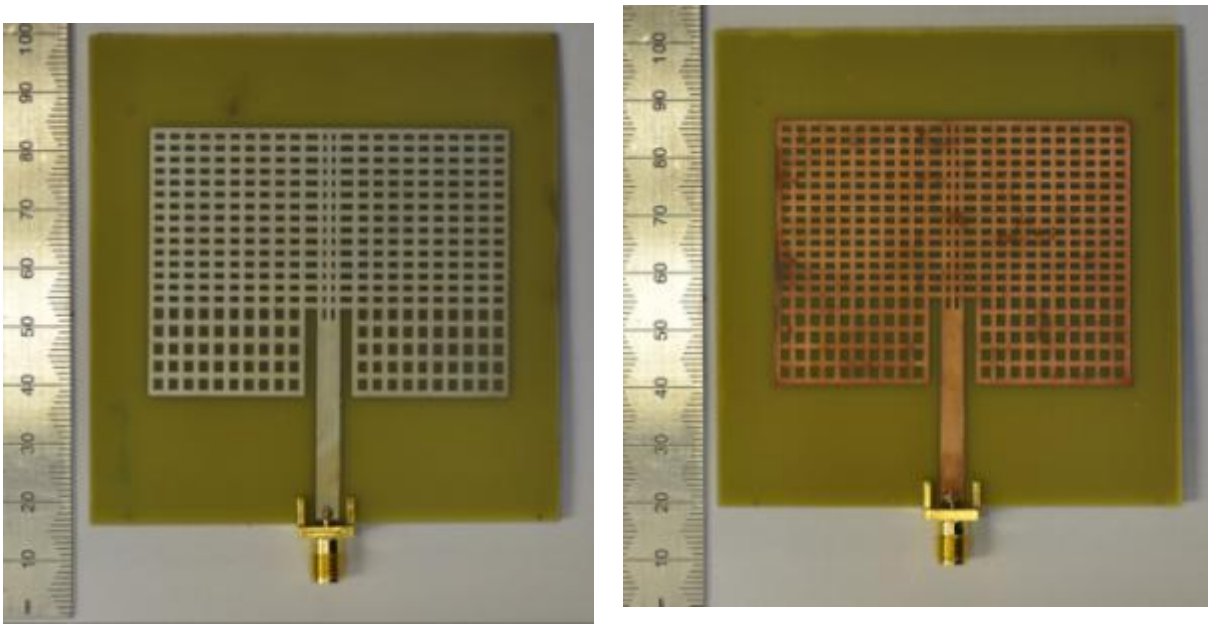

A. B.

Figure 10:8: A. 3 layer Inkjet patch antenna B. Copper plated inkjet patch antenna

10.2.1 Return Loss (reflection coeficient) Measurments

Using a VNA the S11 return loss or more appropriately called reflection coefficient (when a negative number is used) of the printed antenna can be measured. The reflection coefficient is the amount of power reflected back to the VNA for a given input power the rest of the power is either radiated or absorbed by the antenna as losses. This measurement is useful as it gives the resonant frequency and bandwidth of the antenna. The predicted reflection coefficient for the designed patch antenna is shown in Figure 10:9. As can be seen the patch is designed to radiate at approximately 1575MHz with a bandwidth of approximately 0.2MHz at -5dB.

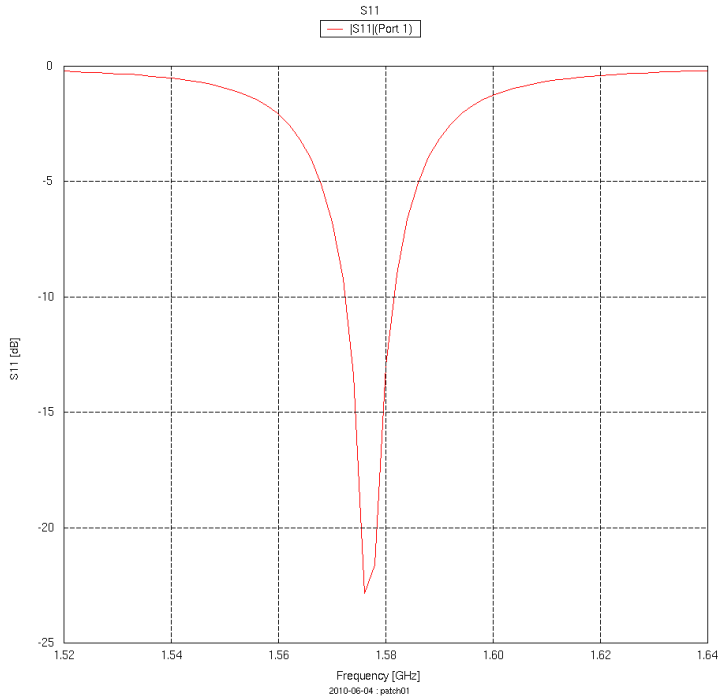

Figure 10:9: Predicted reflection coeficient from antenna design (supplied by BAE Systems)

The S11 measurement for DW patch antennas was measured using an Anristu 37397C VNA at the University of Bristol. The results for the oven and iCure[tm] cured DW patch antennas are given in Figure 10:10 and Figure 10:11.

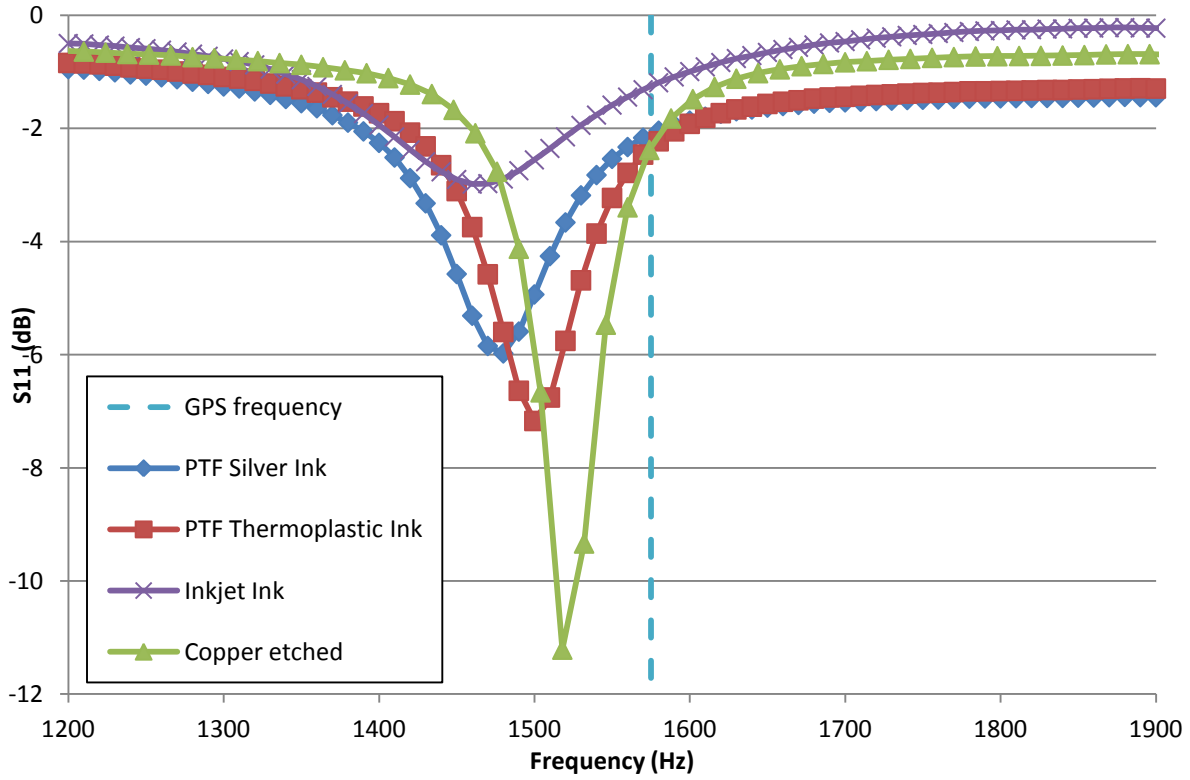

Figure 10:10: Return Loss measurements for oven cured DW patch antennas compared to a copper etched antenna

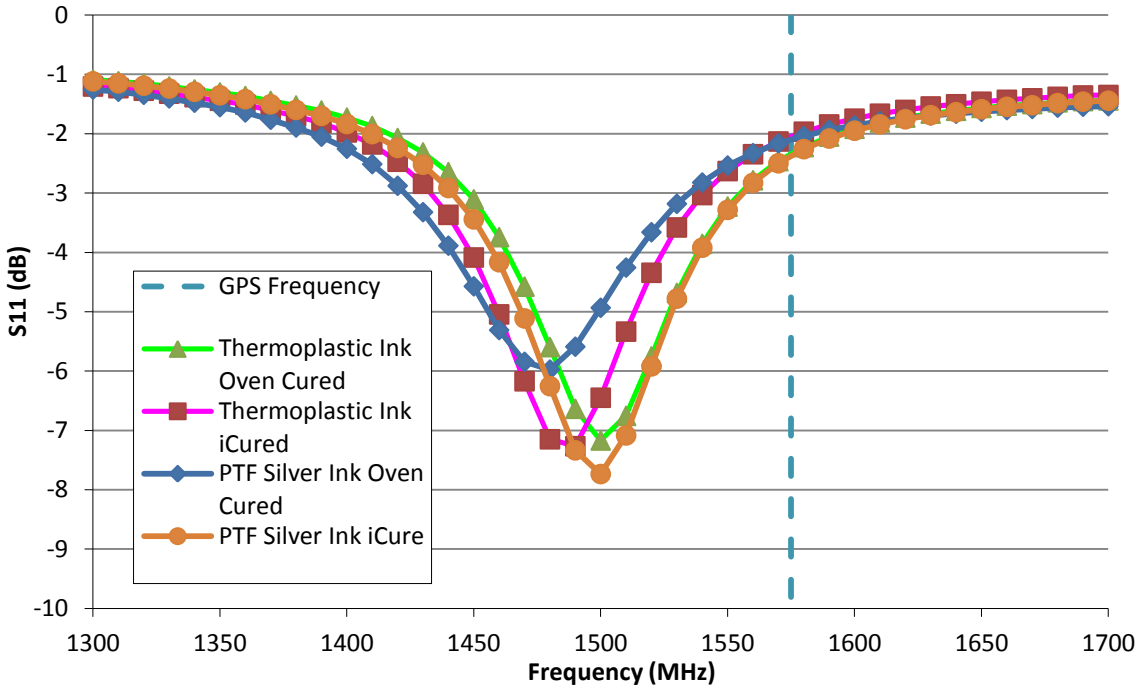

Figure 10:11: S11 measurement showing comparison between iCure[tm] and Oven cured DW patch antennas

It is evident from Figure 10:10 that the benchmark copper etched antenna has a much lower reflection coefficient than the theoretical value in the model. The lower signal could be down to a number of factors such as the high loss tangent of the dielectric material, the surface roughness of the FR4 and poor connection at the SMA interface. The resonant frequency of the fabricated antenna also deviates from the prediction in the model. This is not necessarily surprising as the print process was not optimised to give the exact dimensions of the antenna (i.e. ink rheology was not taken into account when printing the antenna using the inkjet and micro-nozzle DW techniques). This means that due to wetting and spreading effects the dimensions of the antenna ended up slightly larger than the design. The resonant frequency can be easily adjusted in each of the antennas by simply modifying the dimensions of the antenna by the factor it is out by, for example, the PTF thermoplastic patch antenna resonates at approximately 1500MHz which is a factor of 0.952 out from the desired resonant frequency of 1575MHz. By decreasing the dimensions of the antenna by a factor of 0.952 the resonant frequency should theoretically by much closer to the GPS frequency.

The S11 measurements of the DW inks follow similar trends to transmission line experiments in section 9.1 i.e. the lower conductivity inks give better signals with lower losses. The exception to this is the measurements made with the inkjet printed antenna which had the poorest reflection

coefficient. The main reason for this could be attributed to high surface resistivity caused by the low thickness of the inkjet deposit (~0.5μm) when compared to its skin depth (4.12μm at 1575Mhz).

As expected processing using the iCure[tm] system gives similar S11 performance to the oven cured DW patch antennas. Similar to the transmission line results this suggests that the high heat energy imparted from the iCure[tm] system does not affected the dielectric properties of the substrate as most of the energy is restricted to highly localised area.

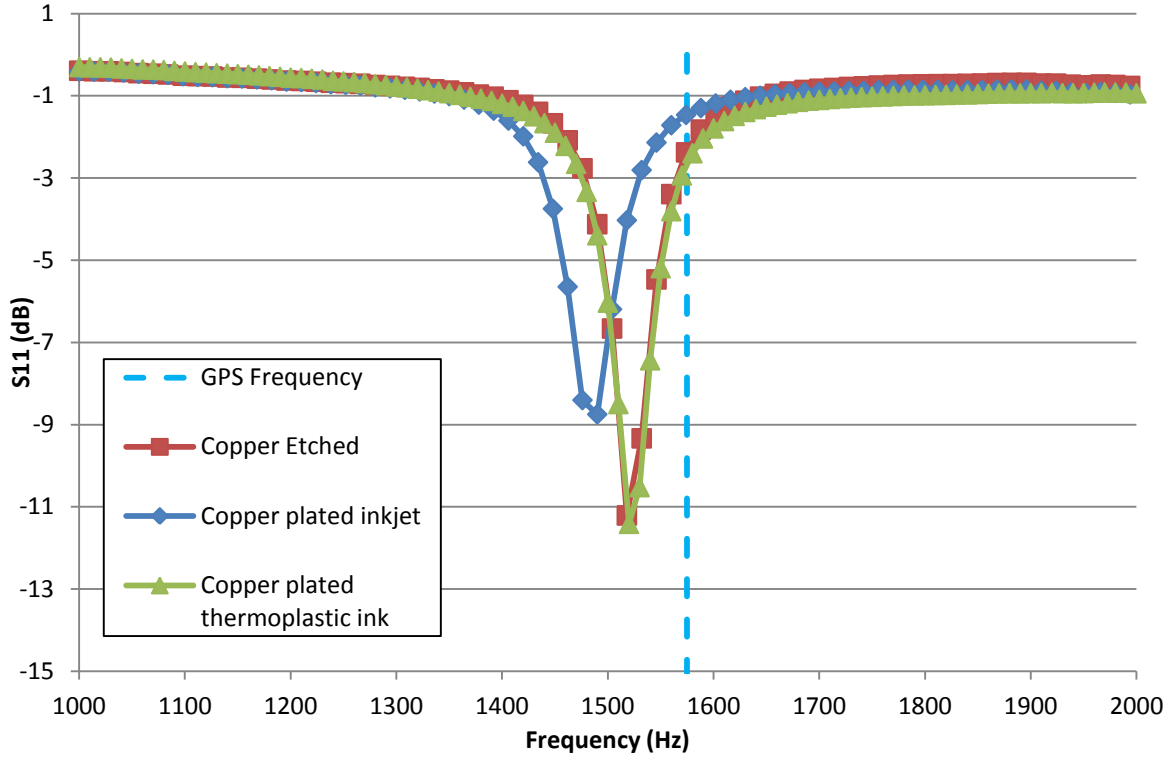

Figure 10:12: S11 measurements of copper plated DW patch antennas

Figure 10:12 shows the S11 measurements for the copper plated DW patch antennas. As can be seen, the return loss for the copper plated thermoplastic patch antenna is near identical to the benchmark copper etched antenna. The inkjet antenna is not quite as good with a reflection coefficient of only -9dB compared to the -11dB obtained with the thermoplastic ink. This, like before, is due to the low thickness of the antenna (2.1μm) when compared to its estimated skin depth (2.03μm).

10.2.2 Gain Measurements

The predicted radiation pattern for the antenna design (Figure 10:7) on an infinite ground plane in both the E-plane and orthogonal H-plane are given in Figure 10:13 and Figure 10:14. The figures show that the antenna is more directive in the H-plane perpendicular to the antenna (where the angle, $\theta = 0$). As expected the antenna is designed so that the majority of the signal radiates in the polarised component of the field.

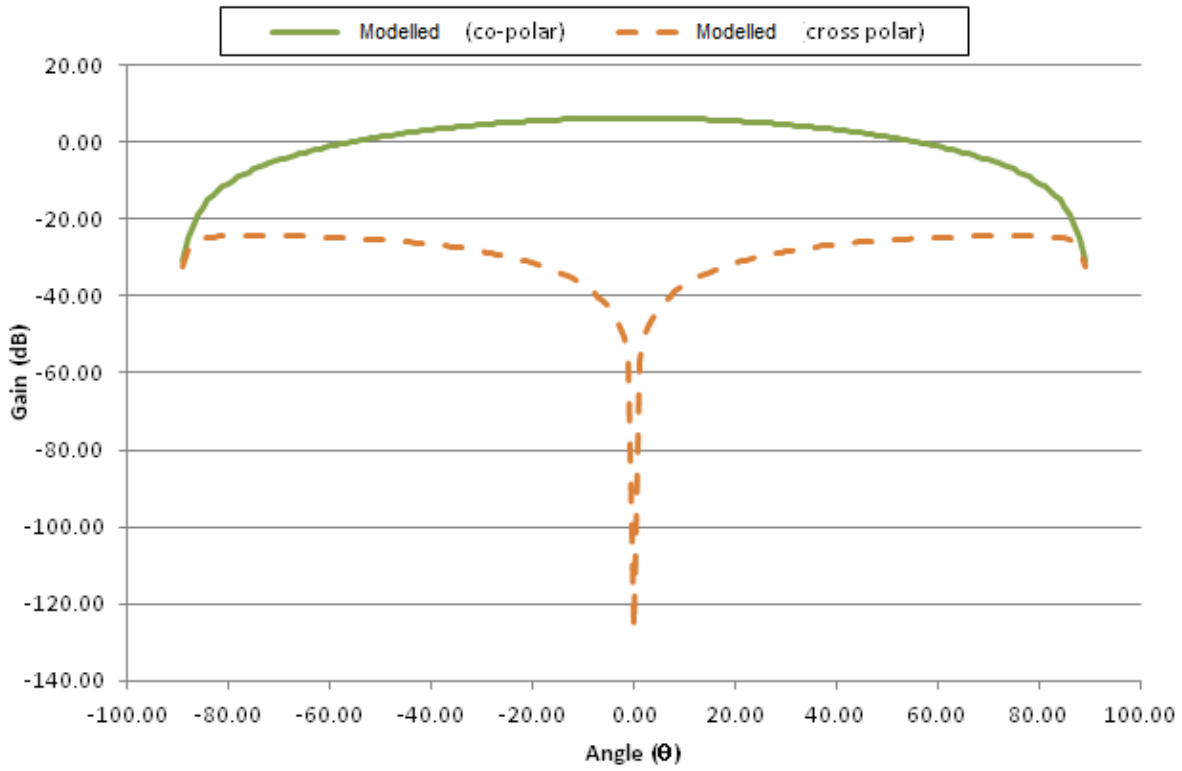

Figure 10:13: Predicted radiation pattern for DW patch antenna in the H-plane

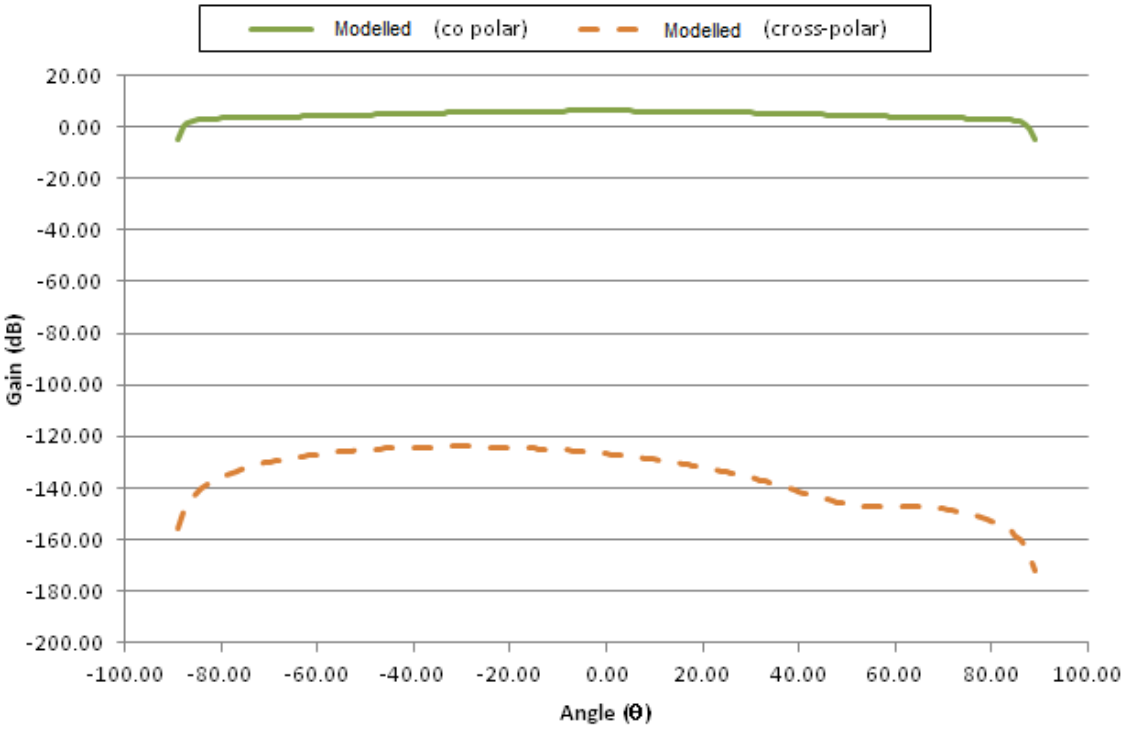

Figure 10:14: Predicted radiation pattern for DW patch antenna in the E-plane

To measure the radiation patterns from the DW patch antennas they were placed in an anechoic chamber. The Antenna Under Test (AUT) was connected to a Anristu 37397C VNA and acted as a receiver for the reference antenna. The reference antenna used for this measurement was a Flann dual polarised Horn. The AUT was placed on to a motion stage to allow for horizontal and rotational movement so that the respective eclectic and magnetic field vectors could be measured as a function of angle with respect to the reference antenna. All measurements were made at the antennas respective resonant frequency (e.g. 1500MHz for the thermoplastic patch antenna). A schematic of the antenna setup is shown in Figure 10:15.

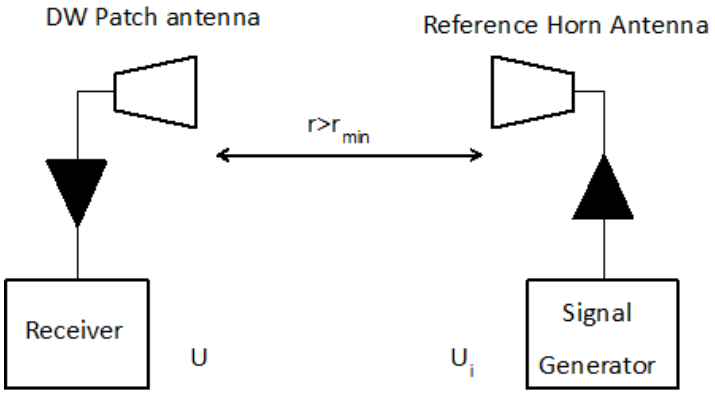

Figure 10:15: Experimental setup used to measure the radiation pattern of the DW patch antennas

To extend the ground plane of the DW patch antenna it was connected to a circular conductor approximately 400mm in diameter. Electrically large ground planes produce stable radiation patterns and also lower the environmental sensitivity of the antenna [184]. Although it is useful for this experiment to minimise variations in the radiation pattern, real world antennas do not have large ground planes in order to minimise the size of the antenna.

All antenna gain patterns are shown in Appendix E, in general the radiation patterns between the DW patch antennas show nearly identical shapes in both the H-plane and E-plane. This is not surprising considering the radiation pattern is a function of the antenna shape and design. The patterns are slightly different to the predicted antenna pattern in that at θ=0 there is a slight dimple or drop in antenna gain. This difference could be caused by the feed line in the DW patch antenna which was printed as a solid line but is designed to be a grid pattern in the design.

The gain of the DW patch are all close to -4dB (within +/- 0.5dB) which is significantly lower than the theoretical value of 6dB. The drop in gain can be caused .l-by losses in the connector through impedance mismatching, high surface resistivities and the poor loss tangent of the FR4 dielectric material. It has also been reported that meshed or gridded antennas can suffer from lower gain (by up to 3dB) which may not be captured in the model [185].

The radiation patterns for the copper plated thermoplastic antenna and copper etched antenna are given in Figure 10:16 and Figure 10:17. The figures show that the co-polar radiation patterns are close approximation to each. The results also show that the cross-polar radiation patterns have a higher gain (-24dB) than the predicted values shown in Figure 10:13 and Figure 10:14. The high cross-polar radiation can also be a by-product of the gridded antenna design; this can be improved by optimising the correct mesh line geometry as described by Clasen, G et al [185].

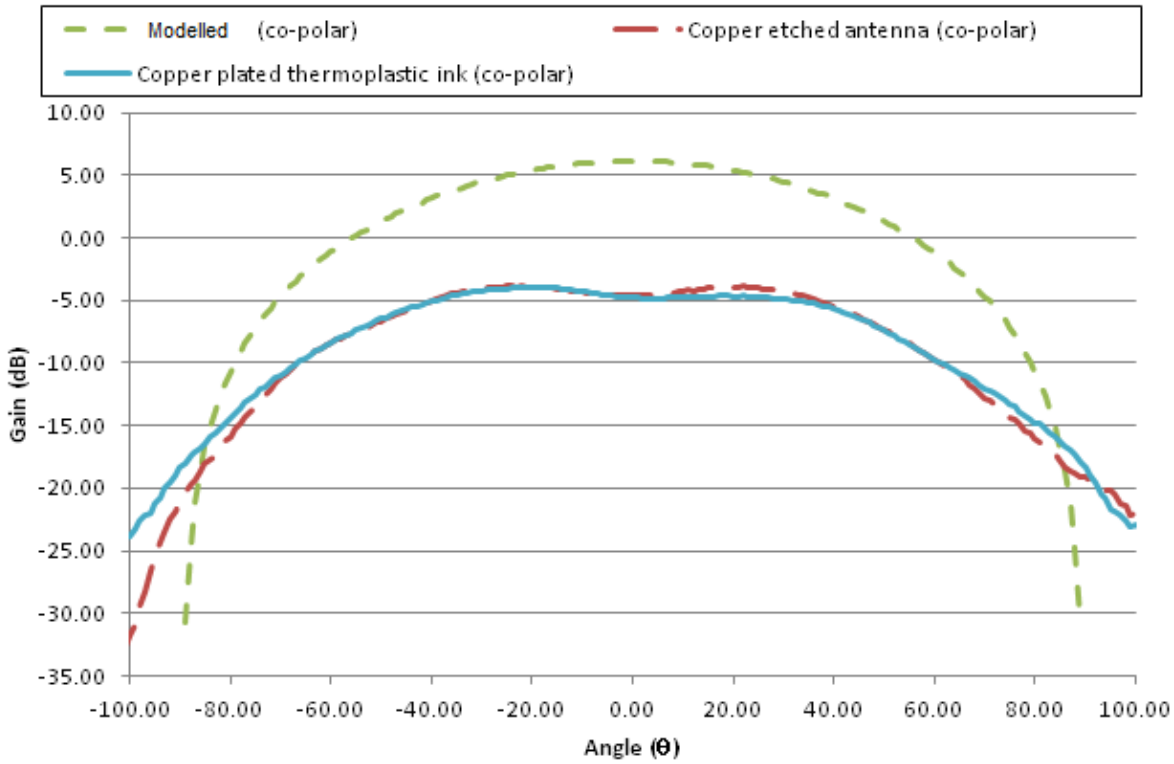

A.

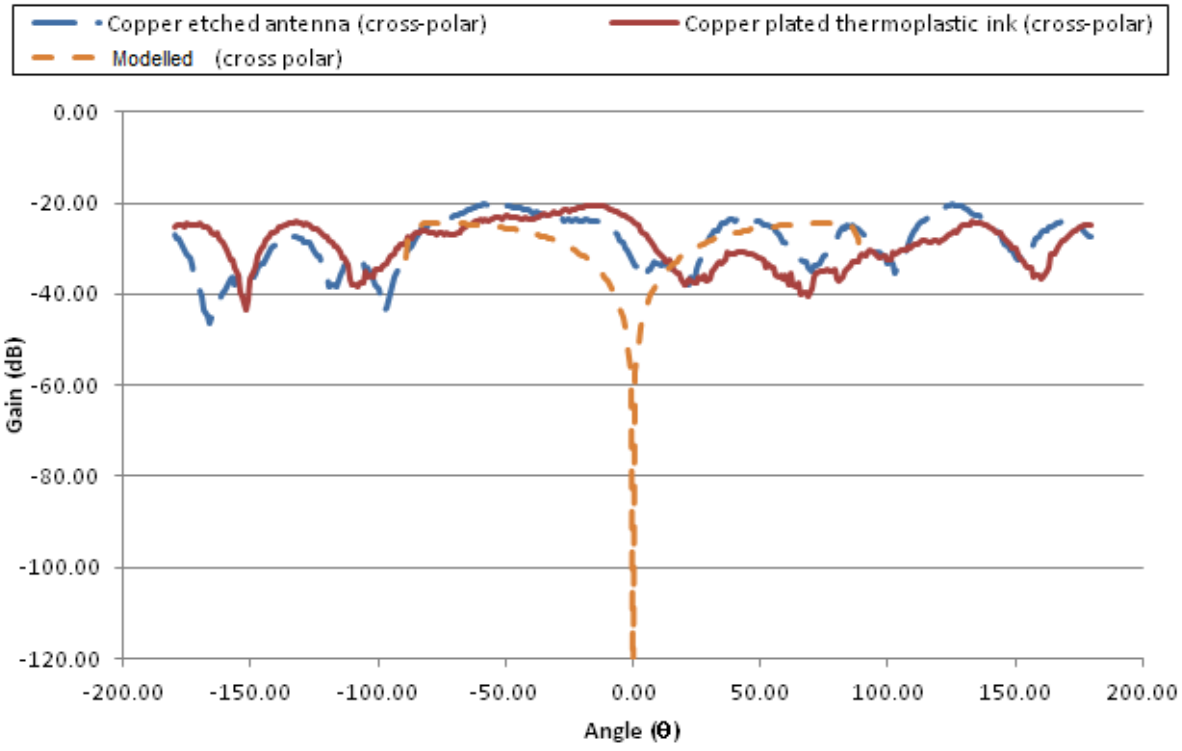

B.

Figure 10:16: A. Co-polar and B. Cross-polar, radiation patterns for copper plated thermoplastic antenna and copper etched antenna in H-plane

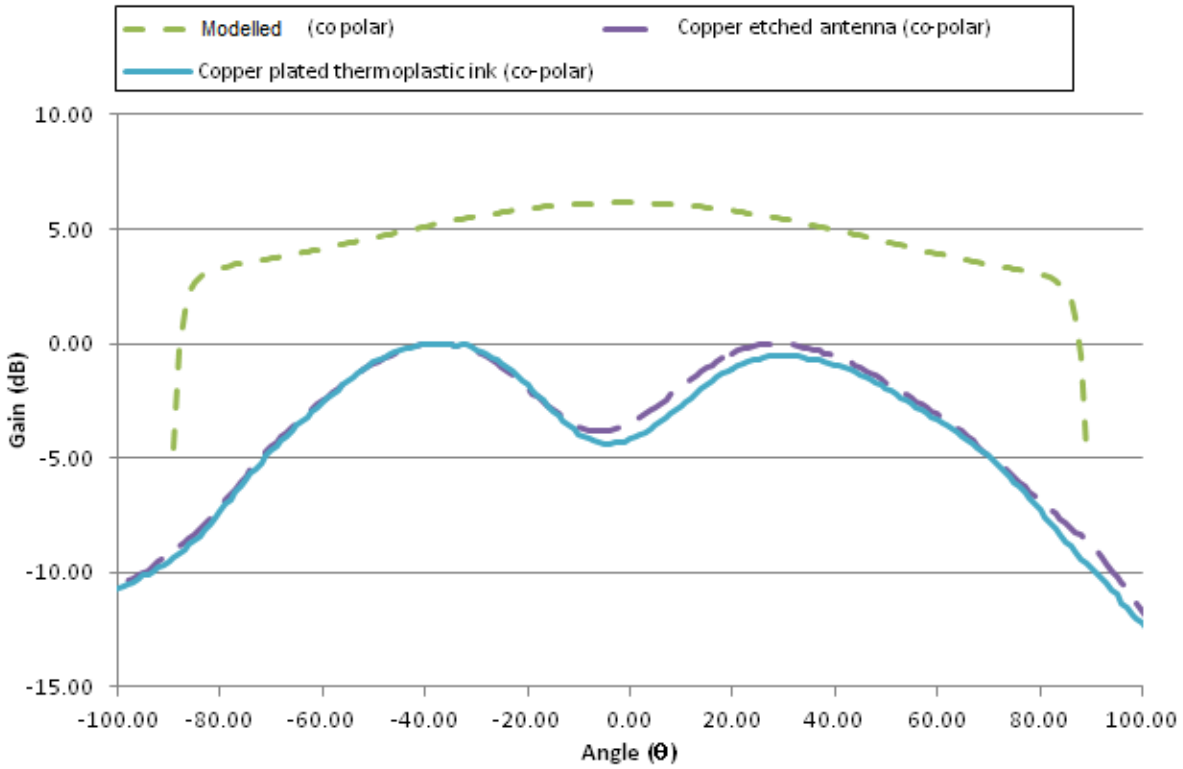

A.

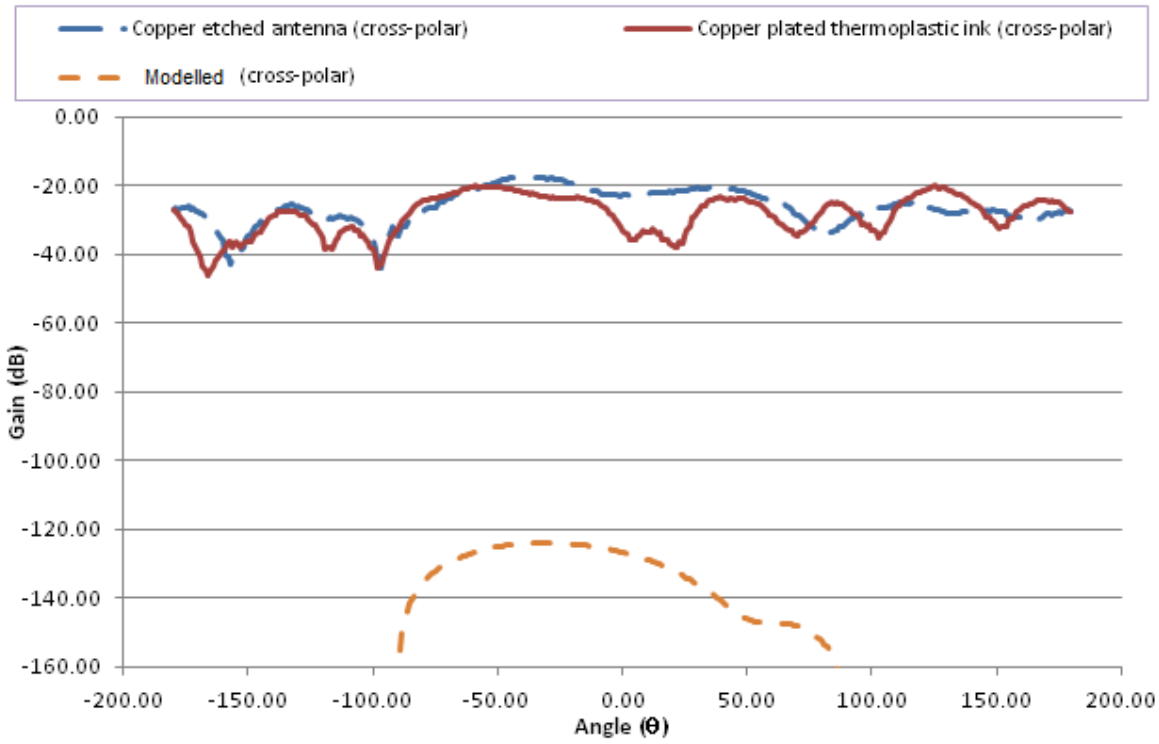

B.

Figure 10:17: A. Co-polar B. Cross-polar, Radiation patterns for copper plated thermoplastic antenna and copper etched antenna in E-plane

10.2.3 Discussion

A patch antenna designed to operate at a GPS frequency of 1.575GHz was fabricated using the DW micro-nozzle and inkjet techniques. The return loss and radiation patterns of the DW antenna were measured and benchmarked against a copper etched antenna using the same FR4 dielectric material.

The return loss showed that the conductivity of the DW ink material could have a large influence on the amount of power that could be radiated by the antenna. Significantly, whilst the return loss for the DW inks was lower than the benchmark copper etched antenna, copper plating of the DW inks showed a marked improvement. It was shown that localised copper plating of the thermoplastic ink results in a return loss near identical to the copper etched antenna.

From the co-polar radiation patterns it was found that the gain that could be achieved with the copper plated thermoplastic ink was close to the copper etched antenna. Relatively high gains were also observed in the cross-polar radiation patterns. This could be a by-product of the gridded antenna design rather than the ink material itself.

10.3 DW Dielectric Considerations

So far the majority of this investigation has concentrated on the development of DW conductor materials for the fabrication of micro-strip antenna structures. For the measurements so far a pre-fabricated dielectric has been used. To realise the full benefits of the DW approach it is important to be able to fabricate both the conductor and dielectric using the same technique. As shown in Chapter 3, the quality and thickness of the dielectric material is important as it affects the loss in the antenna and transmission line as well as the bandwidth of the antenna. The key considerations for the dielectric are:

- Dielectric constant (ε_r)
- Low dielectric loss tangent (tan δ_d< 0.005 for frequencies greater than 1GHz [100])
- High dielectric thickness ($h>\lambda/1000$ [87])
- Low surface roughness ($R_a>\delta_z$ [72])

The dielectric constant has a number of effects on the construction of the antenna. A high dielectric constant will increase the quality factor, Q, of the antenna essentially reducing its electrical size. This can be particularly advantageous if space is an issue but comes at a cost to both the antenna

bandwidth and antenna gain [186]. The bandwidth can be increased by using lower dielectric constant materials and increasing the thickness of the of the antenna substrate. A high dielectric constant will also increase the dissipation losses in the micro-strip feed line to the antenna.

For the majority of DW inks applications inks with relative permittivity (high dielectric constant) have been mainly used. These inks are more suited to the electronics industry (for increased capacitance) but are not desirable for antenna fabrication. More recently thick film pastes made from liquid polyimide have been made available [74] [187], polyimide has a low dielectric constant 3.5k but still a relatively high loss tangent of 0.02 [188]. In this experiment the liquid polyimde was printed with a thickness of 150μm using the N-Scrypt micro-nozzle system [74], however, larger print thicknesses have so far not been demonstrated. If we consider a microstrip patch antenna operating at a GPS frequency of 1.575GHz then the minimum recommended thickness for operation is a 190μm. To increase the bandwidth and efficiency of the antenna and microstrip line thicknesses of greater than 1mm are required (see Chapter Three). In a paper produced by Das, Rabindra N. et al. low k discusses the use of Fluoropolymers, fluorinated polyimides, polyimide-silica hybrid and bismaleimide-triazine in combination with epoxies to form pintable low loss and low dielectric constant materials [189]. However, to knowledge of this author these types of inks are not yet commercially available.

Figure 10:18 (A) shows a thermosetting Commercial off The Shelf (COTS) [129] dielectric ink printed as a single 100μm layer before being oven cured at 130°C for 30mins. After curing the ink layer undergoes significant deformation leading to an uneven layer. This affect is similar to the observations made when laser or locally curing the ink samples where solvent entrapment was causing the printed layer to form blisters.

Figure 10:18 (B) shows an alternative method of building up the dielectric height by printing in three successive 40μm layers, each layer being cured between successive prints. As can be seen the ink deposit has much less distortion or blisters, however, there are still a number of small bubbles and air gaps present in the surface of the layer. When adding more layers, the dielectric eventually starts to deform again, is it thought that apart from solvent entrapment this could be due to changes in the physical properties of the underlying layers as they go through the glass-transition temperature (as T_g < curing temperature).

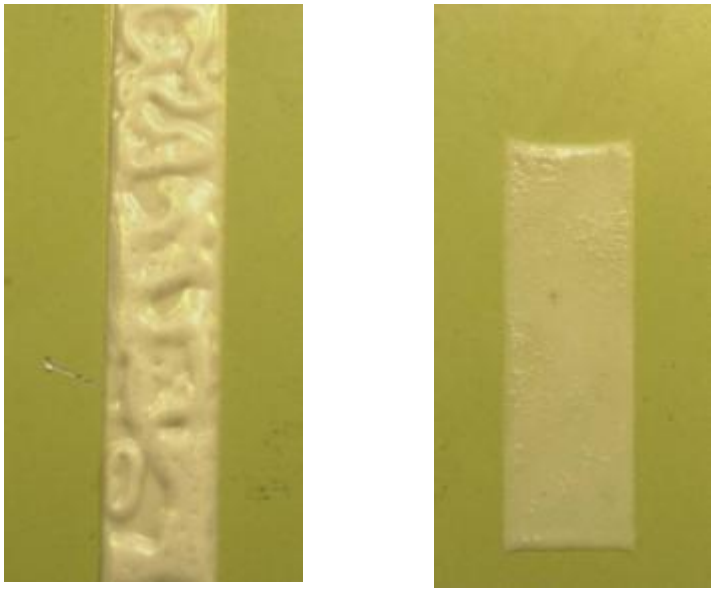

A B

Figure 10:18: DW dielectric layering A. Single 100mm layer B. Three 40mm layers

To test the viability of commercial-off-the-shelf (COTS) DW dielectric ink [129] for RF applications a 100mm micro-strip line was fabricated. To construct the micro-strip line the DW dielectric was printed on to a primed Aluminium substrate which acted as both a support structure for the DW inks and as a ground plane. A hole was drilled in either end of the substrate so that an SMA connector could be fed through for connection to a VNA. Before printing the SMA was positioned in such a way as to protrude through the top surface of the substrate. The clearance between the SMA connector and the substrate was dependant on the projected thickness of the dielectric. Once the dielectric was deposited and cured a DW conductor was printed on to the top surface making sure to make contact with the copper contact on the SMA connector. Figure 10:19 shows a schematic of how the DW micro-strip line was constructed.

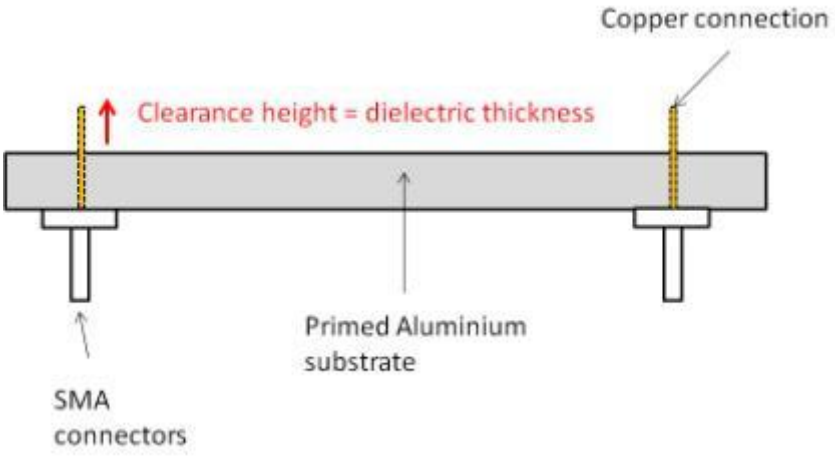

Before Application of DW inks

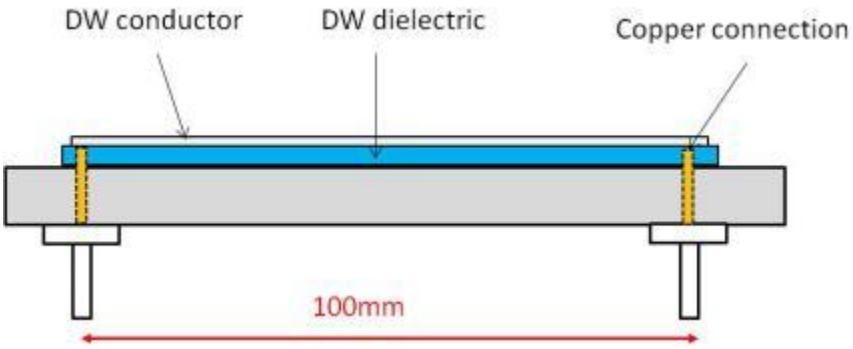

After application of DW inks

Figure 10:19: Fabrication of a 100mm long micro-trip line using DW dielectric and conductive inks

The dielectric was printed on to the aluminium substrate with a width of approximately 8mm and a length of approximately 95mm (to allow the conductive ink to make contact with the SMA). The dielectric height was varied so that different thicknesses could be investigated. The dielectric thickness was increased by printing and curing successive 40μm layers. It was found that the upper limit for the dielectric thickness before large air gaps and bubbles started to form was 340μm. The COTS dielectric ink was estimated to have a dielectric constant of approximately 30k although this was not confirmed experimentally. A further dielectric ink was also acquired later in the project with an estimated dielectric constant of 12k [129] although due to time considerations this was only tested at one dielectric thickness. The thermosetting PTF silver ink was used as the micro-strip conductor material. This was printed as a single (40μm thick) line with a length of 100mm. The optimum width (to match the impedance of the line at 50Ω) of the conductor micro-strip line depends on the thickness of the dielectric, the dielectric constant and the frequency of operation. For low dielectric thicknesses (at 100μm) the width of the conductor track may need to be as narrow as 20 to 30μm which is difficult to achieve accurately using the tape cast print method with the PTF inks. As a number of these parameters will be variable during this investigation it was decided to try

and keep the width of the conductor constant at 100μm (this was nominally achieved between +/-20μm). Although this will add some error in the measurements due to impedance mismatching it allows a consistent print to be achieved with the conductor material. Figure 10:20 shows the complete DW micro-strip line.

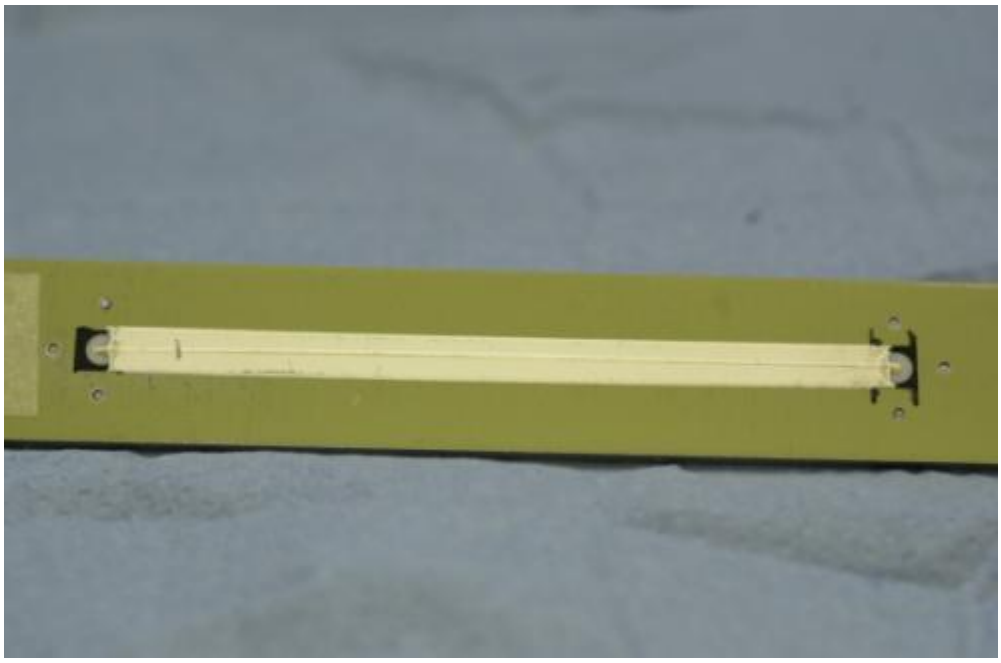

Figure 10:20: Example DW micro-strip line with printed dielectric and conductor inks on to a primed Aluminium substrate

The transmission line loss for the DW micro-strip line is shown in Figure 10:20. When making the measurements there seemed to be fluctuations in the line loss adding an error of approximately 0.5dB to the results. It was found that the main reason for this was poor connection at the interface between the DW silver ink and the copper contact on the SMA connector. As expected the measurements show that the line loss reduces as the dielectric thickness increases. It can also be seen that the line loss of the lower (ε_r=12) dielectric printed at 120μm thickness is lower than the loss of the 30k dielectric at 340μm.

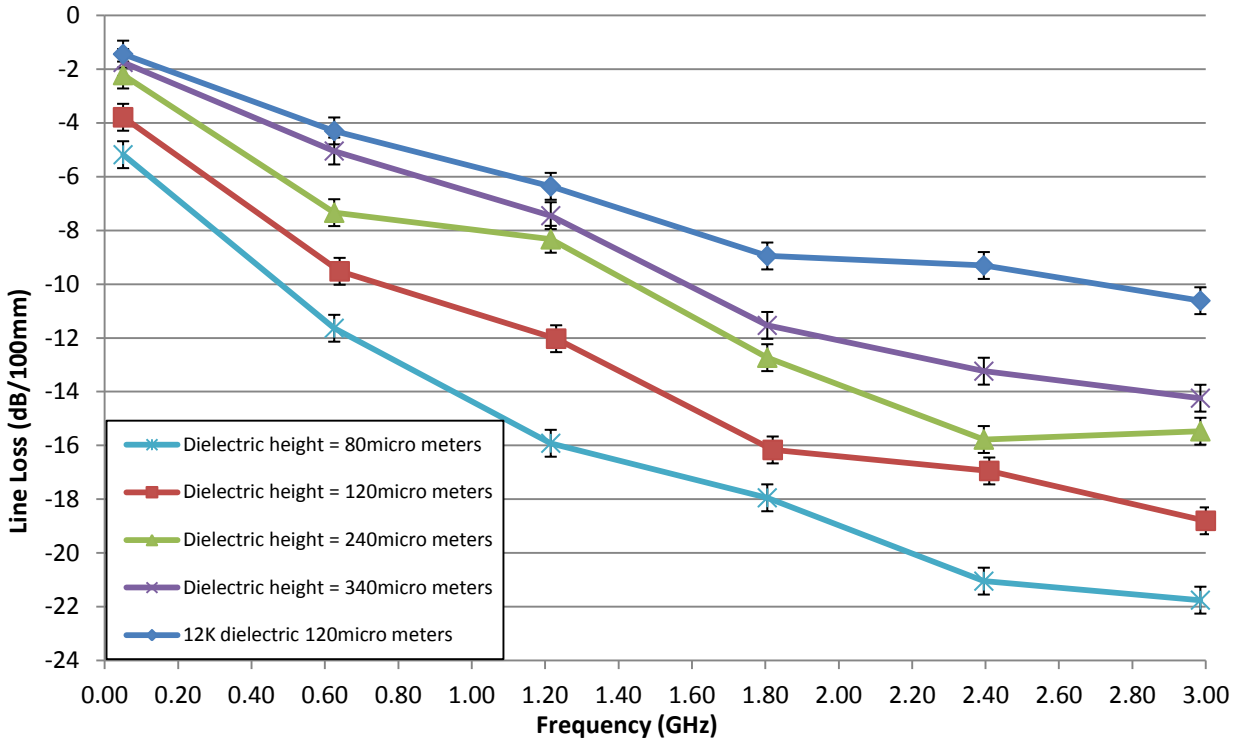

Figure 10:21: Frequency against line loss for a 100mm microstrip line for different DW dielectric thicknesses.

To estimate the loss tangent for the DW dielectric inks the line loss was modelled in TXLINE software [98] and compared to the measured values in Figure 10:21. The following parameters were used in TXLINE:

- Conductivity: 12280 S/cm (2% bulk conductivity of silver)
- Conductor thickness: 40μm
- Conductor thickness: 100μm
- Line length: 100mm
- Dielectric constant: ε_r = 30 and ε_r = 12

Using an iterative method it was found that the closest match between the software model and the measured values occurred when dielectrics were measured with a loss tangent of 0.1 and 0.08 for the higher (ε_r=30) and lower (ε_r=12) dielectric materials respectively. The comparison between the model and the measured values are shown in Figure 10:22.

The predicted loss tangent of the DW dielectrics are high compared to the FR4 substrate which has a loss tangent of 0.014 and higher still then microwave dielectrics such as Duroid which has a loss tangent of 0.0012 [99].

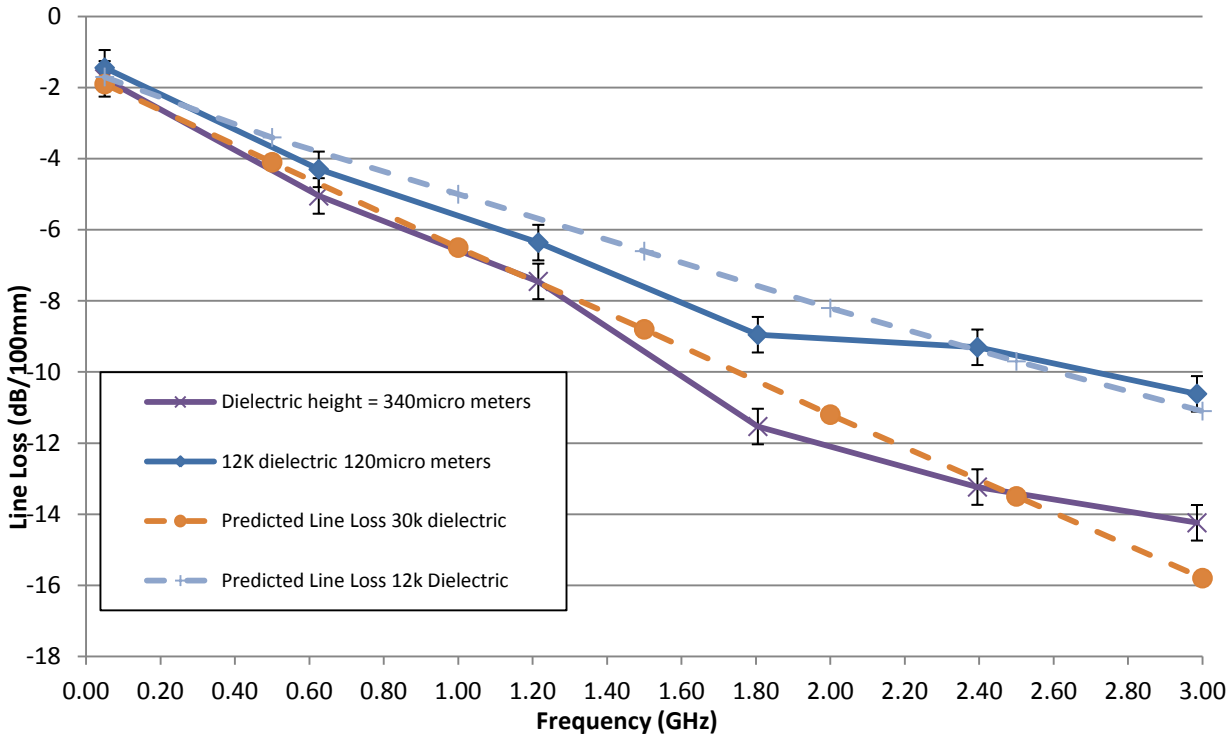

Figure 10:22: Modelled line loss against measured line loss for DW inks

10.3.1 Discussion

The PTF DW dielectric inks investigated in this study are primarily designed as insulating ink for electronics applications. These inks therefore have high dielectric constants and are designed to be printed in thin layers. An assessment of these inks for RF applications was made by fabricating a micro-strip line for testing using a VNA. When fabricating the micro-strip line it was found that the maximum thickness that could be achieved was 340µm before the ink started to deform under thermal stresses and solvent entrapment. From the resulting S21 measurements it was found that the dielectrics exhibited high losses but this could be reduced by increasing the thickness of the layer and by using a dielectric with a lower permittivity. By comparing the measurements with losses predicted on TXLINE software it was found that the 30 and 12 dielectric had a loss tangent of approximately 0.1 and 0.08 respectively. These loss tangents are much higher than those that would be used in RF applications.

It can be concluded that dielectric PTF inks require a number of improvements before they can be used in the fabrication of RF devices especially at frequencies above 1GHz. Suggested improvements include:

- Using lower boiling point solvents to enable larger layer thicknesses to be printed

- Increasing glass transition temperatures so that multiple layers can be printed to build up the dielectric thickness.
- Decreasing the dielectric constant using appropriate fillers
- Decreasing the dielectric loss tangent

10.4 ASTREA Demonstrator

The ASTRAEA (Autonomous Systems Technology Related Airborne Evaluation and Assessment) project is a major £32m program to open up opportunities for the civil use of UAVs by allowing their routine use in segregated and non segregated airspace [190]. This complements work in the military use of UAVs. The consortium of partners in this project includes Agent Oriented Software, BAE Systems, EADS, Flight Refuelling, QinetiQ, Rolls-Royce and Thales UK, renowned research and academic bodies and specialist Small to Medium Enterprises (SMEs).

BAE Systems were contracted to help build and test fly a UAV based on the HERTI design (Figure 10:23) within the first year of this program. This led to a unique opportunity within the business as a whole to test fly additional technologies not directly related to the ASTRAEA program but potentially important to civil/military aircraft programs. One of the technologies earmarked for this was DW specifically for its capability to fabricate conformal antenna device on to 3D structures.

The main aims of this project were to demonstrate the concept of fabricating a DW antenna on to the leading edge of a carbon fibre UAV wing. The UAV aircraft is based on the HERTI design which is pictured in Figure 10:23.

Figure 10:23: HERTI Aircraft (images taken from The A Register [191])

The UAV was originally scheduled to undergo flight trials in October 2008, however, due to delays in the flight programme and subsequent prioritisation of technology demonstrations, it was not possible to fly the printed DW antenna. To continue the development of the technology decision was made to print the antenna on a non flying section of the HERTI aircraft wing. Furthermore, this was a Glass-Reinforced Plastic (GRP) HERTI wing section instead of the originally planned carbon fibre wing. The modified objectives of this program were to:

- Demonstrate Conformal writing capability: Printing on to leading edge of the wing
- Demonstrate a Localized curing approach: DW processing within the tolerances of a carbon fibre substrate surface.
- Use Commercial of the Shelf (COTS) inks to fabricate an antenna as a first trial benchmark
- To develop and understand the requirements for DW antenna fabrication
- Consider how such an application could be integrated into the aircraft manufacturing steps

To meet these objectives an antenna was designed to operate at a nominal frequency band, 2.4 GHz, which is commonly used for public wireless comms and therefore no additional license was needed. The antenna was fabricated on to the leading edge of the HERTI wing. This location gives the chance to demonstrate the conformal printing capabilities of DW technology on the most 'curved' section of the wing, however, it also imposes a strict aerodynamic requirement which limits the maximum profile of the DW coating on the surface to 200μm.

10.4.1 ASTREA Demonstrator Setup

In order to fabricate the antenna on the GRP wing a number of processing adjustments had to be made to the original 3-axis DW system. The first adjustment required an alteration to the motion control stages to accommodate the wing section. In addition to this a method of locally heat treating/curing the DW material was necessary. This requirement stems from the size of the wing (which is too large for conventional oven curing) and the temperature limitation on the GRP/carbon fibre wing. For carbon fibre, the upper operating temperature limit is 90^{o}C [192]. As most micro-nozzle DW inks cure at temperatures above this limit (90-200^{o}C) a method of restricting heat penetration into the components is necessary.

Two curing methods were chosen to fabricate the antenna. The first consisted of a thermally insulating housing used to hold a heat gun in close proximity to the GRP wing. The housing was designed so that airflow coming in through the top of the structure can flow over the surface of the

wing and out through the exit vent. The whole structure was fabricated using Accura Duraform Polyimide material by Airbus using their Selective Laser Sintering (SLS) technology, an illustration of this housing is shown in Figure 10:24.

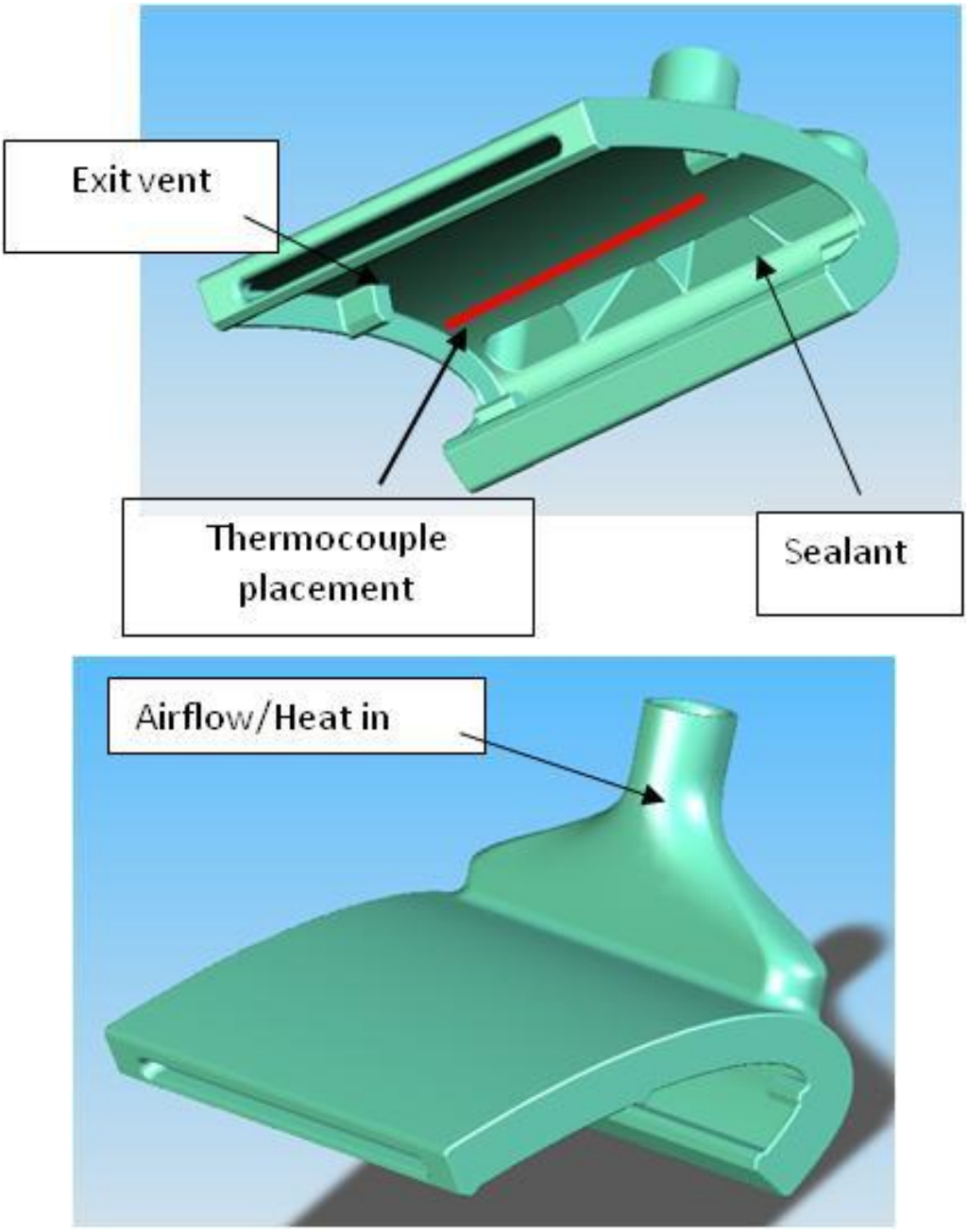

Figure 10:24: Housing produced by Airbus UK to confine the convection current generated by two heat guns placed in close proximity to the GRP wing.

By selecting the most appropriate settings on the heat gun a steady convection current could be generated within the housing leading to a relatively even distribution of heat over the surface. To monitor the temperature distribution across the housing a number of thermocouples were placed

across the surface and the temperature was logged against time by a National Instruments PX-1011 data logger.

The convection curing method detailed above allows a large area to be cured relatively quickly but is only suitable for low temperature curing materials. This method was used to cure the 30k dielectric (from section 9.3) as it is able to solidify at temperature as low as 80°C if long curing times (approximately 2hours) and thin print layers (40µm) are used. For conductive DW inks however, the processing temperatures required to generate low print resistances is much higher, usually between 120-200°C. The PTF silver ink, for example, requires a cure of at least 130°C for 20mins in a conventional oven. To process this ink an 808nm fibre delivered laser diode was used. This method was chosen following successful curing trials shown in Chapter 8. To cure the silver ink a laser power of 3W was used with a traverse speed of 1mms^{-1}, the spot size of the laser was approximately 450µm. The DW system setup with the wing section and the integrated laser head is shown in Figure 10:25.

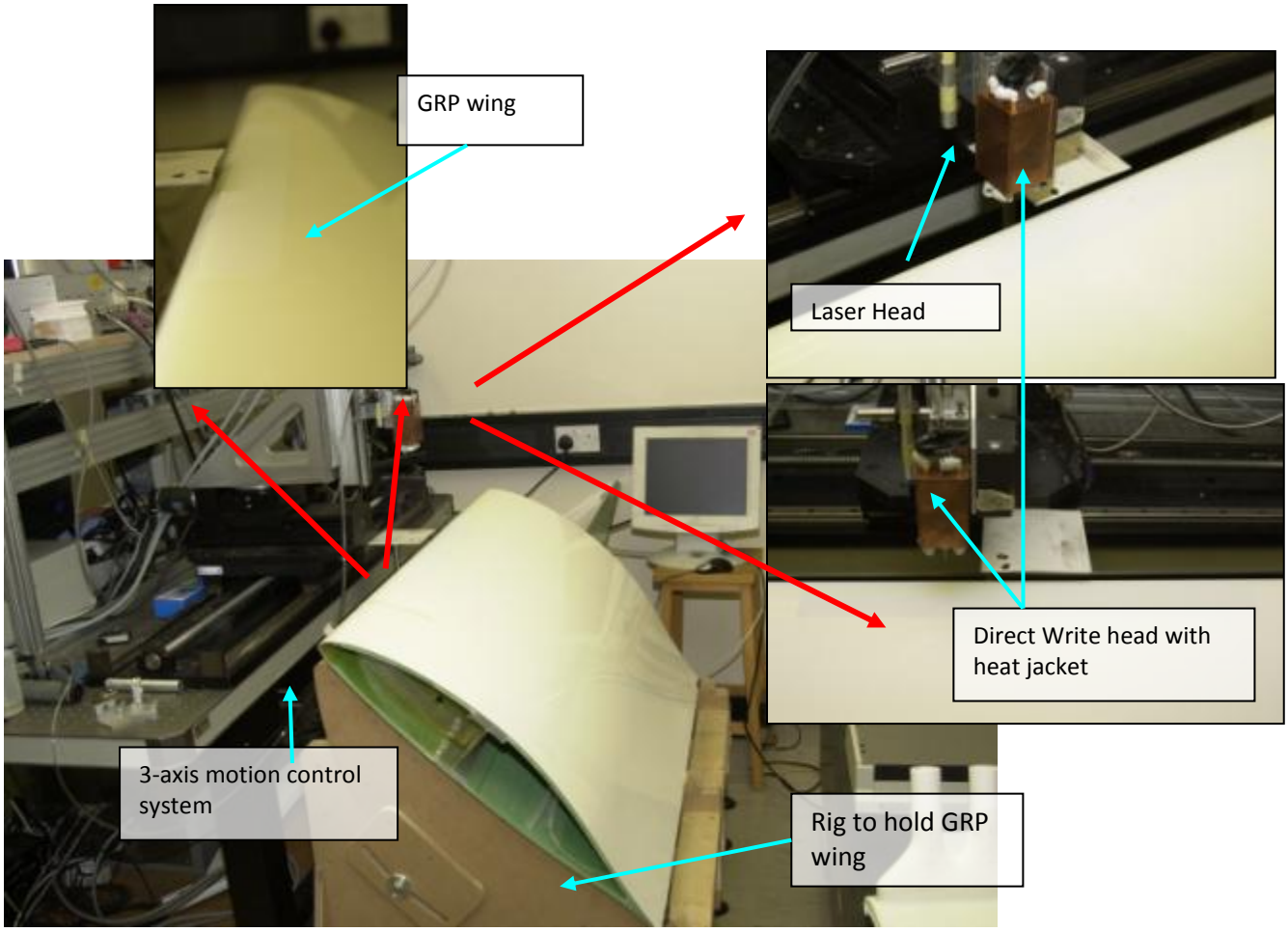

Figure 10:25: DW setup for ASTRAEA demonstrator

The system setup includes the DW micro-nozzle head and laser diode attached to a 3-axis gantry system. A fit-for-purpose heating jacket was also used with the micro-nozzle system to maintain an ink temperature of 28°C. This was used to maintain consistent rheological properties during printing (see Chapter 6). When attached to the 3-axis gantry the micro-nozzle system is able to print across curvatures ranging from +/- 10°. To accommodate this limitation the GRP wing was mounted in such a way as to allow the antenna to be printed across the leading edge of the wing.

10.4.2 ASTRAEA Antenna Printing

The ASTREA DW antenna was designed to operate over a curved surface at 2.4GHz by Richard Orton at the Advanced Technology Centre, BAE Systems, in Great Baddow. The Design is shown in Figure 10:26.

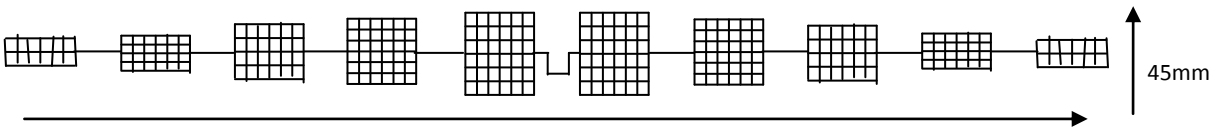

2.4GHz antenna design

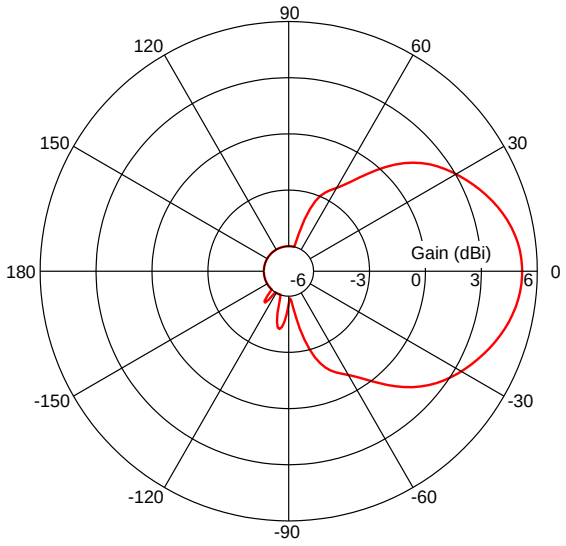

Gain pattern as modelled over the leading edge of the GRP wing

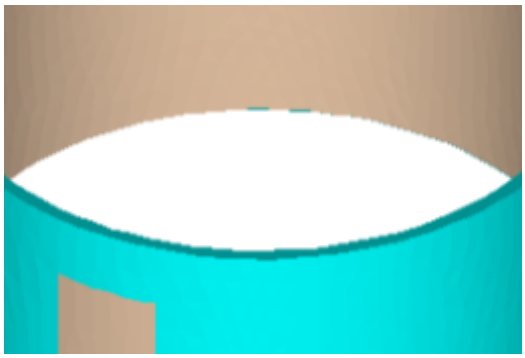

13° curvature over which antenna gain was modelled

Figure 10:26: Antenna design. Available gain coverage +/- 40^{o} from boresight (pointing normal to the antenna surface) modelled on a cylinder with equivalent radius of curvature to the leading edge of the HERTI wing (13^{0} radius of curvature)

The micro-nozzle printed antenna on the HERTI GRP wing is shown in Figure 10:27. The demonstrator proves the concept of being able to use DW technology in combination with localised curing methods to fabricate an antenna on to the leading edge of a wing without compromising the flightworthiness of the aircraft. As discussed in this chapter there are still a number of developments which are required before a DW antenna could be deemed suitable for operation, particularly for DW dielectric materials.

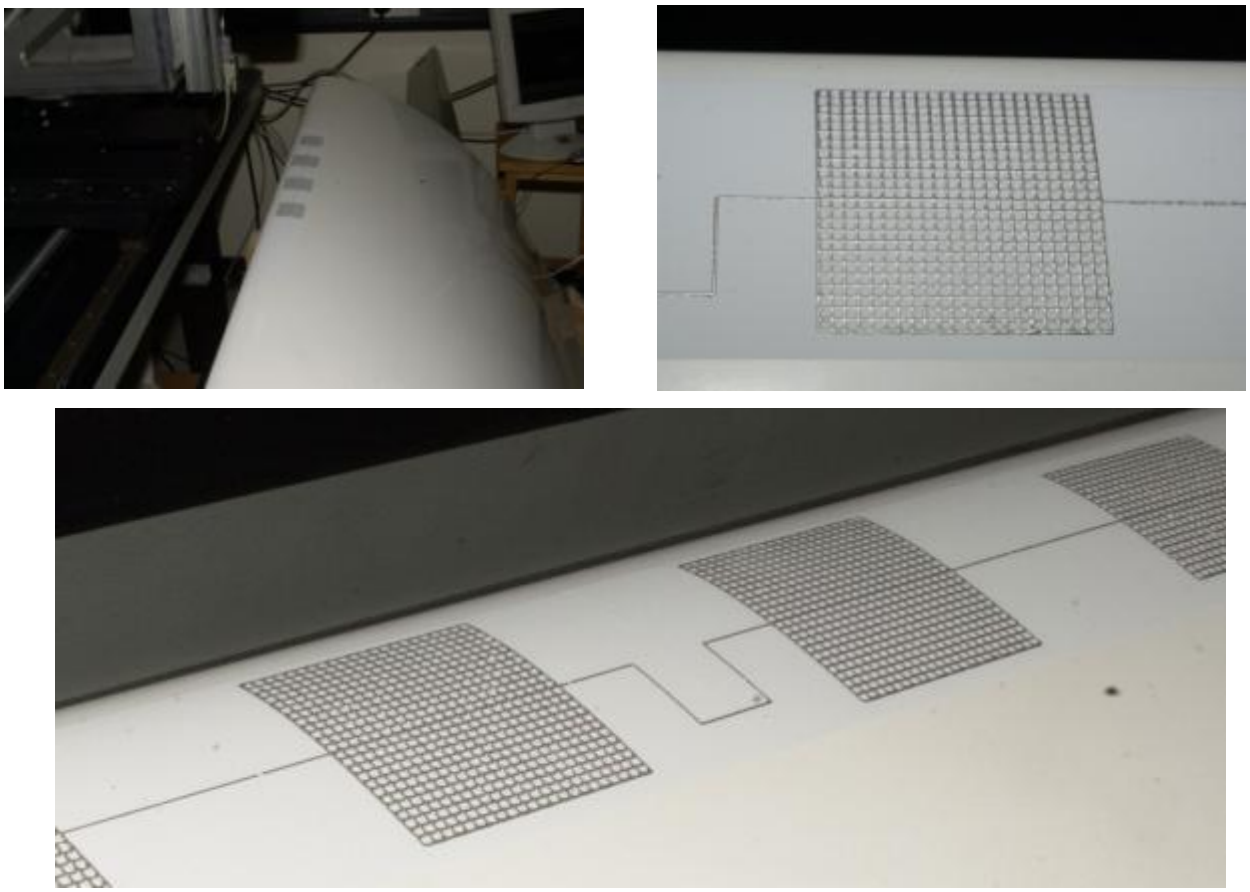

Figure 10:27: Micro-nozzle printed laser cured antenna on to a GRP wing section

10.5 Conclusion

This chapter builds on previous work which has investigated DW process such as inkjet [15] [193], thermal spray [72] and micro-nozzle printing [83] [75] for the fabrication of RF devices. To enable DW to be used for the fabrication these devices on to aerospace components a number of developments have made in both broadband curing (to enable the inks to be cured on large structures) and localised electroplating (to reduce RF losses). Past experiments have shown that copper plating of inkjet inks using electroless plating is a viable method in reducing RF losses [73], however, this process is not particularly applicable for fabricating devices on to large structural components.

The results showed that that the localised electroplating method increased the conductivity of the PTF and inkjet inks sufficiently so that transmission line losses become equivalent to those obtained by an equivalent bulk copper line. Furthermore, broadband curing allowed the inks to be cured without affecting the dielectric properties of the FR4 material. Similarly, the return loss of the DW patch antennas also improved after copper plating. It was found that localised copper plating of the thermoplastic ink resulted in a return loss and gain pattern near identical to the copper etched antenna.

This study has found that whilst DW conductive inks could be used for antenna applications through process optimisation and localised electroplating the same could not be applied to COTS DW dielectric inks. For patch antenna applications relatively large dielectric thicknesses are required with low dielectric constants and loss tangents. This immediately rules out inkjet printing which is suited to very low print thicknesses. Current PTF dielectric inks are currently designed to printed in a single coating (40-80μm) and have high dielectric constants. By printing and curing these dielectrics in successive layers it was found the thickness could be increased to 340μm. Even at this print thickness it was found the transmission line loss was significantly high. Furthermore through comparison with predicted models it was found that the loss tangent of these dielectrics was a factor of a 100 higher than conventional microwave dielectrics such as Duroid and factor of 10 higher FR4 which is considered a to be poor microwave dielectrics.

11 Conclusions and Recommendations

This final chapter presents a summary of the main results achieved by the research described in this thesis, and lists the principal conclusions that can drawn from the work. It provides a synopsis of the main contributions made to scientific and technological knowledge in the subject area, as well as an evaluation of the work and a review of the limitations and problems encountered. This is followed by a section offering suggestions for further research in this area

11.1 Summary of work

This thesis has identified DW as a suitable manufacturing technique for the fabrication of conformal, low profile antennas on to large aerospace structures. Previous studies have also investigated DW ink processes for antenna and RF fabrication using PTF inks [75], inkjet inks [73] [180] and thermal spray techniques [72]. From the background literature it was found that there were three main areas which require development if DW is to be used for antenna fabrication for aerospace and military applications:

- Characterisation of DW material for environmental durability
- Improvement in localised curing methods particularly on temperature sensitive materials
- Optimisation of DW material properties for antenna fabrication

In this thesis two different print processes have been investigated for antenna fabrication, micro-nozzle and inkjet systems. These systems can be easily integrated with CAD/CAM controlled robotics for conformal deposition and can deposit a variety of material types including dielectric and conductive materials. In Chapter 6 a number of conductive inks used in these processes were characterised for adhesion, electrical conductivity and durability. It was found from this analysis that the thermosetting and thermoplastic silver PTF inks used in micro-nozzle printing had relatively high adhesion but very poor electrical conductivity which is similar to past literature published on these inks [16] [27]. The functional properties of these inks could be improved by increasing cure temperatures although conductivities were still much lower than the required values for antenna fabrication. The conductivities of PTF inks have been investigated extensively in the past [16] [27] but there is very little data on the environmental durability of these inks. An assessment of the durability of the thermosetting PTF ink in a number of different environments was therefore performed. It was found that whilst these inks were resistant to high and low temperatures,

humidity and highly corrosive environments, the inks degraded significantly when immersed in skydrol fluid. The exact reasons for this were unknown but it may be that DW devices require additional coatings to protect them from these environments. Inkjet inks on the other hand had higher conductivities than the PTF inks but exhibited poorer adhesion on substrates with low surface roughness. This observation again ties up with previous literature on the subject [73] [57]. At very high processing temperatures the conductivity of inkjet inks could be improved much further than the DW PTF inks as they are not restricted by a polymer resin matrix. The downside to higher processing temperatures is that it can restrict the applications (the types of substrate materials) the ink can be used for. A hybrid PTF silver and nano-particle ink was also investigated in this chapter, unfortunately the small increase in conductivity was offset by poor interlayer adhesion rendering this ink less useful.

To improve the conductivity of the DW inks for antenna applications electroplating was investigated. Electroplating of inkjet DW seed layers has been considered before using electroless plating techniques [73], however, this technique requires the use of very aggressive chemicals and a chemical bath which is not suitable when processing on large structures. To overcome this, a novel brush plating tool was used to locally copper plate both PTF and inkjet ink seed layers. Whilst the process demonstrated in this thesis was relatively slow, requiring multiple scans to build up a uniform copper layer on the surface of the DW seeds layers, the results showed that copper with conductivities of approximately 66% bulk copper on the silver inkjet inks and 56.6% on the thermoplastic silver ink could be plated. These values were higher than the 50% bulk copper conductivities that were reported when electroless plating inkjet inks [155] [73]. From the results it seemed the efficiency of the brush plating tool was a function of the surface area of silver that was available to plate on, for the PTF inks this was limited by the polymer resin. It was predicted that the plating efficiency of the inkjet ink could be increased further by removing or reducing the ‘coffee staining’ effect (by heating the substrate [60]) which causes silver to migrate to edge of the printed track (which again reduced the effective surface area that could be electroplated on).

Localised heat treatment of the DW inks was also investigated in Chapter 8 and Chapter 9. Localised heat treatment is necessary when fabricating DW inks on to large structures where conventional oven processing is not suitable. Previous literature has presented the successful application of lasers to process DW materials as an alternative to conventional oven treatment [68] [70]. However, spectral analysis of DW PTF inks show that silver inks are particularly reflective at IR wavelengths but absorb irradiation at UV wavelengths whereas the resin binder and dielectric inks have multiple

absorption bands. This suggests these inks could be more suited to curing using a broadband source. To investigate this, conductive inks were processed with a diode laser and a fibre delivered broadband thermal spot curing system for comparison. Results showed that PTF and inkjet ink resistances equivalent to high temperature oven cured samples could be achieved at lower energy densities with the broadband system than the laser diode system. Broadband curing is particularly advantageous for curing inks that may have low thermal conductivity but have particularly well defined absorption bands (e.g. dielectric inks). One of the problems with localised heat treatment is that the high temperatures can cause blistering of the ink and high surface roughness. One of the reasons for this could be the fast evaporation of low boiling point solvents within the ink composition. Using pre-heating methods it was found that surface roughness could be reduced significantly, for some inks such as the thermoplastic PTF ink this be done easily by using low temperature drying. Inkjet inks on the other hand have much higher boiling point solvents which need removing before the silver nano-particles can be sintered. Once this is achieved track resistances of approximately 60% bulk silver can be achieved although adhesion of these deposits was known to be an issue.

One of the potential advantages of localised curing is the reduced heat input into the substrate material. This would allow inks to be cured on temperature sensitive materials. To determine the penetration depth from the broadband white light source a FEM modelling technique was used. This follows on from the work conducted by Kinzel [28] who showed that the heat from a laser source incident on a silver track only penetrated a few microns into an FR4 substrate. To make the results more accurate a method of determining the thermal properties of the ink was used. This method consisted of using FEM modelling with measurements made with thermal imaging camera. From the modelling results it was found that although temperatures from the broadband white light source were high (above the operating temperature of the substrate material) at the surface of the substrate (directly underneath the ink layer) this was restricted to only a small penetration depth (a few 100μm) at very short exposure times (<1s). It is yet to be determined if this is sufficient to cause any significant damage to the composite although cross section micrographs of samples cured with the broadband source revealed no visual damage and line loss measurements of broadband cured transmission lines (in Chapter 10) showed no significant deviation between oven cured samples.

By bringing together the developments made in this thesis the RF properties of PTF and inkjet inks were investigated. As expected line loss measurements from the copper plated ink tracks gave the most promising results with loss measurements similar to those obtained with a copper etched

transmission line. A patch antenna (resonating at a frequency used for GPS comms) was also deposited using both micro-nozzle and inkjet processes. The return loss and gain measurements indicated that the copper plated thermoplastic ink was closest to the copper etched antenna although these results were skewed by the fact the inkjet antenna was fabricated using a different printing system to the one used in previous experiments. This meant the total thickness of the deposit was only ~0.5μm rather than the 6.88μm lines obtained when fabricating the inkjet transmission lines. The calculated skin depth of the inkjet antenna at the resonant frequency of the antenna (1575MHz) was approximately 3.7μm meaning that the conductor height of the inkjet antenna was lower than the skin depth which would have increased conductor losses. Had the print parameters remained consistent for the inkjet antenna and transmission line then this may have given slightly better results than the thermoplastic ink due to the high conductivity of the inkjet ink and increased plating efficiency with the brush plating tool.

Whilst it has been shown that DW conductive inks can be used for antenna applications, through process optimisation and localised electroplating, the same could not be applied to COTS DW dielectric inks. For patch antenna applications relatively large dielectric thicknesses (~mm's) are required with low dielectric constants and loss tangents. Although inkjet printable Polyimide dielectrics (with low dielectric constants) are available [194] [66] they still have high loss tangents and large print thicknesses have not been demonstrated. Current PTF dielectrics inks are currently designed to printed in a single coating and have high dielectric losses. Higher thicknesses are difficult to achieve due to solvent evaporation and thermal stresses causing the ink to deform or blister. Furthermore, experimental measurement of these inks showed that loss tangents could be factor of a 100x higher than conventional microwave dielectrics such as Duroid and factor of 10 higher FR4.

Finally to demonstrate the concept of DW antenna a 2.4GHz comms antenna was designed and printed onto a mock HERTI wing section. This process required printing of a dielectric layer before curing with an air gun and then depositing a conductive antenna pattern before curing with a laser source. The design of the deposition system had to modified in such a way as to accommodate a wing section and if needed be transportable to a different location. One of the areas which did crop up as the antenna was being designed was how to connect this with a signal generator/receiver located within the wing section. This is something that was not explored in detail here but requires investigation in future studies.

11.2 Recommendations & future work

Conformal fabrication of a complete patch antenna is not yet possible using DW methods mainly down to the lack of available COTS off the shelf dielectric inks which have low dielectric permittivity and dielectric loss tangents. However, this thesis has shown that DW printing of conductive elements for RF applications on large temperature sensitive components is possible if a combination of processes is used. These processes are required to print, locally cure/sinter the DW material and optimise the conductivity of the deposit through localised electroplating. This improves on previous studies which have used electroless plating methods to increase the conductivity of inkjet inks [73] .

The results have shown that currently the thermoplastic ink is more suited when used in combination with broadband cutting and localised electroplating. Whilst the inkjet ink had the highest copper plating efficiency the trade off is small (66% compared to 58% with the thermoplastic ink) when considering the high pre drying conditions required to successfully process the inkjet ink with the broadband spot curing system. The inkjet inks would be more suitable for these applications if they were adapted to be more suitable for localised sintering.

One area of comparison that is missing in this investigation is how the thermoplastic and inkjet inks match up to the durability and adhesion offered by the thermosetting PTF silver ink which was characterised in Chapter 5. In addition further characterisation of the environmental durability and adhesion of the electroplated DW seed layers is needed as copper is susceptible to corrosion in harsh environments.

Deposition of the dielectric layer has also not been extensively covered in this study. If the dielectric and the conductor can be fabricated using the same processes then it removes more design constraints and allows the process to be more flexible in terms of 3D printing capability. For this to be successful new printable low dielectric loss compositions need to be available. These materials would require printing into relatively thick layers (>1mm) so the printing and processing requirements would need also need to be revisited. For example inkjet systems are limited to low viscosity solutions which limit the print thickness of the deposits, this means that this system would be unsuitable for printing dielectric layers. One approach is to use the micro-nozzle system to print the dielectric and the inkjet system to print the conductor track (as inkjet inks can have higher conductivity than micro-nozzle inks) [194]. However, this creates a more complex and expensive system. Alternatively the work conducted in this thesis has shown that the micro-nozzle inks (PTF

silver and thermoplastic silver ink) can be electroplated to improve conductivities therby removing the need to use an inkjet system to print the conductor lines.

Alternatively Additive Manufacturing (AM) technologies such as Selective Laser Sintering (SLS) of suitable polymer powders [195] or Fused Deposition Modelling (FDM) could be used to fabricate dielectric structures onto which a conductive pattern could be printed using DW. This type of integration has been shown by combining a micro-nozzle system with a Stereo-lithography system, to form devices with both structural and functional properties [196].

Another area which has not been explored is true 3D printing of the antenna. For a full appreciation of the capabilities of DW 3D printing onto large structures needs to be demonstrated further through integration with 5-axis robotics. This may bring up further limitations of the technology such as the ability to print upside down or orthogonal to gravity. Successful integration into 5-axis motion systems will open up further possibilities to antenna design engineers and system integrators who want to make stealthy or novel antennas.

11.3 Requirements Traceability

It is useful to trace the research activities performed in this thesis back to the requirements defined in Chapter 4. By doing this it can be seen if requirements have been met and if not where the current technology gaps are. This can then determine the next phase of development for future projects.

Table 11:1 shows the current status of each requirement defined in Chapter 4 as a result of the research activities conducted in this thesis. As can be seen there a number of requirements that are yet to be fulfilled. Analysis needs to be conducted on the accuracy of DW systems and their effect on antenna properties as well as develop DW dielectric materials that satisfy all the relevant performance requirements. Although some inks have been tested for their durability these experiments were not exhaustive. It would also be to measure the durability of the inkjet inks as well as inks that are cured with the broadband thermal spot system and plated with copper.

Subsystem	Functional Requirements (How's)	Performance Requirements	Progress
Printing System	Position DW Head Accurately	Positional Accuracy (to be defined)	To be measured not conducted in this thesis
		Repeatability (to be defined)	To be measured not conducted in this thesis
	Control material rheology	Viscosity	Viscosity can be kept constant by maintaining the nozzle temperature below the onset of cure
	Deposit DW material	Print Dimensions	Conductive and dielectric inks were deposited using both micro-nozzle and inkjet systems
DW material	Low Dielectric constant	dielectric constant <10	COTS dielectrics had relatively high dialectic constants of 12k and 30k although lower polyimide dielectric inks can be obtained
	High Conductivity	>30% bulk silver	>50% bulk conductivities of copper can be achieved through localised electroplating of inkjet and thermoplastic PTF inks
	Low Surface Roughness (dielectric)	<Skin Depth	Surface roughness effects need to be investigated further
	Dielectric Layer thickness	Track height >1mm	Only dielectric thicknesses of 340mm was achieved due to blistering and deformation of the printed layer]
	Low Loss Tangent	<0.001	Predicted Loss tangents of COTS dielectric inks were very high (approximately 0.1)
	Temperature resistance	Mil Std	PTF inks exhibited high and low temperature resistance. Inkjet inks and electroplated DW inks have not been investigated
	Adhesion	ASTM D4541	PTF inks exhibit high adhesion. Inkjet inks have poor adhesion on surfaces with low surface roughness which could cause a problem at high frequencies where dielectric surfaces need to be smooth
		ASTM D3359	
	Solvent/Skydrol resistance	Mil Std	PTF inks were not Skydrol Resistant
DW Localised Processing	Enable sintering and curing of DW material	Optimise Functional Properties by Curing	Oven cured resistances were obtained using a fibre delivered broadband thermal spot system. Process parameters need to be optimised to increase speed and reduce surface roughness
	Restrict Heat Penetration	No structural damage to substrate	Thermodynamical modelling of the curing process showed that heat penetration into the substrate was restricted to only a few hundred microns below the surface of the ink coating. HAZ analysis showed no visible signs of damage.
DW Transmission Line	Transmission at GHz frequencies	Line Loss	S21 measurements of copper plated inkjet and thermoplastic silver inks were equivalent to a bulk metal transmission line.
		Impedance (50Ohms)	Characteristic impedance of DW transmission line measured approximately 52-55ohms. This can be modified by altering the track dimensions accordingly
DW Antenna	Operate at GPS frequency	Resonant frequency matched to model	Resonant frequency of DW antennas was different from model. This can be modified by altering the print dimensions accordingly
		High return loss	Return loss of copper plated thermoplastic ink was equivalent to copper etched antenna
		Gain matched to model	Gain pattern of copper plated thermoplastic antenna was equivalent to copper etched antenna

Table 11:1: Requirements traceability

[1] S. W. Shneider, C. Bozada, R. Dettmer and J. Tenbarge, “Enabling Technologies for Future Structurally Integrated Conformal Apertures,” 2001.

[2] L. Josefsson and P. Persson, Conformal Array Antenna Theory and Design, John Wiley, 2006.

[3] Sensor Systems Inc, [Online]. Available: http://www.sensorantennas.com/antenna/VHF_LBAND.htm. [Accessed 12 6 2011].

[4] G. Leflour, C. Calnibalosky and H. Jaquet, “Reduction of Time and Costs for Antennas Integration Through Computational Electromagnetism,” Paris, 2002.

[5] J. Kunze, “Design and Manufacturing of a Low RCS, X-band SATCOM Antenna System,” 2008.

[6] R. Engle, “Embedded and Confromal Antennas,” COBHAM, 2008. [Online]. Available: http://chesapeakebayaoc.org/documents/AOC%20Briefing_Oct08_Embedded%20Antenna%20rev%20c.pdf.

[7] R. Sreekrishna., B.R.Karthikeyan and G. R. Kadambi., “Design and Development of a Compact Wideband Conformal Antenna for Wireless Applications,” vol. 10, no. 1, 2011.

[8] J. R. James, P. S. Hall and C. Wood, Microstrip Antenna Theory and Design, Peter Peregrinus Ltd, 1981.

[9] E. Alboni and M. Cerretelli, “Microstrip Patch Antenna for GPS Application”.

[10] P. Kabacik and M. Bialkowski, “Cylindrical Antenna Arrays and their Applications in Wireless Communication Systems”, personally received paper from Prof. Marek E. Bialkowski, Department of Information Technology and Electrical Engineering,” 2002.

[11] B. H. King, D. Dimos, P. Yang and S. L. Morissette, “Direct-Write Fabrication of Integrated Multilayer Ceramic Components,” vol. 3, no. 2, 1999.

[12] B. Stuart, “Write stuff from BAE,” 2007.

[13] Y. Liu, T. Cui and K. Varahramyan, “All-polymer capacitor fabricated with inkjet printing technique,” vol. 47, 2003.

[14] Q. Chen, T. Tong, J. Longtin, S. Tankiewicz, S. Sampath and R. Gambino, “Novel Sensor Fabrication Using Direct-Write Thermal Spray and Precision Laser Micromachining,” vol. Vol. 126 (4), 2004.

[15] V. Subramanian, P. Chang, D. Huang, J. lee, S. Molesa, D. Redinger and S. Volkman, “All-Printed RFID Tags: Materials, Devices, and Circuit Implications,” 2006.

[16] A. Piqué and D. Chrisey, Direct-Write Technologies for Rapid Prototyping Applications, San Diego: Academic Press, 2002.

[17] DTI, “Direct Writing: Global Status and Opportunities for the UK in Advanced Manufacturing – Scoping Study,” 2004.

[18] M. J. Wilhelm, D. H. Weme, P. L. Wemer, K. Church and R. Taylor, “Direct Write Processes as Enabling Tools for Novel Antenna Development,” 2002.

[19] R. Auyeung, M. Nurnberger, D. Wendland, A. Piqué, C. Arnold and A. Abbott, “Laser fabrication of GPS conformal antennas,” San Jose, CA, 2004.

[20] A. Pique, R. C. Y. Auyeung, M. W. Nurnberger, D. J. Wendland, C. B. Arnold and L. C. Schuette, “Rapid Prototyping of Conformal Antenna Structures”.

[21] S. Rea, D. Linton, E. Orr and J. McConnell, “Electromagnetic Shielding Properties of Carbon Fibre Composites in Avionic Systems,” 2005.

[22] B. W. Anderson, “The impact of carbon fibre composites on a military aircraft establishment,” vol. 20, 1986.

[23] D. Harvey, 2008. [Online]. Available: http://news.bbc.co.uk/1/hi/england/bristol/7473838.stm. [Accessed 21 08 10].

[24] V. Browning. [Online]. Available: http://www.darpa.mil/dso/trans/mice.htm.

[25] H. Nakahara, “PCB Market and Opportunity,” 2008. [Online]. Available: http://www.ipcaindia.org/pdffiles/PCBMktOppDrNakahara.pdf.

[26] J. Sidhu, “Direct Write Overview,” BAE Systems Internal Pubication, 2004.

[27] J. J. Licari and L. R. Enlow, Hybrid Microcircuit Technology Handbook (2nd Ed.), Westwood, New Jersey: Noyes Publications, 1998.

[28] E. C. Kinzel, “Laser Microfabrication of Thick-Film Microelectronics,” 2005.

[29] D. B. Chrisey, “Material Processing: The Power of Direct Writing,” 2000.

[30] L. Lin and X. Bai, “Ink-jet Technology: Status Quo and Future Relevance to Surface Coatings,” vol. 33, no. 4, 2004.

[31] D. Wallace, D. Hayes, T. Chen, V. Shah, D. Radulescu, P. Cooley, K. Wachtler and A. Nallani, “Think Additive: Ink-jet Deposition of Materials for MEMS Packaging,,” Long beach California, 2004.

[32] B. Gans De, P. C. Duineveld and U. S. Schubert, “Inkjet Printing of Polymers: State of the Art and Future Developments,” vol. 16, no. 3, 2004.

[33] E. Menard, M. A. Meitl and Y. G. Sun, "Micro and nanopatterning techniques for organic electronic and optoelectronic systems," vol. 107, no. 4, 2007.

[34] Z. Yin, Y. HUANG, Y. BU, X. WANG and Y. XIONG, "Inkjet printing for flexible electronics: Materials, processes and equipments," vol. 55, no. No.30, 2010.

[35] B. King, “Maskless Mesoscale Material Deposition,” vol. 43, no. 2, 2003.

[36] M. Carter, T. Amundson, J. Colvin and J. Sears, “Characterization of Soft Magnetic Nano-Material Deposited with M3D Technology,” 2006.

[37] B. E. Kahn, "The M3D aerosol jet system, an altrernative to inkjet prinitng for printed electronics," Organic and Printed Electronics, 2007. [Online]. Available: http://www.optomec.com/downloads/Optomec_Organic_and_PrintedElectronics.pdf. [Accessed 18 05 2014].

[38] "Optomec," [Online]. Available: http://www.optomec.com/Additive-Manufacturing-Systems/Printed-Electronics-Lab-Systems.

[39] Stony Brook State University of New York, “Center for Thermal Spray Research,” 2007. [Online]. Available: http://www.matscieng.sunysb.edu/ctsr/.

[40] H. Herman, S. Sampath and R. McCune, “Thermal Spray Current Status and Future Trends,” vol. 25, 2000.

[41] Q. Chen, T. Tong, J. P. Longtin, S. Tankiewicz, S. Sampath and R. J. Gambino, “Novel SensorFabrication Using Direct-Write Thermal Spray and Precision Laser Micromachining,” 2004.

[42] S. Sampath, H. Herman and R. Greenlaw, "Method and Apparatus fo rFine Feature Spray Deposition," 2003.

[43] J. Longtin, S. Sampath, S. Tankiewicz, R. J. Gambino and R. J. Greenlaw, "Sensors for Harsh Environments by Direct-Write Thermal Spray," vol. Vol 4, no. 1, 2004.

[44] D. B. Chirsey, A. Pique, J. Fitz-Gerald, R. C. Y. Auyeung, R. A. McGll, H. D. Wu and M. Duignan, “New Approach To Laser Direct Writing Active and Passive Mesoscopic Circuit Elements,” 1999.

[45] Y. Lin, G. Huang, Y. Huang, T.-R. J. Tzeng and D. Chrisey, “Effect of laser fluence in laser-assisted direct writing of human colon cancer cell,” 1995.

[46] C. Zhang, D. Liu, S. A. Mathews, J. Graves, T. M. Schaefer, B. K. Gilbert, R. Modi, H. D.

Wu and D. B. Chirsey, “Laser direct-write and its application in low temperature Co-fired ceramic (LTCC) technology,” vol. 70, 2003.

[47] Intertronics, [Online]. Available: http://www.intertronics.co.uk/products/dispensing_machines_01.htm.

[48] B. H. King, D. Dimos, P. Yang and S. L. Morissette, “Direct-Write Fabrication of Integrated Multilayer Ceramic Components,” vol. 3, no. 2, 1999.

[49] A. Karwa, “Printing Studies with Conductive Inks and Exploration of New Conducting Polymer Compositions Thesis, Center for Materials Science and Engineering,” 2006.

[50] R. A. Dorey and R. W. Whatmore, “Electro-ceramic Thick Film Fabrication for MEMS,” vol. 12, 2004.

[51] Y. Liu, T. Cui and K. Varahramyan, “All polymer capacitor fabricated with inkjet printing technique,” vol. 47, 2003.

[52] R. Parashkov, E. Becker, G. Ginev, T. Riedl, H. Johannes and W. Kowalsky, “All-Organic Thin-Film Transistors Made of Poly(3-butylthiophene) Semiconducting and Various Polymeric Insulating Layers,” vol. 95, 2004.

[53] L. Gasman, “Inks for the printable electronics market, NanoMarkets,” 2006. [Online]. Available: www.nanomarkets.net/resources/download/Ink%20Perspective.pdf.

[54] K. Gileo, Polymer Thick Film, 1996: Van Nostrand Reinhold, New York.

[55] P. J. Smith, D. Y. Shin, J. E. Stringer and B. Derby, “Direct Ink-Jet Printing and Low Temperature Conversion of Conductive Silver Patterns,” vol. 41, 2006.

[56] GOLDPRICEtm, [Online]. Available: http://silver-and-gold-prices.goldprice.org/. [Accessed 05 04 2012].

[57] Fuller, E. J. Wilhelm and J. M. Jacobson, “Ink-Jet Printed Nanoparticle Microelectromechanical Systems,” vol. 11, no. 1, 2002.

[58] L. Hsien-Hsueh, C. Kan-Sen and H. Kuo-Cheng, “Inkjet Printing of Nanosized Silver Colloids,” vol. 16, 2005.

[59] J. Perelaer, W. M. A. de Laat, C. E. Hendriksa and U. S. Schubert, "Inkjet-printed silver tracks: low temperature curing and thermal stability investigation," 2008.

[60] Z. Xiong and C. Liu, "Effect of Substrates Surface Condition on the Morphology of Silver Patterns Formed by Inkjet Printing," 2011 .

[61] J. Mei, M. R. Lovell and M. H. Mickle, “Formulation and Processing of Novel Conductive Solution Inks in Continuous Inkjet Printing of 3-DElectric Circuits,” vol. VOL. 28, no. 3,

2005.

[62] A. Y. Xiao, Q. K. Tong and A. C. Savoca, “National Starch and Chemical Company,” 1999.

[63] A. L. Dearden, P. J. Smith, D. Y. Shin, N. Reis, B. Derby and P. O'Brien, “A Low Curing Temperature Silver Ink for Use in Ink-Jet Printing and Subsequent Production of Conductive Tracks,” vol. 26, 2004.

[64] P. J. Smith, D. Y. Shin, B. Stringer and B. Derby, “Direct Ink-Jet Printing and Low Temperature Conversion of Conductive Silver Patterns,” vol. 41, 2006.

[65] M. Ukena, “UV Curable Inks: Will They Work for Everyone?,” Printed environmental technology, PNEAC, [Online]. Available: www.pneac.org/sheets/screen/UVCurableInk.pdf.

[66] Gwent Electronics Materials (GEM), “C2110414D7 product data sheet,” 2012. [Online]. Available: http://www.gwent.org/gem_data_sheets/polymer_systems_products/flexographic_inks/uv_silver_c2110414d7.pdf. [Accessed 21 05 2014].

[67] J. P. Kruth, X. Wang, T. Laoui and L. Froyen, “Lasers and Materials in Selective Laser Sintering,” vol. 4, 2003.

[68] V. R. Marinov, “Electrical Resistance of Laser Sintered Direct-Write Deposited Materials for Microelectronic Applications,” vol. Vol 1, 2004.

[69] J. Chung, S. Ko, N. R. Bieri, P. C. Grigoropoulos and D. Poulikakos, “Conductor Microstructures By Laser Curing of Printed Gold Nanoparticle Ink,,” vol. 84, no. 5, 2003.

[70] T. Sato, E. Fearon, C. C, K. G. Watkins, G. Dearden and D. Eckford, “Laser-assisted DirectWrite for aerospace applications,” vol. 223, 2009.

[71] J. Perelaer, B. J. Gans and U. S. Schubert, “Ink-jet Printing and Microwave Sintering of Conductive Silver Tracks,” vol. 18, 2006.

[72] V. Marinov and Y. Atanasov, “Improved Direct Write Technologies for High Frequency Interconnects on Flexible Substrates,” 2006.

[73] A. Sridhar, J. Reiding, H. Adelaar, F. Achterhoek, D. J. van Dijk and R. Akkerman, “Injet printing and electroless plating based fabrication of RF circuit structures on high frequency substrates,” vol. 19, 2009.

[74] K. Kirschenmann, K. W. Whites and S. M. Woessner, “Inkjet Printed Microwave Frequency Mulitlayer Antennas”.

[75] R. C. Y. Auyeung, M. W. Nurnberger, D. J. Wedland, A. Pique, C. B. Arnold and A. R.

Abbott, “Laser fabrication of GPS conformal antennas,” 2004.

[76] J. J. Adams, E. B. Duoss, T. F. Malkowski, M. J. Motala, B. Y. Ahn, R. G. Nuzzo, J. T. Bernhard and J. A. Lewis, "Conformal Printing of Electrically Small Antennas on Three-Dimensional Surfaces," *Advanced Materials,* 2011.

[77] A. Chauraya, W. G. Whittow, C. Vardaxoglou, Y. Li, R. Torah, K. Yang, S. Beeby and J. Tudor, "Inkjet printed dipole antennas on textile for wearable communications," *IET Microwaves, Antennas & Propagation,* vol. 7, 2013.

[78] A. K. Sowpati, V. K. Palukuru, V. PynttÄari, R. MÄakinen, M. V. Kartikeyan and H. Jantunen, "Performance of Printable Antennas With Different Conductor Thinkness," *Progress In Electromagnetics Research Letters,* vol. 13, 2010.

[79] V. Pynttäri, E. Halonen, M. Mäntysalo and R. Mäkinen, "The Effect of Sintering Profile and Printed Layer Variations with Inkjet-Printed Large-Area Applications," *IEEE,* 2012.

[80] D. Herold, L. Griffiths and T. Y. Fung, "Lightweigh, high bandwidth confromal antenna system for ballistic helmets," *IEEE,* 2007.

[81] A. Ferrer-Vidal, Rida, Amin, S. Basat, L. Yang and M. M. Tentzeris, “Integration of Sensors and RFID’s on Ultra-low-cost Paper-based Substrates for Wireless Sensor Networks Applications,” 2006.

[82] Mesoscribe, [Online]. Available: http://www.mesoscribe.com/products/conformal-antennas/. [Accessed July 2013].

[83] DuPont, “Processing Guide For Printing Smart Card Antennae,” [Online]. Available: http://www.solutions.dupont.com.au/MCM/en_US/PDF/designguides/Smart-20Card-20Design-20Guide.pdf.

[84] R. C. Johnson, Antenna Engineering Handbook 3rd edition,, New York: McGraw-Hill Inc, 1993.

[85] A. K. Singh, "Dish to digital: Amazing growth in military radar antenna technology," vol. Vol 90, no. 3, 2010.

[86] C. A. Balanis, Antenna Theory: Analysis and Design, Wiley, 1996.

[87] R. C. Johnson, Antenna Engineering Handbook Third edition, Mc Graw Hill.

[88] J. N. Chengalur, Y. Gupta and K. S. Dwarakanath, “Jayaram N Chengalur,” National Centre for Radio Astrophysics, [Online]. Available: http://www.ncra.tifr.res.in/gmrt_hpage/Users/doc/WEBLF/LFRA/LFRA.html. [Accessed 12 2 2012].

[89] F. T. Ulaby, Fundamentals of Applied Electromagnetics, Prentice Hall.

[90] S. N. Makarov, Antenna and EM modelling with MATLAB, John Wiley and Sons Inc, 1997.

[91] J. Kraus and R. Marhefka, Antennas for All Applications, Third Edition, McGraw-Hill, 2002.

[92] W. L. Stutzman and G. A. Thiele, Antenna Theory and Design, John Wiley and Sons Inc, 1998.

[93] M. T. Islam, M. N. Shakib, N. Misran and T. S. Sun, "Broadband Microstrip Patch Antenna," 2009.

[94] J. R. James and P. Hall, Handbook of Microstrip Antennas, IEE Electromagnetic Waves series 28.

[95] D. M. Pozar, Microwave Engineering, Second Edition, John Wiley and Sons.

[96] H. A. Wheeler, "Transmission-line properties of a strip on a dielectric sheet on a plane," 1977.

[97] Y. Atanasov, D. Vaselaar, A. Khan and V. Marinov, "Enhanced Direct-Write for High Frequency Applications on Low Temperature Substrates," North Dakota University, 2006.

[98] "TX-line," AWR, [Online]. Available: http://web.awrcorp.com/Usa/Products/Optional-Products/TX-Line/. [Accessed 10 03 09].

[99] Rogers Corporation, "Reliability and Key Propoerties RT/duroid 6002," [Online]. Available: www.rogerscorp.com/documents/754/acm/Reliabiity-and-Key-Properties-of-RT-duroid-6002.aspx.

[100] J. R. Aguilar, M. Beadle, P. T. Thompson and M. W. Shelley, "The Microwave and RF characteristics of FR4 Substrates".

[101] J. Martin, Systems Engineering Guidebook, CRC Press.

[102] A. P. Sage, Introduction to Systems Engineering, John Wiley & Sons, 2000.

[103] D. Sten, INCOSE SE Terms Glossary, Seattle: INCOSE, 1998.

[104] US Department of Defence System Engineering Standards, Mil-STD-499A, M.-S. 4., 1974, 1991.

[105] C. Elliot and P. Deasley, Creating Systems that Work: Principles of Engineering Systems for the 21st Century, The Royal Academy of Engneering, 2007.

[106] K. Forsberg, H. Mooz and H. Cotterman, Visualizing Project Managment: Models and Frameworks for Mastering Complex Systems, Hoboken: Wiley, 2005.

[107] J. Martin, Systems Engineering Guidebook, CRC Press, 2000.

[108] UK, Ministry of Defence. (n.d.), "Applying Technology Readiness Levels," 2009. [Online]. Available: Ministry of Defence Aquisition Operational Framework: http://www.aof.mod.uk/aofcontent/tactical/techman/content/trl_applying.htm.

[109] F. J. Romero Rojo, R. Roy, E. Shehab and P. J. Wardle, "Obsolescence Challenges for Product-Service Systems in Aerospace and Defence. 1st CIRP Industrial Product-Service Systems Conference (p. 255)," Cranfield University, 2009.

[110] A. Medwell, "Defence software systems development: the benefits of a systems approach," 2008. [Online]. Available: http://www.purplesecure.com/Documents/BenefitOfASystemsApproach_FULL.pdf.

[111] L. M. Smith, "Project Clarity Through Stakeholder Analysis".

[112] S. Burge, "The Systems Engineering Tool Box," [Online]. Available: http://www.burgehugheswalsh.co.uk/uploaded/documents/STA-Tool-Box-V1.pdf.

[113] R. Thompson, S. Moyers, D. Mulvaney and C. Vassilios, "The UML-based design of a hardware H.264/MPEG-4 AVC video decompression core. Axilica Limited, Loughborough Innovation Centre," [Online]. Available: www.Vassilios-Chouliaras.com..

[114] T. Paolo and A. Potrich, "Reverse Engineering of Object Oriented Code," 2007.

[115] R. C. Martin, "Object Mentor, UML tutorial," [Online]. Available: http://www.objectmentor.com/resources/articles/umlClassDiagrams.pdf.

[116] QFD Online, [Online]. [Accessed 2013].

[117] H. Wijshoff, "The dynamics of the piezo inkjet printhead operation," vol. 491, 2010.

[118] T. L. Floyd and D. M. Buchla, Electroics Fudamentals: Circuits, Devices and Applications, Pearsons.

[119] FLUKE, [Online]. Available: http://www.fluke.com/fluke/uken/bench-instruments/bench-multimeters/8845a-8846a.htm?PID=55451. [Accessed 12 5 12].

[120] T. R. Kuphaldt, All About Circuits: Volume I—DC, 2003. [Online]. Available: http://www.allaboutcircuits.com/vol_1/chpt_8/9.html. [Accessed 23 6 12].

[121] E. M. Bock, "Low-Level Contact Resistance Chracterization," vol. 3, 1993.

[122] K. Bautista, "Four Point Probe Operation," University of Texas Dallas, 2004. [Online].

Available: http://www.utdallas.edu/research/cleanroom/manuals/documents/4pointFinal.pdf. [Accessed 24 6 12].

[123] PTB Sales, [Online]. Available: http://sharedresearchfacilities.wvu.edu/SOPs/SRF_Manual_StepProfiler_TencorAlphastep.pdf. [Accessed 23 4 12].

[124] BSI Brumely South, [Online]. Available: http://www.brumleysouth.com/as200.php. [Accessed 26 6 12].

[125] Elcometer, "Elcometer 110 PATTI Tester: Operating Manual," [Online]. Available: http://www.elcometer.com/. [Accessed 12 4 11].

[126] Suntronic, "Jettable Silver U5714 datasheet," [Online]. Available: www.sunchemical.com. [Accessed 12 January 2011].

[127] Acheson, "Electrodag 725A silver ink," [Online]. Available: http://tds.loctite.com/tds5/docs/ELECRODAG%20725A%20(6S-54)-EN.PDF. [Accessed 09 July 2010].

[128] "Direct Write Elements and Sensor (DW Easy) project," 2009. [Online]. Available: http://www.dweasy.co.uk/project_7.asp.

[129] Gwent Electronic Materials, "Silver ink (C2050712D58), hybrid ink (C2080929D6), 30k dielectric ink (D2070209D6), 12k dielectric ink (D2091022D2)," [Online]. Available: www.g-e-m.com.

[130] M. P. K. Turunen, P. Marjamaki, M. Paajanen, J. Lahtinen and J. K. Kivilahti, "Pull-off test in the assessment of adhesion at printed wiring board metallisation/epoxy interface," vol. 44, 2004.

[131] L. Hau, S. Raja, M. Sloan, R. Robinson, J. McDonald, J. Sidhu, C. Tuck and R. Hague, "Printing Characteristics and Performance of Polymer Thick Film Inks for Direct Write Applications,".

[132] N. P. Cheremisinoff, Polymer Characterization: Laboratory Techniques and Analysis, 1997.

[133] J. R. Fried, Polymer Science & technology, Second Edition, Prentice Hall, 2003.

[134] Mettler Toledo, Thermal Analysis Information for users., User Com 23, 2006.

[135] Department of Defence, MIL-STD-810G Environmental Engineering Considerations and Laboratory Tests, 2008.

[136] W. Q. Song, P. Krauklis, A. P. Mouritz and S. Bandyopadhyay, “The effect of thermal ageing on the abrasive wear behaviour of age hardening 2014 Al/sic 6061 Al/SIC composites,,” Vols. 185,, 1995.

[137] H. Kacar, E. Atik and C. Meric, “The effects of precipitation-hardening conditions on wear behaviors at 2024 aluminium wrought alloy,” vol. 142, no. 3, 2003.

[138] G. Sala, “Composite degradation due to fluid absorption,” vol. 31, no. 5, 2000.

[139] M. Buggy and K. O'Byrne, “Effects of Skydrol (A Hydraulic Fluid) on the Network Structure of TGDDM/DDS-Based Resins,” vol. 65, no. 10, 1997.

[140] P. Vassiliou and C. T. Dervos, “Corrosion Effects on the Electrical Performance of Silver Metal Contacts,” vol. 46, no. 2, 1999.

[141] P. Acevedo-Hurtado, P. A. Sundaram and P. G. Caceres-Valencia, “Characterization of Atmospheric Corrosion In AL/AG Lap Joints,” 2007.

[142] Kang and S. J. L., Sintering: densification, grain growth, and microstructure, Elsevier, 2005.

[143] [Online]. Available: www.matweb.com. [Accessed 23 January 2011].

[144] Moon, Kyoung-sik, Hai, Maric, Radenka, Pothukuchi and Suresh, “Thermal Behavior of Silver Nanoparticles for Low-Temperature Interconnect Applications,” 2005.

[145] M. Schlesinger and M. Paunovic, Modern Electroplating, John Wiley & Sons.

[146] H. Fan, “Electroplating of Compound Ni-SiC Coatings and Improvement of Wear Resistance,” 2010.

[147] US Department of Health and Human Services, “Formaldehyde, Report of Carcinogens, Eleventh Edition,” 2005. [Online]. Available: http://ntp.niehs.nih.gov/ntp/roc/eleventh/profiles/s089form.pdf. [Accessed 10 Febuary 2011].

[148] R. Suchentrunk, Metallizing of Plastics - A Handbook of Theory and Practice, ASM International, 1993.

[149] J. W. Dini, “Brush Plating: Recent property data,” vol. 96, no. 6, 1998.

[150] W. Bin, X. Bin-shi, J. Xue-dong, L. Cun-long and Z. Bin, “Automatic brush plating technology for component remanufacturing,” vol. 12, 2005.

[151] “Additive Process Technologies (APT),” [Online]. Available: www.addprotec.com.

[152] J. Perelaer, P. J. Smith, M. M. P. Wijnen, E. van den Bosch, R. Eckardt, P. H. J. M.

Ketelaars and U. S. Schubert, “Droplet Tailoring Using Evaporative Inkjet Printing,” vol. 210, 2009.

[153] D. Soltman and V. Subramanian, “Inkjet Printed Line Morphologies and Temperature Control of the Coffee Ring Effect,” vol. 24, 2007.

[154] E. Tekin, B. J. de Gans and U. S. Schubert, “Ink-jet Printing of Polymers From Single Dots to Thin Film Libraries,” vol. 14, 2004.

[155] S. Busato, A. Belloli and P. Ermanni, “Inkjet printing of palladium catalyst patterns on polyimide film for electroless plating,” vol. 123, 2007.

[156] T. Sato, E. Fearon, C. Curran, K. W. Watkins, G. Dearden and D. Eckford, "Laser-assisted Direct Write for aerospace applications," vol. 223, 2009.

[157] M. A. F. Scarparo, Q. J. Chen, J. H. Miller, J. H. Zhang and S. D. Allen, "Mechanisms of Carbon Dioxide Laser Stereolithography in Epoxy-Based materials," vol. 62, no. pp491-500, 1996.

[158] J. Sidhu and J. McDonald, "Direct Write and Additive Manufacturing Processes". United States of America Patent 20100171792, 2010.

[159] E. Fearon, T. Sato, D. Wellburn, K. G. Watkins and G. Dearden, “Thermal Effects of Substrate Materials used in the Laser Curing of Particulate Silver Inks,” 2007.

[160] W. Demtroder, Laser Spectroscopy: Volume 2, Springer.

[161] Gwent Electronic Materials, "Silver ink (C2050712D58), hybrid ink (C2080929D6), dielectric ink (D2091022D2)," [Online]. Available: www.g-e-m.com.

[162] J. D. Majumdar and I. Manna, "Laser processing of materials," vol. Vol. 28, 2003.

[163] W. M. Steen, J. Mazumder and K. Watkins, Laser Material Processing, Springer.

[164] X. Zeng, B. Zhu, Z. Tao and K. Cui, "Analysis of energy conditions for laser cladding ceramic-metal composite coatings," vol. 79, 1996.

[165] "HexPly 8552 Epoxy matrix data sheet," Hexcel, [Online]. Available: www.hexcel.com.

[166] I. Photonics. [Online]. Available: www.icure-irphotonics.com. [Accessed 05 July 2011].

[167] C.I.F, "CIF photoboard FR4 datasheet," [Online]. Available: http://www.cif.fr/.

[168] D. Ranjit, N. Melikechi and F. Eichmiller, “The effect of irradiation wavelength bandwidth and spot size on the scraping depth and temperature rise in composite exposed to an argon laser or a conventional quartz-tungsten-halogen source,” vol. 18, 202.

[169] E. B. Franco, J. C. Periera, R. F. Mondelli and L. G. Lopes, “Effect of Light Curing Units and Activation Mode on Polymerisation Shrinkage and Shrinkage Stress of Composite Resins,” vol. 16, 2008.

[170] S. Raja, N. Court, J. Sidhu, C. Tuck and R. Hague, "Localised Broadband Curing of Directly Written Inks for the Production of Electrical Devices for the Aerospace Industry," Austin Texas, 2010.

[171] ASTM Standard, *E 2336-87 Standard Test Method for Thermal Conductivity of Solids by means of the Guarded-Comparative-Longitudinal Heat Flow Technique,* 1997.

[172] A. J. Slifka, "Thermal Conductivity Apparatus for Steady-State, Comparative Measurement of Ceramic Coatings," vol. Vol. 105, no. No. 4, 2000.

[173] Infrared Services Inc., [Online]. Available: http://www.infrared-thermography.com/material-1.htm. [Accessed September 2011].

[174] M. Darif and N. Semmar, "Numerical Simulation of Si Nanosecond Laser Annealing by COMSOL Multiphysics," 2008.

[175] M. Santarsiero and R. Borghi, "Correspondence between super-Gaussian and flattened Gaussian beams," vol. Vol 16, no. No. 1, 1999.

[176] G. W. Kaye and T. H. Laby, "Table of Physical and Chemical Constants," [Online]. Available: http://www.kayelaby.npl.co.uk/.

[177] W. Jones and M. Norman, Theoretical Solid State Physics, Courier Dover Publications, 1985.

[178] H. Rosenberg, The solid state, Oxford University Press, 2004.

[179] J. C. Rautio, “Microstrip Conductor Loss Models for Electromagnetic Analysis,” vol. 51, no. 3, 2003.

[180] Z. Radivojevic, K. Andersson, K. Hashizume, M. Heino, M. Mantysalo, P. Mansikkamaki, Y. Matsuba and N. Terada, “Optimised Curing of Silver Ink-Jet Based Printed Traces,” 2006.

[181] T. W. Turpin and R. Baktur, “See Through Antennas and Their Optimization,” 2008.

[182] J. Siden, T. Olsson, A. Koptioug and N. H-E, “Reduced Amount of Conductive Ink with Gridded Printed Antennas”.

[183] PEL Printed Electronics Ltd, [Online]. Available: http://www.printedelectronics.com/.

[184] J. Huang, “The finite ground plane effect on the microstrip antenna radaiting patterns,” Vols. AP-31, 1983.

[185] G. Clasen and R. Langley, “Meshed Patch Antennas,” vol. 52, no. 6, 2004.

[186] E. E. Altshule, T. H. O'Donnell, S. R. Best and B. Kaanta, “A Reveiw of an Electrically Small Antenna Immersed in a Dielectric”.

[187] Creative Materials, "POLYIMIDE ADHESIVE / COATING 122-01," [Online]. Available: https://server.creativematerials.com/datasheets/DS_122_01.pdf. [Accessed 23 05 2014].

[188] L. M. Minges, Electronic Materials Handbook: Packaging, ASM international.

[189] R. N. Das, H. T. Lin, J. Huang, J. M. Lauffer, F. D. Egitto, M. D. Poliks and V. R. MarkovichV, "Printable Materials and Devices for Electronic Packaging," 2010.

[190] ASTRAEA, [Online]. Available: http://www.projectastraea.co.uk/. [Accessed 2008].

[191] The A Register, [Online]. Available: http://www.theregister.co.uk/2007/11/08/bae_mouse_click_robot_spy_dover_over/. [Accessed 07 10 2008].

[192] CYCOM, *CYCOM 823-1 RTM technical datasheet for carbon fibre resin,* 2004.

[193] V. Pynttäri, E. Halonen, H. Sillanpää, M. Mantysalo and R. Mäkinen, “RF Design for Inkjet Technology: Antenna Geometries and Layer Thickness Optimization,” vol. 11, 2012.

[194] D. Redinger, “An Ink-Jet-Deposited Passive Component Process for RFID,” vol. 51, no. 2, 2004.

[195] M. J. Thompson, D. C. Whalley and N. Hopkinson, “Investigating Dielectric Properties of Sintered Polymers For Rapid Manufacturing,” Austin, Texas, 2008.

[196] F. Medina, A. Lopes, A. Inamdar, R. Hennessesy, J. Palmer, B. Chavez, D. Davis, P. Gallegos and R. Wicker, “Hybrid Manufacturing: Integrating Direct Write and Stereolithography,” 2005.

[197] "D20702090D6 Data sheet," GEM, [Online]. Available: www.gwent.org.

[198] J. F. Ready, D. F. Farson and T. Feeley, LIA Handbook of Laser Materials Processing, New York.

[199] P. Calvert, “Inkjet printing for materials and devices,” 2001.

[200] 3D systems, *Accura Duraform PA MSDS,* 2004.

[201] M. Carter, J. Colvin and J. Sears, “Characterization of Conductive inks deposited with Maskless Mesoscale Material Deposition (M3D)”.

[202] J. R. Groza and A. Zavaliangos, “Nanostructured bulk solids by field activated sintering,”

vol. 5, 2003.

[203] S. Merilampi, L. Ukkonen, L. Sydanheimo, P. Ruusjanen and M. Kivikoski, “Analysis of silver ink bow-tie RFID tag antennas printed onto paper substrate,” 2007.

[204] M. Panitz, D. C. Hope, T. Sato and C. D. Harley, “The Opportunities and Challenges for Wireless Interconnects in Aircraft,” 2009.

[205] M. Schmidt, R. Kusche, B. Issendorf and H. Harberland, “Irregular variations in the melting point of size-selected atomic clusters,” vol. 393, 1998.

[206] V. Pynttäri, E. Halonen, M. Mäntysalo and R. Mäkinen, "The Effect of Sintering Profile and Printed Layer Variations with Inkjet-Printed Large-Area Appliciations," *IEEE,* 2012.

A. Appendix A: Class Diagram Notations

The class box or icon contains three pieces of information about an object or system component, the name, its attributes (variables) and its objectives (functions). A typical class box is shown in Figure A:1.

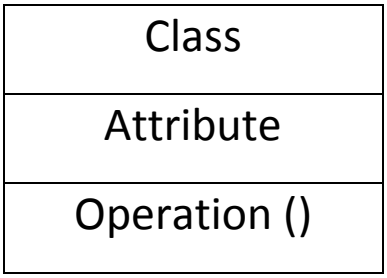

Figure A:1: Class Icon [115]

Relationships between classes are denoted by different types of arrows. An Association arrow, Figure A:2, depicts that the classes have a relationship between each other. There is an association if one class has to know about the other one in order to perform. A Composition arrow, Figure A:3, indicates that one class belongs or is composed of another class. Finally a generalisation or inheritance arrow, Figure A:4, indicates that one or more classes can shares properties described by a super-class. Multiplicities can also be added between an association end which shows the number of possible instances of the class associated with a single instance of the other end. Multiplicities are single numbers or ranges of numbers.

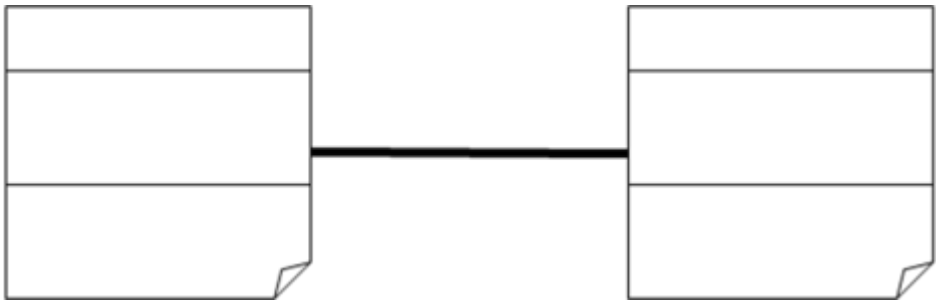

Figure A:2: Association Arrow

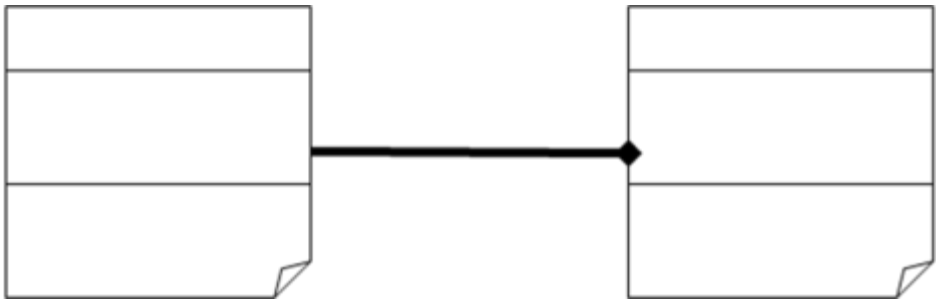

Figure A:3: Composition

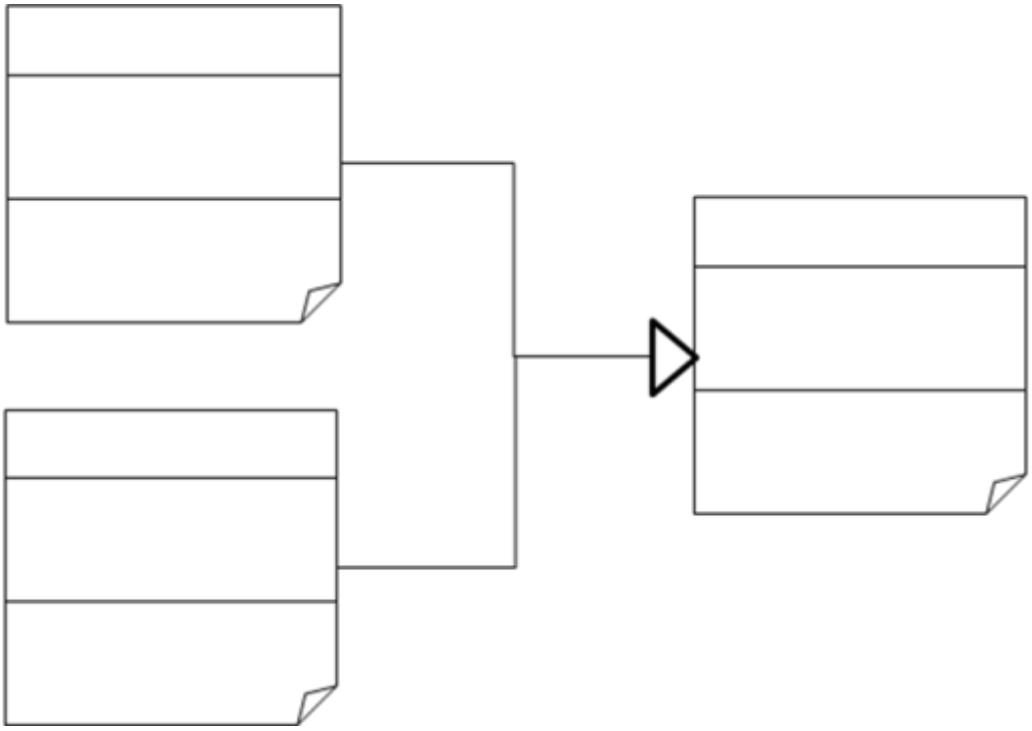

Figure A:4: Generalisation Arrow

B. Appendix B: Technical Performance Measures

Subsystem	Functional Requirement (How's)	Performance Requirement	TP Id Number	Technical Parameter (TP)	Technical Performance Measure (TPM)	TPM Id Number
Printing System	Position DW Head Accurately	Positional Accuracy (to be defined)	DW/P/TP1	Positional Accuracy (mm)	laser sensors to measure positioning of motion system	DW/TPM1
		Repeatability (to be defined)	DW/P/TP2	Repeatability (mm)	laser sensors to measure consistency of motion System	DW/TPM2
	Control Material Rheology	Viscosity	DW/P/TP3	Viscosity (cp)	Rotational rheometer	DW/TPM3
	Deposit DW Material	Print Dimensions	DW/P/TP5	Track width and height (mm)	Measure track profile using a touch probe	DW/TPM4
DW material	Low Dielectric Constant	Dielectric constant <10	DW/M/TP 6	Dielectric Constant	Capacitive measurement (by manufacturer)	DW/TPM5
	High Conductivity	>30% bulk silver	DW/M/TP 7	Sheet Resistance (Ohms)	Four-point probe measurement	DW/TPM6
			DW/M/TP 8	Line Resistance (Ohms)	Two-wire resistance measure	DW/TPM7
	Low Surface Roughness (dielectric)	<Skin Depth	DW/M/TP 9	Surface Roughness (μm)	Measure track profile using methods DW/P/TPM4	DW/TPM4
	Dielectric Layer thickness	Track height >1mm	DW/M/TP 10	Track Thickness (μm)	Measure track profile using methods DW/P/TPM4	DW/TPM4
	Low Loss Tangent	<0.001	DW/M/TP 11	Loss Tangent	Measure the line loss in a DW transmission line to infer the loss tangent	DW/TPM8
	Temperature resistance	Mil Std	DW/M/TP 8	Line (Ohms)	measure the line resistance as the DW material is held at high and low temperatures	DW/TPM9
	Adhesion	ASTM D4541	DW/M/TP 12	Adhesion (MPa)	PATTI pull-off measurement	DW/TPM10
		ASTM D3359	DW/M/TP 13	Adhesion	Peel test measurement	DW/TPM11
	Solvent Resistance	Mil Std	DW/P/TP8	Line Resistance (Ohms)	measure the line resistance as the Dw material is immersed in solvent	DW/TPM12
DW Localised Processing	Enable Sintering or Curing of DW Material	Optimise Functional Properties by Curing	DW/P/TP8	Line Resistance (Ohms)	Two-wire resistance measure	DW/TPM16
			DW/M/TP 13	Adhesion	Peel test measurement	DW/TPM17
			DW/M/TP 14	Crosslink density (Tg, temperature °C)	Dynamic Mechanical Analysis	DW/TPM18
			DW/M/TP 15	Particle density (%)	Cross-section micrography and image analysis	DW/TPM19
	Provide Localised Heat Rise	Temperature > cure/sintering temperature	DW/M/TP 16	Temperature (°C)	Thermal imaging camera	DW/TPM20
					Thermodynamical Modelling	DW/TPM21
	Restrict Heat Penetration	No structural damage to	DW/M/TP 17	Heat Affected Zone (μm)	Measure by cross-section and inspection, Structural	DW/TPM22

		substrate			tests before and after processing	
			DW/M/TP 16	Temperature (°C)	Thermodynamical Modelling	DW/TPM21
DW Transmission Line	Transmission at GHz frequencies	Line Loss	DW/M/TP 18	Line Loss (dB)	Fabricate DW transmission line and compare it to base line measurement. Measure resulting S21 line loss in a Vector Network Analyser	DW/TPM24
		Impedance (50Ohms)	DW/M/TP 19	Impedance	Fabricate DW transmission line and compare it to base line measurement. Measure resulting S21 line loss in a Vector Network Analyser (VNA)	DW/TPM25
			DW/P/TP5	Track dimensions (mm)	Measure track profile using a touch probe	DW/TPM4
DW Antenna	Operate at GPS frequency	Resonant frequency matched to model	DW/M/TP 20	Frequency (MHz)	Fabricate DW antenna and measure S21 resonant frequency in a VNA	DW/TPM26
		High return loss	DW/A/TP 21	Return loss (dB)	Fabricate DW antenna and measure S21 return loss in a VNA	DW/TPM27
		Gain matched to model	DW/A/TP 22	Gain (dB)	Fabricate DW antenna and measure S11 Gain pattern with a VNA in an anechoic chamber	DW/TPM28

Table B:1: Technical Performance Parameters and Measures

C. Appendix C: Comsol Global Expressions

Constants and global expressions used in COMSOL Multiphysics simulation.

Name	Expression	Description
E	0.5 [W]	Laser Power
t_0	0.5 [s]	Exposure Time
G_fac	2.5	Super Gaussian Factor
G_G	7.09E-06	Normalisation Factor (calculated in math cad)
σ	0.0015 [m]	Beam Width σ
Rho	2600 [kg/m^3]	Density of DW Coating
k_c	8[W/(m.k)]	Thermal Conductivity DW Coating
Cpc	235[J/(kg.k)]	Specific Heat Capacity of DW Coating
To	297 [K]	Ambient Temperature
P_W	E*(t<t_0)	Applied Power
L_int	P_W*exp(-(((abs(x)/σ)^G_fac)+((abs(y)/σ)^G_fac))) [W]	Gaussian Input Power
L_xy	L_int*(1/G_G) [W/m^2]	Normalised Gaussian Input Power

Table C:1: Constants and global expressions used in COMSOL Mulitphysics simulation

D. Appendix D: Transmission Line Results

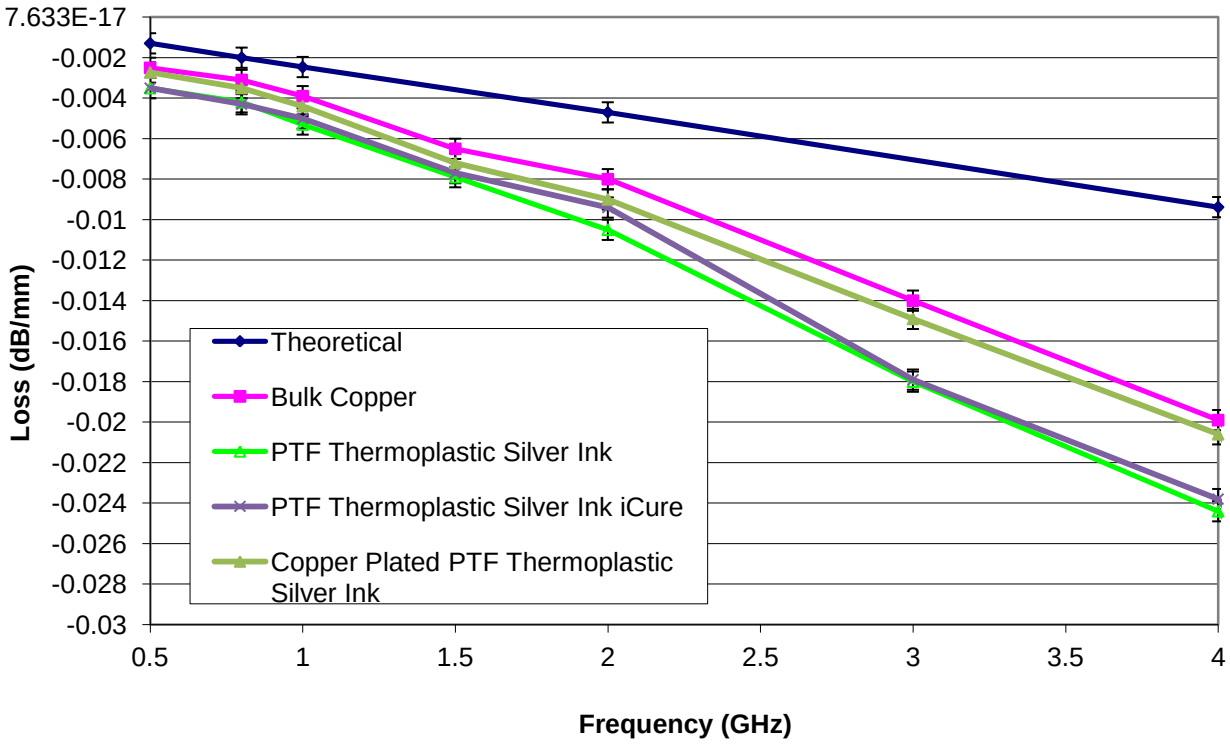

Figure D:1: S21 transmission line loss against frequency for PTF thermosetting silver ink micro-strip lines

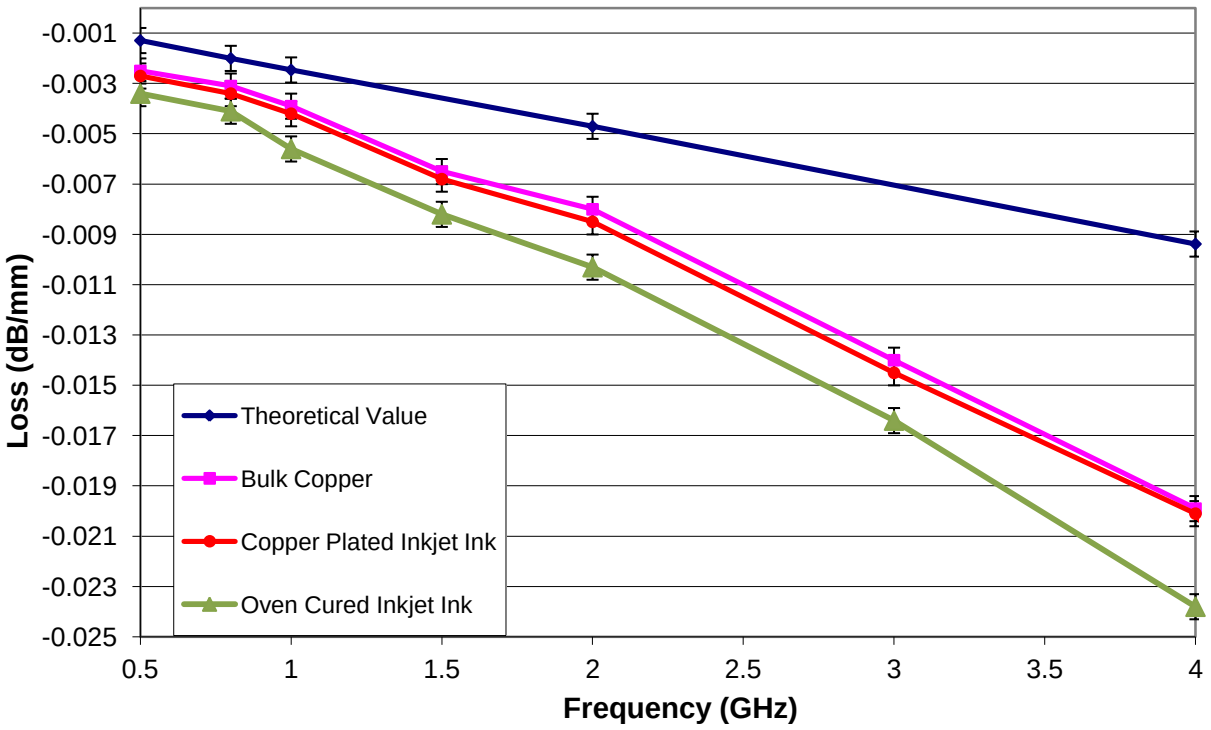

Figure D:2: S21 transmission line loss against frequency for Inkjet silver ink micro-strip lines

E. Appendix E: Antenna Gain Patterns

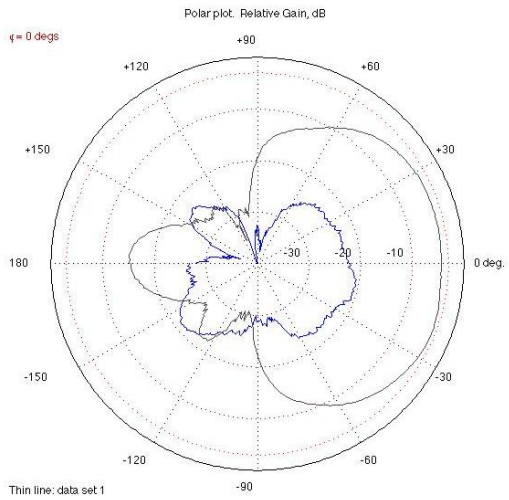

H Plane Oven Cured Silver Ink

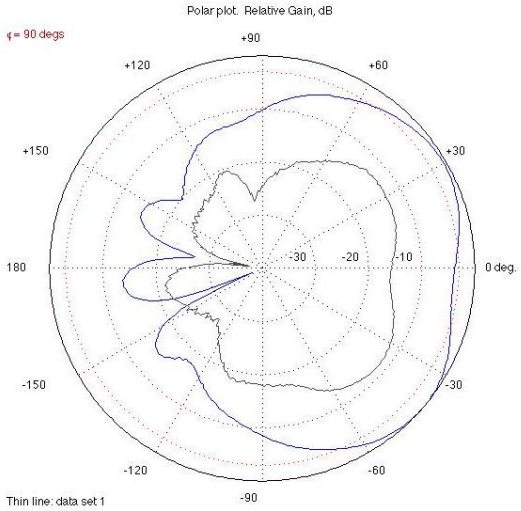

E Plane Oven Cured Silver Ink

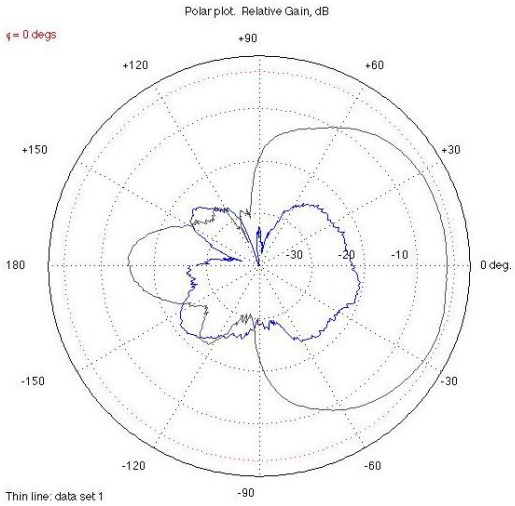

H Plane Broadband Spot Cured Silver Ink

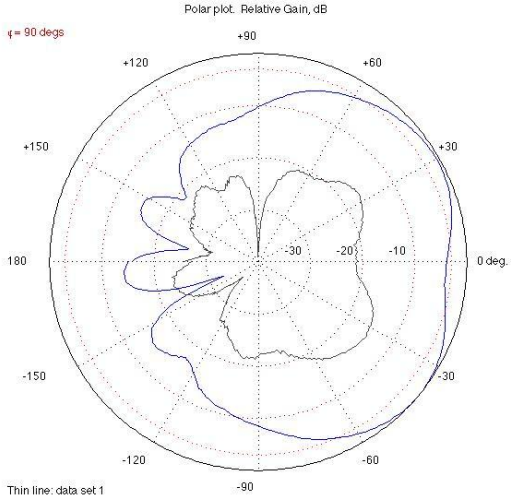

E Plane Broadband Spot Cured Silver Ink

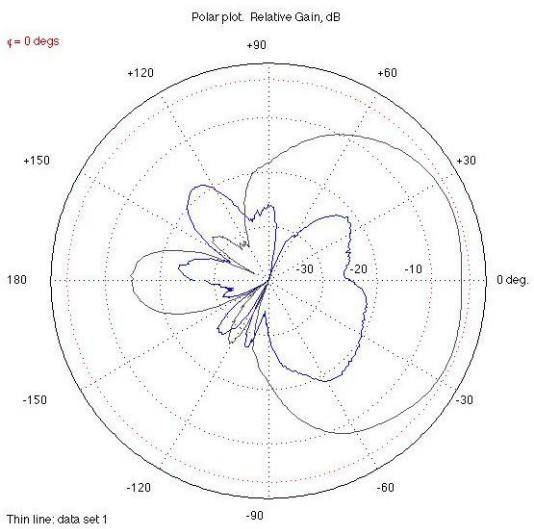

H Plane Oven Cured Thermosetting Silver Ink

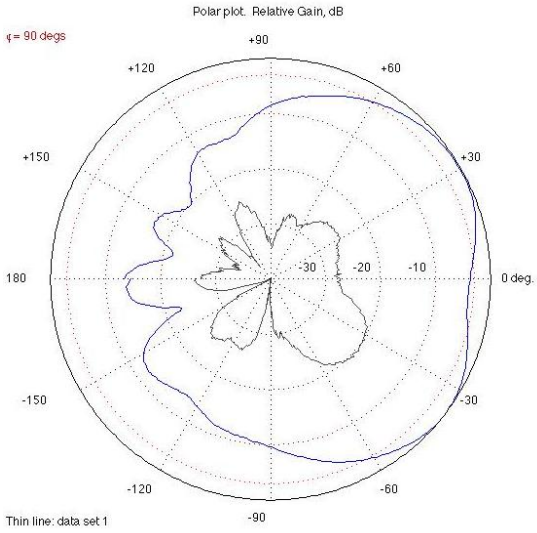

E Planve Oven Cured Thermosetting Silver Ink

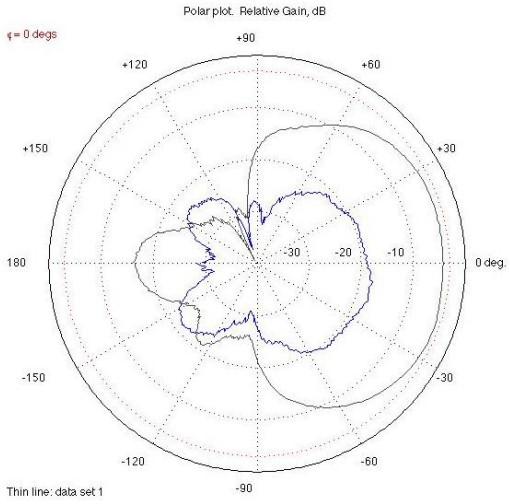

H Plane Broadband Spot Cured Thermosetting Silver Ink

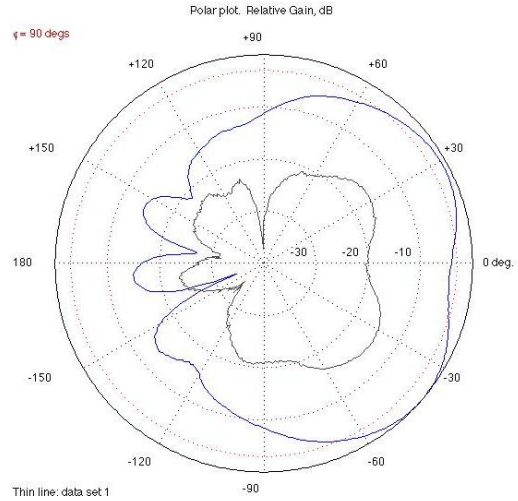

E Plane Broadband Spot Cured Thermosetting Silver Ink

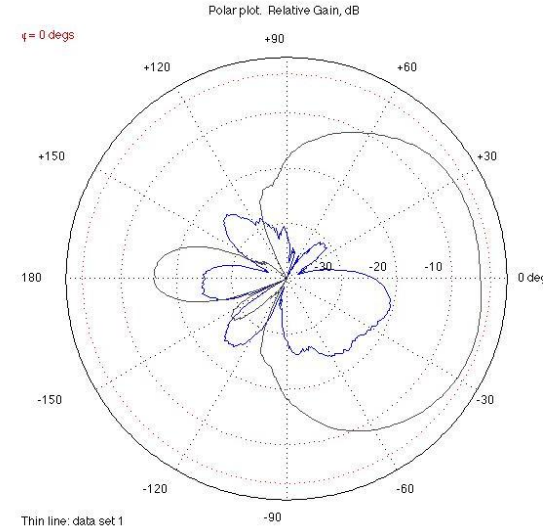

H Plane Copper Plated Thermosetting Silver Ink

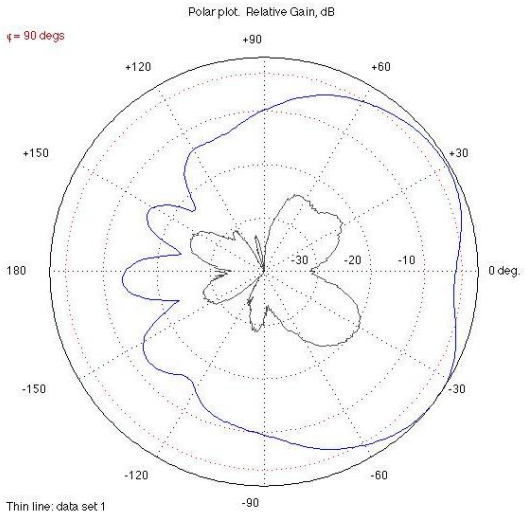

E Plane Copper Plated Thermosetting Silver Ink

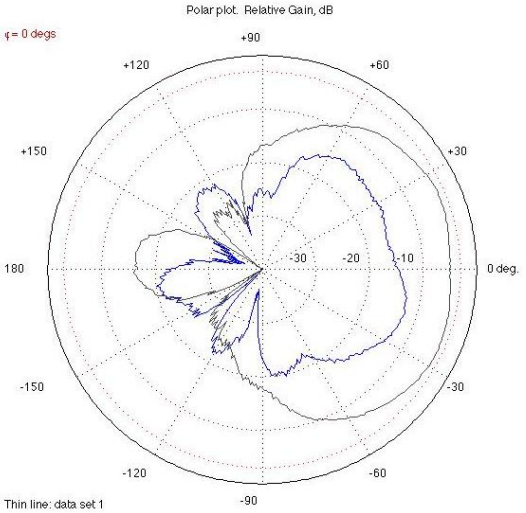

H Plane Oven Cured Multilayer Inkjet Ink

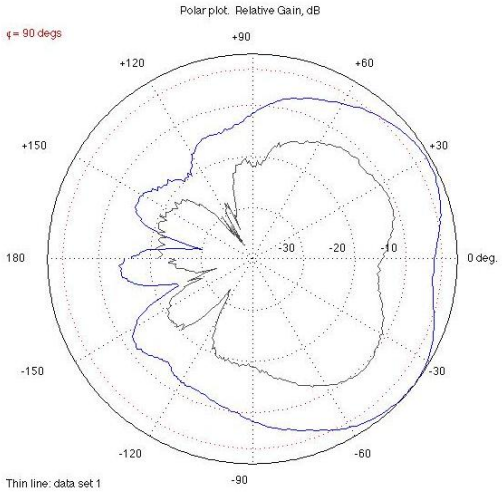

E Plane Oven Cured Multilayer Inkjet Ink

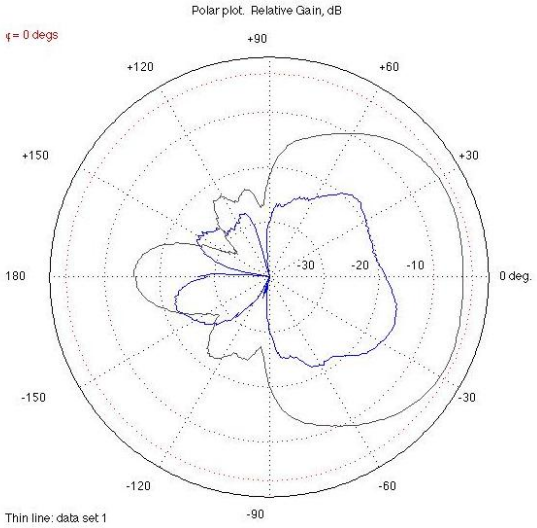

H Plane Copper Plated Multilayer Inkjet Ink

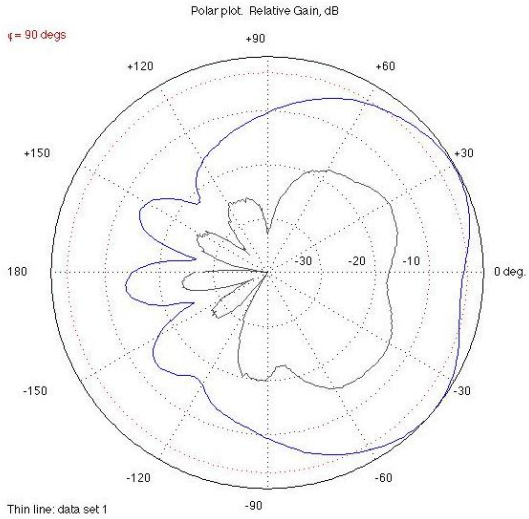

E Plane Copper Plated Multilayer Inkjet Ink

Figure E:1: Antenna gain measurements for DW patch antennas

Document End